CHAPTER ONE

INTRODUCTION

1. General background

The Cradle of Humankind World Heritage Site (COH WHS) is situated in the Gauteng Province of South Africa. COH WHS is well known for its extensive fossiliferous deposits of various species belonging to the Animalia Kingdom. A number of fossil-rich sites (mostly caves) have been discovered in this area, which includes among others Gladysvale, Sterkfontein, Swartkrans and Kromdraai, just to mention but a few. The samples used for the characterisation of both the fossil and modern bones were obtained from one of these prominent sites: Gladysvale. The global position of this site is described in detail under sampling site, Chapter Five, section 5.1. Fossil research work at this site started in 1936 following the collection of fossil remains by Dr. Robert Broom (Berger and Tobias, 1994). Following other activities which were carried out, Berger pioneered the long-term survey and excavation of the Gladysvale Cave deposits in April 1993.

The site contains extensive fossil remains of large vertebrates (Berger, 1992; Lacruz *et al*., 2002) and micro-fauna (Avery, 1995), including a diverse avian fauna (Stidham, 2004), from both *in situ* fossiliferous cave fill and mined breccias from a three chambered cave system which developed from dolomite, quartz and limestone rocks. These fossils occur in three forms: (i) breccias exposed in the walls of three chambers of the cave, (ii) several old, external and subterranean mine dumps and (iii) calcified and decalcified breccias that have been exposed by weathering, roof collapse and mining activities (Berger and Tobias, 1994).

1.1 Cave formation

Formation of caves and their features takes place when rainwater seeps into the cracks or joints in the rock material, usually limestone or dolomite. The combination of rainwater with carbon dioxide from the air and soil forms a weak carbonic acid. When this carbonic acid comes into contact with the limestone, then dissolution of the rock begins. Over a long period of time, the dissolution process results in cracks and joints becoming larger and larger (http://www.uwec.edu/jolhm/cave/caveform2.htm, accessed on 14/09/09). The concentration of the acid gradually increases due to increased amounts of carbon dioxide absorption from vegetation and soil surrounding the area. Large tunnels, networks of tunnels and joints, and actual caves form and become established, as more and more limestone is dissolved (http://school.discoveryeducation.com/ accessed on 14/09/09).

Various speleothems (distinctive limestone features) begin to form once the caves and network of tunnels have formed, and these include among others stalactites, stalagmites, columns, popcorns, rimstone pools and cave pearls (Figure 1.1). Stalactites also known as soda straws (flowstones) are speleothems that hang from the ceiling of the cave, while stalagmites grow up from the floor of the cave (http://www.nps.gov/wica/Speleotherms.htm accessed on 14/09/09). Stalagmites form from the drops that have fallen from stalactites or flowstone i.e. following landing of many drops on the same spot a stalagmite is formed.

Water drips out of the walls; the calcite falls out of the solution and clusters on the cave walls, creating shapes that resemble popcorn (University of Wisconsin, http://www.uwec.edu/jolhm/cave/caveform2.htm, accessed on 14/09/09).

Figure 1.1. Numerous stalactites (many soda straws) on the ceiling of the cave. (The Legendary Black Water Rafting Company, 2004, University of Wisconsin, http://www.uwec.edu/jolhm/cave/caveform2.htm accessed on 14/09/09).

Figure 1.2 is a diagrammatic representation of the stages involved during dolomitic cave formation.

Stage 1: Phreatic cave passages are formed along a fracture or crack below the water table (the saturated zone) by water flowing under pressure. These cave passages (caverns) vary in size and shape due to differences in the nature of the fractures and planes of weakness in the rock.

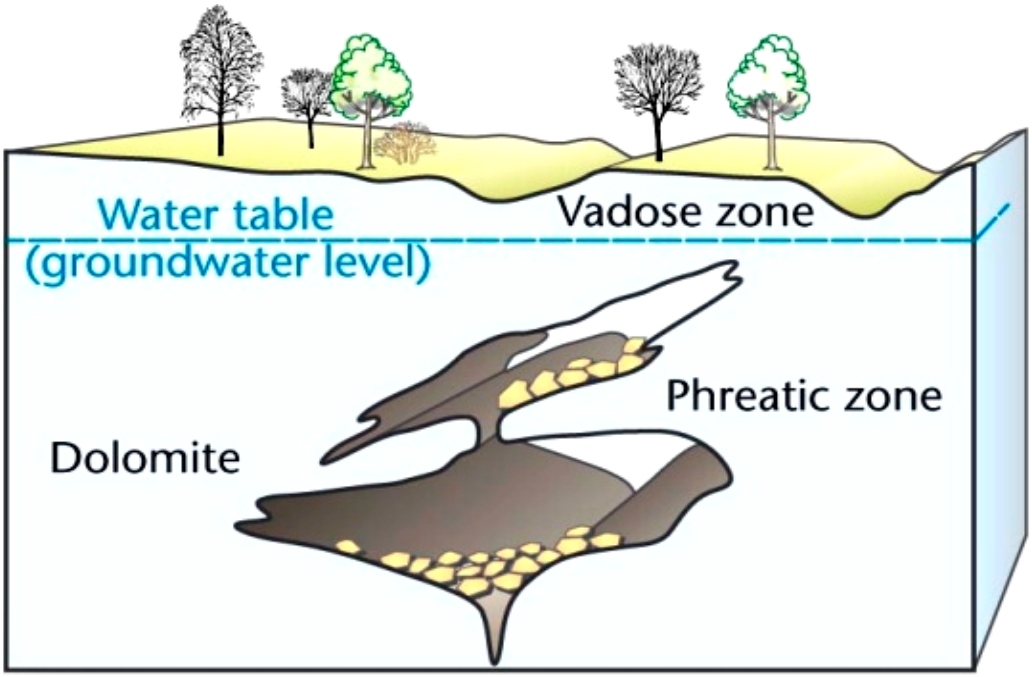

Stage 2: Later, as water levels drop and the cave becomes air-filled, several cave features (such as stalactites, stalagmites and flowstone) begin to form as water saturated with calcium carbonate drips through the ceiling of the cave.

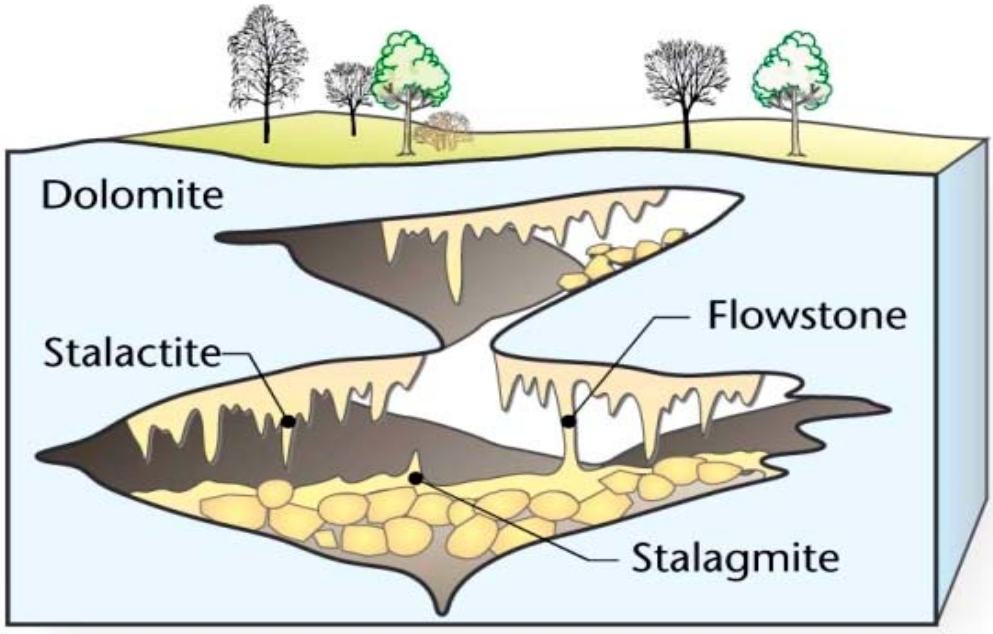

Stage 3: Shafts are formed that will finally break through to the surface, creating an opening into the cave. Through natural events such as erosion, a debris cone (i.e. deposition of bones of animals, soil and other organic matter derived from the surface) is formed in the cave. Cave breccias are formed by dripping of lime-bearing water on the debris cone.

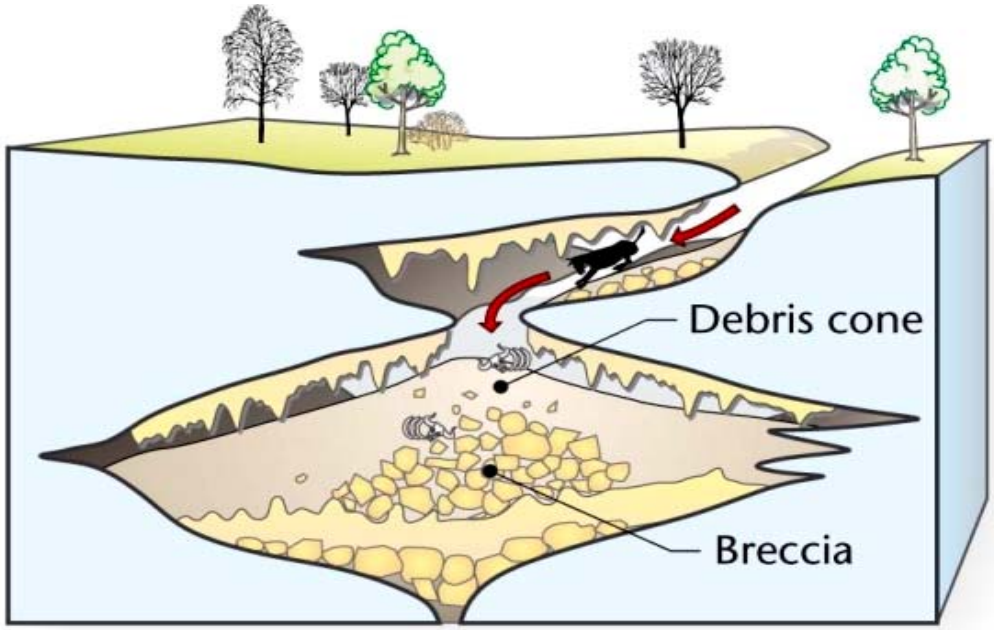

Stage 4: The cave entrance keeps on widening due to surface erosion.

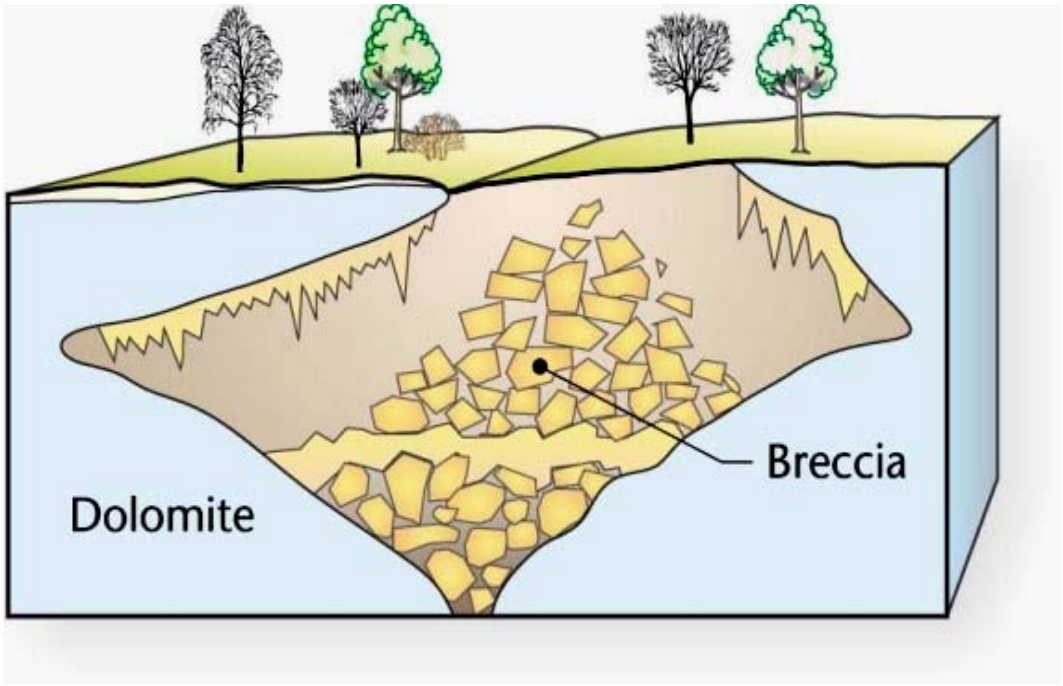

Stage 5: Finally the entire cave roof has been removed by surface erosion, exposing bone-bearing breccia on the surface.

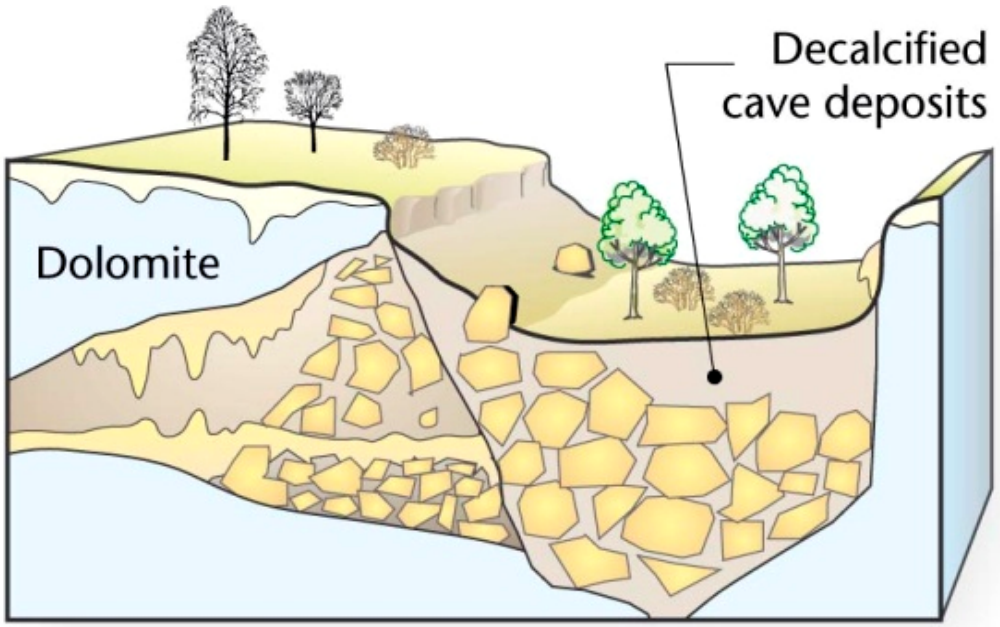

Figure 1.2. Stages in dolomitic cave formation and later infilling, (McCarthy and Rubidge, 2005).

Figure 1.3 is a schematic diagram showing the final stage of cave formation, where erosion has de-roofed part of the cave forming an entrance into the cave, and the bone bearing breccia is now exposed on the surface. The cave deposits start to decalcify, mixing with the fragments from the breccia. The diagram also shows the presence of stalactites, stalagmites, flowstones among many other cave features.

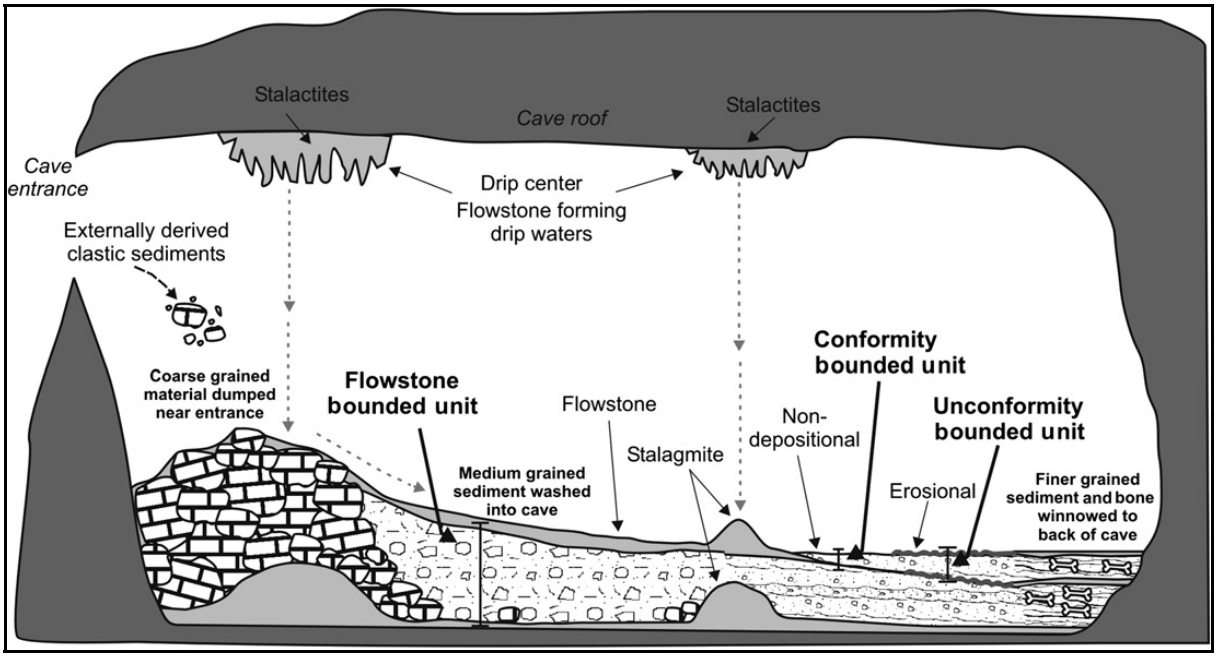

Figure 1.3. The final stage of cave formation, where erosion has de-roofed part of the cave forming an entrance into the cave, and the bone bearing breccia is now exposed on the surface (Pickering *et al*., 2007).

1.2. Diagenesis

In order to determine the molecular information remaining within fossilized vertebrate tissues, taphonomic and diagenetic processes operating at molecular level should be well understood (Schweitzer *et al*., 2008). Diagenesis is the cumulative physical, chemical and biological environment; these processes will modify an organic object's original chemical and/or structural properties and will govern its ultimate fate, in terms of preservation as fossils and their chemical and mechanical alteration or destruction (Wilson and Pollard, 2002; Behrensmeyer *et al*., 1989). Whereas taphonomy focuses mainly on the alterations from the original living state of the bone that occur at any point between death and discovery of the fossil remains (Efremov, 1940; Lawrence, 1979; Hagelberg, *et al*., 1991). Once organism remains have been buried, they became prone to a number of taphonomic processes. Mineralization and deformation are the most common ones with microbial decay, biogeochemical interactions, and autolytic breakdown of cell and tissue components being some of the processes contributing to taphonomic loss (Rafalska *et al.,* 1991). Hence chemical and

structural alteration and/or loss of both the organic and inorganic components of the bone provide a potential source of valuable data on the bone's taphonomic history (Bell, 1990). Figure 1.4 below is a case study by Gutierrez (2001) on guanaco bone recovered from the Paso Otero 1 site in Argentina, showing typical taphonomic history of the bone. Diagenesis of skeletal tissue is affected by intrinsic factors of the tissue specimen, such as its size, porosity, chemical and molecular structure and by extrinsic factors such as sediment pH, water and temperature regimes and bacterial action (Von Endt and Ortner, 1984). Diagenetic alterations at the molecular level include: intramolecular and/or intermolecular bond disruption, denaturation of three dimension molecular structure, crosslinking of proteinaceous fragments with the soil organic components resulting in the formation of melanoidins and humic acids (Rafalska, 1991), deamination, depurination, racemization of amino acids or methylation of organic compounds (Schweitzer *et al*., 2008).

The process of diagenesis can be conveniently considered as occurring in three different environments: the bone tissue itself, the pore spaces and cavities within the bones, and the sediment around the bone. In the first, ionic substitution of apatite minerals with other minerals regularly occurs. In the second, pore spaces and trabeculae are filled with diagenetic minerals. Comparison of these with those of the surrounding sedimentary matrix may indicate transport prior to the final burial of the bone if the two sets of minerals differ (Martill, 1990).

Ultimately, the sedimentary matrix in which the vertebrate remains are buried affects (a) the outer surface of the bone (b) the nature of ground water (Lyman, 1994). It has been observed that the composition of ground water depends primarily on the local geology and that a wide range of trace element compositions occur in different potential host soils and sediments, for instance limestones are characterised by high Sr and Mn levels, whereas clays and mudstones by high Na, Fe, REE, Th and U levels (Williams, 1989). (c) Whether buried vertebrate remains are crushed or deformed based on the presence or absence of diagenetic cements in the sediment (Lyman, 1994).

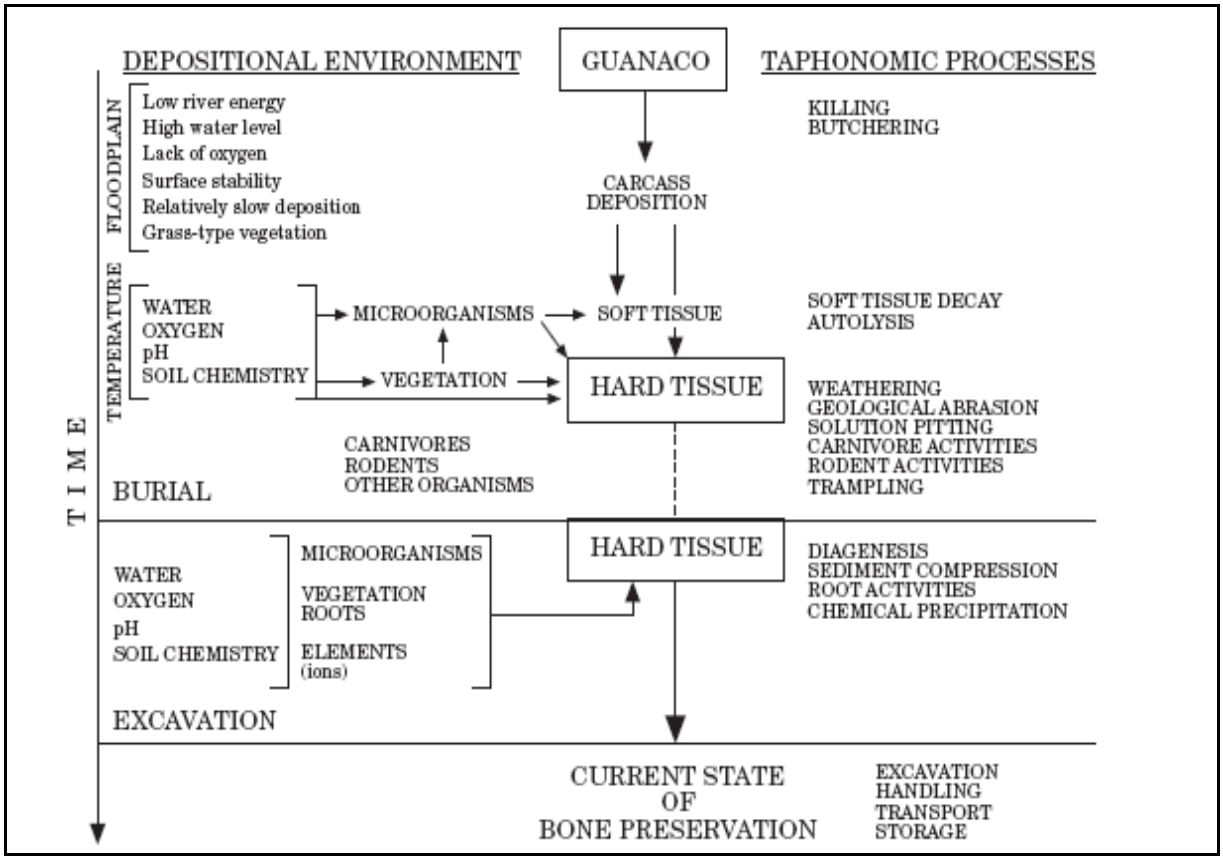

Figure 1.4. Model of the taphonomic history of Paso Otero 1. After Gutierrez (2001).

The process of diagenesis can be divided into two major successive stages, early and late diagenesis. The former deals with the decay processes of organic compounds within the bone itself (mostly through hydrolysis and other degradation reactions for example: non-enzymatic deamination, decarboxylation, ester formation and the Maillard reaction, all of which transform certain amino acids into derivatives (Bada and Miller, 1970)), recrystallization process and ion exchange between the surrounding water and the bone matrix (Pfretzschner, 2004). Hence early diagenesis is always associated with significant bone alterations in protein content, histology, apatite crystallinity, porosity and mineralogy (Tuross *et al*., 1989; Hedges *et al*., 1995; Nielsen-Marsh and Hedges, 2000), facilitating elemental and isotopic exchange with ambient fluids and/or embedding sediment. The chemical environment of early diagenesis is therefore characterized by high phosphate content mixed with the decay products of bone protein, and this stage ends with the replacement of the collagen by minerals (Pfretzschner, 2000). This high phosphate content buffers the pH to high

values leading to an environment having pH values of between 8 and 10 and extremely low redox potential, lower than -200 mV. Equation 1.1 represents the buffering process (Pfretzschner, 1998):

$$PO_4^{3-} + 3\ H_2O \leftrightarrow HPO_4^{2-} + OH^- + 2\ H_2O \leftrightarrow H_2PO_4^- + 2\ OH^- + H_2O \leftrightarrow H_3PO_4 + 3\ OH^- \quad (1.1)$$

Increase in pH is also a direct result of the release of ammonia during the decay of collagen, thus the degradation of collagen (which also involves gelatinisation of collagen by successive splitting into shorter protein chains), is to a certain extent due to non-biotic leaching and also partly due to microbial activity on the bone. The faster the rate of collagen gelatinisation process, which is pH dependent and is considerably fast under high pH, the faster the rate of protein hydration (Walrafen and Chu, 2000). Hydration of the gelatinised protein causes swelling leading to development of microcracks in the bone. These cracks plays a crucial role in enhancing the process of diagenesis by opening pathways through the entire bone volume, thereby increasing the rate of decay and leaching as well as ion exchange with the surrounding environment. Early diagenesis roughly lasts for 50 to 500 years under natural conditions (Pfretzschner, 2000).

At late diagenesis much of the organic remains have disappeared except for some traces which may persist in the apatite matrix, and this process is characterized by slow rates of chemical reactions, mainly substitution and precipitation of minerals within the bone (DeNiro and Weiner, 1988). Under these highly reducing environments (high pH due to the presence of phosphate), metal ions in aqueous solutions which come in contact with the fossil bone or enter it by diffusion will be reduced and precipitate as hydroxides or oxides and/or carbonates. For instance manganese which naturally occurs in higher concentrations in groundwater, enters the bone as mobile Mn^{2+} and is precipitated as $Mn(OH)_2$, which transforms, by loss of water, into MnO and later into pyrolusite, (MnO_2). Similarly under the same conditions, mobile ferric ion (Fe^{3+}) approaching the bone will be reduced to ferrous iron (Fe^{2+}) which rapidly precipitates to $Fe(OH)_2$ and later undergoes transformation

to hematite, (Fe_2O_3). Alternatively, pyrite (FeS_2) is formed instead of hematite via precipitation of iron sulphide (FeS, equation 1.2) (decaying collagen will release sulphide ions into the water) (Pfretzschner, 2004):

$$Fe^{2+} + H_2S \rightarrow FeS + 2\ H^+ \qquad (1.2)$$

The black or dark brown colour of the fossil bones is a result of high levels of pyrite, hematite and pyrolusite coatings. During the later stages of late diagenesis, external oxidants can find their way into the fossil and transform the existing mineral through the oxidation process (Pfretzschner, 2004).
Basically, diagenesis occurs in three distinct phases:

(i) Syndiagenesis which involves bacteria in shallow sediments metabolizing organic matter in the skeletal tissue. This phase was used by Andrews & Cook (1985) to signify taphonomic processes that occur simultaneous with burial.

(ii) Anadiagenesis is the deep burial phase of compaction and cementation; inorganic chemical reactions predominate in this phase.

(iii) Epidiagenesis can result in the disappearance of the fossil itself leaving only a mould (Rolfe and Brett, 1969). Properties of the embedding sedimentary matrix which include among others: acidity, chemistry, moisture content, as well as permeability, are also of great significance to the process of diagenesis (Retallack, 1984; Tuross *et al.,* 1989).

Figure 1.5 is a schematic overview of the successive stages in bone diagenesis, the chemical conditions in the bone and the main minerals that may occur in fossil bone.

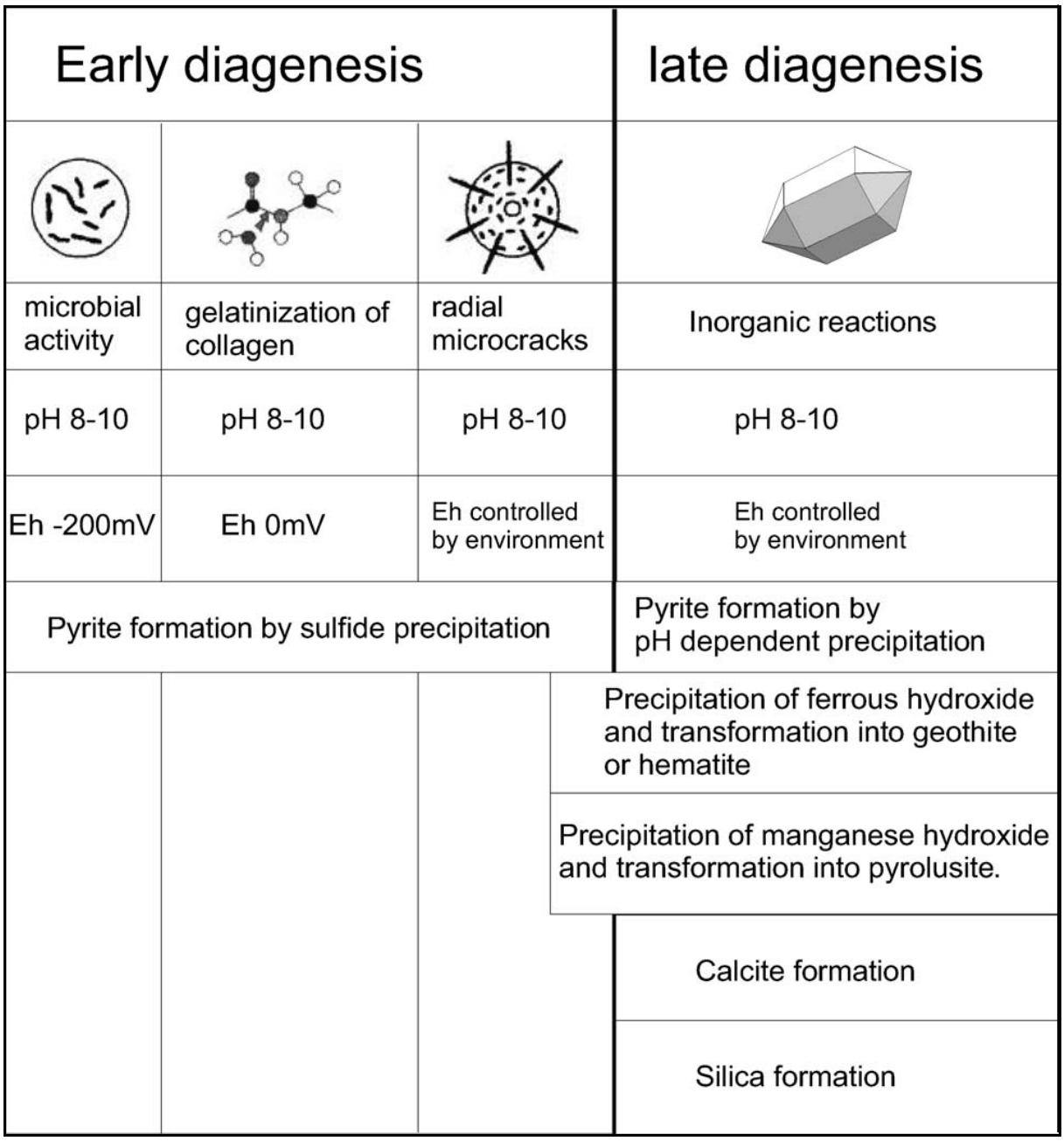

Figure 1.5. An overview of the successive stages in bone diagenesis, the chemical conditions in the bone and the main minerals that may occur in fossil bone, after (Pfretzschner, 2004).

1.3. Fossilisation

Fossilisation is the alteration of an organism's remains, impressions or activities by physical, biological or chemical changes retaining the original material in some form.

Therefore fossils are the preserved remains or traces from the remote past of organisms or plants. Bartsiokas and Middleton (1992) defined fossilisation process as a "naturally occurring physico-chemical process that preserves the gross morphology by ionic exchange and increase in the size of the apatite crystallites; this process also involves the loss of organic material of the bone and the filling of the voids with minerals". During the process of fossilisation, the bone's components are generally modified as follows:

(a) Gradual disappearance of all organic structures, i.e. the osteocytes and the collagen;

(b) Their replacement by material carried in the ground water;

(c) Substitution of the chemical elements constituting the crystalline lattice of the apatite (Ascenzi, 1969).

It is hypothesized that once buried, minerals (e.g. calcite, silica, gypsum, selenite, and many others) in overlying sediments are solubilized and then redeposited or precipitates in pore spaces within the fossil as the saturated ground water moves through them, while at the same time removing any endogenous organic constituents (Schweitzer *et al*., 2008). A permineralized or petrified fossil is formed when the mineral-bearing solutions infiltrate into pores of skeletal tissue, depositing their mineral content in those spaces. Whereas a mineralized fossil is formed by the substitution of the original hard parts of an organism with exogenous minerals; thus skeletal tissue's chemical constituents are dissolved and removed while minerals dissolved in the ground water are deposited in their place (Matthews, 1962). Leaching can be best described as the removal of soluble matter and enrichment as the addition of soluble matter. Hence mineralization and petrification, in a way, are enrichment processes. Hydrolysis is often regarded as a leaching process involving the combination of water with other molecules (Lyman, 1994). Calcification which is the precipitation of calcium carbonate salts is characteristic of some fossil remains recovered from arid areas where moisture is insufficient to flush the salts from the sedimentary matrix. The presence of these coating on the bones with such salts and /or minerals can obscure the information necessary to recognize them and requires intensive cleaning (Stahl and Brinker, 1991). The extent of alteration of fossils

through these processes (diagenesis) is variable and is directly proportional to molecular preservation and its state of preservation depends on the nature of the environment during burial. The less the extent of alteration that has occurred at the gross, microscopic and elemental levels from the living state, the higher the probability of finding fragments of original biomolecules being retained (Hagelberg, 1991; Hedges, 2002). Bone dissolution can lead to substantial loss of the bone mineral, and this process proceeds rapidly at low pH (that certainly occurs when organic matter is oxidized) as opposed to presence of calcite in sediments, which stabilises pH at around 8.0 and thus minimises dissolution. However, dissolution accompanied by reprecipitation should leave original decomposition traces in the fossil (Stiner *et al*., 2001). So the availability of calcite and/or dahllite in sediments indicates that conditions are conducive to good preservation of bones (Shiegl *et al*., 1996). Thus fossilisation process is a complex series of activities that take place over a variable timescale leading to preservation, destruction or modification of bone structure.

1.4. Fossil Formation

Fossils are normally found in sedimentary rocks, which are produced by the accumulation of sediment such as sand or mud. Quick burial (over moist sediments) is one of the best conditions favouring fossilisation process. This prevents the animal or plant from being eaten by other organisms or from undergoing natural decay through exposure to oxygen. Usually the soft parts of an animal decay more quickly than its hard parts. Teeth and bones are therefore more likely to be preserved than skin, tissues, and organs (http://www.fossils-facts-and-finds.com/fossil_formation.html. Accessed 19/03/09). Figure 1.6 is showing a lizard fossil from Solnhofen limestone formation.

Figure 1.6. A lizard Fossil from Solnhofen Limestone Formation, http://pro.corbis.com/ (accessed 19/03/09).

Below is a general sequence of events leading to fossil formation (http://www.fossils-facts-and-finds.com/fossil_formation.html. Accessed 19/03/09).

(i) The animals must die and get buried quickly by sinking in mud or in soil, or other areas.

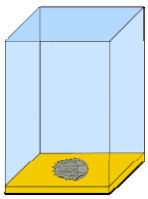

(ii) Over time, more and more sediment covered the remains (sedimentation process). The faster this happens the greater chances of fossilisation occurring. These sediments continue to pile on, the lower layers become compacted by the weight of layers on top and over some period of time this pressure turns the sediments into a rock.

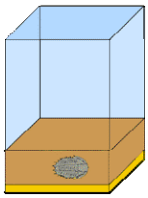

(iii) The process of fossilisation involving the dissolution and replacement of the original minerals in the bone with other minerals and/or permineralization, the filling up of spaces in fossils with minerals, and/or recrystallization in which a mineral crystal changes its form continued. This process results in a heavy, rock-like copy of the original bone (a fossil). The fossil has the same shape as the original object, but is chemically more like a rock. Some of the original hydroxy-apatite (a major bone constituent) remains, although it is saturated with silica and other minerals.

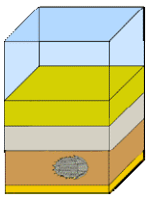

(iv) Now fossil formation is complete but the bone is still buried under hundreds or even thousands of feet in a rock. As the continental plates moves around the earth, crashing into each other, mountains are formed and former sea floors are lifted up becoming dry land and the bone will come closer to the surface.

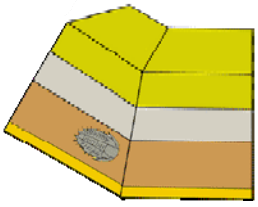

(v) The fossil is eventually revealed by erosion. Wind, rain, freeze and thaw, even earthquakes will help force the fossil out of its burial ground and out into the light.

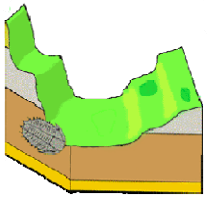

Figure 1.7 is a flow chart illustrating conditions necessary for fossil formation in the geochemical environment.

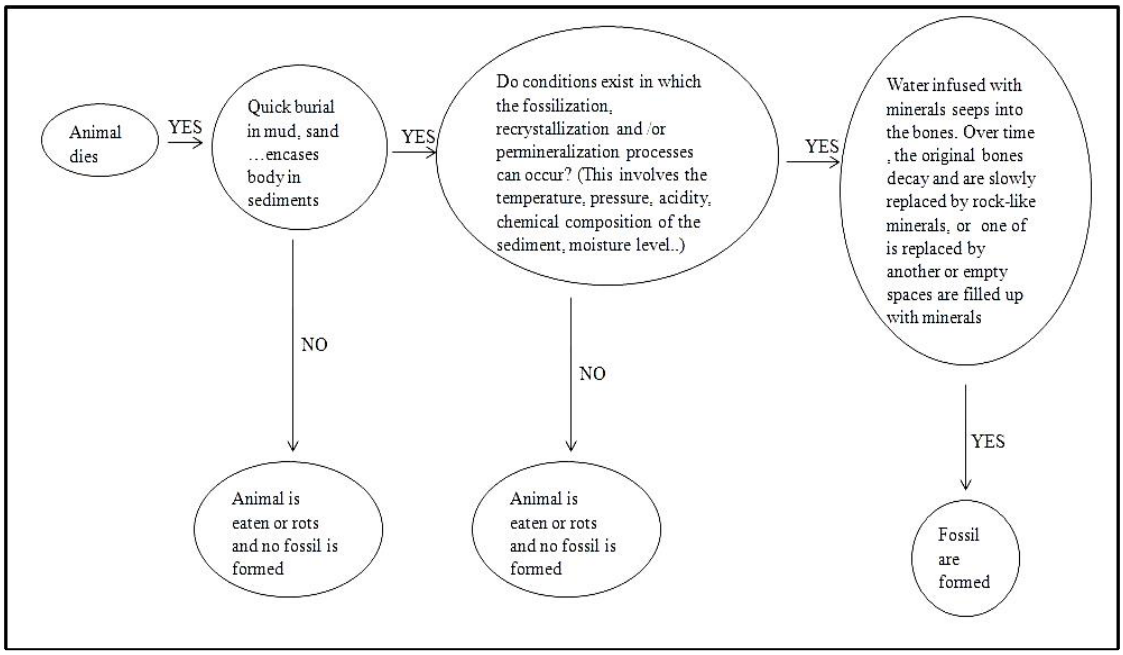

Figure 1.7. Flow chart illustrating conditions necessary for fossil formation. Modified from Col, Jeananda, http://www.enchantedlearning.com (Accessed 06/04/09).

1.5. Fossil Preservation

Preservation refers to the survival of the organism's remains after death and its transition into a fossil. Skeletal material (bones) can be well-preserved retaining many of the physico-chemical characteristics found in modern fresh bone (Smith *et al*., 2007). The process of bone diagenesis leading to this preservation over a given geological time is a highly complex phenomenon involving the physical, chemical, histological and mechanical alterations that take place at different time scales from the time of death and is entirely depended on the local geochemical conditions (Trueman *et al*., 2004). The state of preservation is a direct result of the past events, which are the processes that had occurred to bones from the time of death, through burial up to the time when the bone was recovered. Normally, the biological information contained in the living organisms is either obscured or completely destroyed as a result of the complex physical and chemical changes that usually take place in bones after burial (Gutierrez, 2001). As a result the state of preservation is quite variable depending on the environmental conditions. Some of the processes affecting bone preservation are: (i) dissolution of the mineral phase, leading ultimately to the loss of the bone. Bone apatite dissolution is pH dependent, and in low pH environments (pH< 6.5) the bone mineral phase is relatively soluble (Berna *et al*., 2004), this may lead to rapid leaching of both major and trace elements from the bone, and consequently bone apatite is usually lost from the sediment system. Therefore bone apatite solubility increases with decrease in pH, and decreases as pH is increased above 7 and hence bones are more likely to be preserved in environments with high pH. (ii) Bone porosity, roughly 40% of the volume of a fresh bone is made up of collagen, and as collagen degrades during the process of diagenesis, additional pore volume is created which may be filled through diagenetic recrystallization of primary bone crystallites and growth of secondary apatite (Truemen *et al*., 2006). The pore structure of the bone determines how it interacts with the groundwater and as a result the extent of diagenesis and hence the state of preservation, consequently the higher the density and lower the porosity of a given bone sample the less the rate of alteration. Thus the greater the porosity of a bone tissue the more susceptible it is to diagenetic change and the more rapid the ion exchange reactions between the tissue and the sedimentary

matrix in which it is embedded (Hanson and Buikstra, 1987). In addition, measuring the porosity of modern bone material can potentially provide a method for assessing the relative likelihood of survival for different skeletal elements. (iii) recrystallization; recrystallization of the apatite matrix transforms the fossil bone into a rather more stable mineral phase and decreases the accessible surface of the crystals, and thereby reducing and/minimising the rate of chemical reactions and substitutions occurring in the apatite (Pfretzschner, 2004), thus preserving the fossil's original components. The rate of recrystallization in buried bones is site specific, and is basically dependent on hydrological, chemical and microbial variables (Kohn and Law, 2006). Throughout diagenetic recrystallization of bone, trace elements are scavenged from the surrounding waters and/or sediments into the bone via a diffusion-adsorption process (Millard and Hedges, 1999) Therefore post-mortem uptake of these trace elements is only limited by their supply and availability in the environment where the bone is buried and effectively ceases when recrystallization closes all porosity initially occupied by collagen (Trueman *et al*., 2006). (iv) Climate, different climatic conditions (being frozen, alternately wet and dry, or constantly wet and dry), all determines the rate and types of chemical reactions that can occur. In cold environments (at low temperatures) the rate of collagen hydrolysis in the bone is very low; hence collagen remains can be preserved for a long time. The action of micro-organisms for example the bacteria and fungi that attack collagen, is less pronounced in dry environments as compared to moist environments (Sillen, 1989). Furthermore the rate of decomposition of the bone protein is more rapid in an aerobic environment, than under anaerobic conditions as the former environment can sustain a larger population of micro-organisms and also the decay processes are naturally faster during oxidation. However, a rapid growth of aerobic micro-organisms may lead to anaerobic conditions when the rate of oxygen consumption surpasses the rate of oxygen diffusion (Child, 1995). The location of bone deposition also determines the rate of its burial, and bones that are weathered sub-aerially would respond differently to diagenetic processes as compared to unweathered bones (Sillen, 1989) bringing about different state of preservation. Finally, a short temporal duration of burial may result in a bone being deprived access to various diagenetic processes that it would be exposed to were it buried for a long time.

Due to these complex physical, chemical and biological processes taking place during fossilisation, molecular preservation is considered to be highly unlikely, or totally impossible. More often than not, taphonomic factors combine to completely destroy tissues leaving no trace of the organism behind. The existence of fossil remains is evidence that at least some of these processes were arrested before complete degradation occurred. In the event of outstanding preservation, in which the fossil displays: preservation of original skeletal elements, preservation of original, unaltered mineral composition and orientation, labile soft tissues, or cellular structure, shows that destructive processes were stopped very early, and/or that mineralization outpaced degradation to preserve those components that are normally lost (Schweitzer *et al*., 2008).

1.6. The chemical composition of the mineral phase of calcified tissues – bone

The bone in living animals is a heterogeneous dynamic tissue composed of collagen, water, hydroxylapatite crystals, little amounts of protein and noncollagenous molecules (Martin *et al*., 1998). The mineral phase of calcified tissue that make up bones and teeth is a calcium phosphate that closely resembles the naturally occurring mineral, hydroxylapatite ($Ca_5 (PO_4)_3OH$) (Gaines *et al*., 1997), and is often referred to as bioapatite due to its intimate association with biological activity and molecules. Thus small crystals of hydroxylapatite and bundles of collagen fibres are bound together by amorphous cement consisting of organic and inorganic ingredients (Hare, 1980). However the bioapatite mineral does not have a precise/definite composition and crystal structure, and therefore the following formula is a more appropriate representation of bioapatite $(Ca,Na,Mg[\ ])_{10}\ PO_4\ ,HPO_4\ ,CO_3)_6\ (OH,F,Cl,CO_3,O,[\ ])_2$. The brackets show vacancies in some lattice sites within the solid to achieve a charge-balanced solid phase (Skinner, 2004). Thus skeletal tissues (bones, enamel and dentine) mainly consist of mineral carbonate-bearing hydroxyl apatite (dahllite) particles ($Ca_{10}(PO_4)_{6-x}(CO3)_x(OH)_{2+x}$) imbedded in an organic collagen matrix and their composition varies with age, nutrition, nature, type and location of the tissue (Reiche *et al*., 1999). This is shown in Table 1.1. Variations are mainly due to differences in protein content, crystal size and porosity; resulting in different

properties of these skeletal tissues with enamel being the least susceptible to diagenesis (Zazzo *et al*., 2004). Whole cortical bone is approximately 69% inorganic, 22% organic, and 9% water (Triffitt, 1980). Collagen, a protein, constitutes 90% of the organic portion of the dry fat free bone (McLean and Urist, 1968) and amongst its main functions in the body; it also provides nucleation centers for the initiation of bone calcification (Price *et al*., 1985). Different bioapatites display different elemental compositions with the Ca/P ratios always differing from the ideal or stoichiometric value. For example Table 1.2 shows Ca/P *wt*% deviating by a range of 1.3 to 2.2 from 2.15, the stoichiometric value for hydroxylapatite (Zipkin, 1970).

Table 1.1. Bulk composition of bone, dentine, and enamel. Modified table after Skinner (2004).

	Bone *wt%*	Dentine *wt%*	Enamel *wt%*
Inorganic	70	70	96
water	6	10	3
Organic	24	20	1

Table 1.2. Composition of major elements and the Ca/P ratio of the Bioapatites in three tissues (wt% on a dry, fat-free basis). From Zipkin (1970).

	Bone	Dentine	Enamel
Ash	57.10	70.00	95.70
Ca	22.50	25.90	35.90
P	10.30	12.60	17.00
Ca/P	2.180	2.060	2.110
Mg	0.260	0.620	0.420
Na	0.520	0.250	0.550
K	0.089	0.090	0.170
CO_2	3.500	3.190	2.350
Cl	0.110	0.000	0.270
F	0.054	0.020	0.010

These variations are a direct result of ionic substitutions within the mineral by carbonate, citrate, and wide range of minor and trace elements from food and water ingested during the life of the organism (Pate and Hutton, 1988). Figure 1.8 shows the schematic model of the structure and formation of the mineral, hydroxylapatite in the bone in close association with solution (fluid) containing a wide range of possible ionic substituting groups. All positions of the crystal lattice, the Ca, phosphate, and hydroxyl take part in these substitutions (Neuman and Neuman, 1958; Neuman, 1980; LeGeros *et al.,* 1970; McClellan, 1980; Boskey and Posner, 1984).

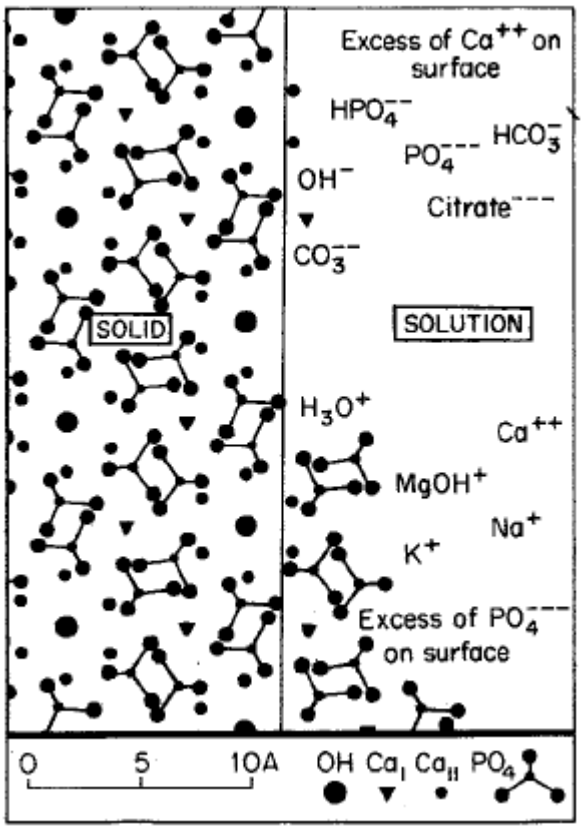

Figure 1.8. Schematic model of structure and formation of hydroxylapatite in bone, (Engström *et al.,* 1957).

Mammals discriminate against certain elements for instance barium and strontium with respect to calcium in the digestive tract and kidneys (Walser and Robinson, 1963; Kostial *et al*., 1969; Spencer *et al*., 1973; Kobayashi and Suzuki, 1990; Leggett,

1992; Sips *et al*., 1997), and as a result modern bones usually contains lower Ba/Ca and Sr/Ca ratios when compared to fossil bones. This is so because after burial a bone is no longer subject to biological discrimination against minor and trace elements (Spencer *et al.,* 1960, 1973; Walser and Romnson, 1963; Kostial *et al.,* 1969). Hence, the chemical composition of any postmortem diagenetic phases will reflect the composition of the soil solution and would deviate from *in vivo* values (Pate and Hutton, 1988).

1.7. The crystal structure of hydroxylapatite

Hydroxylapatite has a composition of $Ca_5(PO_4)_3OH$, normally expressed as $Ca_{10}(PO_4)_6(OH)_2$ to indicate that there are two formula units in the crystallographic unit cell (Wopenka and Pasteris, 2005). Figure 1.9 is a diagrammatic representation of the three-dimensional arrangement of the atoms that make up the hydroxylapatite structure. This projection presents a view down the *c*-axis (with a plane perpendicular to *c*), showing the spatial distribution of the PO_4 tetrahedral ionic groups, Ca ions and channel sites making–up the unit cell (Skinner, 2004). In this sketch (sizes of atoms are not drawn to scale) the parallelogram indicates an outline of the crystallographic representation of the repeating unit cell. Six of the Ca^{2+} atoms form a six-fold site (shown by dashed lines) in which the channel ions reside. All crystallographic sites/positions including channel sites are size specific and hence not every atom or ionic group will fit (with flexibility) into each site. The channel sites in the hydroxylapatite structure are not assigned to OH^- ions only, but can also be occupied by the substituting ions F^- and/or Cl^-, as represented by the general formula $Ca_5(PO_4)_3(F, OH, Cl)$ (Pan and Fleet, 2002; Picolli and Candela, 2002). When the channels are occupied by OH^- the mineral is known as hydroxylapatite, and in the event that they are occupied by Cl^- and F^- the name is chlorapatite and fluorapatite respectively, which are other existing members of the calcium apatite mineral group (Hughes *et al*., 1989; Skinner, 2004).

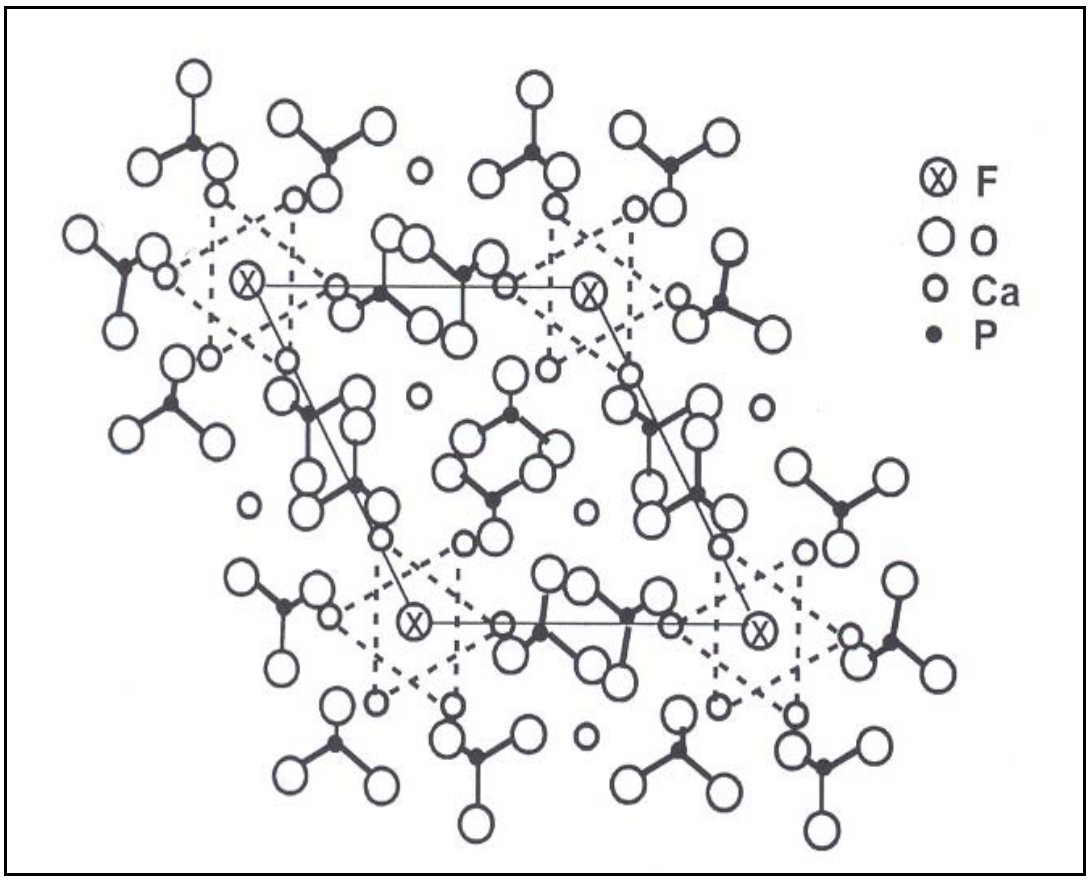

Figure 1.9. Three dimensional structure of fluorapatite, (ideal formula $Ca_5(PO4)_3(F)$), showing PO_4^{3-} tetrahedral ionic groups, Ca-ions and channel ions. Parallelogram indicates outline of unit cell and the diagram is viewed down the *c*-axis, (Wopenka and Pasteris, 2005).

Figure 1.10 further illustrates the distribution of the tetrahedral orthophosphate groups (PO_4^{3-}) in the apatite crystal, which are the building blocks of the apatite backbone structure. In the diagram the phosphorous atom (yellow) is in tetrahedral coordination, bonded to two white oxygen atoms in the same plane as the phosphorous and also to two light purple oxygen atoms one above the plane and the other below it. As shown by the diagram, there are two distinct sites where cations can reside (also known as cationic exchange sites) and they are discretely coloured orange and raspberry red. One is linked to the tetrahedral phosphate (PO_4) backbone oxygens and the atoms in channel ways (OH, F, or Cl) that runs parallel to the c-axis, and the

other is linked to the trigonal a axes in the centre of the cell. The two cationic sites are designated Ca1 and Ca2 in Figure 1.10 (Skinner, 2004).

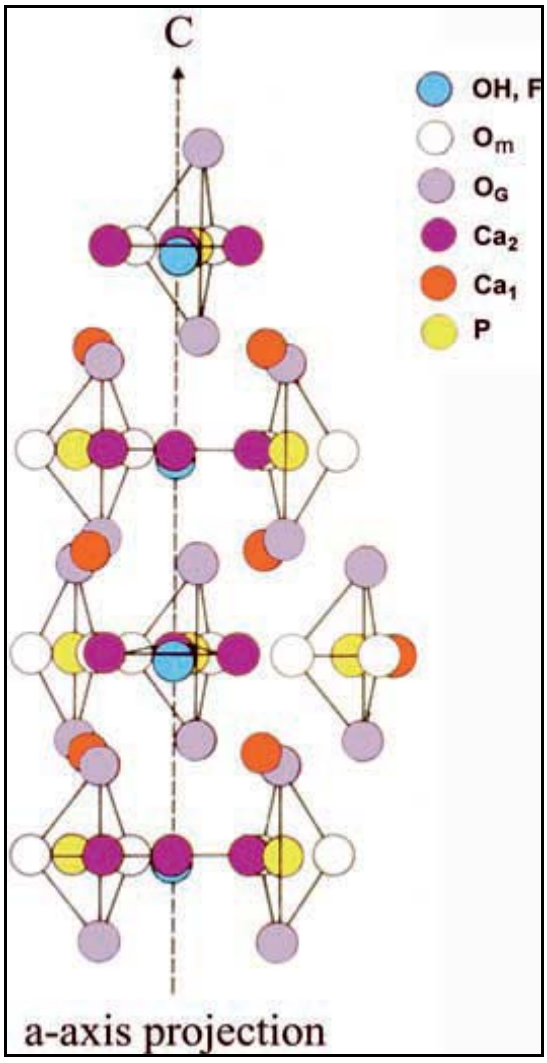

Figure 1.10. Three dimensional crystal structure of hydroxylapatite, showing the distribution of the tetrahedral orthophosphate groups (PO_4^{3-}). The diagram is a projection down the a-axis of the unit cell (Skinner, 2004).

They are basically four different types of crystallographic positions in the apatite unit cell: (i) tetrahedral sites for six P^{5+}-ions, each in 4-fold coordination with oxygen, (ii) Ca sites for four of the Ca^{2+} ions, (iii) Ca sites for the six other Ca^{2+} ions, and (iv) the channel site, which is typically occupied by two mono-valent anions, most commonly

OH^-, F^-, and/or Cl^- per unit cell (Wopenka and Pasteris, 2005). It is crucial therefore to take note of such differences in symmetry of apatite since they do affect the natural growth morphology of the crystals, which plays a vital role towards the bulk mechanical properties of a composite material like bone.

1.8. Possible ionic substitutions in the crystal

The mineral composition of any given apetite is not fixed, but the chemical substitutions that may occur must maintain the overall charge balance in the mineral and provide a geometric fit for the replacing ions within the crystal lattice (Wopenka and Pasteris, 2005). It should be noted that bioapatite (e.g. in fossils) composition always reflects the elemental bioavailability. Trace elements can be incorporated into the crystal structure of the bioapatites where they will occupy definite positions through substitution reactions. These substitutions may proceed in various positions on the crystal: (i) Hydroxyl site: The hydroxyl (OH^-) ion can be substituted by fluoride (F^-) and chloride (Cl^-) ions in the channel ways, forming fluorapatite and chlorapatite minerals respectively (Hughes *et al*., 1989). The rate of substitution for each other of these anions (OH^-, F^- and Cl^-) in the channel sites becomes more rapid at elevated temperatures. (ii) Phosphate backbone: Anions–complexes which include among others arsenate (ASO_4^{3-}), vanadate (VO_4^{3-}) which has a charge and size very similar to PO_4^{3-}, and other tetrahedral anionic groups, sulfate (SO_4^{2-}) and silicate (SiO_4^{4-}), although of different charge to PO_4^{3-}, can substitute the phosphate (PO_4^{3-}) anion in the apatite structure (Skinner, 2004). (iii) Cation sites: Both cationic locations designated Ca_1 and Ca_2 in hydroxylapatite (Figure 1.10) can also undergo cationic substitution by monovalent (e.g. Na^+, K^+) divalent (Mg^{2+},Ni^{2+},Cu^{2+}, Zn^{2+},Sr^{2+},Ba^{2+}, Pb^{2+}, Cd^{2+}) and trivalent ions of the rare-earth metals (Y^{3+}) for calcium (Piccoli and Candela, 2002; Pan and Fleet, 2002). In general the substituting ion should be of similar ionic radius to that which it replaces, and apparently experimental observations show that substitution reactions are more likely to proceed given that the radii of the two ions fall within 25% of each other. For instance, Sr^{2+}, Ba^{2+}, Zn^{2+}, $(UO2)^{2+}$, REE $^{3+}$ and Th $^{4+}$ substituting Ca^{2+}; $(VO_4)^{3-}$ and $(AsO_4)^{3-}$ substituting

(PO4) $^{3-}$; and F- for $(OH)^-$ (Williams, 1989). When substitution of one ion by another of the same sign but different charge (e.g. CO_3^{2-} for PO_4^{3-}) occurs, coupled ionic substitutions are likely to follow. In so doing charge neutrality is maintained either by a second substitution by an ion with dissimilar charge or by vacancies elsewhere in the lattice (e.g., one Ca^{2+} substituted by one K^+ plus one vacancy in place of OH^-) (Wopenka and Pasteris, 2005). Figure 1.11 shows the processes that influence element-uptake in the buried bone.

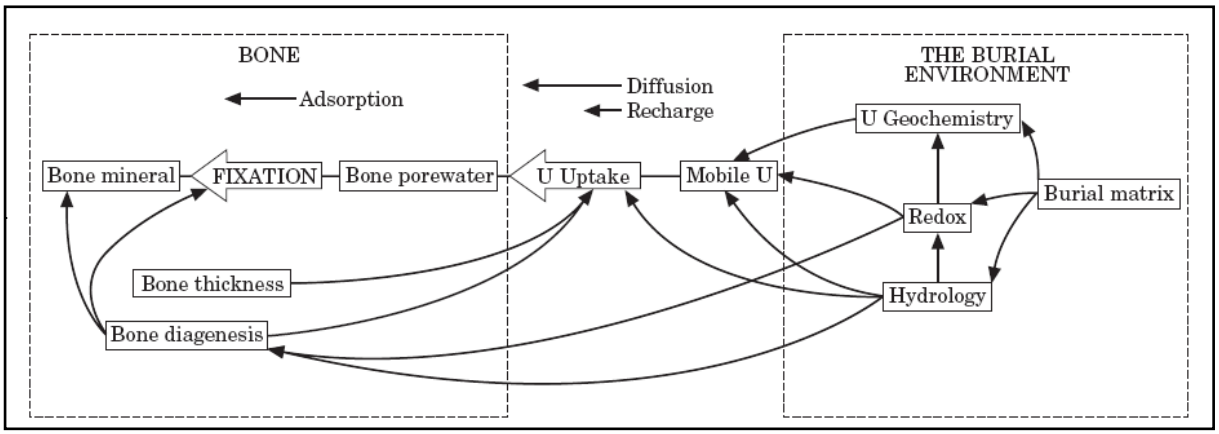

Figure 1.11. The processes controlling U (element) uptake in archaeological bone (from Pike, 2000). Uptake of other elements is likely to be controlled by similar processes.

Various analytical techniques, such as X-ray diffraction (XRD) and Raman spectroscopy can be used to detect structural changes following incorporation of any ions in the hydroxylapatite structure. Thus, the incorporation of F^- instead of OH^- gives better fit of the anion in the channel position, and results in the contraction of the unit cell along the a-axis direction (Hughes and Rakovan, 2002). Ionic substitutions in biological apatite are virtually less as compared to that in geologic apatites due to the limited number of available elements in the body. F^-, Cl^-, Na^+, K^+, Fe^{2+}, Zn^{2+}, Sr^{2+}, Mg^{2+}, citrate, and carbonate are some of the known and reported substituting ions in bone and tooth mineral (Gross and Berndt, 2002; LeGeros, 1991; McConnell, 1973).

CHAPTER TWO

LITERATURE REVIEW

2.1. Ionic exchange between soil solution and bone

Ionic interactions between the bone and soil solution are associated through competition between a wide ranges of ions for the various lattice positions in bone mineral (Pate *et al*., 1989), resulting in substitution reactions. Substitution of the original bone constituents by exogenous elements results in bone contamination. Contamination of buried bone takes both physical and chemical forms. The porous structure of the bone tissue is susceptible to infiltration by foreign materials, primarily trace elements (Price *et al*., 1992). The process of infiltration into the bone structure by an element can be considered as a three-stage process. Mobility is the first requirement, hence the element must migrate from the soil to the groundwater where it is mobile. Secondly, from the groundwater to the water held within the bone's pores, and finally it must be fixed in the bone (Pike and Richards, 2002).

Thus exogenous chemical species may move into the bone matrix by several different ways, including exchange with natural bone constituents (heteroionic exchange), deposition in unfilled voids or defects, and adsorption on the surface (Neuman and Neuman, 1958). Basically there are two common mechanisms by which trace elements may become incorporated into fossil bones: (1) by simple (or coupled) isomorphic substitution where the trace element, in ionic form, is able to fit into the bone apatite structure in a thermodynamically stable manner, substituting for one of the major ions, i.e. Ca^{2+}, $(PO_4)^{3-}$ or OH^- (Williams, 1989). (2) Through adsorption onto bone apatite crystal surfaces, this requires the element to be complexed to be in anionic or cationic form (Rae and Ivanovich, 1986). Since adsorption is a surface phenomenon, it is a more significant mechanism for uptake of trace elements where the degree of recrystallisation is small and bone porosity is high (Williams, 1989).

Therefore soil solution analyses from each interment site can be used to reveal which ions will be competing for exchange sites in buried bone.

2.2. Relating soil chemistry data to post-mortem diagenesis in bone

Information regarding relative and chronometric dates (Oakley, 1970; Taylor, 1987; Pickering 2008) palaeodiet (Klepinger, 1984; Lambert *et al.,* 1984; Ericson, 1985; Price *et al.,* 1985), palaeoclimate/palaeoenvironment (Luz *et al.,* 1984) as well as diagenetic alteration can be obtained from chemical composition of human and faunal bone excavated from palaeontological and archaeological sites, which in this study comprise cave deposits. The diagenetic processes occurring in these bones are considerably variable from one environment to the next and depend on a wide range of interactions, which include among others biological, chemical, and physical factors (Hedges and Millard, 1995). Hence these applications become complicated due to post-mortem chemical contamination and alteration occurring in the fossil bone through exogenous and endogenous transport of substances from the surrounding soil matrix. In order to overcome these complications, chemical analysis of soils, sediments and rocks (breccias) where the bones have been buried, followed by comparison with those of the fossil bone need to be considered. Comparative studies of the elemental concentrations in fossil bone and associated soils have been employed (e.g. Kyle, 1986; Waldron, 1983; Nelson and Sauer, 1984 to address chemical exchanges between bone mineral and the soil. The use of total elemental soil composition or acid soluble extracts instead of the soluble and exchangeable ions available to solution under field conditions introduce slight errors in these studies. Generally inorganic chemical reactions in the soil environment occur in solution, and the relative amounts of elements in a soil will not reflect the ionic concentrations in solution due to the differential solubilities of the various mineral and salt constituents (Pate and Hutton, 1988). For instance, the major components of highly weathered soils (i.e. Fe, Al, Ti and Mn) occur in insoluble forms and are therefore less available to the soil solution (Milnes and Hutton, 1983; Bohn *et al.,* 1985).

To understand soil solution chemistry, basic knowledge of the colloidal properties is a requirement. Metal oxides are available in soils as; free oxides, clay mineral coating and/or clay edges. These metal oxides exhibit charge due to protonation and deprotonation of the oxygen bonded to the metal (e.g. Fe^{3+}, Mn^{3+}, Mn^{4+}, Al^{3+} and Si^{4+}). This charge is referred to as variable charge or pH dependent charge, and it can be positive or negative depending on the pH of the system (Evangelou, 1998). Soil particle surfaces normally possess a net negative charge emanating from the negative charges on silicates and organic matter that attracts cations and repels anions. It then follows that anions are more easily leached from soils than cations (Pate and Hutton, 1988). These electrostatic relations are expressed by Coulomb's law:

$$F = qq`/Dr^2 \qquad (2.1)$$

Where F is the force of attraction or repulsion (dynes), q and q` are the electrical charges represented by the soil surface and ions in solution, r is the distance of charge separation (cm), and D is the dielectric constant. Besides variable charge caused by dissociation of mineral –edge hydroxyls, surfaces of mineral particles also contain permanent charge due to isomorphous substitutions. These permanent charges occur when coordinating cations of higher valence are replaced by cations of lower valence (e.g. replacement of Al^{3+} by K^{+}), a net negative charge on the mineral surface is generated. Thus to maintain electrical neutrality in the system, exchangeable cations from the solution are adsorbed onto the negatively charged mineral/soil surface (Evangelou, 1998).

According to Coulomb's law, the strength of ionic retention or repulsion decreases with (1) decreasing ionic charge and (2) increasing ionic radius or distance between the charge and soil particle surface. Thus because of their greater charge, trivalent cations are held more tightly by the soil surface as compared to divalent or monovalent cations, whilst cations with the same valence but smaller radius are held more tightly due to the reduced distances between the positive and negative charges. Therefore, a higher cation concentration on soil particle surfaces than in the surrounding solution can be expected. Bulk solution cations are known as soluble ions

and the bound hydration layer cations as exchangeable ions and it is the exchangeable ions that contribute greatly to the soil solution in more humid climates or in areas where irrigation is practiced (Adams, 1971; Rhoades, 1982; Thomas, 1982; Tucker, 1983; Bohn *et al*., 1985). In the geochemical environment pH is one of the major environmental parameters that is determined by all of the simultaneous equilibria existing in a given environment. Therefore the degree of dissociation of weak basic and acidic compounds (minerals) and the resulting solubility of otherwise insoluble weak basis are controlled by the activity of H^+ in that environment (Faure, 1992). Thus availability of various elements to the soil solution depends on the soil pH. In basic environments, iron, magnesium, aluminium and manganese will occur as relatively insoluble oxides and hydroxides, and phosphorous as sparingly soluble calcium and magnesium phosphates (Pate and Hutton, 1988). For example, under alkaline conditions magnesium and iron form the highly insoluble minerals brusite ($Mg(OH)_2$), and bernalite respectively. The precipitation reaction for Mg occurs in two steps (Faure, 1992):

$$Mg^{2+}_{(aq)} + OH^-_{(aq)} \leftrightarrow Mg(OH)^+_{(aq)} \qquad (2.2)$$

$$Mg(OH)^+_{(aq)} + OH^-_{(aq)} \leftrightarrow Mg(OH)_2(s) \qquad (2.3)$$

$$Fe^{3+}_{(aq)} + 3\ OH^-_{(aq)} \rightarrow Fe(OH)_{3(S)} \qquad (2.4)$$

Whereas, phosphorus and heavy metals such as copper, zinc, cobalt, manganese, lead and nickel will be adsorbed by silicate clays (Taylor *et al*., 1983; Norrish and Pickering, 1983) as well as iron oxides and hydroxides as illustrated in the example of γ-FeOOH (lepidocrocite) described later under section 2.5 of this chapter, and therefore will be less available to solution. Therefore, most of the soil solution ions will come from water-soluble carbonate, sulphate and chloride salts of calcium, magnesium, potassium and sodium (Bower and Wilcox, 1965; Isbell *et al*., 1983;

Hubble *et al*., 1983). It is thus the degree of acidity and alkalinity that determines the dominating ionic species in any solution (Garrels and Christ, 1965; Salomons and Forstner, 1984; Moore and Ramamoorthy, 1984).

2.3. Soil and sediment processes causing pH changes (Evangelou, 1998):

- Nitrification

$$NH_4^+ + 1.5\ O_2 \rightarrow NO_2^- + 2\ H^+ + H_2O \qquad (2.5)$$

- Denitrification

$$H_2O + NO_3^- + 2e^- \rightarrow NO_2^- + 2\ OH^- \qquad (2.6)$$

$$2\ H_2O + NO_2^- + 3e^- \rightarrow 0.5\ N_2 + 4\ OH^- \qquad (2.7)$$

$$1.5\ H_2O + NO_2^- + 2e^- \rightarrow 0.5\ N_2O + 3\ OH^- \qquad (2.8)$$

- Oxidative metabolism (enzymatically available organic matter + $O_2 \rightarrow CO_2 + H_2O$).

$$H_2O + CO_2 \leftrightarrow H_2CO_3 \qquad (2.9)$$

- Other electron acceptors for microbiological respiration

$$2\ H_2O + MnO_2 + 2e^- \rightarrow Mn^{2+} + 4\ OH^- \qquad (2.10)$$

$$Fe(OH)_3 + e^- \rightarrow Fe^{2+} + 3\ OH^- \qquad (2.11)$$

$$6\ H_2O + SO_4^{2-} + 8e^- \rightarrow H_2S + 10\ OH^- \qquad (2.12)$$

- Sulfur oxidation

$$H_2O + S + 1.5\ O_2 \rightarrow SO_4^{2-} + 2\ H^+ \qquad (2.13)$$

2.4. Geochemical conditions and Mineral occurrence in fossil bones

Understanding the processes of mineral formation during early diagenesis requires basic knowledge of the chemical environment within the decomposing bone. In this respect, bone histology (morphology) must be taken into account. Most types of bone are very dense and the most readily available means by which external reactants can reach the interior of the bone is by diffusion (Pfretzschner, 2004). Precipitation, recrystallization and mineral replacement are some of the dominant complex diagenetic physicochemical processes which take place during infilling of bone voids throughout the process of diagenesis (Downing and Park, 1998; Pate *et al*., 1989). The process of precipitation during early diagenesis occurs only in those cavities and cracks in bone that are accessible at that particular time, such as Haversian canals, osteocyte lacunae and the proximal parts of canaliculi (Figure 2.1a) (Pfretzschner, 2004). From a study done by Wings, (2004), carbonates ($CaCO_3$, $FeCO_3$, $BaCO_3$), sulphides (FeS, ZnS), oxides (FeO, Fe_2O_3), and sulphates ($BaSO_4$, $CaSO_4$) were found to be the most common infill minerals. In general the kind and availability of infilling minerals depends on the chemical composition of the ground water and the presence of bacteria influencing mineral precipitation where the bone is buried. The presence of other minerals in the fossil bone other than hydroxylapatite may indicate diagenetic change from original, unaltered bone mineral, consisting of microcrystalline, non-stoichiometric carbonate hydroxylapatite $Ca_5(PO_4)_3(OH)$. Bone decomposition environment is associated with high pH values, normally between 8 and 10, and extremely low redox potential (less than –200 mV) (Pfretzschner, 1998). Laboratory experiments conducted by Pfretzschner (1998), in which pH measurements were done on decaying bone gave results with good agreement to the theory. The measured pH in the surrounding water ranged from 8 to 8.5. These high pH values are a result of buffering effect of phosphates which occur at relatively high concentrations in the bone.

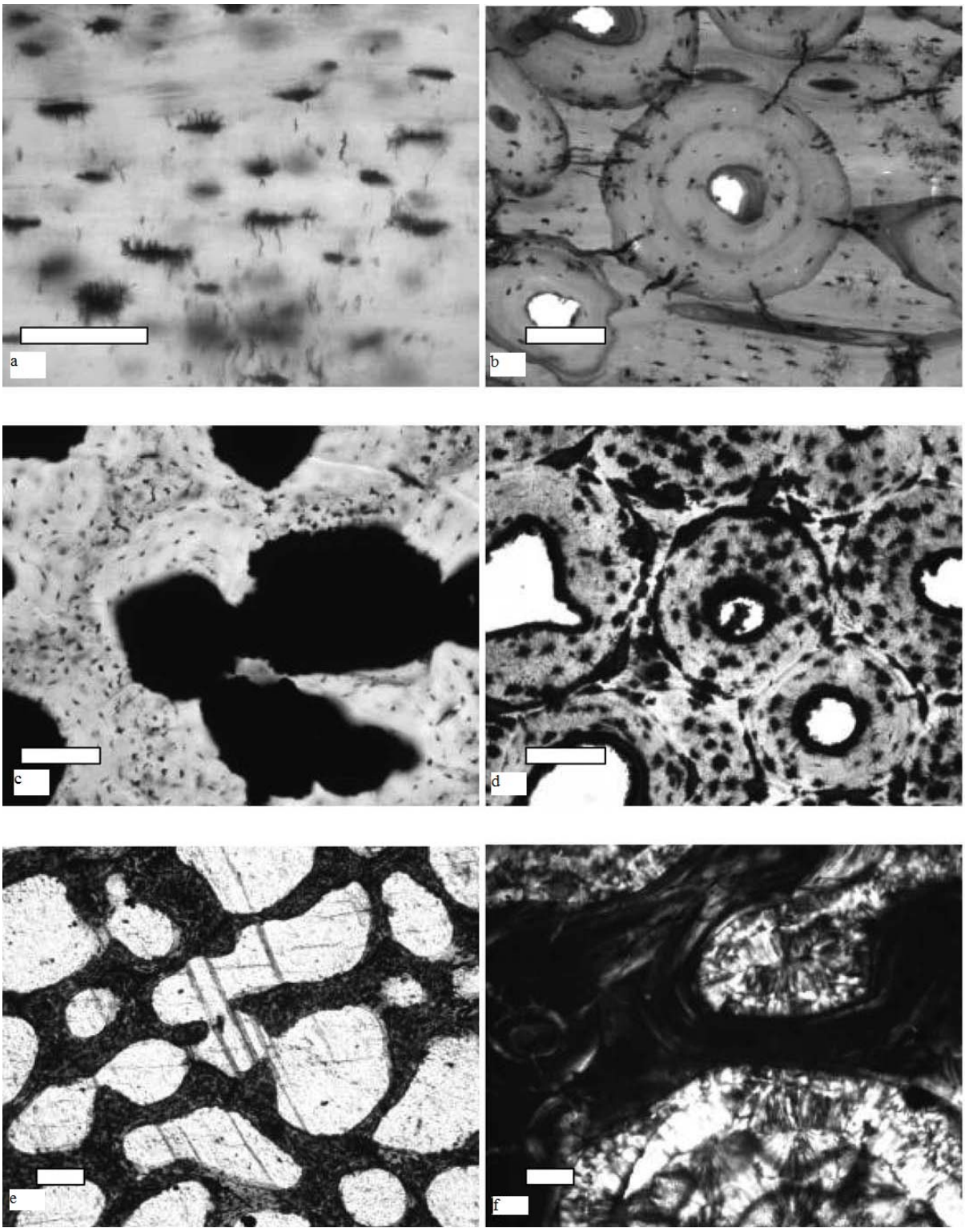

Figure 2.1. (a) Early diagenetic pyrite formation through sulphide precipitation in bone osteocyte lacunae in a Pleistocene *Equus* metatarsal, Rhine gravel. Scale bar: 50 µm. (b) Radial microcracks on a *Camarasaurus* longbone. Scale bar: 100 µm. (c) Late diagenetic pyrite formation through pH-dependent precipitation, demonstrating

extensive replacement of bone matrix by pyrite. Scale bar 100 μm. (d) Hematite fillings formed by pH-dependent precipitation of ferrous hydroxide and transformation into hematite. Extensive replacement of bone matrix by hematite in a *Barosaurus* tibia, Tendaguru Formation, Africa. Scale bar: 100 μm. (e) Late diagenetic calcite formation in the porosities of trabecular bone in a *Stenopterygius* vertebra, Posidonian shale, Dotternhausen, Germany. Scale bar: 100 μm. (f) Late diagenetic silica filling of the porosities of trabecular bone. No replacement of the bone matrix by silica. Dinosaur indet. Morrison Formation, Utah. Scale bar: 100 μm. After Pfretzschner (2004).

Consequently, when mobile metal ions in aqueous soil/sediment solutions from the burial environment come into contact with the fossil bone surface, or enter it by diffusion or any other mechanism, they will meet high pH conditions and precipitate as hydroxides (Pfretzschner, 2004):

$$M^{n+} + nOH^- \rightarrow M(OH)_n \qquad (2.14)$$

As illustrated by the equation (2.14) above, these precipitation reactions are characterized by reduction in pH following the consumption of OH^- ions and, according to LeChartelier's Principle, a small amount of apatite will dissolve and the phosphate buffers again the pH to its original high equilibrium value, as illustrated by equation (1.1).

Besides hydroxides, sulphides and oxides, carbonates can also be precipitated through raised pH (Figure 2.1e). Below are examples of pH-dependent mineral precipitation occurring in the fossil bone at high pH:

(i) Ferrous iron can be precipitated from aqueous solution of its more soluble compounds such as iron (11) sulphate as $Fe(OH)_2$.

$$FeSO_4 + 2\ OH^- \rightarrow Fe(OH)_2 + SO_4^{2-} \qquad (2.15)$$

Ferrous hydroxide can later be transformed to hematite, Fe_2O_3 or goethite FeOOH through some oxidation processes (as illustrated in Figure 2.1d).

(ii) Likewise manganese oxides such as pyrolusite, MnO_2 are initially precipitated as hydroxides, $Mn(OH)_2$ which is then transformed by loss of water into MnO and later into pyrolusite MnO_2 (Pfretzschner, 2004) and hausmannite, Mn_3O_4 (John, 1981):

$$3\ Mn^{2+} + 0.5\ O_{2(aq)} + 6\ OH^- \rightarrow Mn_3O_4 + 3\ H_2O \qquad (2.16)$$

Alternatively, hausmannite can be precipitated in the bone under highly oxidizing conditions (Hem and Lind, 1983):

$$3\ Mn^{2+} + 4\ H_2O \leftrightarrow Mn_3O_{4(s)} + 8\ H^+ + 2e^- \qquad (2.17)$$

(iii) Carbonates e.g. calcite $CaCO_3$, $FeCO_3$, $BaCO_3$

(iv) Sulphates e.g. $BaSO_4$, $CaSO_4$

(v) Sulphides e.g. FeS, ZnS

Pyrite is first precipitated as iron sulphide, FeS, and then later transformed to pyrite FeS_2

$$Fe^{2+} + H_2S \rightarrow FeS + 2\ H^+ \qquad (2.18)$$

The precipitation of certain minerals, for instance pyrite and silica, does not damage the bone, but instead simply fills up the cavities in the bone wall, and the resulting pyrite and silica usually forms precise casts of the histological structures (Figure 2.1a and 2.1f respectively) (Pfretzschner, 2004). Pyrite formation on the bone surface is mainly dependent upon the availability of sulphide (Canfield *et al*., 1992; Raiswell and Berner, 1985) and on the Eh/pH conditions caused by decay of organic matter, as iron is usually available in excess in the natural environment (Pfretzschner, 2004). Whereas pyrite precipitation within the bone is iron-controlled, because decaying

protein releases a lot of sulphide, and access of iron into the bone is limited by low diffusion constants. As time progresses sulphide production ceases, leaving behind virtually no free sulphide and with the development of diagenetic cracks (which allows entry of more iron), pyrite formation may be sulphide-controlled. In the event that bone is buried under seawater, reduction of additional sulphate (SO_4^{2-}) to sulphide (S^{2-}) rapidly occurs due to the high natural concentration of sulphate ($C_{sulphate}$ = 2.65 g kg^{-1}sea water). Hence pyrite in fossil bones from marine deposits is a common feature, with these bones containing considerably higher amounts of pyrite as compared to those found in bones from cave or terrestrial sediments. In such environments sulphide supply is higher relative to the amount of iron present, and pyrite precipitation is often iron-controlled (Pfretzschner, 2004).

Krumbein and Garrels (1952) point out that "far more common in the fossil record is the nearly concurrent precipitation of pyrite and calcite", which is confirmed by a study done by Wings (2004) (Figure2.2a and 2.2b). In this work, Wings used the following techniques; petrographic microscopy, X-ray diffractometry and scanning electron microscopy –energy dispersion spectrometry to study cavity infills of fossilized vertebrate bone and the distribution of minerals in these bone voids. Carbonates, sulphides, oxides, and sulphite-containing minerals (including calcite and pyrite among others) were identified as the most abundant void fillers in this study, as illustrated in Figure 2.2a and 2.2b.

The simultaneous appearance and occurrence of calcite and pyrite in the samples reflect the presence of the ions of both minerals in the pore fluids and that they are being precipitated interchangeably (Wings, 2004). Figures 2.1a to 2.1f show mineral precipitation both on the bone surface and within the bone occurring at different stages during bone diagenesis. Silica mineral often fills the fossil Haversian canals, cracks and intertrabecular cavities of the bone (Hubert *et al*., 1996) as shown in (Fig. 2.1f).

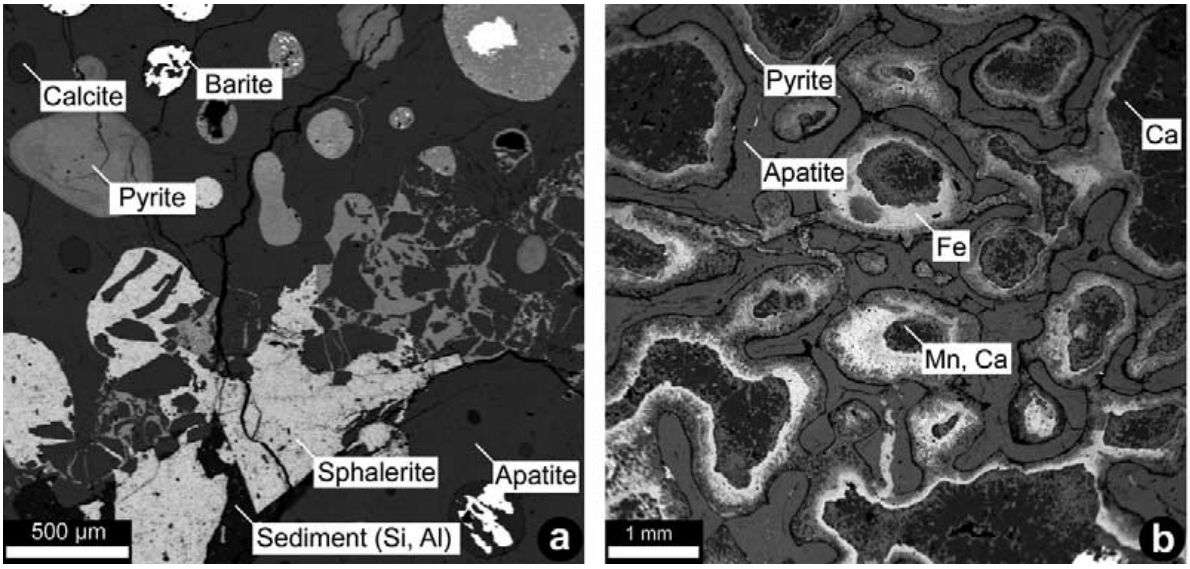

Figure 2.2. (a) BSE-image of a Lyme Regis thin section of a bone sample showing four authigenic minerals in voids and brecciated bone. (b) BSE-image of an Isle of Wight thin section of a bone sample showing close interactions between precipitated minerals. The minerals siderite (Fe), calcite (Ca), and kutnohorite (Mn, Ca) feature a gradual transition. Note that the kutnohorite is a later infill, predated by siderite. After Wings (2004).

Since the silicification process of is not pH-dependent, but associated with recrystallization of the silica (Landmesser, 1994), this process has a tendency of preserving, rather than destroying, bone histological structure. Transformation of the already precipitated minerals in bones can occur via oxidation reactions. One such a transformation is the oxidation of pyrite, which formed earlier, during diagenesis into hematite (Pfretzschner, 2001):

$$2\ FeS_2 + 7.5\ O_2 + 7\ H_2O \rightarrow 2\ Fe(OH)_3 + 4\ H_2SO_4 \qquad (2.19)$$

Contrary to the silicification process, oxidation of pyrite on and/or within the bone affects the bone negatively by promoting secondary replacement of apatite by iron oxides, since oxidation of pyrite produces sulphuric acid that will etch or dissolve the bone matrix (Pfretzschner, 2004).

2.5. Chemistry of different forms of minerals commonly found in fossil bones, in varying environmental conditions.

After iron, manganese is the second most abundant transition metal in the earth's crust. Generally, the cycling and movement of elements (e.g. iron and manganese) in natural systems depend upon their redox chemistries, and the ever-present distribution of ferromanganese in different environments, including a range of soil types, desert conditions, marine and fresh water, including stream bed deposits, as reported by Sung and Morgan (1981). Thus iron and manganese often occur together in nature as ferromanganese compounds, and ferrous iron oxygenation occurs rapidly under natural conditions. Because of the above mentioned facts, in this project the chemistry, availability and occurrence of metal ions in the environment is focused mostly on iron and manganese, and to a lesser extent other elements. Jenne (1968) postulated that the surfaces of iron and manganese oxide and hydroxide act as sinks and sources of other trace metals. For instance the study done by Sung and Morgan (1981) has shown that adsorption of Mn(II) on γ-FeOOH (lepidocrocite), a ferric oxyhydroxide formed by oxidation of ferrous iron in solution, is significant at higher pH (pH>7) and is an approximately linear function of pH over the pH range of 8-9.5 as illustrated in Figure 2.3. Several studies on the adsorption of trace metals on iron hydroxide and oxide surface have been conducted. Forbes *et al*. (1976) reported that the affinities of metal ions for α-FeOOH in 0.075M $NaNO_3$ increase in the order Cd< Co< Zn < Pb< Cu. A similar trend was observed by Grimme (1968) for α-FeOOH in 0.1M KNO_3 with the order Mn< Co< Zn< Cu. Similar reactions as such are also prevalent in the natural environment under similar conditions. A typical Mn(II) adsorption on γ-FeOOH equation can be expressed as (Sung and Morgan, 1981):

$$\equiv FeOH + Mn^{2+} \leftrightarrow \equiv FeOMn^{+} + H^{+} \qquad (2.20)$$

Where ≡FeOH is a schematic representation of surface site.

It must be noted that several possibilities in the adsorption of Mn(II) species on the γ-FeOOH surfaces are widespread in the environment:

$$Mn^{2+} + 2 \equiv FeOH \leftrightarrow (\equiv FeO)_2Mn + 2H^+ \quad (2.21)$$

$$MnCl^+ + \equiv FeOH \leftrightarrow \equiv FeOHMnCl + H^+ \quad (2.22)$$

Therefore the presence of iron oxide and/or hydroxide minerals within or on the surface of the fossil bone may result in adsorption of trace elements from the burial environment as described above, leading to elemental enrichment (contamination) in the fossil bone.

Mineral dissolution plays a pivotal role in a variety of natural processes, including among others weathering of minerals and rocks, the availability of elements in the environment, and heavy metal release in natural and waste water (Garc`ia- San`chez and A` lvarez-Ayuso, 2002; El-Korashy, 2003). The study of mineral–water interactions (i.e. dissolution – precipitation equilibrium reactions) and the rates of mineral weathering, are therefore of great interest to numerous fields (Ruiz-Agudo *et al*., 2009), including research on diagenesis processes. A study done by Dongarrà *et al*. (2009) on the geochemistry of water circulating in the mineralised area of north-eastern Sicily, Italy, has shown that water chemistry in that area is mainly dominated by dissolution of carbonates and hydrolysis of aluminosilicate minerals. These dissolved carbonates occur in the environment predominantly as HCO_3^- due to pH range.

Their results indicated that weathering of more soluble minerals (i.e. carbonates) and less soluble minerals (e.g. aluminosilicate) increases the water salinity together with the concentrations of Ca^{2+}, HCO_3^- and SO_4^{2-} with respect to Na^+ and Cl^-.

The solubility of calcite and dolomite is largely controlled by CO_2 fugacity and pH, expressed by the following equations (Dongarrà *et al*., 2009):

$$CaCO_3 + H_2O + CO_{2(g)} \leftrightarrow Ca^{2+} + 2\ HCO_3^- \quad (2.23)$$

$$(Ca_{1-x}Mg_x)CO_3 + CO_{2(g)} + H_2O \leftrightarrow (1-x)\ Ca^{2+} + x\ Mg^{2+} + 2\ HCO_3^- \quad (2.24)$$

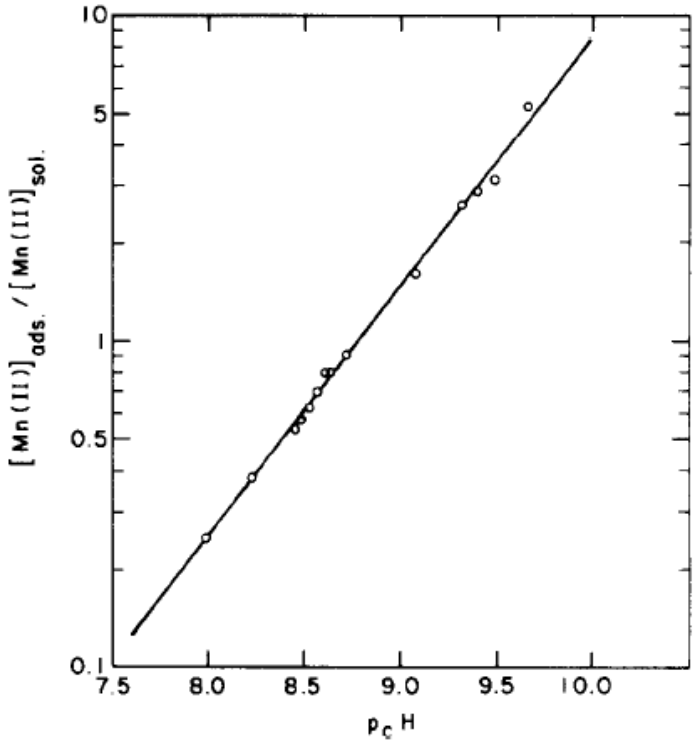

Figure 2.3. Adsorption of Mn(II) on γ-FeOOH as a function of pH.10-3M Fe(III) as γ-FeOOH, 0.7M NaCl at 25°C. After Sung and Morgan (1981).

Sodium can also be released into the environment through dissolution of Na-feldspar mineral or exchange with clay minerals according to the reaction equations below (Dongarrà *et al*., 2009):

$$2\ NaAlSi_3O_8 + 2\ CO_2 + 3\ H_2O \rightarrow Al_2Si_2O_5(OH)_4 + 2\ Na^+ + 4\ SiO_2 + 2\ HCO_3^- \quad (2.25)$$

$$(Ca, Mg)^{2+} + 2\ Na_{ex} \rightarrow (Ca, Mg)_{ex} + 2\ Na^+ \quad (2.26)$$

The solubilities of the iron (III) minerals $Fe_2O_{3(s)}$, $Fe(OH)_{(s)}$ and $FeOOH_{(s)}$ as a function of pH are given by (Millero *et al*.,1995):

$$Fe_2O_{3(s)} + 6\ H^+ \rightarrow 2\ Fe^{3+} + 3\ H_2O \quad (2.27)$$

$$Fe(OH)_{3(s)} + 3\ H^+ \rightarrow Fe^{3+} + 3\ H_2O \quad (2.28)$$

$$FeOOH_{(s)} + 3\ H^+ \rightarrow Fe^{3+} + 2\ H_2O \qquad (2.29)$$

Following multi-step complex calculations the equilibrium solubility of [Fe(III)] for the various minerals can be determined for any natural water using:

$$[Fe(III)] = \{KFe_2O_3\boldsymbol{\gamma}H^6[H^+]^6/(\boldsymbol{\alpha}Fe^2\boldsymbol{\alpha}H_2O^3\boldsymbol{\gamma}Fe^2)\}^{0.5} \qquad (2.30)$$

$$[Fe(III)] = KFe(OH)_3\boldsymbol{\gamma}H^3[H^+]^3/ (\boldsymbol{\alpha}Fe\boldsymbol{\alpha}H_2O^3\boldsymbol{\gamma}Fe) \qquad (2.31)$$

$$[Fe(III)] = KFeO(OH)\boldsymbol{\gamma}H^3[H^+]/ (\boldsymbol{\alpha}_{Fe}\boldsymbol{\alpha}H_2O^2\boldsymbol{\gamma}Fe) \qquad (2.32)$$

Where **α** is the activity and **γ** is the activity coefficient.

The solubilities of hydrous ferric oxide ($Fe(OH)_{3(s)}$), goethite ($FeOOH_{(s)}$), and hematite ($Fe_2O_{3(s)}$) as a function of pH are shown in Figure 2.4

Alternatively a thermodynamic approach can be used to estimate the solubility product (K) for a given mineral as illustrated below (Marion *et al.*, 2009):

$$Al(OH)_3(cr) + 3\ H^+ \leftrightarrow Al^{3+} + 3\ H_2O \qquad (2.33)$$

And

$$K = \frac{(\boldsymbol{\alpha}_{Al}{}^{3+})(\boldsymbol{\alpha}_w)^3}{(\boldsymbol{\alpha}_{H}{}^{+})^3} = \frac{(\boldsymbol{\gamma}_{Al}{}^{3+})(\mathbf{m}_{Al}{}^{3+})(\boldsymbol{\alpha}_w)^3}{(\boldsymbol{\gamma}_{H}{}^{+})(\mathbf{m}_{H}{}^{+})^3} \qquad (2.34)$$

Where α is the activity of the subscripted component, γ is the activity coefficient, and m is the molality [mol $kg(H_2O)^{-1}$]. Given experimental measurements of the molalities (m) and an equilibrium model that can calculate γ and the activity of water, α_w, one can directly estimate the value of K using equation (2.34).

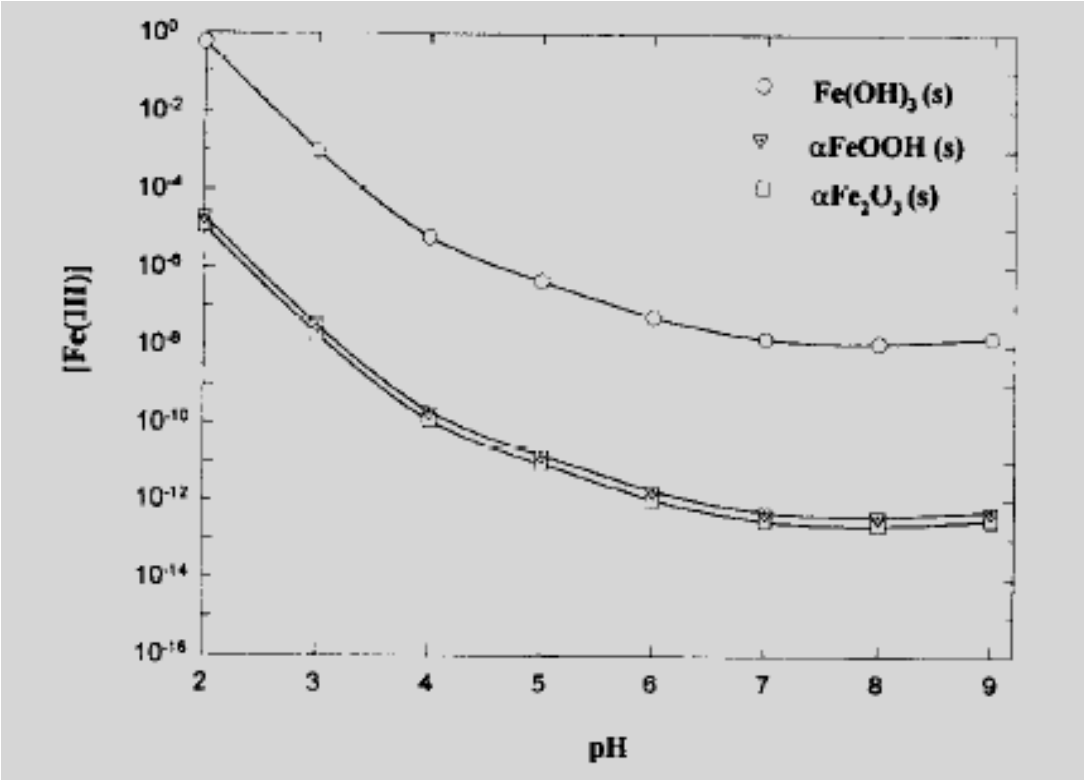

Figure 2.4. The solubility of Fe(III) minerals in seawater as a function of pH (after Millero *et al*., 1995).

The liberation of Si and Al into the environment occurs when primary aluminosilicate rock minerals are attacked by acid, either H_2CO_3, from dissolution of atmospheric CO_2 or H_2SO_4 , from oxidation of sulphides (Dongarrà *et al*., 2009):

$$NaAlSi_3O_8 + H^+ + 7\ H_2O \leftrightarrow 3\ H_4SiO_4 + Al(OH)_3 + Na^+ \qquad (2.35)$$

$$CaAl_2Si_2O_8 + 2\ H^+ + 6\ H_2O \leftrightarrow Ca^{2+} + 2\ H_4SiO_4 + 2\ Al(OH)_3 \qquad (2.36)$$

$$KAlSi_3O_8 + H^+ + 7\ H_2O \leftrightarrow 3\ H_4SiO_4 + Al(OH)_3 + K^+ \qquad (2.37)$$

The liberation of other metal ions commonly found in the natural environment, from their mineral containing rocks, basically follows the same dissolution mechanism as described above. Generally the lower the pH (acidic conditions) the higher the rate of

mineral dissolution and the higher the solubility, mobility and availability of trace metals in the burial environment. Hence the higher the rate of exchange reactions between the bone and its surroundings. Table 2.1 is a summary of the potential modes of element occurrence, potential mechanism and parameters controlling the mobility of various types of elements, and compounds in the natural environment based on the sequential chemical extraction (SCE) results.

Table. 2.1. The potential modes of occurrence and leach behaviour on the basis of SCE test results after (Broadhurst *et al*., 2007).

Fraction	Potential mode of element occurrence	Potential mechanism and parameters controlling element mobility
Water soluble	Present as highly reactive and liberated salts	Mobility will be instantaneous or rapid and will be dependant only on the concentration in this fraction
Exchangeable components	Weakly adsorbed onto clay minerals, iron and magnesium oxides/hydroxides, organic matter and other colloids.	The mobilisation of exchangeable components from solid will most likely occur as a result of rapid ion-exchange reactions, and will be dependant on the soluble salt concentrations and pH
Carbonate bound and/or specifically adsorbed components	Present as or occluded in carbonates and/or chemically adsorbed onto surfaces of simple and complex oxides of iron, manganese and aluminium compounds (simple and complex oxides).	Mobility is likely to be controlled by the rate and extent of carbonate and oxide dissolution/precipitation or by surface adsorption reactions, and will be dependant on pH.
Fe/Mn oxide bound	Present as or occluded in manganese and iron oxides	Mobility is likely to be controlled by rate and extent of Fe and Mn oxide dissolution/precipitation, and will be largely dependant on pH and Eh
Sulphide bound	Present as or occluded within organic matter and/or sulphide minerals	Mobility will be governed by the rate of organic matter/sulphide mineral oxidation, which will be largely controlled by oxygen diffusion
Residual	Present as or occluded in stable primary mineral phases	Element phases are likely to either be inert, or mobilised at extremely slow rates under most disposal conditions

Thus the chemical mobility of solid mineral and soil constituents in the environment, including where the bones are buried, will be determined in the first place by the stability or reactivity of the primary mineral and soil phases as a function of environmental conditions within the deposit, primarily redox potential, oxygen concentrations, microbial activity and pH, and secondly by the extent of attenuation or

reduction of the solubilised constituents via precipitation/dissolution and adsorption/desorption reactions. Usually these attenuation reaction mechanisms are known to be rapid, fully reversible equilibrium-controlled reactions, which are dependant on a number of parameters, such as constituent activity, redox potential, the nature and concentration of major soluble ions, exchangeable ions, and pH (Broadhurst *et al*., 2007). These processes results in the alteration of the fossil bone following the enrichment and/or leaching of elements or minerals through precipitation/dissolution and adsorption/desorption reactions. In some cases, the rates of withering or alteration of the primary phases vary considerably, ranging from rapid equilibrium-controlled reactions, leading to a short-period of mobilisation of associated elements, to slow kinetically-controlled reactions, which result in a long-term, significant mobilisation of associated elements in the medium (both the burial environment and the fossil bone) (Brown *et al*., 2000). Brown *et al*. (2000) state that "In some cases the weathering reactions may be so slow that they do not result in any significant mobilisation of elements within the time frame of consideration and can therefore be discounted".

2.6. Redox chemistry of Mn and Fe: the most common bone staining/coating minerals in the geochemical environment

Most metals and metalloids in soil-water systems have the potential to change oxidation states. For instance iron and manganese can be present in soil and in water as iron (II) (Fe^{2+}) or elemental iron (III) (Fe^{3+}) and manganese (II) Mn^{2+}, manganese (III) Mn^{3+}, or manganese (IV) Mn^{4+} respectively. In oxidized soil-water systems, the environment is considered electron deficient, and the higher oxidation states of iron or manganese (i.e. Fe^{3+}, Mn^{3+}, or Mn^{4+}) are most stable (Evangelou, 1998). Under such conditions iron and manganese occur as insoluble oxyhydrooxides and oxides. In reduced soil-water systems, the environment is considered electron-rich and the lowest oxidation states of iron and manganese (i.e. Mn^{2+} of Fe^{2+}) are most stable (Evangelou, 1998). Thus the chemistry of manganese is related to that of iron. One of the most apparent similarities is the high solubility of the reduced species Mn^{2+} and

Fe^{2+} in comparison to the oxidized species $Mn^{3+/}Mn^{4+}$ and Fe^{3+}, which tend to precipitate as oxides, hydroxide and oxyhydrooxide minerals (Sposito, 1989).

Usually, soil-water systems vary in Eh from roughly 800 mV under well-oxidized conditions to about -500 mV under strongly reducing conditions as shown in Table 2.2.

Table 2.2. Range of Eh measurements of soil-water systems (after Evangelou, 1998)

Very well-oxidized soil	800 mV
Well-oxidized soil	500 mV
Poorly-oxidized soil	100 mV
Much-reduced soil	-200 mV
Extremely- reduced soil	-500 mV

Under relatively intermediate reduced environments, often sulphur would be present in the sulphate form (SO_4) and its potential to precipitate Fe^{2+} as $FeSO_4$ would be limited due to the high K_{sp} of ferrous sulphate. Whereas in strongly reduced environments, sulphur would be reduced to S^{2-} and FeS, a highly insoluble mineral, will be precipitated (Evangelou, 1998). Hence FeS-mineral precipitation and deposition within and/or on surfaces of fossil bones occur more rapidly where the fossil is buried in a strongly reduced environment.

Therefore, oxidation-reduction (redox) processes in nature control the behaviour and availability of elements or substances in different forms. Figure 2.5(a) shows a stability field diagram of the pe-pH range in the soils with oxic-anoxic systems. In nature redox couples may also involve solution and solid phases, for example, Fe^{2+},$Fe(II)(OH)_3$; Mn^{2+}, $Mn(III)(OOH)_3$; $Fe(II)CO_3$, (Evangelou, 1998). From Figure 2.5b, it can be shown that the insoluble Fe^{3+}-oxide phases are thermodynamically favoured over the pH-range of 5-8 in soils under oxic conditions, (i.e. in the presence

of oxygen), while the reduction of Fe^{3+} to soluble Fe^{2+} occurs under suboxic or anoxic conditions. On the other hand Figure 2.5c shows that the insoluble Mn-oxide minerals are stable only at the highest pe's and pH's, whereas soluble Mn^{2+} is thermodynamically stable even under oxic conditions.

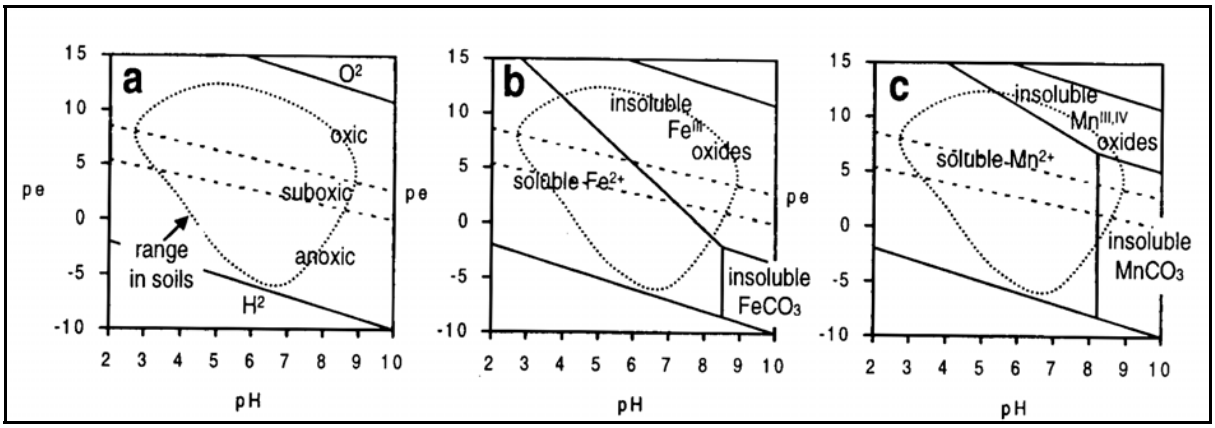

Figure 2.5. (a). Stability diagram showing pe-pH range in soils with oxic and anoxic systems, (b). Stability field (pe-pH) diagram showing the soluble and insoluble Fe forms (c) pe – pH diagram with manganese (Sposito, 1989). Most of the metals follow the same trends under the same geochemical conditions.

Figure 2.6 illustrates typical reaction mechanisms occurring both inside and on fossil bone surfaces.

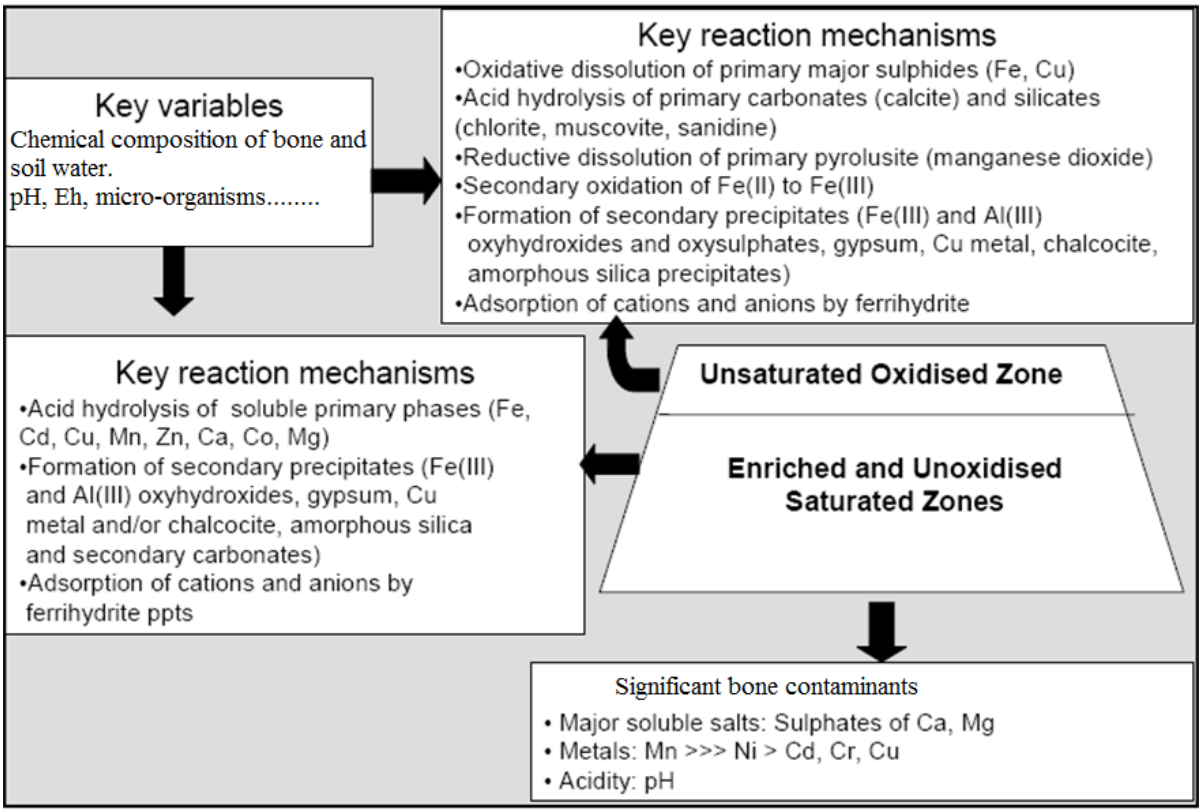

Figure 2.6. Typical processes occurring in the environment as well as fossil bone (modified from Broadhurst *et al*., 2007).

2.7 Effects of diagenesis on the chemical composition of bones

Quantification of diagenetic alteration of fossil bones is accomplished by assessment of the structural, chemical and physical differences between the diagenetic parameters of the fossil and the modern bone standard. A higher degree of diagenetic alteration is normally associated with reduced amounts of collagen, increased porosity and crystallinity. Increased crystallinity is a result of the transformation of the bioapatite into a more thermodynamically stable apatite (Smith *et al*., 2005). The process of bone diagenesis can be fully explained analytically by considering all diagenetic parameters. Hence measurements of the diagenetic paremeters such as crystallinity, microporosity, macroporosity, nitrogen (%N), carbonate (C/P) and calcite content (%calcite), as well as histological integrity (morphology) can give adequate chemical, structural and microscopic information for the quantification of the post-mortem

alteration of the bone (Gutierrez, 2001). Several methods, which include among others scanning electron microscope (SEM) (coupled with various kinds of detectors), inductively coupled plasma atomic emission spectroscopy (ICP-AES), inductively coupled plasma mass spectroscopy, particle induced X-ray emission (PIXE), particle induced gamma-ray emission (PIGE), X-ray diffraction (XRD), Fourier transform infrared spectroscopy (FT-IR), and X-ray fluorescence (XRF) can be employed to achieve characterization of both modern and fossil bones. ICP-AES, ICP-MS, PIXE, PIGE, CHNS, XRF-mapping and other elemental analysis methods can be applied to qualitatively and quantitatively determine the specimen's post-mortem alterations: elemental loss, contamination and/or enrichment (at ultra-trace levels) and examine the elemental distribution across bone transverse sections. SEM, XRD, RT-IR, and porosity and density measurement techniques provide the topographic image of the sample and information about the local and global crystallinity of bone apatite, the precipitation of foreign minerals in the bone matrix and the presence of preserved collagen (Reiche *et al*., 2003). The combination of all these different analytical methods can be employed in the laboratory to provide essential information on bone diagenesis. In the following section attention shall be given to elemental, crystallographic and morphological studies conducted.

Elemental post-mortem changes in fossil are of great significance to the study of diagenesis, a process that alters the original composition of the bone following its burial, through events such as leaching, decomposition and exposure to groundwater, which ultimately result in enrichment, depletion and/or substitution of the original elements in the bone. The development of highly sensitive, accurate and improved analytical techniques for elemental (skeletal tissue) analysis has lead to the diversification of bone chemistry studies and the identification of a variety of elements and isotopes in bone as indicators of past conditions (Price *et al*., 1985). Reiche *et al*. (2003) used scanning electron microscopy coupled with energy dispersive X-ray analysis (SEM-EDX), particle-induced X-ray emission and particle–induced gamma for elemental determination on fossil and modern unaltered sheep bones. They observed relatively higher concentrations of exogenous elements like F, S and Sr and a depletion of light elements like Na, Mg and Cl in fossil bones compared to modern bones. Elements like Mn, Fe, Al, Si, Ba and Cu were present only in fossil bones and not in the modern bone with manganese and iron having the

highest concentrations, thus the fossil bones were enriched in Mn, Fe, Al, Si, Ba, Sr, S, F and Cu and depleted in Na, Mg and Cl most probably through leaching process. They also studied the morphology and mineral inclusions in the samples using SEM-EDX and XRD and they detected the presence of pyrite (FeS_2) precipitates together with some sulphur and barium-bearing precipitates in fossil/archaeological bone. From the XRD patterns all bones, modern and fossil, contained mainly hydroxylapatite, with the fossil bone revealing more crystalline apatite and the presence of quartz and calcite. A significant increase in porosity (2.5 times) in fossil compared to modern bone was also observed. This has lead to mass elemental enrichment of the buried bone by chemical species which are abundant in the soil constituents (such as clays, oxides, sulphates, carbonates) containing Si, Al, S, Sr, Mn, Fe, Cu. In a separate study, Goodwin *et al*. (2007) used PIXE analysis to identify and map the elemental composition of dinosaur bone bioapatite at ppm sensitivity and submicron-scale spatial resolution. The elemental maps allowed them to identify local patterns of enrichment and depletion within micron-scale regions of fossil bone that are ordinarily lost in alternative bulk analyses. As in most related studies, (e.g. Bocherens *et al*., 1994; Schoeninger *et al*., 1989; Lambert *et al*., 1985; Denys *et al*., 1996; Greenlee, 1996; Kohn *et al*., 1999; Reiche *et al*., 1999; 2003) iron and manganese concentrations were found to be very high in fossil bones as compared to modern bones. Their results also indicate As enrichment in the fossil bone, and they concluded that "elevated As levels in the dinosaur bone bioapatite is likely a result of adsorption, porosity change, recrystallization on the crystallite surface area, and/or ionic substitution". Reiche *et al*. (1999) used PIXE and PIGE to determine the elemental composition of archaeological bones (approximately 6000 years old) and post mortem alteration in the burial environment. Modern sheep and horse bones were subjected to the same analyses under the same conditions as reference standards for comparison. Al, Si, Mn, Fe, and Cu were found to be present only in the archaeological sample and not in the modern bones. The concentrations of iron and sulphur for archaeological samples show a tendency for surface enrichments, with both elements also penetrating deeply to the centre of the bone core. Schoeninger *et al*. (1989) used X-ray diffractometry and thin sections to assess the preservation of biogenic bone mineral and histological structure in archaeological and fossil samples. They used XRD on un-ashed, powdered bone samples to check for any alteration in

the crystallinity of the bone mineral. Their results displayed that all buried bones analysed appeared to be altered to some extent, with those samples indicating lack of histological structure also showing X-ray patterns which deviated markedly from that of fresh bones. Besides XRD and thin section, Schoeninger *et al*. (1989) also used present results of amino acid analysis of gelatin by extraction of the organic component of the bone by demineralization of bone samples in weak acid (1% HCl). The results showed patterns of amino acid composition similar to collagen. This is an indication that even though the archaeological and fossil bones were altered, they managed to retain to some extent their original biological signatures (i.e. collagen in this case). Conclusions of the degree to which diagenetic alteration has occurred in a bone cannot be drawn from a single diagenetic parameter measurement. However, a combination of these parameters can give adequate information to address the 'real' extent of diagenetic alteration of a given specimen. In a study carried out by Hedges *et al*. (1995), the relationship among only four diagenetic parameters were considered; histological preservation, protein content, crystallinity and porosity, to represent the state of diagenesis of bone buried on archaeological sites. The data obtained show that diagenetic change in most bone samples involved a shift in pore size distribution and an overall increase in porosity in a quite defined way. Increase in porosity is a result of dissolution of bone micro-crystallite and histological destruction by microbes such as bacteria and fungi. Their results indicated less correlation between the measured diagenetic parameters than (they) expected and they concluded that that "the processes by which protein is lost, by which micro-morphology is destroyed, and by which the bone mineral is restructured, might operate at different timescales".

2.8. Burned bones versus mineral coated bones

The recognition of burning in modern bones is not that complicated, since the blackening caused by char is easily identified with the naked eye. Contrary to this, use of a visual approach is unsatisfactory for fossils, because they may be blackened due to the incorporation of diagenetic metals, mainly oxides of iron and manganese (Sillen and Hoering, 1993). Burning of modern bones can be recognized by alterations in

their colour, crystallinity, shape and the presence of a black char with characteristic chemical properties. Black is the most easily identified colour indicative of burning, due to the carbonization of the bone's organic matrix (Gross *et al*., 1997). The establishment of the precise and/or rather the exact temperature to which a bone has been heated is difficult due to the fact that prolonged heating (for example at 300^{o}C), may yield the same effect as a short interval of heating at a much elevated temperature. Several studies have indicated that at about 300^{o}C, a fresh bone undergoes carbonization of its collagen and other organic components, resulting in the specimen turning a black colour. The carbonization process proceeds as follows: subjecting the bone specimen to prolonged subsequent heating results in oxidation of this carbon, which will then in turn escape as carbon dioxide, leaving behind only the mineral component of the bone, the hydroxyapatite. In this form the bone is referred to as being calcined. It is complicated, however, to tell whether a white, calcined bone had lost its carbon rapidly at a high temperature, or more slowly during prolonged heating at low temperature (Brain, 1993). At temperatures of about 350°C to 500°C, fire visibly alters and damages flint, as evidenced by typical macrofracture deformations such as pot lids, shrinkage, fractures, and cracks. These damage patterns give a clear distinction between the burned and unburned flint items without the aid of a microscope (Goren-Inbar *et al*., 2004). In a study carried out by Stiner *et al*., (1995) in which they compared both experimentally burned modern bones and fossil burned bones, they compared changes in mineralogy and the organic matrix components due to both burning and diagenesis. They concluded that HCl-insoluble fraction technique together with macroscopic changes in internal bone, more reliably diagnose burning damage on archaeological bones. Sillen & Hoering (1993) characterized the composition of char (the organic insoluble fraction) using CHNS microanalysis, analytical pyrolysis, gas chromatography/mass spectrometry (GC/MS) and high performance liquid chromatography (HPLC), and they concluded that the bones were not stained but burned. In a related study, Person *et al*. (1996) investigated the effects of heating fresh powdered cortical cow bones at different temperature with the main focus being on colour changes, remaining weight, crystallinity index, and carbon and nitrogen percentage. Following these experiments, they observed that the cream-coloured powder of fresh bone turned black after one hour of heating at 300^{o}C. The colour progressively became lighter, beige, and grey with increasing temperatures

from 400°C to 600°C. Finally, the sample turned white and chalky following heating at temperatures above 625°C. At 300°C, the X-ray diffractogram of the bone was found to be identical to that of fresh bone. Another interesting observation was that of a clear and progressive increase in splitting of the peaks of carbonate hydroxylapatite with increase in temperatures, "generally, peaks tend to become sharper with increasing temperature in the other regions of the X-ray profiles" (Person *et al*., 1996).

Using X-ray diffraction, Infra-red spectroscopy and the HCl-insoluble fraction extract techniques; we can differentiate between the three most common causes for black-coloured fossil bones: bones that are burned, bones that are stained, and bones that are both burned and stained (Gross *et al*., 1997). Whereas, gross microscopic surface characteristics such as colour, cracking and warping, and degree of calcination, are typical specimen properties that can be manipulated to characterize the degree of their exposure to a heat source or lack thereof (Taylor *et al*., 1995).

In a related study, Stiner *et al*. (1995) explored the relationship between imported factors aiding in the interpretation of burning damage caused on the bones, which includes among other factors, visible changes in bone colour, changes in bone mineral and matrix, and alterations in the mechanical properties of the bone that promote fragmentation. A number of research projects have been carried out using fire experiments involving practical heating of modern bones at a range of given temperatures to investigate the effects of burning on bones and to try to establish possible temperatures to which fossil bones found in caves were exposed. Shipman *et al*. (1984) conducted a series of experiments involving the effects of burning sheep or goat remains under controlled conditions. They assessed changes in: shrinkage, crystal structure, colour and microscopic morphology induced by heating on natural surfaces of bones and teeth, with the aim of deducing past events involved in heated or burned skeletal material. Their results on colour changes agreed with those of other authors that bones pass through a range of colours from normal bone colour (unburned), to dark brown (for non-incinerated bones) to a black colour (for incompletely incinerated bone), and finally to white (for completely incinerated or calcined bones) with increased heating temperature. For crystal structure, results from X-ray diffraction show a gradual increase in hydroxylapatite crystal size with increase

in temperature. This size increased was indicated by increase in sharpening and narrowing of peaks with increase in temperature. There was a gradual change in sample morphology from normal state at low temperatures below 185^{o}C, to increased surface roughness (185-<285), to a glassy and smooth surfaces (285-<440^{o}C), to a frothy or fleecy appearance (400-<800^{o}C), and these frothy protuberances coalesce into smooth-surfaced globules or nodules (800-<940^{o}C) (Shipman *et al*., 1984). A related study carried out by Stathopoulou *et al*. (2005) on the origin of black colour of skeletal remains from the fossilisiferous site of Aghia Napa in Cyprus has shown that the colouration was certainly a result of staining with oxides of Fe and Mn. They also observed no proof of change in the microstructure of the bone apatite due to high temperatures and no remains of fire in the excavation. Several techniques, which include among others Optical microscopy, Scanning Electron Microscopy (SEM), X-Ray Diffraction (XRD), and Infrared Spectroscopy (FTIR) were employed during their investigation.

2.8.1 Magnetic and archaeomagnetic dating

The recognition of indisputable evidence of human–controlled fire is extremely challenging in archaeological contexts where obvious remains, such as charcoal fragments, as well as burned bones, shells and ash, have not been preserved (Bellomo, 1993). The best evidence for the use of fire is the occurrence of well conserved hearths. These well preserved hearths are often found in a round or oval shape with an upper layer composed of light coloured minerals, a lower layer loaded with charcoal and a substrate of reddened sediment (Schiegl *et al*., 1996). Where such physical evidence is missing, magnetic and archaeomagnetic dating (on sediments) should be employed to confirm whether there has been existence of fire in any suspected area. Archaeomagnetic dating is dating of archaeological artifacts or elements by comparison of magnetic direction or /and intensity information with known spatial-temporal changes of the earth's magnetic field. Materials that are normally used are those with magnetic records that depends on thermoremanent magnetization (TRM)

which span a wide diversity of archaeological elements such as burned sediments, ceramics, kilns and others (Hueda-Tanabe *et al*., 2004).

Bellomo (1993) used several parameters of investigation including among others: (1) magnetic susceptibility, (2) macroscopic examination of fire features on surfaces and profiles, (3) analyses of magnetometer data, (4) studies of isothermal remanent magnetization (IRM) acquisition, (5) analyses of alternating field demagnetization characteristics to identify and discriminate between archaeological evidence of fire resulting from human activities and natural processes. Bellomo (1993) predominantly emphasized magnetic and archaeomagnetic methods of analysis, since magnetic susceptibility, magnetic stability, magnetic grain size and magnetic mineralogy are all affected by temperature.

In most cases the remains of a fireplace will be degraded by wind and water, trampling and scavenging. Ash and charcoal are dispersed fairly readily if uncovered, while debris such as bone and animal or plant matter may be scavenged. More often than not, little evidence of a fireplace will be enclosed and preserved by sediments. One of the features most likely to survive, however, is the substrate that is the sediment under the fire or on the sides of a pit. In the case that the remains of a fireplace are covered over, weathering and degradation continue. Plant and animal matter, wood and bone will undergo considerable alteration and decay with time, so too will ash and the delicate features like discolouration in baked sediments and stones. In any case it must be noted that charcoal and particles of carbonized organic materials are chemically stable and durable, and more likely to survive in the archaeological record (Barbetti, 1986). Hence in such cases where the evidence has not been preserved magnetic and archaeomagnetic studies have to be done to demonstrate that fire was once used at an archaeological site.

2.8.2 Magnetic susceptibility

Magnetic susceptibility can be simply described as the degree of magnetization of a material (in this case sediment) in response to an applied magnetic field (http://en.wikipedia.org/wiki/Magnetic_susceptibility. Accessed 03/02/09). The

changes in the magnetic minerals induced by heating of sediment, which causes magnetic field irregularities around a fireplace, can also be studied by direct measurement of the magnetic susceptibility. This can be done on small samples of sediment, or in the field with a portable susceptibility meter and search coil (Barbetti, 1986). Minerals which can be magnetized in sediments include the ferromagnetic minerals (strongly magnetizable) and any of the paramagnetic (moderately magnetizable) minerals. The former include magnetite, haematite, iron titanium oxides, pyrrhotite, maghemite, greigite and goethite, minerals capable of acquiring remnant magnetization and useful for palaeomagnetic studies. The latter include a broad array of substances, all of which contain Fe^{2+}, $Fe^{3+,}$ or Mn^{2+} ions. These paramagnetic minerals may include clay minerals (chlorite, smectite and glauconite), iron and manganese carbonates (siderite, rhodochrosite), ferromagnesian silicates as well as a variety of ferric-oxyhydroxide mineraloids, (University of Minnesota, http://www.cartage.org.lb/en/themes/sciences/physics/. Accessed 03/02/09).

2.8.3 Palaeomagnetism

Palaeomagnetism refers to the study of the record of the earth's (i.e. sediments in this case) magnetic field preserved in various magnetic minerals (http://en.wikipedia.org/wiki/Paleomagnetism. Accessed 03/02/09). Thermoremanent magnetisation is the most understood magnetic effect caused by past human habitation. When materials that contain iron-oxides are heated above their Curie temperature and then allowed to cool in the ambient earth's magnetic field they have the potential to acquire a considerable thermoremanence that is fixed in the material unless they are reheated or disturbed (Schmidt, 2007). In general, when clay (materials that contains iron) is heated, the microscopic iron particles within it attain remnant magnetism parallel to the earth's magnetic field. They also point toward the location around the geographic North Pole where the magnetic North pole was at that moment in its wandering. Once the clay cools, the iron particles maintain that magnetism until the clay is reheated. By using another dating method (dendrochonology, radiocarbon dating) to obtain the absolute date of an

archaeological feature (such as a hearth), and measuring the direction of magnetism and wander in the clay today, it is possible to determine the location of the magnetic North pole at the time this clay was last fired. A magnetometer is used to measure the orientation of the iron particles in the samples. The location of the magnetic pole and age are determined for that fire-pit by looking at the average direction of all samples collected (Eighmy, 1980, 1990; Butler, 1992).

2.8.4 Magnetic field surveying

Heating induces changes in the iron oxide minerals in the sediment, generally enhancing their capacity to carry a magnetism induced by the Earth's field. Some of the iron oxide particles will remain with a weak remanent magnetism, imparted as they cool down. Both the induced and the remanent magnetism contribute to the magnetic field anomaly (Barbetti, 1986). The measured magnetic susceptibility depends on the amount of iron oxides available prior to its alteration by humans, and also on the extent of conversion due to the anthropogenic influences. As a result, the absolute value of magnetic susceptibility can vary widely between different sites and enhancement can only be recognized as a contrast between areas of higher susceptibility compared to background measurements (Schmidt, 2007). This method can be applied to archaeological sites to show the presence fireplaces. It would hence complement visual observations, and help establish whether (for example reddening) was feasible to be due to heating (Barbetti, 1986).

2.8.5 Shortfalls of Palaeomagnetic and Archaeological dating.

Although fireplaces (i.e. sediments) can be directly dated using the above techniques where evidence of burning has not been preserved, there are a number of limitations associated with them:

(a) Palaeomagnetic dating can only date deposits that are hundreds of thousands to millions of years old. This is useful when studying early fossil hominids, but is not useful when studying modern human beings.

(b) The ability of the archaeologist obtaining the sample, and the number of the samples used to calibrate the archaeomagnetic master curve has an effect on the precision with which archaeologists can determine a date for a feature (Eighmy, 1980, 1990; Butler, 1992). This is because 'the potential precision of the technique varies with the rate at which the magnetic pole position was moving at different periods. Where movement was rapid, features can be dated to within a smaller time window than in periods where the movement was slow. This places a limit on the relative precision with which the dates of features from different periods can be determined, regardless of the quality of the calibration evidence' (Linford, 2004).

(c) Due to complex oxidation reactions as the igneous rock or sediments cool after crystallization, the orientation of the earth's magnetic field are not always accurately recorded (http://en.wikipedia.org/wiki/Paleomagnetism. Accessed 03/02/09).

(d) It appears that the magnetic pole has reoccupied the same positions at different times over the last 3000 years. This implies that the calibration curve crosses itself and can result in uncertainty as to which of the two dates is accurate for a particular remanence direction (Linford, 2004).

(e) The microscopic iron particles in several sediments go through chemical changes after they have settled through the water into strata. These chemical alterations cause the iron particles to realign themselves with the Earth's magnetic field at the moment of the chemical change or modification. This is called chemical remanent magnetization. The identification of the particular iron minerals that are susceptible to this change can be an early warning that errors can be expected (Eighmy, 1980, 1990; Butler, 1992).

(f) Indirectional dating technique (as developed by Thellier and Thellier, 1959) demands numerous measurements compared to directional dating, hence more sources of errors are involved. Such errors can arise from: sample inhomogeneity, sample anisotropy, differences between the original and laboratory: (i) firing atmosphere (ii) heating and (iii) cooling rates.

(g) Directional archaeomagnetic dating can only be effectively utilized if the types of archaeological features to be dated meet three basic conditions, which are: (i) they must contain magnetic minerals capable of carrying a stable remanent magnetization (ii) should have experienced a remanence-inducing event at some time in their history and (iii) should have remained undisturbed since acquiring the remanence so that its direction is still meaningful (Linford, 2004).

In this research much attention was given to distinguishing: bones that are burned, bones that are stained, and bones that are both burned and stained by chemical cleaning of bones, elemental analysis by ICP-AES, CHNS analysis. Self ignition temperature of organic matter found in the vicinity of burnt bones were experimentally obtained which we have assumed to have caused a spontaneous combustion of this organic matter (bat guano) therefore resulting in burning of the bones

CHAPTER THREE

OBJECTIVES OF THE STUDY

Fossil material plays an important role in archaeology as a source of information about the geochemical environment i.e. the sediments, soils and local ground water in which they were buried. However, significant alteration occurs over time at all scales from the macroscopic to nanoscopic level, to the physical and chemical properties of bone during the burial period. Alterations in chemical composition and structure of the bone include among others; partial or complete dissolution, erosion, precipitation, recrystallization, ion uptake by sorption and diffusion, hydrolysis, crystal growth, and repolymerization. The state of preservation of these fossil remains therefore varies greatly and depends mainly on direct environmental conditions, such as ground water and sediment composition, soil hydrology and pH, redox potential and temperature, soil solution fluoride and carbonate concentration, mechanical pressure, microbial activity, duration of interment and particle transport. Hence an understanding of the diagenesis process is crucial to the evaluation and understanding of the preservation state of the original biochemical signatures of fossil bones.

Several studies have been conducted and were mainly focused on bones exposed to weathering under harsh climatic conditions (e.g. Tuross *et al*., 1989; Trueman *et al*., 2004), or buried in soil (e.g., Child, 1995; Bocherens *et al*., 1997; Pfretzschner, 2004). Cave sediments or soils have rarely been considered. In addition, most of these studies have been done on teeth rather than bones, based on the widespread assumption that tooth enamel is more resistant to diagenetic alteration and is therefore the material of choice for diagenesis studies. Hence not much has been done on bones. In addition to this, another major drawback of such studies is that they concentrated mainly on chemical trends of bulk materials and rarely investigated the mechanisms by which chemical compositions and mineralogical alterations occur during the burial period. Furthermore, even though fossil bones have been commonly investigated, little

attempt, if any, has been made to combine morphological, mineralogical, and chemical information for both modern and fossil bones.

The purpose of this study was to characterize the morphological, mineralogical, and chemical features of fossils from Gladysvale Cave, South Africa in comparison with modern samples from the same geological area, and also to investigate the mechanisms by which bone chemical compositions and mineralogical alterations occurred during the burial period. Here, investigation of diagenetic parameters that quantify the post-mortem alteration of bones (i.e. bone morphology, porosity, protein content, crystallinity of bone apatite, enrichment and leaching of chemical species) was done to identify, not only the effects of the burial environment on the sample sets, but also whether relationships between these parameters could provide clues to how bone alteration occurs in different geochemical environments, providing a deeper understanding of the diagenetic process.

This was achieved by accomplishment of the following objectives:

- Collection of fossil bones of known anatomical element and taxon, and modern bones from the same geological area.
- Determination of the composition of elements in the modern and fossil bones.
- Determination of the elemental composition of the surrounding soil.
- Determination of the mineralogical composition of modern and fossil bones.
- Morphological examination of modern and fossil specimens.
- Comparison of the distribution of elements in the soil, modern and the fossil bones (identifying which elements were replaced in the fossil, and how it happened).

Samples of a modern bone of the same species as the fossil, from the same geological area, were submitted to the same analyses for comparison. Finally comparison of the studied diagenetic parameters that quantify the post-mortem alteration of bones

between modern and fossil specimens was carried out and any modern versus fossil changes were attributed to diagenesis, and any similarities to diagenetic resistance.

On the other hand, black-coloured bone remains are a common scene in most South African caves. Questions normally arise as to whether changes in bone colour were a result of burning or surface coating from minerals? Presumed that the bones are burnt, and then the need to find out what would have caused this fire- whether natural or human controlled fire. Hence the need to differentiate between black fossil bones that are burned and unstained, burned and stained, and stained but not burned.

Thus the other objectives of this study are to:

- Investigate whether the black colour observed on the bones was a result of burning or surface mineral coating.

- Differentiate between black bones that are burned and unstained, burned and stained, and stained but not burned.

- Investigate what could have started this fire (natural or accidental), in the event that the bones are burnt, by determining the self-ignition temperature of the organics collected from the same site in the vicinity of the black bones.

3.1. Key questions

This study therefore seeks to address the following questions:

- How does the surrounding matrix influence the fossil formation?
- In which order did the mineral replacement occur?
- Why do fossils occur in one site and not another?
- Is black colour in bones a result of burning or mineral coating?

3.2. Significance of research

- Potential for modelling of the diagenesis process.
- Potential for fingerprinting the origin of fossils that are out of context.
- Potential for direct dating of radioactive material in fossils.
- Potential for study of original mineral composition of an individual fossil.

3.3. Outline of methods

Characterization of the bones was performed using scanning electron microscopy (SEM) for morphological studies; (XRF) mapping for the identification of elemental distribution within the bone samples; Powder X-Ray Diffraction (PXRD) for mineral determination; Inductively Coupled Plasma Atomic Emission Spectroscopy (ICP AES) for elemental determination, bone porosity and density measurements and Carbon, Hydrogen, Nitrogen and Sulphur (CHNS) for detection of light elements, particularly nitrogen, whose concentration is correlated to the collagen content of the bone. These analytical techniques determined quantitatively the sample's post-mortem contamination and elemental loss, even at trace level, and examined the elemental distribution across bone transverse sections. They also provided information on the local and global crystallinity of bone apatite, the precipitation of foreign minerals in the bone matrix and the presence of preserved collagen. A combination of these different complementary analytical techniques was therefore used to give information on bone diagenesis.

CHAPTER FOUR

AN OVERVIEW OF ANALYTICAL METHODS USED IN BONE CHARACTERIZATION

This chapter offers an overview of analytical methods that have been employed in the characterization of bones in both previous and recent studies and the ones that were used here. Various studies were done on bone characterization using different techniques yielding either the same information (for instance the use of AAS, ICP AES, ICP MS, and EDX for elemental analysis) or different information for an example the use of PIXE for the spatial distribution of elements in a sample and PXRD for mineral identification. In cases where different analytical techniques can be used to obtain the same information, chances are that some will give more reliable and more accurate data than the others due to differences in instrumental parameters, like detection limits, limits of quantification, specificity, linearity and precision, just but to mention a few. The major objective of this chapter is to provide adequate information on the suitable analytical technique to be used for a specific analysis when attempting to address specific questions concerning the process of diagenesis. This is achieved by outlining the strengths, limitations and the nature of information that is obtained from each technique.

4.1. Various analytical methods used in bone characterization

The study of the physical features of the specimen, which mainly include deformation, prior post-mortem fracture and state of preservation, and microscopic dissolution, recrystallization and permineralization, can be compared and contrasted with modern specimens to estimate the type and extent of post-mortem processes and diagenetic alteration. These physical features offer essential information on the nature of the geochemical environments in which the bone specimen has been buried over a given period of time. On the other hand a chemical and/or molecular analysis renders

a higher resolution identification of alterations that have occurred in fossils. Such analyses can also be applied to identify the types of molecules or molecular fragments present in fossil material, thus elucidating depositional/chemical environments most likely to preserve endogenous biomolecules, or to show whether retained organic material is original, or if it has been incorporated in fossil matrices through diagenesis. The observed chemical alterations, for instance bond breakage, exogenous ligands, and functional group modifications, can also point us towards the possible mechanisms of molecular diagenesis (Schweitzer, *et al*., 2008). As described earlier in Chapter One, diagenesis involves the processes of dissolution, precipitation, adsorption, mineral replacement, recrystallisation, elemental enrichment and leaching (Carvalho *et al*., 2004). These processes will ultimately lead to significant alteration of the original crystal structure of bioapatite, resulting in modifications to fossil bones and teeth from different burial sites and ages (Parker and Toots, 1970; Toots, 1963; Wycoff, 1972). Therefore post-mortem diagenesis always results in a wide range of chemical and mineral changes to the organic and inorganic constituents of fossil bone and teeth. The need to identify and quantify the degree of these alterations caused by either one or a combination of these diagenetic processes has triggered development of new analytical techniques of analysis as well as improvement of the existing ones. The resolution and precision of these analytical methods has improved since the 1960s and early 1970s (Schweitzer, *et al*., 2008) with systematic studies of chemical and physical changes of fossilisation (Blake *et al*., 1997; Bocherens *et al*., 1994; Chillón *et al*., 1994; Elorza *et al*., 1999; Goodwin *et al*., 2007; Henderson *et al*., 1983; Hubert *et al*., 1996; Kohn, 1999; Kohn and Cerling, 2002; Lee-Thorp and Van der Merwe, 1991; Pate *et al*., 1989; Person *et al*., 1995; Trueman, 1995).

Hence this chapter gives a brief outline (i.e. description and principle) of various suitable methods for characterisation of bone material that have already been used in such studies.

4.2. Ion beam techniques

A particle accelerator equipped with an external beam line is often applied to the elemental analysis of archaeological samples in order to infer from their major, minor

and trace elements, post-mortem alteration processes on the original mineral part of bones due to their burial environment (dissolution, uptake and diffusion of foreign ions). Ion beam analyses are suitable for such studies because they are non-destructive, sensitive, multi-elemental and do not necessarily need preparation prior to measurement. Such techniques includes among others, Particle Induced X-ray Emission (PIXE), Particle Induced Gamma-ray Emission (PIGE), Electron Diffraction Pattern Analysis (EDPA), Scanning Electron Microscopy (SEM), X-Ray Fluorescence mapping (XRF), Electron probe microanalysis (EPMA), and have been used in previous studies to detect micro elemental distribution patterns and thus identify post depositional contamination. The spatial localisation and distribution of elements can also provide vital information as to the probable mode of association/ interaction of particular elements.

4.3. Proton Induced X-ray Emission (PIXE)

Proton Induced X-ray Emission (PIXE) of bio-minerals (such as bones) is a higher resolution analytical technique that provides relevant information to various fields of research such as archaeology (Tapper *et al*., 1990; Elliott and Grime, 1993; Reiche *et al*., 1999; Brenn *et al*., 1999), biology (Tang *et al*., 1997), biomedical research (Pålsgård *et al*., 1997; Preoteasa *et al*., 2004; Gomez *et al*., 2006), and palaeontology (Bruckschen *et al*., 1995; Wu *et al*., 1997). Microbeam PIXE is a typical X-ray fluorescence (XRF) technique. Therefore the principle behind this technique is similar to that of XRF. Basically the microscopic regions of a mineralogical or biological specimen are bombarded with a three Million electron Volt (MeV) energy proton beam focused to micron-sized dimensions (Roberts *et al*., 1999). These MeV accelerated protons will interact with the inner shell atomic electrons in the specimen creating vacancies in the inner shell orbits. This vacancy is filled by transition of an outer shell electron of the atom and the energy (X-ray photon) emitted during this transition is characteristic of the emitting atom, which is known as X-ray fluorescence. These processes are represented diagrammatically in Figure 4.1. X-ray energy spectra for each selected beam location are produced, as the beam is scanned across the specimen (Antolak *et al*., 1994). The recorded X-ray spectra corresponding

to a selected area on the scanned sample are extracted for quantitative analysis (Antolak and Bench, 1994), and ultimately elemental maps are made from this output. Normally coupled to the PIXE is a scanning transmission ion microscope (STIM) which uses a particle detector located behind the sample to measure the residual energy of protons after they have passed through the target specimen. The proton energy losses are then converted into specimen density or thickness (Goodwin *et al*., 2007). Thus bone sections are directly placed in front of the external proton beam for the PIXE and PIGE analyses and depth profiles along the bone sections are measured by scanning the sample in front of the beam in precisely recorded steps.

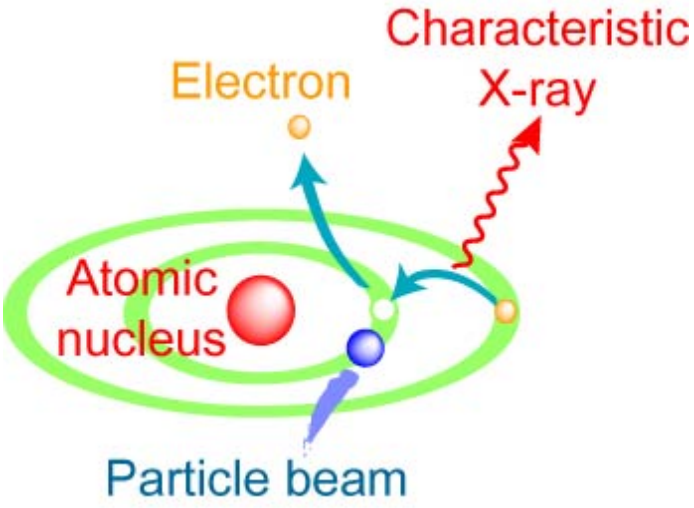

Figure 4.1. Brief summary of the principle of PIXE Analysis i.e. (i) an electron in the inner shell jumps with the interaction with a particle beam, (ii) another electron in outer shell moves to an inner orbit and finally a characteristic X-ray which has particular energy is emitted (www.taka.jaea.go.jp/tiara/663/microPIXE.files/pixe accessed on 20\08\09).

PIXE analysis was employed in a study carried out by Goodwin *et al*., (2007) to identify and map the elemental composition of dinosaur bone bioapatite at ppm sensitivity and submicron-scale spatial resolution. The resultant elemental maps allowed the identification of local patterns of enrichment and depletion within micron-scale regions of fossil bone that are usually lost in alternative bulk analyses. The major advantage of PIXE as a micro-sampling technique is that it provides a more detailed and comprehensive record of physiological and palaeoecological history by

capturing an elemental signal or concentration gradient not obtainable by bulk sampling (Thomas and Carlson, 2004).

4.4. Electron diffraction pattern analysis (EDPA)

This technique relies on the fact that a very high energy electron (200 kV) beam is transmitted through the sample. The beam is then diffracted at angles determined by Bragg's Law, applied to a set of reflecting crystal planes separated by the d-spacings of the crystals (Schweitzer, *et al*., 2008). Diffraction patterns can allow identification of *in situ* mineral phases with high accuracy, and can differentiate between bioapatite and other forms by d-ring spacing (Schweitzer *et al*., 2007), or between different forms of iron-bearing minerals. The EDPA technique is frequently applied in quantifying degree of diagenetic alteration in fossil samples, or in identifying remnants of original biominerals. This method is normally coupled to TEM systems (Schweitzer, *et al*., 2008).

4.5. UV/VIS spectroscopy

The absorption of ultraviolet and visible radiation by organic molecules, such as proteins in bones, is limited to certain functional groups referred to as chromophores that contain valence electrons of low excitation energy. Since the superposition of rotational and vibrational transitions on the electronic transitions give rise to a combination of overlapping lines, these lines appear as a continuous absorption band. Because of such phenomenon the spectrum produced from a molecule containing these chromophores is complex (Sheffield, Hallam University, http://teaching.shu.ac.uk/hwb/chemistry/tutorials/molspec/uvvisab1.htm accessed on 10/08/09).

UV/VIS spectroscopy can be used for the confirmation and identification of organic biomolecules in bone samples. Different organic molecules which includes among others, bone protein (e.g. collagen) absorb radiation at specific wavelengths in the electromagnetic spectrum, and may be identified by the specific absorbance pattern they exhibit. An absorption spectrum will show a number of absorption bands

corresponding to structural groups within the molecule. Both modern and fossil bone organic extracts are solubilized in relevant solvents or sterile distilled water; placed in a special ultraclean quartz cuvet, and a continuous wavelength light (~190–800 nm) is transmitted through the sample. When light interacts with a molecule, it is absorbed in quantum packets, electrons are promoted from their ground state to an excited state. In a molecule, the atoms can rotate and vibrate with respect to each other. These vibrations and rotations also have discrete energy levels, the characteristics of which are dependent upon the atomic make-up and overall molecular structure of the sample. An optical spectrometer will then record the wavelengths at which absorption occurs, together with the degree of absorption at each wavelength. The resulting spectrum is presented as a graph of absorbance (A) versus wavelength.

The absorbance of a sample will be proportional to the number of absorbing molecules in the spectrometer light beam. Absorbance is directly proportional to the path length, b, and the concentration, c, of the absorbing species. Beer's Law states that

$A = \varepsilon bc$, where ε is a constant of proportionality, called the absorbtivity.

4.6. Pyrolysis gas chromatography–mass spectrometry (PY-GC-MS)

Pyrolysis gas chromatography–mass spectrometry relies on the same principle as other methods of mass spectrometry, that is, it capitalizes upon the fact that every molecule consists of a unique combination of atoms that can be determined with high resolution by their atomic masses (Karasek and Clement, 1988). This technique uses high temperature around 600^{o}C to split and volatize molecular components for example collagen, which are then separated according to fragment mass by gas chromatography. A Quadrupole mass spectrometer will then analyse each separated peak in order to identify the number and mass of each volatized fragment, producing a spectrogram. This method has minimum chances of introducing artifacts into the analyses since it does not require any chemical extraction. This technique has been applied in a number of previous studies to identify the remnants of original molecular components, including protein fragments, lignins and chitin of fossils (Stankiewicz *et*

al., 1997a, b, c; Stankiewicz *et al*., 1998; Van Bergen *et al*., 1995). This method is not ideal for identification of DNA, though it is highly sensitive to other biomolecular fragments (Schweitzer, *et al*., 2008).

4.7 X-ray photoelectric spectroscopy (XPS)/Electron Spectroscopy for Chemical Analysis (ESCA)

X-ray Photoelectron Spectroscopy (XPS) is a typical surface analysis technique with a sampling volume that extends from the surface to a depth of approximately 50-70 Angstroms, and is often applied to quantitative determination of atomic composition and chemistry of samples. XPS, also known as Electron Spectroscopy for Chemical Analysis (ESCA), can also be utilized for sputter depth profiling for the characterisation of bones by quantifying matrix-level elements as a function of depth.

The XPS/ESCA process works by focusing monochromatized X-rays on the specimens under ultra high vacuum (UHV) which then produces photoelectrons varying in intensity and kinetic energy. Individual elements within the sample under analysis produce unique characteristic XPS lines corresponding to that particular element, the intensity and position of which determine the concentration and local chemistry or bonding environments of the atom detected (Schweitzer *et al*., 2008). Thus basically XPS/ESCA is an elemental analysis technique that is unique in providing chemical state information of the detected elements, for instance, the sulphur 2p line can show as much as 7eV chemical shift between sulphur in a disulfide environment (S^{2-}) and one in a sulphate (SO_4^{2-}) environment (S^{6+}) (Schweitzer, *et al*., 2008). Therefore this method can distinguish between the oxidised and reduced forms of elements. Since nitrogen is a major constituent of both DNA and proteins, and though its identification in fossil samples does not guarantee the existence and/or presence of these molecular compounds, if nitrogen is not identified in these fossils then it is certain that these molecular compounds are absent. XPS/ESCA is highly sensitive and discrete, confirming the presence of elements identified in other methods like Energy Dispersive X-ray (EDX or EDS), as well as identifying even light elements and their bonding environment unambiguously, such

as nitrogen, which is not detectable or quantifiable by other methods like EDX (Schweitzer *et al*., 2008). Hence this method is an exceptional complement to other methods, for example Time-of-Flight Secondary Ion Mass Spectrometry (TOF-SIMS), Mass Spectrometry (MS) and EDX, in that the oxidation state of the elements identified by EDX, or molecular fragments identified by MS, can be linked to local bonding environments by XPS (Briggs and Seah, 1990). Also, in the case of TOF-SIMS suggesting the presence of sulphur-containing amino acid groups in a bone sample, then XPS will confirm whether that sulphur is present or not and its oxidation state in the sample (Schweitzer *et al*., 1999). Therefore XPS/ESCA can also distinguish between organic sulphurs in bonding environments and those derived from inorganic sedimentary sulphur, among other elements.

Outlined below are the ideal uses of XPS/ESCA analysis, its strengths and limitations (Evans Analytical Group (EAG), http://www.eaglabs.com/techniques/analytical_techniques/ftir.php accessed on 10/08/09).

Uses for XPS/ESCA analysis:

- Surface analysis of organic and inorganic materials, stains, or residues.
- Determining composition and chemical state information from surfaces.
- Depth profiling for thin film composition.
- Silicon oxynitride thickness and dose measurements.
- Thin film oxide thickness measurements (SiO_2, Al_2O_3 etc.).

Strengths of XPS/ESCA analysis:

- Chemical state identification on surfaces.
- Identification of all elements except for H and He.
- Quantitative analysis, including chemical state differences between samples.
- Applicable for a wide variety of materials, including insulating samples (paper, plastics, and glass).
- Depth profiling with matrix-level concentrations.
- Oxide thickness measurements.

Limitations of XPS/ESCA analysis:

- Detection limits typically ~ 0.1%.
- Smallest analytical area ~10 μm.
- Limited specific organic information.
- Sample compatibility with UHV environment.

4.8. Infrared Spectroscopy

Infrared spectroscopy exploits the fact that molecules have characteristic frequencies at which they rotate or vibrate corresponding to discrete energy levels, often referred to as vibrational modes. Thus when exposed to infrared radiation, chemical bonds in molecules absorb radiation at frequencies that match their vibration modes. Measurement of the absorbed radiation as a function of frequency produces a spectrum that can be used to identify functional groups and compounds, since each frequency of vibration corresponds to a particular bond type (Evans Analytical Group (EAG) http://www.eaglabs.com/techniques/analytical_techniques/ftir.php accessed on 10/08/09). Fourier Transform Infrared Spectroscopy (FTIR) is a novel infrared technique which presents vital information about chemical bonding and molecular structures, making it applicable for analysis of bone biomolecules. The major advantage of FTIR compared to conventional infrared spectroscopy is that all wave numbers are measured simultaneously with the aid of a Michelson interferometer. Carbonate is the third most abundant constituent of bone and tooth mineral after calcium and phosphate, and is regarded as a charge trap which produces an electron spin resonance (ESR) dating signal in tooth enamel and bone. As already outlined in Chapter Two, tooth and bone mineral consists of carbonate hydroxyapatite that bear a crystallographic structure similar to that of the mineral dahllite (Lowenstam and Weiner, 1989), and which often contain variable carbonate content according to the formula: $Ca_5[(PO_4)_3\text{-}B(CO_3)_B][(OH)_1\text{-}A(CO_3)_A]$ (Rink and Schwarcz, 1995). Carbonate, can occupy two different sites in the crystallographic structure, denoted by *A* and *B* in the formula above, substituting for OH^- and PO_4^{3-}, respectively. Using the relative intensities of the infra-red (IR) absorption spectrum, the relative amounts of

CO_3^{2-} at the two sites in the bone sample can be estimated. Figure 4.2 is a typical FTIR spectrum of fossil rhinoceros enamel, showing the wave numbers at which both the carbonate and phosphate occur.

Outlined below are the ideal uses of FTIR analysis, its strengths and limitations (Evans Analytical Group (EAG) http://www.eaglabs.com/techniques/analytical_techniques/ftir.php accessed on 10/08/09).

Uses for FTIR Analysis:

- Identifying the molecular structure of organic compounds for contamination analysis.
- Identification of organic particles, powders, films, and liquids (material identification).
- Quantification of O and H in Si, and H in SiN wafers (Si-H vs. N-H).
- Contamination analysis (extracts, out-gassed products, residues).

Strengths of FTIR analysis:

- Capable of identifying organic functional groups and often specific organic compounds.
- Extensive spectral libraries for compound identification.
- Ambient conditions (not vacuum; good for volatile compounds).
- Typically non-destructive.
- Minimum analysis area: ~15 micron.

Limitations of FTIR analysis:

- Limited surface sensitivity (typical sampling volumes are ~0.8 μm).
- Limited inorganic information.
- Typically not quantitative (needs standards).

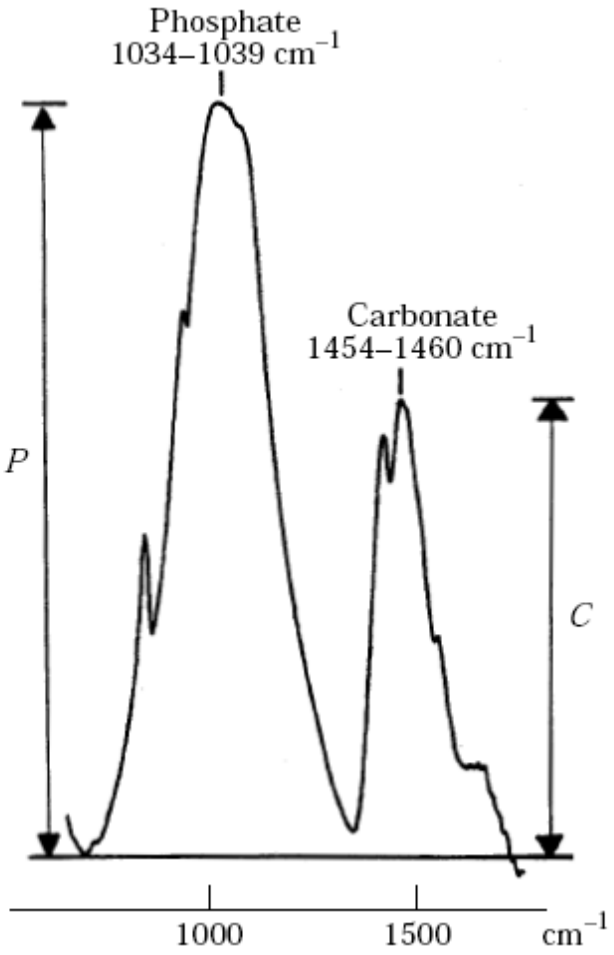

Figure 4.2. Fourier transform infra-red spectrum of fossil rhinoceros enamel, generally typical of most samples. A peak of height *C* composed of contributions from A and B site carbonate ions and a peak of height *P* associated with the phosphate ions gave the ratio *C/P* (after Rink and Schwarcz, 1995).

4.9. Electron paramagnetic resonance (EPR)

In essence Electron paramagnetic resonance (EPR), also known as electron spin resonance (ESR) and electron magnetic resonance (EMR), is an analytical technique based on the resonant absorption of microwave radiation by paramagnetic ions or molecules, which contain at least one unpaired electron spin, and in the presence of a static magnetic field. Hence this technique exploits the fact that some atoms in molecular complexes contain electrons that exist in a state of unequal spin, detectable by EPR. When the bone sample is bombarded by gamma rays or any other form energetic radiation, a characteristic ESR signal is produced, the intensity of which can

then be used to estimate the radiation dose to which the bone sample has been exposed (Grün *et al*., 1987), and this is the basis of ESR fossil dating.

Several authors have pointed out that the ESR dating signal is associated with charges trapped at oxidized carbon-sites, either as the CO_3^{-3} species (Cevc & Schara, 1972; Doi *et al*., 1979, 1980, 1981) or as the oxygen-deficient CO_2^- species (Bacquet *et al*., 1981; Geoffrey and Tochon-Danguy, 1985; Callens *et al*., 1987). Since the existence of ESR dating signal signifies the presence of carbonate in bone samples then it is possible to identify any variations which may have occurred in the carbonate content of bone/enamel since the time of its burial (Rink and Schwarcz, 1995). Thus loss of carbonate due to leaching or its enrichment following uptake processes have a significant effect on the dating studies of fossil bones, since this alters both the ESR signal intensity and its sensitivity to radiation. EPR is therefore a well established method suitable for both identifying and verifying the presence of paramagnetic compounds in extracts of fossil bone, and can definitely provide evidence for the extent of preservation of molecular fragments (Schweitzer *et al*., 1997) in fossil bones. Though the range of applications for EPR is rather limited as compared to Raman or NMR methods, it is known to be more sensitive than NMR, and provides slightly different information, such as characteristics of electron transitions and molecular interactions (Blumberg, 1981) in the specimen under study.

4.10. Total reflection X-ray Fluorescence (TXRF)

Total reflection X-ray fluorescence (TXRF) is a highly surface-sensitive technique well established for chemical analysis of samples deposited as a thin layer (Borgese *et al*., 2009) and is very sensitive to very dilute quantities of material. This technique utilizes extremely low-angle X-ray excitation of a polished sample surface. The incident angle of the X-ray beam typically 0.05° is made to impinge on the surface of a sample such that total reflection occurs. Such a small incident angle causes excitation of atoms in the top below the critical angle of the substrate and limits excitation to the outer most surface layers of the sample. In addition by maintaining an incident angle less than the critical angle greatly increases sensitive analysis as a

result of reduced background signals. The resultant fluorescence is detected by a Si(Li) detector placed above the sample. These fluorescence photons emitted from the surface atoms are characteristic of the elements present in the sample (Evans Analytical Group (EAG), http://www.eaglabs.com/techniques/eds.php accessed 10/08/09). Figure 4.3 is diagrammatic representation of a typical total reflection X-ray fluorescence geometry with the angle of incidence being less than the critical angle and the primary radiation penetrating into the sample below the critical angle of the sample restricting excitation of the outer most surface layers of the sample.

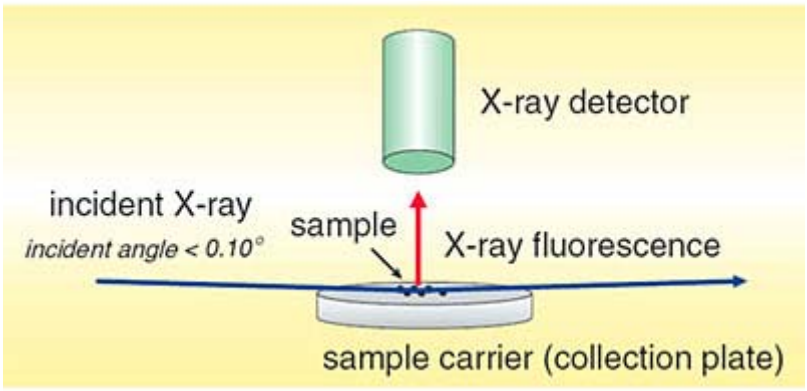

Figure 4.3. TXRF geometry with the angle of incidence being less than the critical angle and the primary radiation penetrating into the sample below the critical angle of the sample (Esaka *et al*., 2003).

This technique has been used by Carvalho *et al*., (2004) in the study of the distribution of trace elements along human bones. In this study quantitative analysis was performed for Ca, Mn, Fe, Cu, Zn, Sr, Ba and Pb with Fe and Mn bearing the highest concentrations, of the same range and magnitude to those in the burial soil. Thus post-mortem Fe and Mn contamination occurred in the whole bone tissue from the surrounding soil. Hence TXRF is a suitable technique for the quantification of the extent of elemental diagenetic alterations of fossil samples using modern bones as the standard reference samples for comparison. The amounts of elements can be then be calculated by comparing the peak intensities of elements with that of the internal standard.

Outlined below are the strengths and limitations of TXRF analysis (Evans Analytical Group (EAG), http://www.eaglabs.com/techniques/analytical_techniques/ftir.php accessed on 10/08/09).

Strengths of TXRF Analysis.

- Trace element analysis.
- Survey analysis.
- Quantitative.
- Non-destructive .
- Automated analysis.
- Whole wafer analysis (up to 300 mm).

Limitations of TXRF Analysis

- Cannot detect elements with low-atomic number (Li, Na, Al).
- Polished surface required for best detection limits.

4.11. Analyses of chemical extracts of fossil material

Numerous analytical methods require fossil and modern bone material to be chemically extracted prior to analysis. Organic extractions using organic reagents are used for isolating particular compounds of interest, such as kerogens, lipids and other geochemical components (e.g. CoBabe and Pratt, 1995) from the sample under investigation. However, different reagents or a suitable mixture of reagents are used for isolation of water-soluble molecular components such as protein fragments.

It is recommended that sample surfaces be thoroughly cleaned by abrasion to remove external contaminants. The bone (fossil and /or modern) material is then crushed to a fine powder using appropriate recommended apparatus or instrument taking all necessary precautions to avoid sample contamination. The powdered sample is then washed 2–3 times in water or dilute salt solution to remove any loosely bound contaminants before the removal of wash buffers by centrifugation. Depending on the particular method used, an extraction buffer is then applied to the bone powder and allowed to incubate for several hours to overnight. Usually ion-exchange column

chromatography or dialysis is used to remove the extracting reagents prior to analyses. By doing this low molecular weight salts are removed together with other remaining buffer components, while the larger organic components of fossil tissues are retained. The bone extracts should then be dialyzed against sterile distilled water or a neutral physiological buffer such as phosphate-buffered saline (PBS), using low molecular weight cut off (MWCO) membrane. Whenever concentrated sample are required, ultrafiltration or lyophilization can be applied following dialysis process, thus optimizing chances of identifying endogenous molecules in low concentration (Schweitzer *et al*., 2008).

4.12. Time-of-Flight secondary ion mass spectrometry (TOF-SIMS)

Time-of-Flight Secondary Ion Mass Spectrometry (ToF-SIMS) is a surface analytical technique that provides detailed surface chemical information; elements, chemical groups, molecules, polymer groups. ToF-SIMS uses a primary ion beam which is pulsed to produce packets of primary ions. Thus a high-energy (e.g., gallium ions, typical energy: 15 keV) primary ionizing beam with a pulse width of ∼1 ns and a repetition rate of 10 kHz is rastered over a predetermined area to release molecular fragments from a sample surface (Vickerman *et al*., 1989).

The sample ion images are generated by scanning the primary beam over the sample surface and recording the number of ion as a function of the position. The secondary electrons which are produced following bombardment process are detected to give secondary electron images. The spatial resolution of the images mostly depends on the diameter of the pulse of the primary ions (http://www.fkf.mpg.de/ga/machines/sims/ accessed on 20\08\09).

The major strength of this technique lies on the ultra high-resolution detector which is capable of differentiating fragments that differ in mass by as little as 0.001 atomic mass unit (amu) (Schweitzer *et al*., 2008).Variation in mass resolution among sample is usually due to differences in primary pulse width, sample type and surface flatness, and charge compensation. Also whether or not detectable secondary ions are generated is highly dependent on characteristics of the sample; therefore, peak

intensities (i.e., peak areas) may differ between samples (Karasek and Clement, 1988), but mass resolution is not affected, therefore the ToF-SIMS spectral patterns will vary because of inherent differences in the surface composition. For this reason, a fresh bone may produce a spectrum with a pattern that is differed from that of a fossil bone, even though they may contain some identical (i.e. same) molecules. Figure 4.4 is an illustration of a ToF-SIMS profile obtained on dinosaur vessels recovered from demineralised bone. The profile is showing a high resolution of organometallics fragments, the unique association/complexation of Fe with organic-derived C, N, and H, as well as purely organic fragments containing C, N, and H.

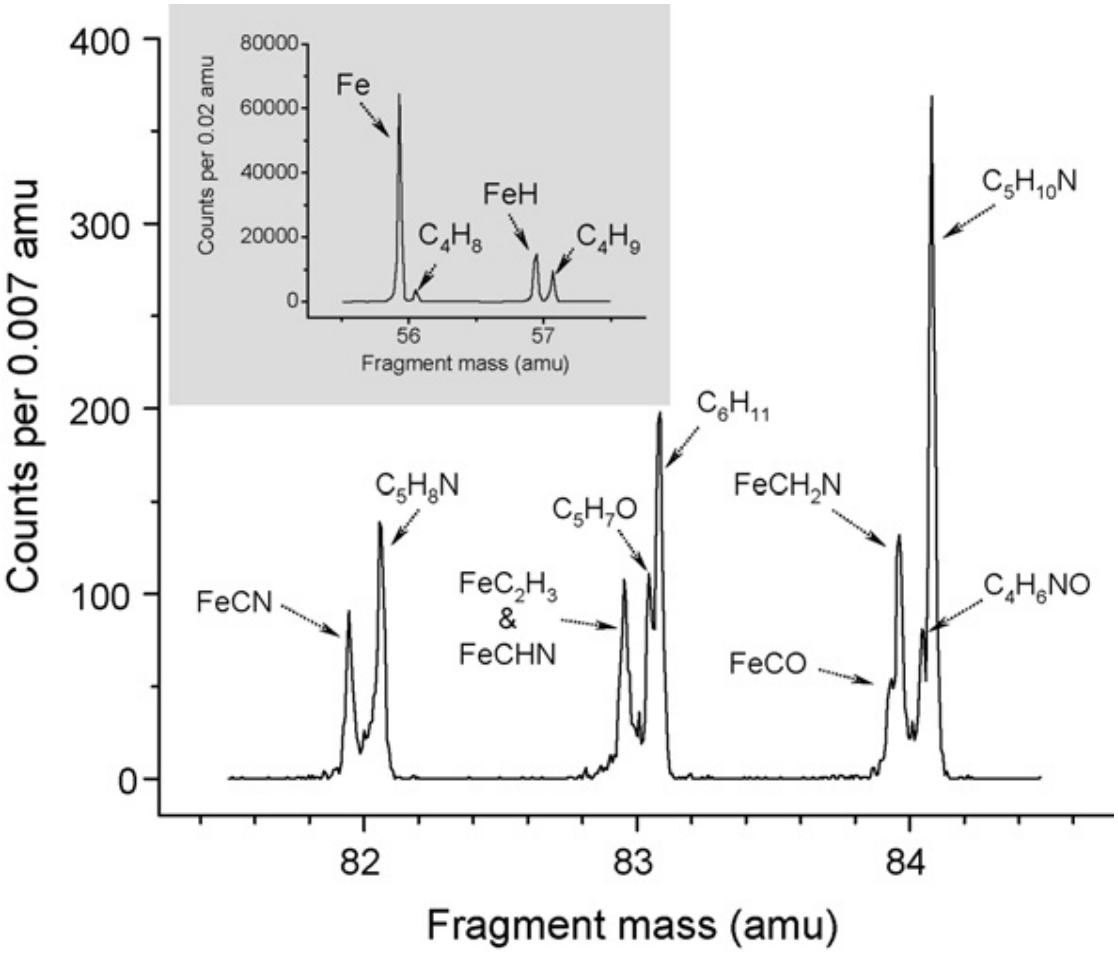

Figure 4.4. High-resolution positive-ion ToF-SIMS spectra obtained from demineralized dinosaur vessels. The inset is an amplified mass region around 56–57 amu, showing the identification of iron in the vessel wall, while the main spectra shows the expanded region around 82–84 amu.

4.12.1. Advantages of ToF-SIMS

- ToF-SIMS can measure both positive and negative ion spectra, thereby providing complementary information about fragmentation patterns of sample derived molecules (Asara *et al*., 2007a; b; Schweitzer *et al*., 2007).

- Compared to other mass spectrometric methods, ToF-SIMS allows the localization of molecular sources to specific regions of the sample. For that reason, in fragile specimens where there is a need to limit handling or sample preparation, the study specimen can be left within the encasing matrix. Then comparative mass data can be obtained from both fossil tissues and the surrounding matrix, indicating that molecular signal originates from the specimen, and not from exogenous environmental contaminants (Schweitzer *et al*., 2008).

- ToF-SIMS is capable of detecting all the elements in the periodic table, including H.

- ToF-SIMS can provide mass spectral information; image information in the XY dimension across a sample; and also depth profile information on the Z dimension into a sample.

- The imaging capabilities of this technique can also offer elemental and molecular information from defects and particles on the micron scale.
- Due to its chemical specificity, ToF-SIMS may be exploited to provide semi-quantitative data where variations in the surface concentrations of different chemical species may be determined by monitoring changes in the relative intensities of their diagnostic signals.

- ToF-SIMS can detect and precisely locate organic compounds in environmental samples.
- Being a non-destructive technique, ToF-SIMS allows successive examination of the studied sample areas using other conventional microscopic techniques

to obtain further sample information. This is important with rare, minute, or fragmentary fossil materials.

4.13. Inductively coupled plasma atomic emission spectrometry (ICP AES)

4.13.1 Effect of diagenesis on bone elemental compositions

The effects of diagenesis on elemental concentrations can be assessed by comparing modern bones with the fossil bones. Elemental composition of fossil specimens can demonstrate diagenetic alteration by identifying exogenous elements incorporated into the pore spaces in bone matrices (Schweitzer *et al*., 2008). These exogenous elements may become incorporated into bone structure from the groundwater and soil through several means. Once inside the bone they may reside in pores, voids or micro-cracks in the bone matrix, form complexes with the organic component, and adsorb onto the surface of hydroxylapatite matrix via ionic exchange. These processes and their rates of reactions are entirely dependent upon the physical and chemical characteristics of the burial environment (Carvalho *et al*., 2004). Several techniques have been used for the study of elemental distribution in fossil bones, which include among others atomic absorption spectrometry (AAS) (Gonzalez-Reimers *et al*., 1999), particle-induced X-ray emission (PIXE) (Brenn *et al*., 1999; Reiche *et al*., 1999; Tapper *et al*., 1990) to examine diagenetic chemical substitutions in the mineral structure, X-ray fluorescence (XRF) for quantitative determinations (Carvalho *et al*., 1998; 2000; 2003; 2004) and nuclear microprobe for elemental distribution (Boscher-Barre and Trocellier, 1993; Elliott and Grime, 1993). Several authors have used inductively coupled plasma atomic emission spectrometry (ICP-AES) technique for elemental analysis in the same field of study. Kniewald *et al*. (1994) determined the concentrations of Pb, Cu, Cd, Zn, Ca, Sr and Ba in fossil and recent human bone using ICP-AES and differential pulse anodic stripping voltammetry (DPASV). All the above mentioned analytical techniques are best suited for the investigation of the effect of diagenesis on bone elemental composition because of the great analytical precision and comparatively small amount of material required.

In this study bone elemental composition was accomplished using ICP-AES. ICP-AES is a technique that offers large linear dynamic range, relative freedom from chemical interference, high specificity, multi-element capability and good detection limits. Hence the extent of diagenetic alteration of fossil samples was quantified by determining the differences between the diagenetic parameters of the fossil bones and the modern counterpart bone standard.

4.13.2 Principal behind ICP-AES

ICP-AES is an emission spectrophotometric technique, exploiting the fact that excited electrons release energy at a given wavelength as they return to ground state. This type of emission spectroscopy makes use of the inductively coupled plasma to excite atoms and ions that will emit electromagnetic radiation (as they return to ground state) at specific wavelengths characteristic of a particular element. The identification of this radiation permits the qualitative analysis of a sample. A quantitative determination takes place on the basis of the proportionality of radiation intensity and element concentration in calibration and analysis samples i.e. the intensity of the energy emitted at the chosen wavelength is proportional to the amount (concentration) of that element in the analyzed sample. Therefore, by determining which wavelengths are emitted by a sample and by determining their intensities, the analyst can quantify the elemental composition of the given sample relative to a reference standard. Figure 4.5 is a schematic diagram of ICP-AES showing all stages involved from sample introduction to detection.

Inductively coupled plasma-atomic emission spectrometer the (1) aqueous sample is pumped and (2) atomized with argon gas into the (3) hot plasma. The sample is excited, emitting light wavelengths characteristic of its elements. (4) A mirror reflects the light through the (5) entrance slit of the spectrometer onto a (6) grating that separates the element wavelengths onto (7) photomultiplier detectors. (U.S. Geological Survey (USGS), http://minerals.cr.usgs.gov/gips/na/5process.html. Accessed 09/01/09).

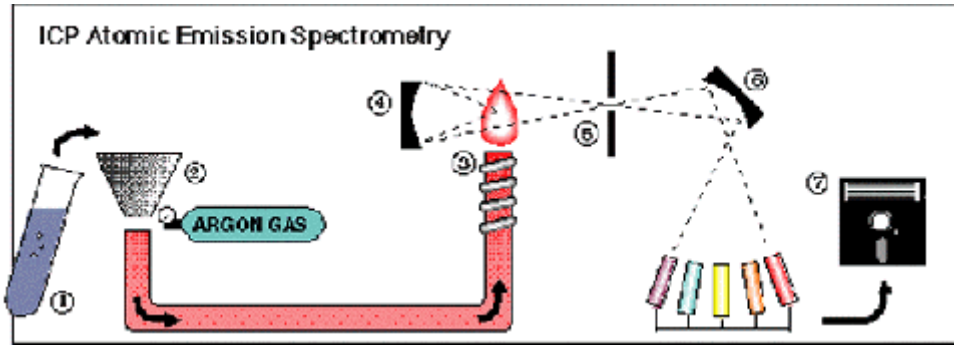

Figure 4.5. Schematic diagram of ICP-AES showing all stages involved from sample introduction to detection. Adapted from (U.S. Geological Survey (USGS), http://minerals.cr.usgs.gov/gips/na/5process.html. Accessed 09/01/09).

4.14. Scanning Electron Microscope (SEM)

The morphological examination of fossil bone at both macro- and microscopic levels provides vital information for the identification of probable agents and processes responsible for bone modification (Gutierrez, 2001), that is its state of preservation, in particular the extent of microbial post-mortem destruction (Bell, 1990). Analyses using Scanning Electron Microscope (SEM) technology coupled with several detectors such as Back-Scattered Electrons (BSE), Electron Backscatter Diffraction (EBSD), and X-ray permits to phase identification, both qualitative and quantitative analyses of the chemical composition of the sample under examination (Poole and Lloyd, 2000; Orr *et al*., 2002). In order to clearly identify and characterize textural changes in Gladysvale fossils in comparison with modern bone samples, high resolution analytical approach was used: scanning electron microscope (SEM) imaging.

Electron microscopy technique is an interdisciplinary technology extensively applied in various disciplines of science. Currently, scanning electron microscopes (SEM) has become the basic measuring and research tool everywhere, where the need to analyze the state of the surface and the estimation of morphology occurs (Kowalewska and Szwedo, 2009). The scanning electron microscope allows the examination and characterization of both heterogeneous organic and inorganic materials on a

nanometre (nm) to micrometer (μm) scale. The popularity of the SEM results from its ability to give three-dimensional images of a wide range of materials (Goldstein *et al*., 2003) including among others fossil bones.

The shorter wavelength and tighter focusing of electrons across the surface of the specimen increase magnification (to about X20 000) and resolution (to about 10 nm) by orders of magnitude over topographical images obtained by the most powerful light microscopy, where resolution is limited to about 1.0–0.5 microns. Such high magnification and resolution are a direct result of the fact that electrons exhibit both particle and dual wave-like nature, which allows them to have a wavelength of the order of 0.1nm when accelerated through a voltage. In addition to secondary electrons used in imaging, backscattered electrons and X-rays are also generated, and these can produce additional data, such as the relative distribution of heavy and light elements, elemental identification and mapping, or crystal phase identification (Schweitzer *et al*., 2008).

4.14.1 Principal behind SEM

An electron gun generates electrons (referred to as an electron beam), which are then accelerated by an electric potential. The electron beam follows a vertical path through the microscope, which is held within a vacuum to minimize electron –gas interactions. Figure 4.6 is a diagramatic representation of the main components of SEM.

The function of the coil is to produce a magnetic field which exerts a force on the moving electrons. The beam travels all the way down through electromagnetic fields and lenses, which directs the beam down toward the final objective lens that finally focuses the beam to a small spot on the sample. When the beam hits the sample, secondary electrons, backscattered electrons, Auger electrons and X-rays are ejected from the sample upon interaction of atoms in the surface layer of the sample with the primary electrons. These ejected electrons collect all the essential information before leaving the surface. They are then captured by the respective detectors and the information is converted into an electric signal, amplified and digitalized (Jim Schweitzer, http://www.purdue.edu/REM/rs/sem.htm. accessed 06/01/09).

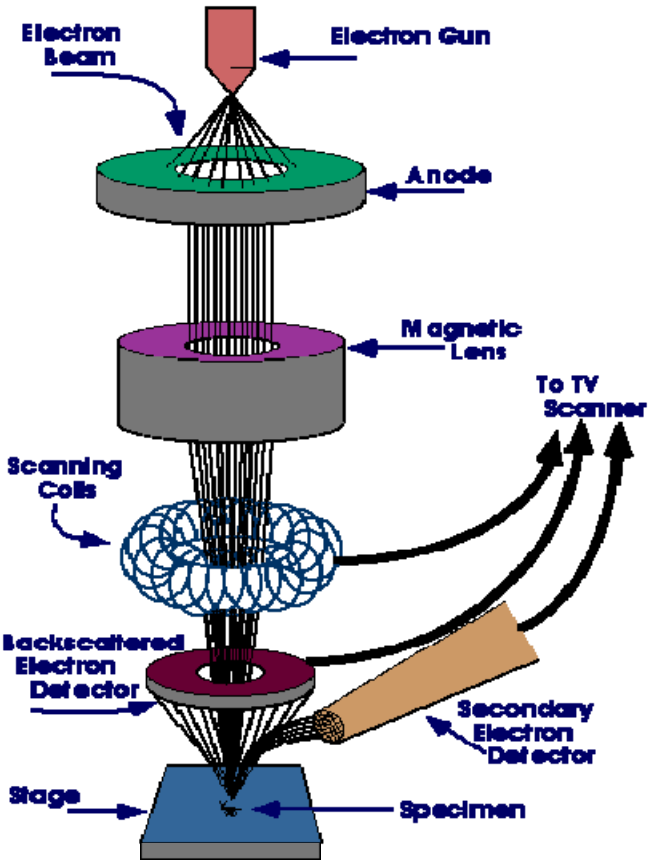

Figure 4.6. Diagramatic representation of the main components of SEM (Jim Schweitzer, http://www.purdue.edu/REM/rs/sem.htm accessed on 06/01/09).

4.14.2 Preparation of SEM samples

- Remove all water, solvents, or other materials that could vaporize while in the vacuum.
- Firmly mount all the samples.
- Non-conductive samples should be coated by covering the sample with a thin layer of conductive material so they are electrically conductive. This should be done in a vacuum (e.g. when using sputter coater) to avoid gas molecules interacting with the argon and gold during coating leading to uneven coating or no coating at all. Recent advances in thermal field emission scanning

electron microscopy (FESEM) technology, coupled with improved electron optics and use of variable pressure environments, allow imaging and analyses of uncoated samples using a wide range of primary beam energies between 0.1 and 30 keV (Schweitzer *et al*., 2008).

In summary, the advantages of SEM system with the various detectors, over the ordinary light microscopy is that it can provide the following**:**

- Higher resolution imaging, so closely spaced features on the specimens can be clearly identified and distinguished at high magnification.
- Provide both qualitative and quantitative analysis.
- Fast elemental mapping and/or analysis of the bulk material.
- Topographical and compositional information can be obtained.
- Digital output, which is easy to read and interpret.
- The fact that SEM uses electromagnets instead of lenses (used in light microscopy), the analyst has much more control in the degree of magnification.
- It gives clear images.

4.15 Powder X-Ray Diffraction (PXRD)

Bones are a composite material, consisting of an intimate interaction between mineral phase and organic component phase. Bone mineral is therefore a very important component of the bone in the preservation of biomolecular information (i.e. proteins like collagen) over archaeological time; hence the development of various screening techniques for the examination of the diagenetic state of the bone mineral fraction (Hiller *et al*., 2004). These techniques include among others the use of Fourier-transform infrared spectra (FTIR) to calculate indices of crystal change (Weiner and Bar-Yosef, 1990; Wright and Schwarcz, 1996); X-ray diffraction (XRD) to determine crystal composition, bone strain and bone density (Farquharson *et al*., 1997; Person *et al*., 1995); and particle-induced X-ray emission (PIXE) to examine diagenetic

chemical substitutions in the mineral structure (Reiche *et al*., 1999). Powder X-ray diffractometry has been used to characterise as well as confirm the state of preservation of the fossil bones, through the identification of the degree of alteration in the crystallinity of bone mineral (following the work of Posner, 1969; Schoeninger, 1979; Shipman *et al.,* 1984). Almost all buried bones analyzed so far using this technique appear to be altered to some extent. Numerous partially and completely fossilized bones still retain structure at this level while, apparently, having undergone some chemical alteration (Walker *et al.,* 1982). In another related study done by Reiche *et al*. (2003) on the morphology and mineral inclusions in the samples using SEM-EDX and XRD, they detected the presence of pyrite (FeS_2) precipitates together with some sulphur and barium bearing precipitates in fossil/archaeological bone. In this study both the fossil and modern bones were analyzed for mineral composition using a Powder X-ray Diffractometry method.

4.15.1 Principal behind XRD

X-ray powder diffraction is a versatile non-destructive analytical technique widely used to identify and characterize unknown crystalline materials. For the past years the primary use of this technique has been limited to phase identification, quantitative analysis and the determination of structural imperfections (strain, and crystal defects) based on material's diffraction pattern. Recently, applications have been extended to new areas, such as recognition of amorphous materials in partially crystalline mixtures, determination of crystal structures, identification of three-dimensional micro-structural properties as well as quantitative determination of different phases in multi-phase mixtures by peak ratio calculations (D. Louër and E. J. Mittemeijer, 2000). Thus PXRD can now reveal detailed information about the chemical composition and crystallographic structures of both natural (geological samples e.g. fossils, rocks and clay minerals) and synthetic/manufactured materials at micro and nano levels (http://www.panalytical.com/ accessed 06/01/09.

4.15.2 Crystal lattice and the diffraction process

Solid matter can be either described as amorphous, that means the atoms are arranged in a random way comparable to the disorder that exist in liquids or as crystalline where atoms are arranged in a regular, repeating planes that form a three-dimensional structure known as a crystal lattice. When a focused X-ray beam interacts with these planes of atoms, part of the beam is transmitted, part is absorbed by the sample, part is refracted, and part is scattered (diffracted). Both the direction and intensity of the diffracted beams depends on the orientation of the crystal lattice with respect to the incident beam. Hence X-rays are diffracted by each material (mineral) differently, based on what atoms make up the crystal lattice and their spatial distribution or arrangement in space. The arranged of atoms is such that they tend to form a series of parallel planes separated from one another by a distance *d*, which varies according to the nature of the material. For any crystal, planes exist in various orientations - each with its own specific *d*-spacing (http://www.aml.arizona.edu/labs/xrd.html. accessed 06/01/09). When an X-ray beam hits a sample, diffraction occurs and the distances between the planes of the atoms that constitute the sample can be measured by applying Bragg's Law (Flohr, 1997):

$n\lambda=2d \sin\theta$.

Where:

n is an integer (1,2.3…); λ (lambda) is the wavelength of the incident X-rays (1.54 Å for Cu); d (d-spacing) is the interplanar spacing generating the diffraction measured in angstrong and θ (theta) is the diffraction angle in degrees.

This law relates the wavelength of electromagnetic radiation to the diffraction angle and the lattice spacing in a crystalline sample. These diffracted X-rays are detected and then processed by a microprocessor converting the signal to a count rate. A scan of the sample through a range of 2θ angles ensures that all possible diffraction directions of the lattice are obtained due to the random orientation of the powdered material. The conversion of the diffraction peaks to d-spacings followed by comparison of these d-spacings with standard reference patterns, thus provide a structural fingerprint of the unknown and enables identification of specific minerals in

the unknown sample, since each mineral has its own set of unique d-spacings (Evans Analytical Group (EAG), http://www.cea.com/techniques/xrd.php. accessed 06/01/09).

4.16. X-Ray Fluorescence (XRF) spectrometry

The XRF mapping method provide information that enables us to examine the post-mortem alteration by determining the distribution and concentration profile of several elements which include among others Mn, Fe, Si, K, Mg, Al, P and Ca in transverse bone sections. Comparison of the concentration profiles of all elements present in fossil with modern bone (standard) reveal the possible acting diagenetic alteration processes and the possible mechanisms by which these exogenous elements find their way into the bone.

X-Ray Fluorescence (XRF) spectrometry is a high-tech, non-destructive analytical technique applied for qualitative and quantitative determination of elemental concentration in samples of various forms and nature by measuring their characteristic radiation (Yellepeddi *et al*., 1996; Birks and Hergoltz, 1978). The emission of to the characteristic radiation from the inner electronic shells of the atoms (Figure 4.8) under certain conditions forms the basis of elements identification of by X-ray methods. Thus the emitted quanta of radiation are X-ray photons whose specific energies permit the identification of their source atoms. The concentration of an element corresponds to the number of counts at a given energy per unit of time and this forms the basis of quantitative analysis. The fact that each atom has a unique energy pattern along with its electrons having distinct quantum numbers, the resulting characteristic X-rays are also unique with specific frequencies (energies) acting as fingerprints of each element.

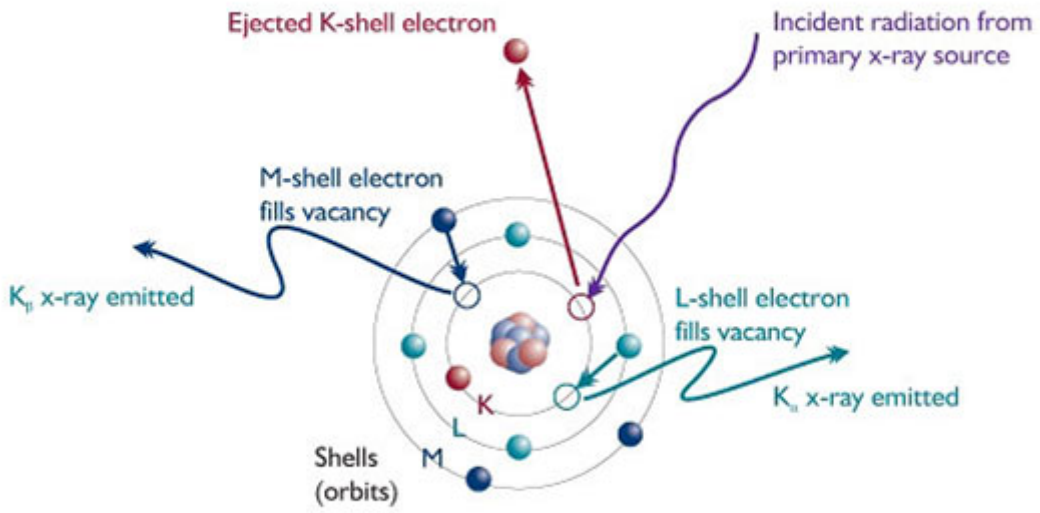

Figure 4.7. XRF process showing: ejection of an inner shell electron by a radioactive source creating an electron vacancy, vacancy is filled by transition of an outer shell electron of the atom, and emission of characteristic X-rays for element identification, (http://www.nmai.si.edu/ accessed 06/01/09).

4.17 Carbon, Hydrogen, Nitrogen and Sulphur (CHNS) elemental analyzer

Protein content

The nitrogen content (%N) in the whole fossil bone is correlated (proportional) to the amount of collagen remaining in the fossil. Generally the amount of collagen decreases as the bone degrades (Hedges and Law, 1989). Processes such as biological demineralisation, autolytic breakdown and deterioration, interaction with groundwater, and chemical degradation of the protein chains all contribute to the loss of collagen in fossil bone (Collins *et al*., 1995; Hedges *et al*., 1995; Jackes *et al*., 2001). Micro-organisms are known to play important roles in biogeochemical cycles, primarily as decomposers of dead organisms and also as participants in many redox processes, hence they are capable of uptake and transport of a variety of ions of

different valency states (Olson, 1983; Grant and Long, 1985). After all the soft tissue is gone, these micro-organisms are capable of metabolizing both the bone collagen and non-collagenous proteins, thus actively participating in bone decomposition process. Such microbial activity may be revealed macroscopically by staining or cracking of the bone (Grupe and Piepenbrink, 1989). However, the association of collagen with bone mineral renders the protein biologically unavailable for microbial degradation (Child, 1995; Collins *et al*., 2002), thereby contributing to its persistence and ultimate preservation in the fossil bones. In this study the amount of preserved protein (mainly collagen) was obtained through the analysis of percentage nitrogen in the bones using CHNS elemental analyzer. Therefore the preservation state of some organic bio-molecules in fossil samples was determined by comparing the amount of nitrogen (i.e. %N) in the fossil bones against that of the modern bone standard.

CHAPTER FIVE

SAMPLE PREPARATION AND ANALYSES

This chapter focuses on the methods used for preparation of samples prior to different kinds of analysis which include among others elemental, mineral, morphological, porosity and density analysis. Detailed procedures including instrumental parameters, reagents, cleaning of various apparatus and digestion steps to mention but a few, employed prior to each analysis are also outlined in this Chapter prior to presentation of the results in Chapter Six. It also gives a brief description of the sampling site, where the samples were collected. Macrographs of bone samples used for the various analyses are also shown. However, not all bone samples are shown in these tables, but only representative samples for each analysis done.

5.1 Sampling site

Bone samples of modern *Equus burchelli* and the fossil *Equus* species from the same skeletal element were obtained from the same region at Gladysvale Cave (GPS coordinates 25^{o} 54' S; 27^{o} 45' E), located in the Cradle of Humankind World Heritage Site (COH WHS), Gauteng, South Africa (Figure 5.1). Gladysvale Cave is located 13 km northeast of Sterkfontein, Swartkrans, and Kromdraai, on the northeastern slope of the Gladysvale Valley in the John Nash Nature Reserve on the farm Uitkomst, in the Krugersdorp District of South Africa (Berger *et al*., 1993). Sterkfontein, Swartkrans, and Kromdraai are the other major fossil hominid-bearing sites in South Africa.

The cave is situated in an eastern side of the valley, surrounded by trees, shrubs, and grass, while higher ground above the cave is grass-dominated (Pickering *et al*., 2007), whereas the region in which it is positioned is mainly open grassland with scattered trees and bushes to more densely wooded valleys (Acocks, 1953). The site consists of fossil-rich calcified and decalcified deposits, and importantly, it provides both modern and fossil animals of the same species. Dating by electron spin resonance (ESR) of the fossil bones from these calcified sediments suggests an age range of 578 to 830 Ky,

(Lacruz *et al*., 2002, 2003). Figure 5.2 is an illustration the cross sectional images of a samples of both the fossil and modern bones, used for CHNS analyses, porosity and density measurements, ICP AES and PXRD analyses. The displayed images are just a few samples selected as representatives from the rest of the other samples.

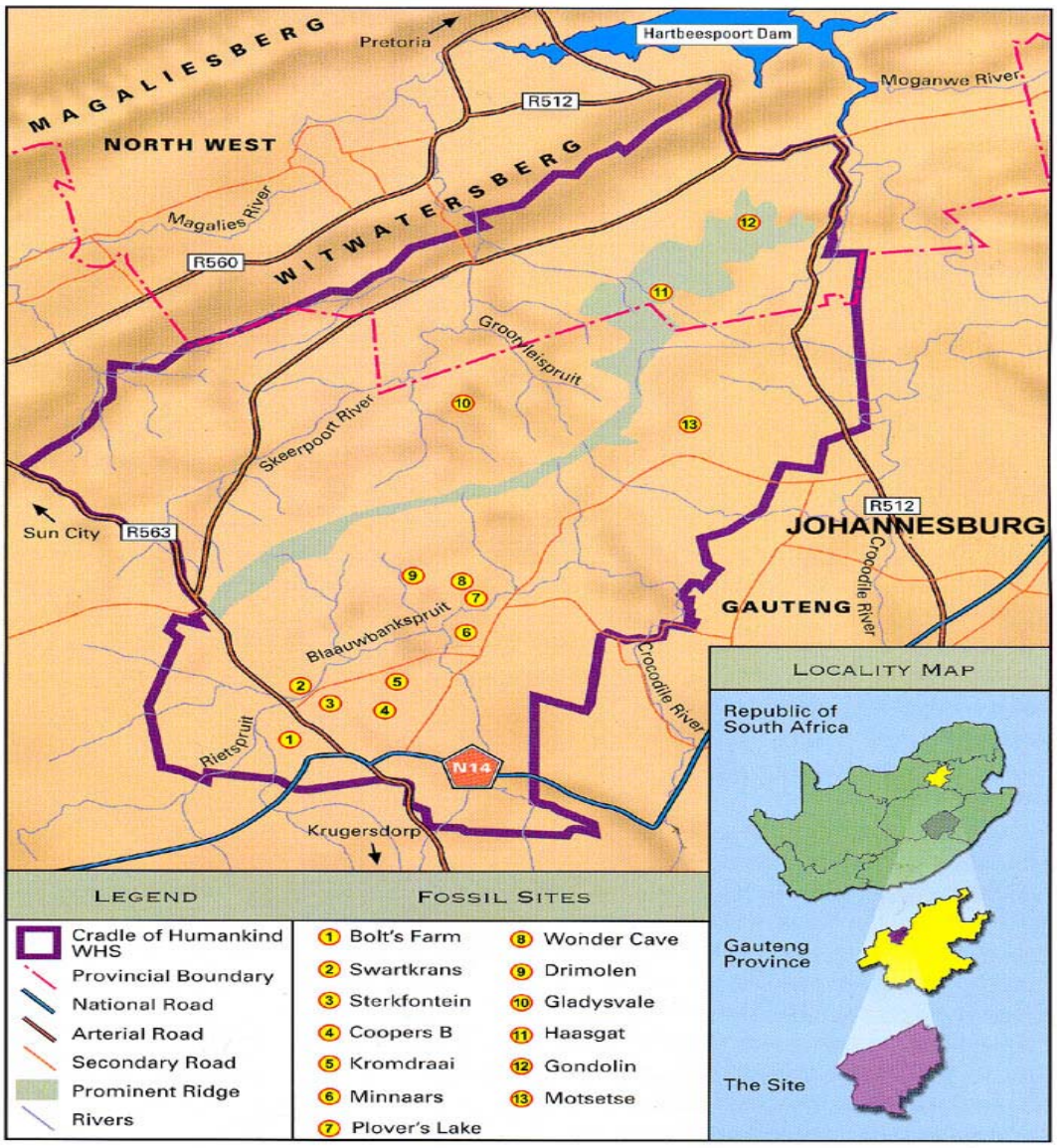

Figure 5.1. Sampling map showing the location of various fossil deposit sites, including Gladysvale where sampling was done, (Barber and Berger, 2002).

Sample	Fossil bone	Modern bone
1		
2		
3		
4		

Figure: 5.2. Macrographs of cross section of a sample of both the fossil and modern bones, used for CHNS analyses, porosity and density measurements, ICP AES and XRD analyses.

5.2 Burned bones

Bone samples were divided into three categories according to their physical outward appearance: black (see Figure 5.3), greyish -brown (see Figure 5.4) and Chalky-white (see Figure 5.5). Since fossil bones may be black due to mineral staining by black iron/manganese oxides (Gross *et al*., 1997), burning and/or both burning and staining, a chemical cleaning to remove the oxides from mineral coated fossil bones was used to differentiate between black fossil bones that are burned and unstained, burned and stained, and stained but not burned. Coated bones were used as standards (Figure 5.6) for comparison and any differences between the coated and burnt fossil bones were attributed to burning effects. The samples were obtained from baboons bones. The organic matter found together (in close proximity) with the burnt bones which is basically believed to be baboon wastes (in drooping) was also divided into five categories depending on the size, nature and appearance (see Figure 6.29, in Chapter Six): big marula, small nuts plus fine drooping, small nuts drooping only, fine drooping in lump form, very fine free drooping and leaves.

Figure 5.3. Category 1 black bones (likely to have been burnt at below 450^{o}C).

Figure 5.4. Category 2 greyish-brown bones (likely to have been burnt at 450 to 600^{o}C).

Figure 5.5. Category 3 chalky-white bones (likely to have been burnt above 700^{o}C).

Figure 5.6. Category 4 Fe/Mn-oxide coated bone (unburned bones)

5.3 ICP-AES: Fossil bone, burnt bone, modern bone and soil elemental analysis

5.3.1 Reagents/Chemicals used

All chemicals used were pure analytical grade reagents obtained from Merck and Rochelle Chemicals and any dilutions were made in 18.3 MΩ cm deionised water (MILLIPORE). Pure analytical grade concentrated nitric, hydrochloric, hydrofluoric and boric acids (Merck), and hydrogen peroxide (Rochelle Chemicals) were used for the sample digestion for soil, fossil and modern bones samples. Certified standard stock solutions containing various elements of interest in 2% HNO_3 from Ultraspec were used for the preparation of working standards.

5.3.2 Cleaning of various apparatus used

All apparatus and sample containers used were thoroughly cleaned with a metal free non-ionic detergent solution, rinsed with tap water, soaked in acid, and then rinsed

again with deionised water to minimize risks of possible contamination. Quartz, TFE, or glass materials were soaked in 10% HNO_3 (v/v) and 10% HCl (v/v), for 24 hours. All plastic materials used were soaked in, 10% HNO_3 (v/v). Reliable soaking conditions are 24 hrs at 70^oC. Thus all vessels to be used were washed, rinsed and then soaked overnight in 10% (v/v) analytical grade nitric acid and hydrochloric acid. Finally before use all the vessels were rinsed in high purity deionized water (MILLIPORE). This cleaning procedure was adapted from Environmental Protection Agency (EPA) method and was applied in order to minimize sample contamination.

5.3.3 Standard preparation and analysis

High purity 10 μg mL^{-1} ICP AES commercial stock standards from Ultraspec Pure Multielement Standard were used for the preparation of working standards. For the purpose of matrix matching, the standard and blank were prepared in the same acid content as the sample. The standard solutions used for the interference scans were also high purity grade in order to eliminate any error that might occur from potential contaminants in the standard solution. The blank was prepared by performing the sample preparation procedure without any sample present. Cr, Fe, Mn, Si, Al, Ca, Mg, S, P, K, Ti, Ni, Ba, Pb, Zn, V, Co, Mn, Cu, Sr, Na standards of 0.050; 0.100; 0.200; 0.500; 1.000 mg kg^{-1} were prepared from Ultraspec certified standard stock solution of 10 mg L^{-1} in 10% HNO_3 (v/v) solution for the instrument calibration and 3 replicates of each sample were run. The results are presented as the average of 3 measurements. Variability due to sample heterogeneity was assessed by analyzing individually prepared sample replicates.

5.3.4 Equipment and Apparatus

- Inductively coupled argon plasma emission spectrometer (GENESIS ICP-AES SPECTRO Analytical Instruments)
- Computer-controlled emission spectrometer with background correction.
- Optional mass flow controller for argon nebulizer gas supply.

- Optional peristaltic pump.
- Argon gas supply -- high purity (from AFROX 99.999%).
- Volumetric flasks of suitable precision and accuracy.
- Volumetric pipettes of suitable precision and accuracy.
- Filter funnel.
- Analytical balance (Precisa 180A).
- Microwave (Anton Paar Multiwave 3000 SOLV).

5.3.5 Soil sample preparation prior to analysis

Digestion: closed system microwave

All sample containers and various glass and plastic apparatus used were prewashed with detergents, acids, and deionized water as described in detail under section 5.3.2 to ensure that they were free of contamination before use.

The dry soil samples were refrigerated upon arrival from sampling. Reduction in sub sampling variance was achieved by reducing the sample particle size, and homogeneously mixing the resulting fines. Thus the samples were crushed and ground using a pulveriser to reduce sub-sample variability. The sample was then mixed thoroughly to achieve homogeneity and size-fractioned using a 90 μm stainless steel sieve. As recommended all equipment used for homogenization was thoroughly cleaned to minimize the potential of cross-contamination. For each digestion procedure, representative samples of up to 0.1000 g were weighed on an analytical balance into a high pressure resistant (capable of withstanding pressures of at least 30 atm (30 bar or 435 psi)) inert polymeric (PTFE) microwave digestion vessels. An acid mixture of 4.00 mL concentrated analytical grade hydrogen peroxide, 4.00 mL concentrated analytical grade nitric acid, 2.00 mL concentrated analytical grade hydrochloric acid and 2.00 mL concentrated analytical grade hydrofluoric acid were precisely and accurately transferred into the digestion vessels (liners) using a 1.00 mL micropipette. The use of several digestion reagents was necessary to achieve complete decomposition as well as total dissolution of the matrix, and the choice of the acid mixture was based on their individual properties discussed Appendix 4. All steps requiring the use of acids were conducted under a fume hood using appropriate

laboratory safety equipment. After the seals had been expanded using a seal-forming tool, they were then fitted on the reaction vessels and closed with a screw cap. The vessels were securely sealed with pressure relief caps and heated in the microwave system. Pressure relief devices were used for safety reasons since certain inert polymeric digestion vessels without pressure relief mechanisms may crack, burst, or explode in the unit under certain pressures during the digestion process. The pressure vessels were inserted in the rotor, and the closed rotor was placed into the microwave (Anton Paar Multiwave 3000 SOLV) and the door was then closed. The decomposition program was defined via a built in microcontroller, which controls the instrument, stores the sample information, has the method library and documents the reaction process. The samples were heated by means of microwave radiation following a preset temperature profile. The temperature profile was specified to permit specific reactions to occur and was set at 800 watts power for 15 minutes and remaining at the same power (holding time) for another 15 minutes for the completion of specific reactions. The microwave is fitted with a rotating turntable employed to ensure homogeneous distribution of microwave radiation within all the sample digestion vessels. The speed of the turntable was maintained at 3 rpm for effective digestion of the samples. The operating decomposing temperature and pressure were recorded simultaneously by means of a contactless pressure-temperature (P/T) sensor, installed in the upper rotor plate in the sensor unit. After the digestion, vessels were allowed to cool in the fume hood. The second step involved the complexation of fluoride where 12.00 mL 1 M boric acid ($H_3BO_{3\ (sat)}$) was added to each digestion vessel, where 1.00 mL HF is equivalent to 6.00 mL of H_3BO_3 to protect the quartz plasma torch of the ICP-AES from being damaged. The vessels were securely sealed and heated again in the microwave system at the same conditions as the first step. Crystal clear solutions were obtained at the end of the digestion process signifying total sample digestion. The solutions were transferred (totally) to a 50.00 mL plastic volumetric flask, and accurately made up to volume with deionized water. The samples were then taken for ICP AES analysis. Table 5.1 gives the microwave conditions used for soil digestion and the elements analysed. Table 5.2 and 5.3 present the acid mixture and the analytical task used respectively.

Table 5.1. Microwave closed system conditions for soil digestion

	Power [W]	**Ramp [min]**	**Hold [min]**	**Fan**
1.	800	15	15	1
2.	800	15	15	1

Table 5.2. Acid mixture and program

Acid Mixture	**H_2O_2**	**HNO_3**	**HCl**	**HF**
First step	4.00 mL	4.00 mL	2.00 mL	2.00 mL

Table 5.3. Analytical task

Sample	Soil samples: S1, S2 and S3
Target weight	0.1000 g
Elements of interest	Cr, Fe, Mn, Si, Al, Ca, Mg, S, P, K, Ti, Ni, Ba, Pb, Zn, V, Mn, Cu, Sr, Na
Analysis Technique	ICP-AES

5.3.6 Bone sample preparation prior to analyses

Bone samples were ground to powder using a milli-grinder (pulveriser). Samples from burnt, fossil, coated and modern bones were obtained from the cross section of each specimen. The powdered samples (0.1000 g) were each weighed into polytetrafluoroethylene (PTFE) liners. The samples were then subjected to closed system microwave digestion, as described in detail below. The solutions were quantitatively transferred to 50.00 mL volumetric standard flasks and were made-up

to the mark with deionized water. Analysis was done with ICP AES immediately after digestion.

Digestion: Closed system microwave

A closed system Microwave (Anton Paar, Multiwave 3000 SOLV) was used for the digestion of the samples. Reduction in analytical variability was accomplished through the use of appropriate recommended sample preparation procedures (adopted from US EPA standard methods) during the digestion process as well as sample analysis. The elements of interest were Cr, Fe, Ca, Ba, Al, Zn, V, Co, Mn and Cu. An acid mixture of 4.00 mL concentrated analytical grade hydrogen peroxide, 4.00 mL concentrated analytical grade nitric acid, 2.00 mL concentrated analytical grade hydrochloric acid and 2.00 mL concentrated analytical grade hydrofluoric acid were precisely and accurately transferred into the digestion vessels (liners) using a 1.00 mL micropipette. The use of several digestion reagents was necessary to achieve complete decomposition as well as total dissolution of the matrix, and the choice of the acid mixture was based on their individual properties discussed in detail in Appendix 4. All steps involving the use of acids were conducted under a fume hood using appropriate laboratory safety equipment. The vessels were securely sealed with pressure relief caps and heated in the microwave system. Pressure relief devices were used for safety reasons since certain inert polymeric digestion vessels without pressure relief mechanisms may crack, burst, or explode in the unit under certain pressures during the digestion process. The temperature profile was specified to permit specific reactions to occur and was set at 600 watts power for 5 minutes and remaining at the same power (holding time) for another 15 minutes for the completion of specific reactions. After the digestion, vessels were allowed to cool in the fume hood. The second step involved the complexation of fluoride where 12.00 mL 1M boric acid ($H_3BO_{3\ (sat)}$) was added to each digestion vessel where 1.00 mL HF is equivalent to 6.00 mL of H_3BO_3 to protect the quartz plasma torch of the ICP-AES from being damaged. The vessels were securely sealed and heated again in the microwave system at the same conditions as the first step. Crystal clear solutions were obtained at the end of the digestion process demonstrating total sample digestion. The

samples were then taken for ICP AES analysis. Table 5.4 gives the microwave conditions used for both fossil and modern bone digestion and the elements analysed, while Table 5.5 and 5.6 present the acid mixture and the analytical task used respectively.

Table 5.4. Microwave closed system conditions for fossil and modern bones digestion

	Power [W]	**Ramp [min]**	**Hold [min]**	**Fan**
1.	600	5	15	1
2.	600	5	15	1

Table 5.5. Acid mixture and program

Acid Mixture	**H_2O_2**	**HNO_3**	**HCl**	**HF**
First step	4.00 mL	4.00 mL	2.00 mL	2.00 mL

5.3.7 ICP-AES Instrumentation

All measurements were performed using a GENESIS ICP-AES atomic emission spectrometer (SPECTRO Analytical Instruments,) with radial plasma observation. The instrument is a simultaneous measurement Inductively Coupled Plasma, (used as a source of excitation of atoms and electrons) with a polychromator and a Charge-Coupled-Device (CCD) detector (for both qualitative and quantitative analyses). Simultaneous measurements of background analyte emission allows for accurate correction of transient background fluctuations.

Table 5.6. Analytical task

Sample	Bone samples: FbS1, FbS2, FbS3, FbS4, MbS1, MbS2, MbS3 and MbS4
Target weight	0.1000 g
Elements of interest	Cr, Fe, Ca, Ba, Al, Zn, V, Mn, Cu, Mg, S, K, Sn, Li, Ni, Pb, Sr, P, Ti, and Si
Analysis Technique	ICP-AES

The system was purged with ultra purity Argon gas (99.999%). The instrument was controlled by Smart Analyzer Window Software. Table 5.7 shows the instrumental operating parameters that were used during the analysis.

Table 5.7. ICP AES operating conditions.

Condition	setting
RF Power	1400 W
Coolant Gas Flow	14.00 L min^{-1}
Auxiliary Gas Flow	1.00 L min^{-1}
Nebulizer Gas flow	1.00 L min^{-1}
Sample Pump Flow	2.00 mL min^{-1}
Sample Aspiration Rate	2.00 mL min^{-1}
Replicates	3
Plasma Torch	Quartz
Plasma Viewing	Radial
Spray Chamber	Single pass
Nebulizer	Crossflow
Processing Mode	Area

Figures 5.7, 5.8 and 5.9 are the calibration curves for various elements analysed for soil, fossil and modern bone samples. The text colour of each equation corresponds to the curve (line) of the same colour.

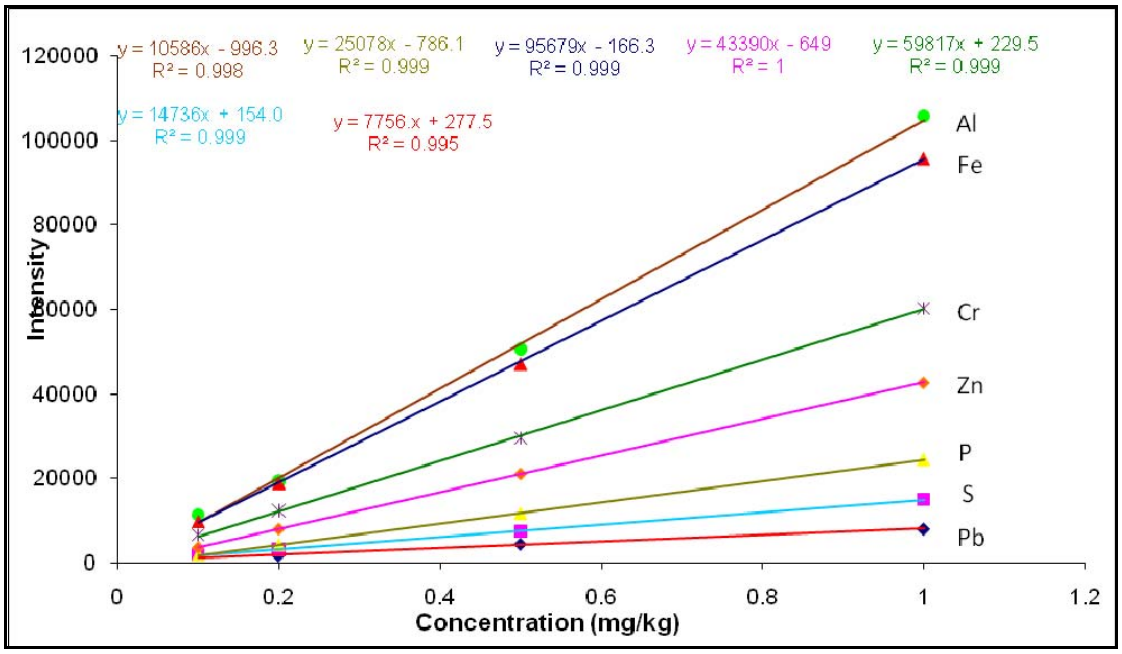

Figure 5.7. ICP AES calibration for Pb, Sn, P, Zn, Cr, V, Fe and Al.

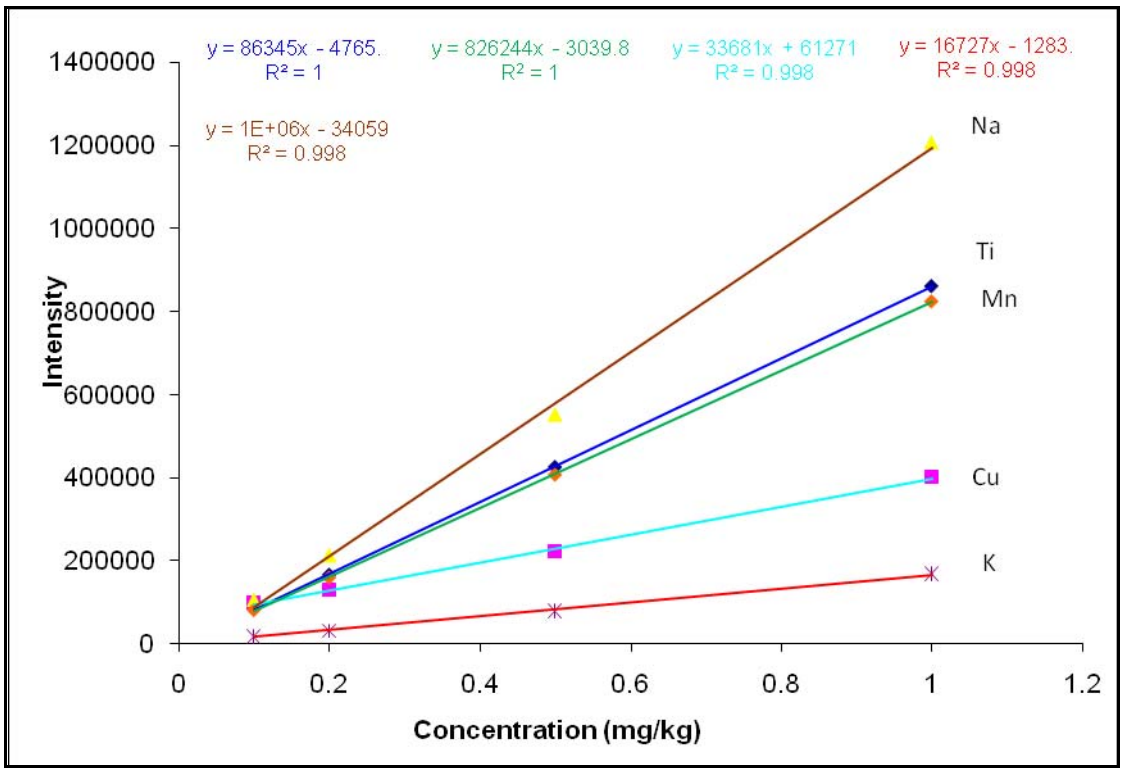

Figure 5.8. ICP AES calibration for K, Cu, Mn, Ti and Na.

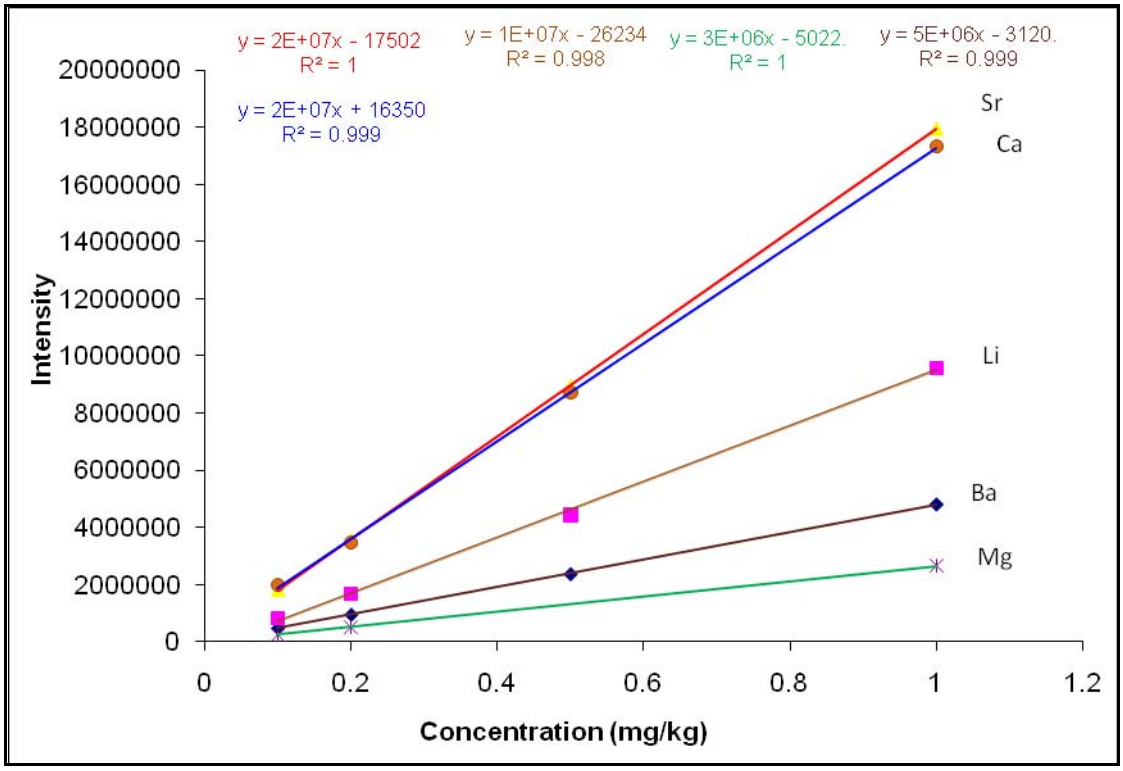

Figure 5.9. ICP AES calibration for Mg, Ba, Li, Ca and Sr.

5.3.8 Burnt bones: Differentiating between burning and oxide staining

It should be noted that colour-based identification (for fossil burned bones) is only applicable to modern burned bones, fossil bones may be black due to mineral staining, such as by black manganese oxides (Gross *et al*., 1997). On the other hand, presence of manganese or some other metal oxide on fossil surface does not automatically imply that the bones are not burned, since they could be black due to both burning and staining (Sillen & Hoering, 1993). Applied here is a new, relatively simple chemical procedure to remove the oxides from soil/mineral coated fossil bones, prior to elemental composition analyses of both burnt and coated fossil bones using CHNS as well as ICP-AES. Therefore an analytical method developed by Cukrowska *et al*. (2005) that makes use of hydrogen peroxide to remove oxides from bones was employed. Coated bones were also subjected to the same conditions, treatment and analysis (as burnt bones) as references for comparison with burnt fossil bones. Any coated versus burnt fossil bones changes were ascribed to burning effects. The

methods mentioned above were used for differentiating between black fossil bones that are burned and unstained, burned and stained, and stained but not burned.

Procedure: Removal of mineral coating (Fe/Mn oxides)

The bones were left in 1.8 Molar, freshly prepared solution Hydrogen peroxide (AR 30%, from Saarchem) for 24 hrs under a fume hood to expel any gas produced during the reaction. The cleaning method relies on the use of hydrogen peroxide as a reducing agent to convert Mn^{4+} into soluble Mn^{2+} under optimized conditions (equation 5.1). Likewise hydrogen peroxide can be used to reduce Fe^{3+} to its soluble Fe^{2+} species (equation 5.2) (Cukrowska *et al*., 2005):

$$MnO_2(s) + H_2O_2\,(aq) + 2\,H^+ \rightarrow Mn^{2+}\,(aq) + O_2\,(g) + 2\,H_2O\,(l) \qquad (5.1)$$

$$Fe_2O_3\,(s) + H_2O_2\,(aq) + 4\,H^+ \rightarrow Fe^{2+}\,(aq) + O_2\,(g) + 2\,H_2O\,(l) \qquad (5.2)$$

The above two equations clearly show the mechanism behind the use of hydrogen peroxide to dissolve (i.e. to reduce) the manganese and iron oxide from the bone surfaces into solution, thereby bringing about surface cleaning.

5.4 Morphological studies (high resolution analysis and imagery) using scanning electron microscopy (SEM)

Textural changes in bones during fossilisation

Scanning electron microscope analyses were performed with a JEOL-JSM-840 microscope. The specimens were coated with a conductive substance, carbon, deposited as a fine film (only nanometers thick) on the surface of the specimen under vacuum. The specimens were introduced into the SEM. High vacuum (10−5 torr or less) was employed which allows the unscattered flow of electrons from the source to the surface of the sample. The high-energy beam generated secondary electrons that were transmitted from the surface at intensities dictated by inherent sample properties

to a detector capable of translating electron counts into a three-dimensional topographic image. Micrographs of both the fossil and modern bones were taken at varying magnifications (X250-X10 000) to fully elucidate the effects and extent of diagenesis and also provide a conclusive morphological comparison between fossil and modern bones, illustrating the degree of alteration or degradation that has occurred in the fossil bones. Thus the morphological examination of fossil bone gives vital information about the state of preservation i.e. the extent of microbial post-mortem destruction.

5.5 Crystallographic characterisation (mineralogical analysis) using Powder X-ray diffractometry (PXRD)

Fossil and modern bone sample preparation prior to analysis

The samples were ground to fine powder of 90 μm using a pulveriser. The samples were then mixed thoroughly to achieve homogeneity. All equipment used for homogenization was thoroughly cleaned to minimize the potential of cross-contamination. Samples from both fossil and modern bones were obtained from the cross section of each specimen. The samples were then taken for mineral composition determination using the PXRD instrument. The samples were then set on the diffractometer fitted with a copper anticathode tube, a scintillation counter and a sample holder rotating at around one hundred times per minute, in order to give a better statistical distribution of the crystallites and thus improved measurement reproducibility.

5.6 Bone porosity, density and water absorption

5.6.1 Apparatus

(i) *Balance*, equipped with a stirrup for weighing the specimen in both air and water to an accuracy of 0.1% of the mass.

(ii) *Water tank*, fitted with a device to maintain a constant water level, and of sufficient size to allow the specimen on the stirrup to be fully immersed to constant depth.

(iii) D*rying oven*, well ventilated.

5.6.2 Procedure for determination of volume

Specimens were placed on the stirrup and fully immersed in the tank. Measures were put in place to ensure that the stirrup did not touch the bottom of the tank and that air bubbles were not trapped on the surface of the specimen and the stirrup. The completely immersed specimens were weighed and their apparent mass m_w recorded (in kg), correcting for the apparent mass of the empty stirrup when weighed immersed in water to the same depth as when holding the specimen. The specimens were removed immediately from the stirrup, weighed in air after wiping the surplus water from the surface using a moist cloth and their mass m_a (in kg) recorded.

Calculation:

Taking the density of water as 1000 kg m^{-3}, the volumes, V (in m^3) of the specimens were calculated from the following formula:

$$V=m_a-m_w/1000 \qquad (5.3)$$

5.6.3 Bone density

Bone density has been considered as one of the key parameters in determining the overall survival of bone in the burial environment. It has been discovered that bones with high bulky density have a greater potential for high rates of chemical degradation than those with low bulky density. Where bulk density (or Volume density) is defined as a measure of the density of a bone including vacant pore spaces, so bones with higher porosity have low bulky density (Smith *et al*., 2008).

5.6.4 Procedure for determination of saturated density

The specimens were fully immersed in water at 20^{o}C until a constant mass was achieved as shown by two measurements, taken 24 hours apart, giving a difference of less than 0.2% in the mass of the wet specimen in air. Before each weighing, surplus water from the specimens' surface was wiped using a moist cloth. The constant mass *m* (in kg) was recorded.

Calculations

The volume (*V*) was obtained by the water displacement method described above and the saturated density was calculated using the formula:

$$P=m/V \qquad (5.4)$$

5.6.5 Water Absorption

Procedure

The samples were placed in the drying oven for 72 hours. The samples were cooled for 24 hours in a desiccator, and then weighed before complete immersion in a water tank at 20^{o}C for 30 minutes. The bulk of water was removed by shaking the samples and drying them with a cloth before weighing.

Calculation

The measured absorption of each specimen was calculated as the increase in mass resulting from immersion expressed as a percentage of the mass of the dry specimen.

5.7 Elemental analysis of carbon, hydrogen, and nitrogen composition in fossil, coated, burnt and modern bones by CHNS

Bone samples for CHNS from both coated and burnt bones were obtained by surface scraping approximately 1.5 mm deep removed using a Teflon spatula to avoid contamination. While bone samples for CHNS from both fossil and modern bones were obtained from the whole bone cross section, to get a homogenous representative composition of the bone. Powdered bone sample (2.000 mg) in a tin capsule and analyzed with a CHNS elemental analyzer (LECO CHNS-932). The samples were placed in the sample loading chamber and held there until a dose of oxygen had been released. Each sample was then dropped into the furnace at the same time the oxygen arrived. The samples were combusted in a quartz oven in an oxygen-rich environment at 1000^{o}C and the evolved gases (CO_2, N_2, and H_2O) were carried through the system by helium carrier gas, swept and purified successively through the oxidation tube packed with tungsten trioxide (which adds oxygen) and then reduced in a copper furnace (with copper sticks, which remove oxygen). The water was swept through the non-dispersive infrared absorption detection system where it was measured. After trapping of water using anhydrone, the amounts of carbon and nitrogen were measured by thermal conductivity detector by comparison of the integrated areas with those of a standard (corngluten). Adjustments for blank, calibration and weights were applied to the final integrated signal and the answers were displayed as weight percent C, N, and H.

5.8 XRF mapping

5.8.1 XRF mapping on the modern bone specimen

XRF mapping analyses was performed on the modern bone sample using the SPECTRO MIDEX Micro-XRF system (in Germany), in order to determine possible diagenetic (i.e. alteration) processes that have occurred in their burial environment (i.e. dissolution, uptake and diffusion of exogenous ions).

Sample Preparation

The sample surfaces were first cleaned from loose particles by using a soft brush. The bone fragments were cut to get a fresh cross sectional surface. The fragments were then mounted into modelling clay to position the bones surface perpendicular to the X-ray beam. Table 5.8 presents the measurement conditions used for qualitative element distribution pattern of modern bone surfaces.

Table 5.8. Measurement conditions used for qualitative element distribution pattern of modern bone surfaces (MB3).

Measurement cycle	1
Spot size	0.5 mm
Tube Voltage	45 kV
Measurement time	60 s per spot

All measurements were performed in helium atmosphere.

5.8.2 XRF mapping on fossil bone specimens

Sample preparation was achieved by cutting each bone fragment into two pieces so as to expose a fresh cross sectional surface. The fragments were then plugged into modelling clay to hold them perpendicular to the X-ray beam. The XRF-maps for fossil bone specimens were obtained from Kuczumow *et al*. (2010). Table 5.9 are the measurement parameters used for different fossil bone samples.

Table 5.9. Measurement parameters used for different fossil bone samples, (Kuczumow *et al*., 2010).

Measurement	**Fossil sample CD 21245**	**Fossil sample CD 21231**
Target	Direct excitation	Direct excitation
Collimator/ mm	0.1	0.1
Spot size/ mm	0.2	0.2
Tube voltage/ kV	45	45
Measurement time/ s	60	10

CHAPTER SIX

RESULTS AND DISCUSSION

Presented in this chapter are the results and detailed discussions of bone characterization conducted using various techniques: Inductively Coupled Plasma Atomic Emission Spectroscopy (ICP AES); Scanning Electron Microscopy (SEM); Powder X-ray Diffractometry (PXRD); X-Ray Fluorescence (XRF) mapping; bone porosity and density measurements as well as carbon, hydrogen and nitrogen analysis (CHN).

6.1 ICP-AES

The results of the soil, fossil and modern bone analyses are shown in Figure 6.4 and Table 2A.1 and 2A.2 in the Appendix. In each case three replicates were analysed and the concentrations are reported as average concentrations for 3 measurements in mg kg^{-1}, Table 2A.1 and 2A.2 in the Appendix. The final concentrations were converted to natural logarithm in order to create the chart in Figure 6.1.Error bars (uncertainty) were also included in the results for statistical reasons.

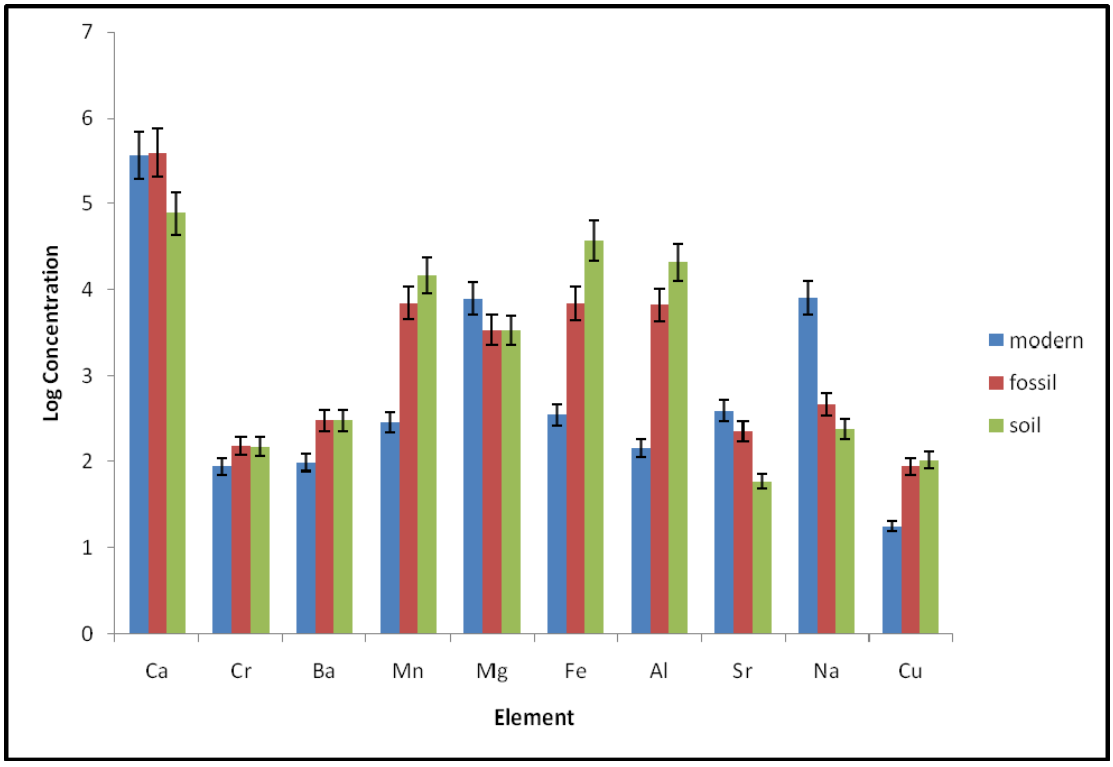

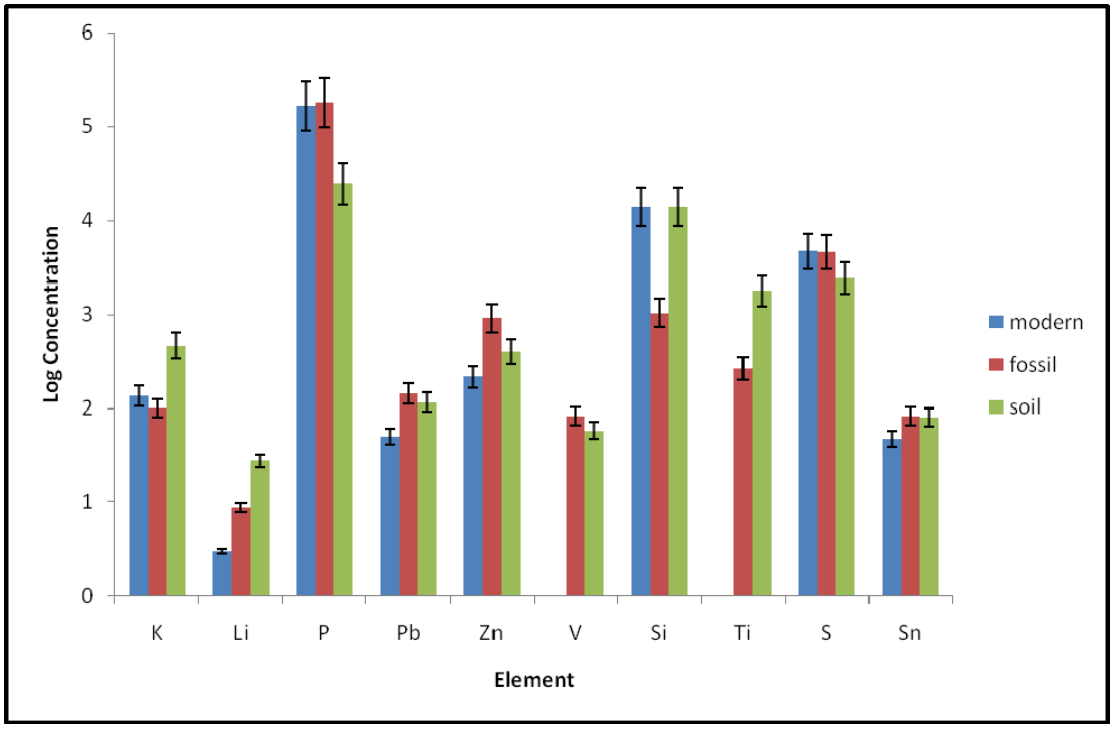

Figure 6.1. Comparison of the elemental concentration in the modern bone, fossil bone and the surrounding soil.

Discussion

The results in Figure 6.1 show no significant differences in the amount S and K between modern and fossil bones. These are statistically indistinguishable, and thus there is no evidence that S and K have been altered in any way through the fossilisation process. Likewise, there is no evidence that exogenous S and K ions have become incorporated to a significant or detectable extent in fossil bones. Hence S and K are not good indicators of elemental enrichment in this case.

It is not the case; however, that no elemental concentrations have increased in the fossil samples, where the exposed bone mineral component hydroxylapatite is well known for its ability to scavenge trace elements from soil pore waters. The mean levels of Mn, Fe, Ba, Cr, Zn, Al, Cu, Ti and V in fossil specimens surpass their biogenic ranges in modern bone (Figure 6.1). Since the average concentrations of these elements are higher than the biogenic range; these bones are interpreted as having undergone a post-mortem gain of these elements. Powder X-ray diffraction results (Figure 6.7-6.10) have also shown the presence of calcium carbonate containing minerals in fossil bones and this can best explain the elevated levels of Al, Ti, Mn, Fe, Cr, Zn, Cu, and V. Due to the fact that the surfaces of calcium carbonate minerals are reactive, they may continuously undergo surface precipitation-dissolution (solubility) reactions with dissolved Ca^{2+} and HCO_3^- (McKinley *et al*., 2007). In the presence of these ions (Al^{3+}, Ti^{3+}, Mn^{2+}, Fe^{2+}, Cr^{3+}, Zn^{2+}, Cu^{2+}, and V^{3+}), the interaction of the solute ions (Ca^{2+} and HCO_3^-) to precipitate or dissolve calcite in these fossil bones could affect the concentration of Al^{3+}, Ti^{3+}, Mn^{2+}, Fe^{2+}, Cr^{3+}, Zn^{2+}, Cu^{2+}, and V^{3+} and limit their mobility through co-precipitation leading to the accumulation of these elements in the fossil bones. This hypothesis has been experimentally proven by Parkman *et al*. (1998) using calcite in the presence of solutions containing Ca^{2+} and Sr^{2+} in which the mobility of Sr^{2+} was limited through co-precipitation. Several other field studies of calcites, where co-precipitated Sr^{2+} showed variation in solid phase concentration, indicating its immobilization during migration in carbonate-bearing media include the work of Ali (1995); Vaniman and Chipera (1996); Wogelius *et al*. (1997). The surface complexation of such cations to fixed–charge and amphoteric sites on mineral surfaces is a competitive reaction dependent upon factors such as surface site concentration, surface charge and relative

solute concentrations (McKinley *et al*., 2007). These elements can also be incorporated into the fossil bone through cation exchange processes.

The mean levels of Na, Mg and Sr in fossil specimens are lower relative to those in the modern bone, indicating post-mortem loss of these elements in fossil bones during the diagenesis process. Thus fossil bone apatite has been shown to become enriched in some elements that are abundant in diagenetic environments (soils, sediments and groundwater), but are characteristically very low in fresh bones, and on the contrary is depleted in some elements that are naturally bound into the apatite matrix. Millard and Hedges (1999) pointed out that during diagenetic recrystallization of the bone trace elements are scavenged from surrounding soil/sediment waters via a diffusion-adsorption process. Thus in this case Mn, Fe, Ba, Cr, Zn, Al, Cu, Ti and V were supplied from external surfaces of the bone, and diffused through the bone pore spaces into the bone before being incorporated into the bone matrix. In this case the process of post-mortem uptake of these elements became limited by their supply and availability in the soil water and effectively ceased when recrystallization closed all pore spaces originally occupied by collagen. Therefore it follows that the duration of uptake of these elements into the fossil bone was controlled by rate of bone recrystallization. This mechanism/model of element uptake in the bone is based on the assumption that the rate–limiting process in diagenetic alteration is the movement of solutes to, from, or within the bone.

Chemical change during fossilisation results in compositional heterogeneities and concentration gradients within the texture of fossil bone. The results confirm that elements are not distributed homogeneously in fossil bone but rather show a pattern of Mn, Fe, Ba, Cr, Zn, Al, Cu, Ti and V enrichment in excavated fossil bones compared with modern bones. This pattern is characteristic of elemental enrichment of the fossil bone from the surrounding soil. The increase in Fe, V, Ba, Cr, Zn, Al, Cu, Ti and Mn and concurrent loss of Na, Sr and Mg in the fossil bone compared to modern bone also confirms how porosity affects post-mortem elemental uptake and loss. Thus porous tissue of bone functions as a pathway of least resistance for postmortem elemental uptake and loss.

The chemical disparities between the modern and fossil bones can be attributed to significant diagenetic alteration, through the introduction of exogenous material to the existing matrix, and chemical alteration of the original bone matrix during the

fossilisation processes. These changes may occur in the form of secondary mineral precipitation in cracks, sorption of extraneous ions or phases onto the surface of the existing bone matrix, exchange of material from the depositional diagenetic environment matrix, chemical leaching and replacement of the original bone matrix by secondary material (Jacques *et al*., 2008). Clay particle inclusions account for the high levels of Al in fossil bones relative to modern bones.

The higher Fe and Mn values in fossil bones as compared to their modern counterparts are not surprising, for fossils from the Cradle of Humankind are commonly stained by iron and manganese as confirmed by the study done by Cukrowska *et al*. (2005). From the results obtained (Figure 6.1), a diagenetic interpretation of the mean elemental concentration identified in the skeletal remains is consistent with the results from the analysis of the soil samples in which the fossil bones were embedded. In most cases, the average elemental concentrations found in the soil are of the same order of magnitude as those found in the fossil bone, with the exception of Zn, P, Ca and S which displayed higher mean values in fossil bone than those found in the soil. These exceptions can be attributed to the accumulation of these elements in fossil bones, as pointed out by Radosevich (1993), that in such instances where concentrations are consistently higher in the bone than in the soil it reflects the accumulative nature of the diagenetic process.

Analysis of the soil which was in contact with the fossil bones indicated relatively higher amounts of Al, Fe, Mn, Ba, K, Si, V and Ti in the soil than in both the fossil and modern bones. High levels of Al and Si is simply due to the presence of clay soils which contains high concentrations of Si and Al. Oxyhydroxides contain abundant Fe, Mn, Ba (Kohn *et al*., 1999) and this explains the strong increase of these elements in soil. Overall, calcium and phosphorous were found to occur in the highest concentration levels in both the fossil and modern bone as compared to other elements since they are the major constituents that make up the bone hydroxylapatite mineral ($Ca_{10}(PO_4)_6(OH)_2$).

The Ca level in fossil is slightly higher than in modern bones. This is a result of the introduction of exogenous Ca into the porous bone structure, most likely in the form calcium carbonate, precipitated at the surface of the bone pores, since the cave

environment contains a lot of calcite and dolomite as confirmed by the PXRD rock results (Figure 6.11; 6.12). The same scenario has been identified in modern human bones experimentally by Shinomiya *et al*. (1998), in which an initial decrease of Ca and P was observed after six months of burial due to the demineralization process. After 24 months the levels of these two elements increased exceeding above the pre-burial levels, supporting the hypothesis that Ca and P migrated into the bone from embedded soils (Goodwin *et al*., 2007). However, our measurement techniques limit us from identifying and distinguishing, on a local scale, between calcium atoms from original bone mineral hydroxylapatite and those from naturally present or exogenous carbonates. Nevertheless other methods exist such as X-ray absorption fine structure measurements, X-ray Absorption Near Edge Structure (XANES) or Extended X-Ray Absorption Fine Structure /EXAFS) that permit the analysis of chemical speciation and could facilitate such discrimination (Reiche, 2003). Modern bones contain high amounts of Mg, Sr and Na than fossil bones. This pattern is characteristic of leaching of the respective elements from the fossil bone to the soil.

Conclusion

Fossil bones are unquestionably altered chemically compared to their modern counterparts. However, Ca, S and K in fossil bones show much less alteration than Mn and Fe. Thus fossilisation is a complex series of events that occurs over a variable timescale resulting in the preservation, destruction or modification of bone bioapatite. Calcium and phosphorous remain the major constituents of these bones. In some cases postmortem uptake and recrystallization may result in variable Ca and P levels surpassing levels found in modern bone.

6.2. Morphological studies (high resolution analysis and imagery) using scanning electron microscopy (SEM)

Textural changes in bones during fossilisation

Modern and fossil microstructures of zebra bones were observed under SEM and the results are shown in Figure 6.2. Several microcracks were observed in fossil bones with differing trajectories from those of natural cleavage of bone tissue, such as cement lines encircling secondary osteons. Microcracks in fossil bones may result from a variety of factors, including the remineralization process due to microbial activity, organic matter loss, which leads to shrinkage of the skeletal structure, or exposure to high temperatures. Increase in bone microcracks is always accompanied by an increase in brittleness of the bone.

Paying more attention to diagenetically altered fossil samples, it was observed that bone microstructure were totally reorganised and characterized by irregular and varying pore sizes. The results are in agreement with those obtained by Guarino *et al*. (2006).

Fossil bone	Modern bone
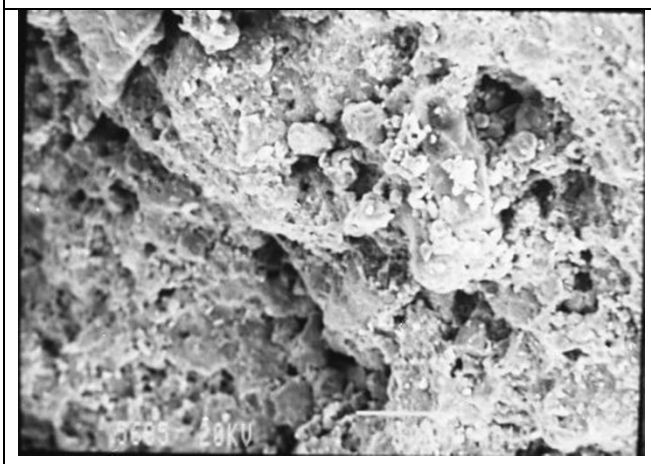	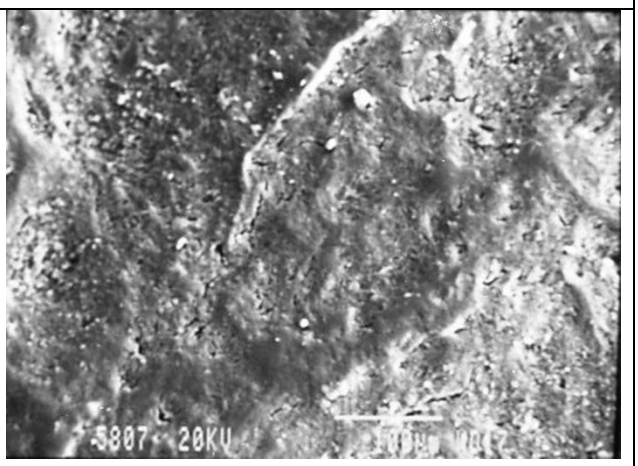
FBS2 X250	MBS4 X250
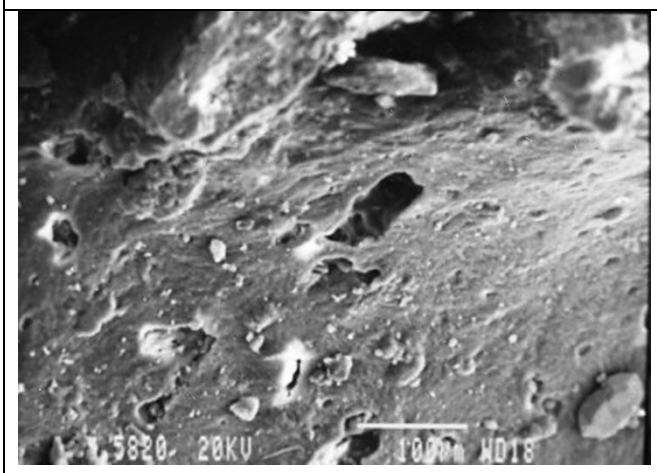	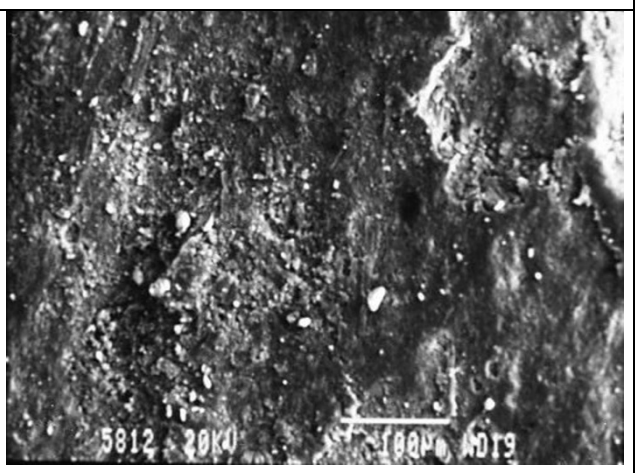
FBS1 X250	MBS3 X250
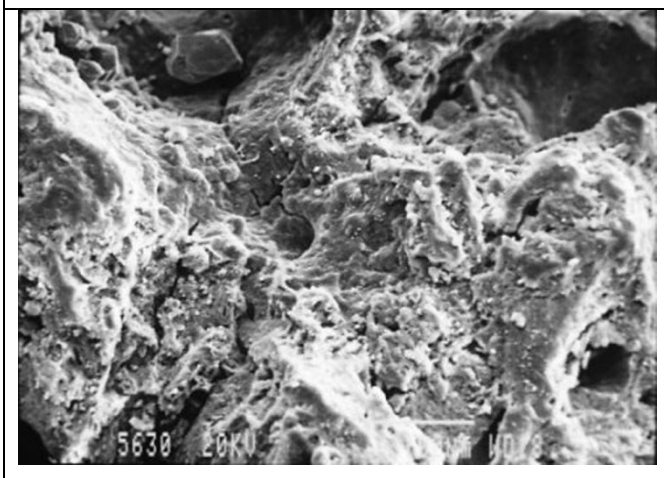	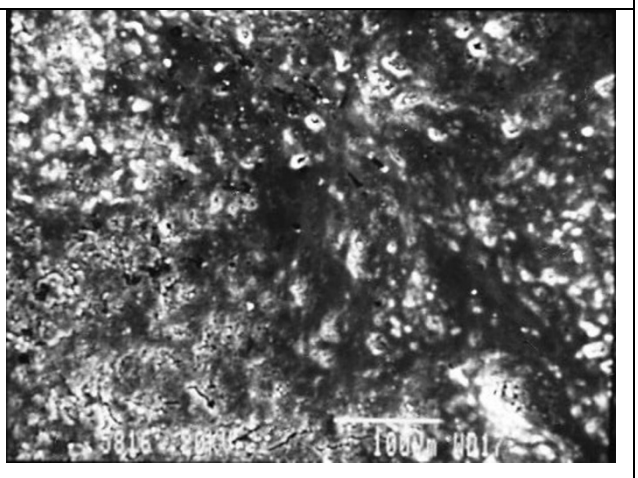
FBS4 X250	MBS2 X250

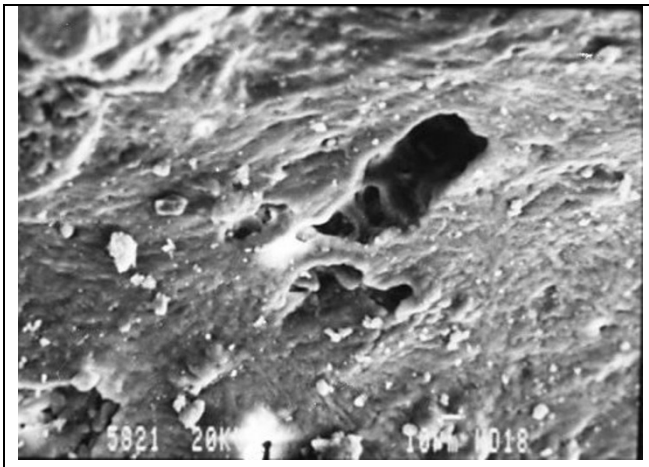	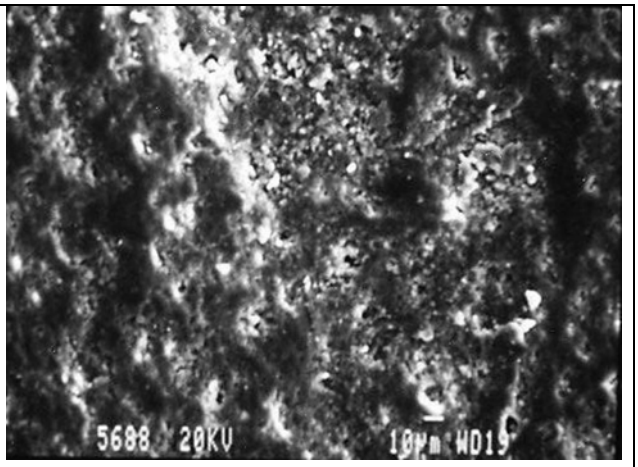
FBS2 X450	MBS1 X450
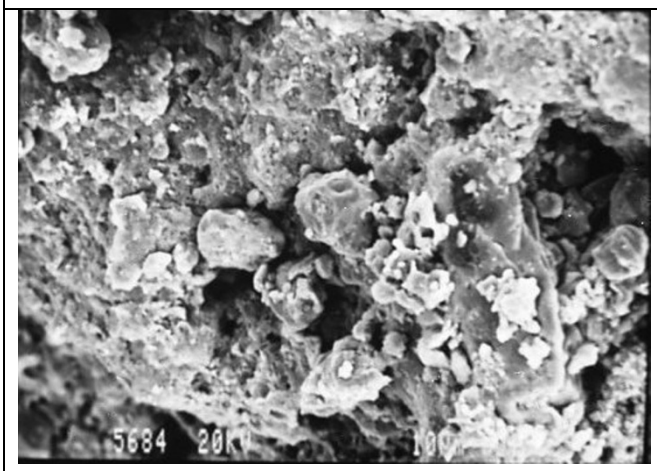	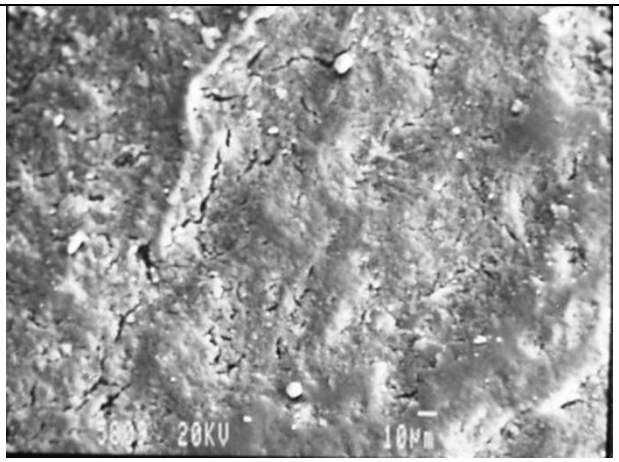
FBS2 X450	MBS4 X450
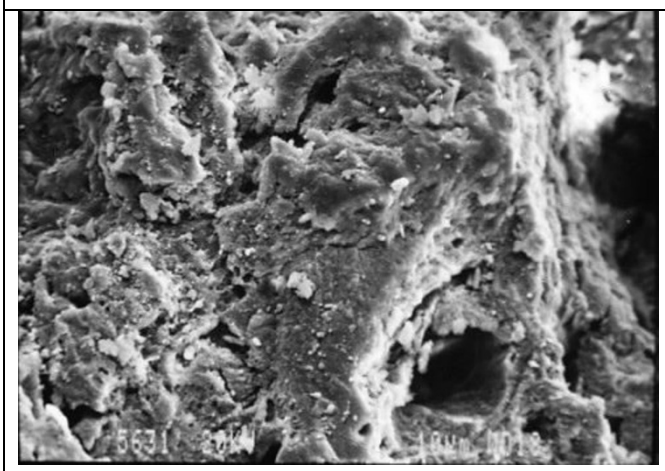	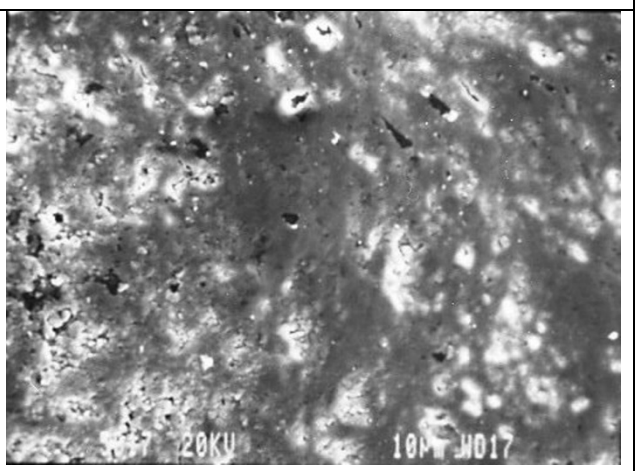
FBS4 X450	MBS2 X450

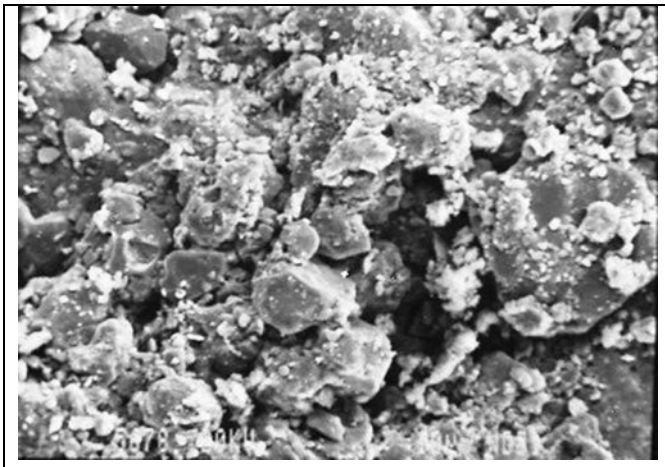	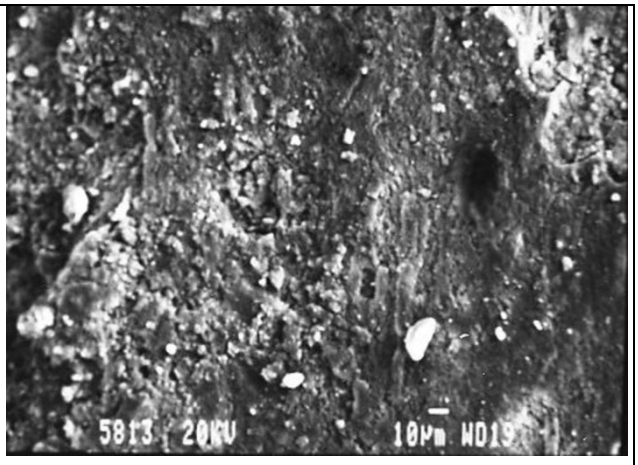
FBS3 X450	MBS3 X450
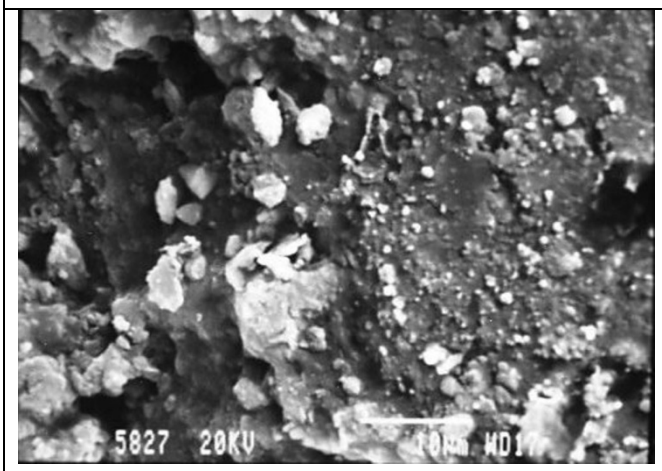	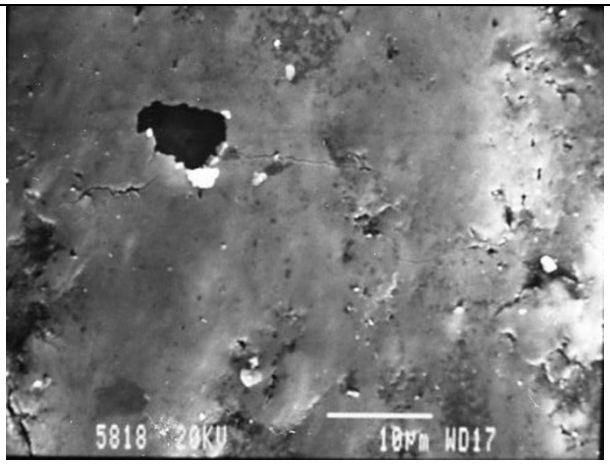
FBS3 X25000	MBS2 X2500
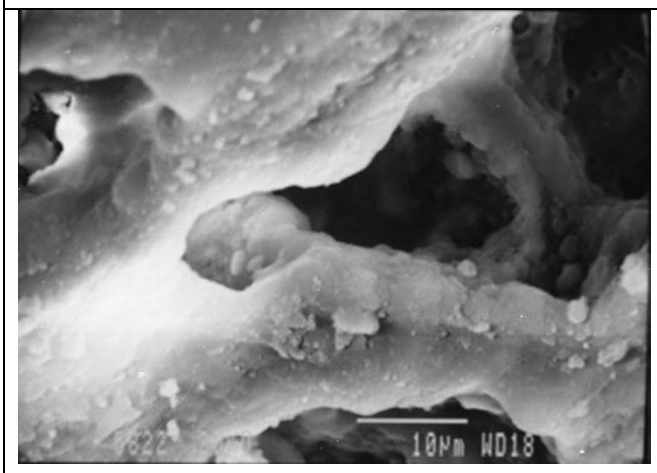	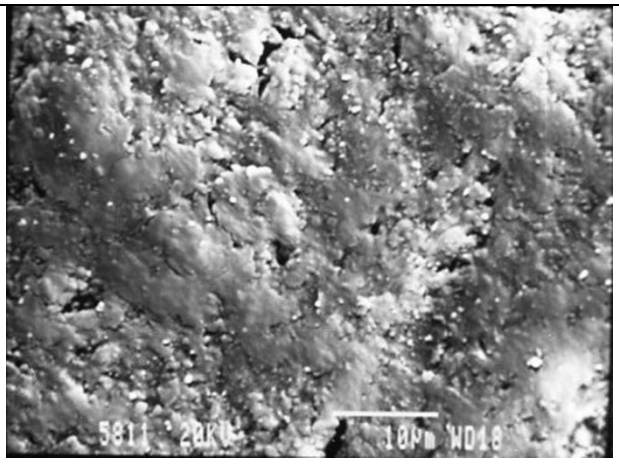
FBS1 X2500	MBS4 X2500

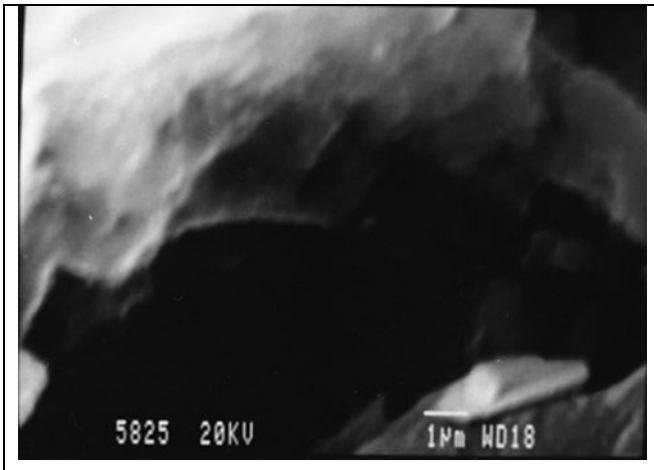

FBS1 X10 000

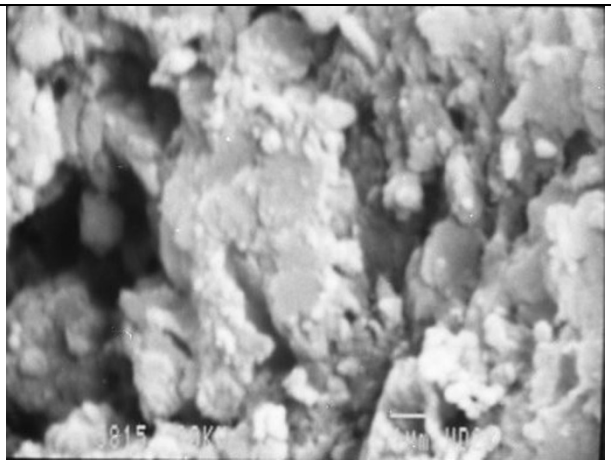

MBS3 X10 000

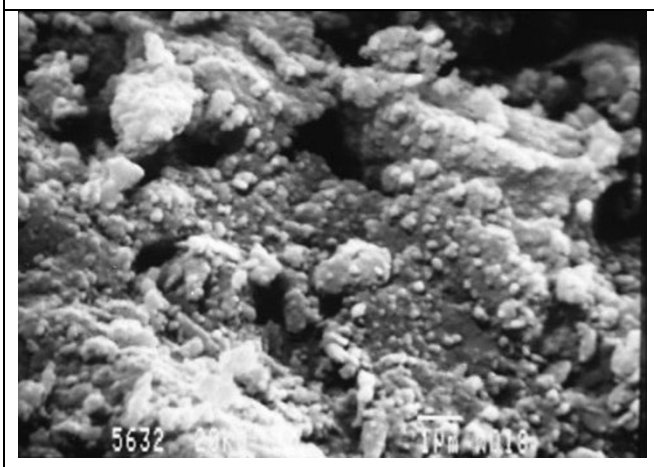

FBS4 X10 000

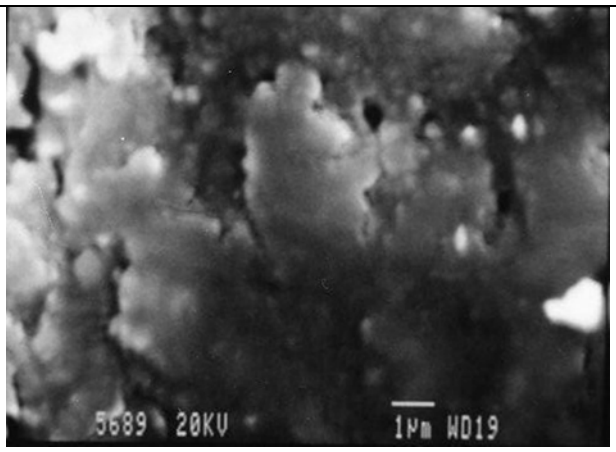

MBS1 X10 000

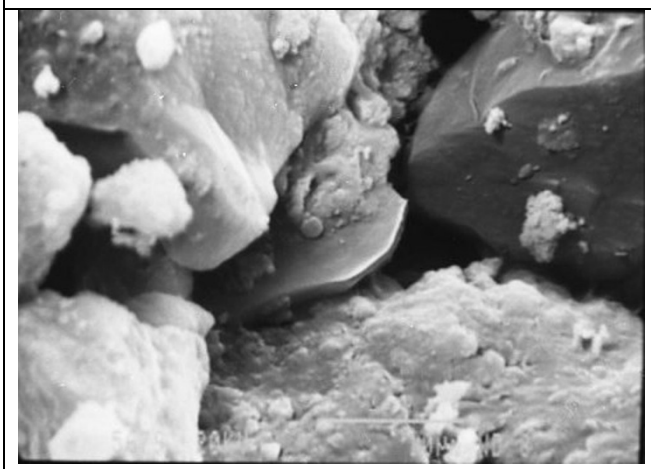

FBS3 X10 000

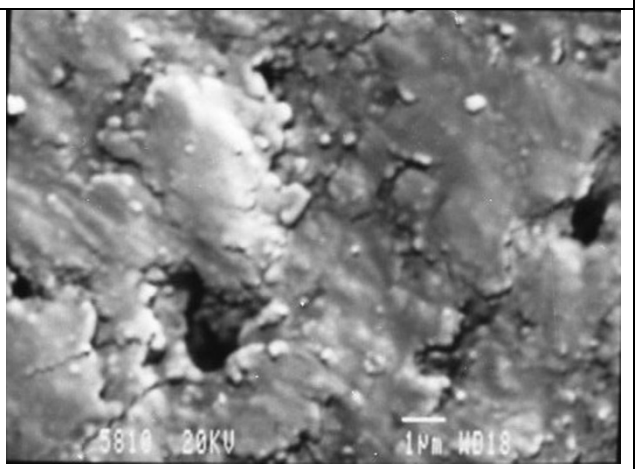

MBS4 X10 000

Figure 6.2. Scanning Electron Micrographs of fossil zebra bone (*Equus* sp.) on the left, versus modern (*Equus burchelli*) from the same geological area on the right, at increasing magnifications.

Discussion

Results from the SEM (Figure 6.2) have shown that fossil bones are highly porous compared to their modern counterparts. This is a direct result of the diagenesis process. Bone material, both the mineral and the organic fractions, were lost due to microbial attack, the most common mechanism of bone deterioration, resulting in a bone becoming more susceptible to hydrolytic infiltration. This increased the rate of leaching of bone components, resulting in an overall increase in bone porosity (Figure 6.14). The results from the modern bones have shown that less alteration has occurred at the gross and microscopic levels; therefore it is likely that parts/constituents of original bio-molecules are retained. Due to large pore spaces in fossil bones as shown by the SEM results, it can be deduced that endogenous components (e.g., proteins, DNA, lipids, carbohydrates), were removed from the bone and exogenous organics from invasive microbes, minerals and trace elements from the surrounding environment were added during the process of diagenesis. This was confirmed by ICP AES (Figure 6.1) results in which the fossil bones contained a lot of exogenous elements relative to the modern bones.

An oxygen-rich environment during dry periods leads to a rapid degradation of the bone's organic matter (disruption of the protein-mineral association) and also favours the activity of micro-organisms (Reiche *et al*., 2003), leading to collagen loss and further increase in porosity. This appears to be the case for the fossil bone studied here, as indicated by the results obtained. It has been hypothesized that when organic remains (in this case bones) are buried, minerals in overlying sediments or soil are solubilized and then re-deposited in pore spaces within the fossil as the saturated water moves through them, while at the same time removing any endogenous organic constituents (Schweitzer *et al*., 2008). The process of degradation of the organic matter, followed by its leaching, induces an increase in bone porosity, (as shown in Figure 6.2). This results in a deeper penetration of pore water containing dissolved chemical species into the bone structure and for the water to be in contact with a larger available surface of apatite crystals. The formation of apatite crystals of a larger size, in fossil compared to the modern bone, is a direct result of increased porosity; organic matter loss and availability of pore water giving rise to dissolution or recrystallization. During the dissolution/recrystallization process, either substitution or

incorporation into apatite crystals or secondary minerals of the chemical species in groundwater is likely to occur.

Water fluctuation also plays a vital role in the trapping of sediments or soil particles in bone pores, for example quartz, clays and the precipitation of calcium carbonate. In such circumstances the trapped particles could act as a diffusion barrier, preventing the water from penetrating deeper into the bone structure and therefore reducing the degree of bone contamination to a certain extent (Reiche *et al*., 2003). In summary, among the main factors that determine whether a bone will survive for a long-period in the fossil record are the effects of microbial attack, pore structure and interaction with soil water. The morphological condition and appearance of the fossil micrographs (see Figure 6.2) points to dissolution and microbial attack as the primary causes of the patchy pore bone distribution. It shows that the modern specimens are still in the early stages and fossil specimens are in their late stages of diagenesis, with both sets displaying varying degree of diagenetic alteration. Therefore studying the hydrological regime of the site and soil water chemistry, as well as bone structure are critical factors in determining the rate of mineral dissolution or recrystallisation, and consequently the survival potential of bone (Smith *et al*., 2008).

6.3. Crystallographic characterisation (mineralogical analysis)

Powder X-ray diffractometry (PXRD)

The XRD results are shown from Figures 6.3 to 6.10. Because particle grain size was fine enough to ensure minimal differences due to preferred orientation between samples, and the diffractometer instrumentation settings were kept constant for all samples, the significant variations in peak intensities between the fossil samples and the modern samples reflect relative degrees of diagenetic alteration within the samples. A clear difference is visible between the mineral composition of fossil and modern bone. From the XRD patterns all modern bones contained mainly hydroxylapatite, while fossil bones are composed of a variety of minerals and more crystalline apatite as compared to much broader and less resolved modern bone peaks. Table 6.1 shows different minerals contained in different samples. A small scaled

(reduced) diffractogram for each sample is included on the top right of the main diffractogram to clearly show the diffraction pattern before mineral loading.

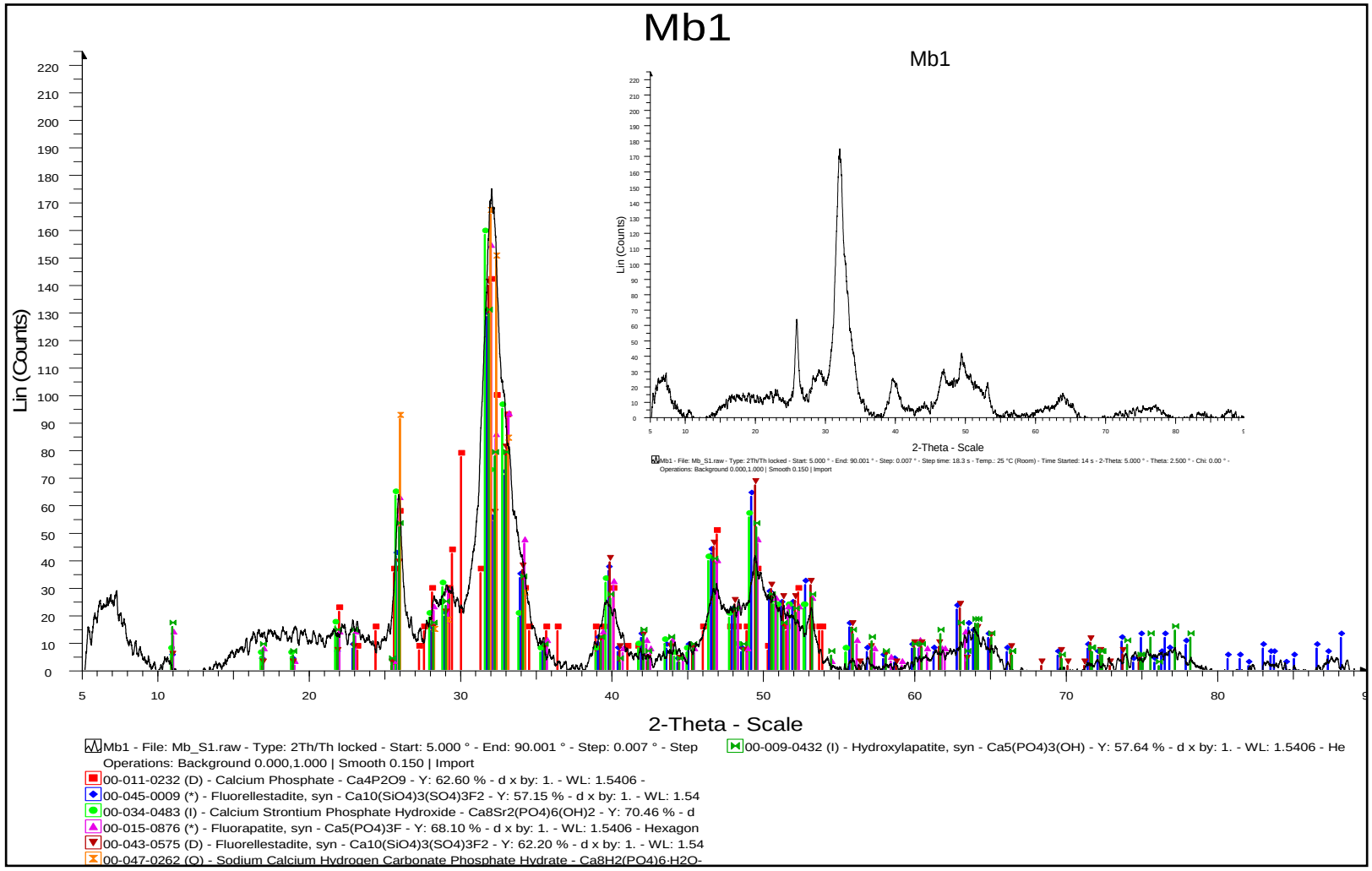

Figure 6.3. Sample (Mb1) modern bone diffractogram before and after mineral loading.

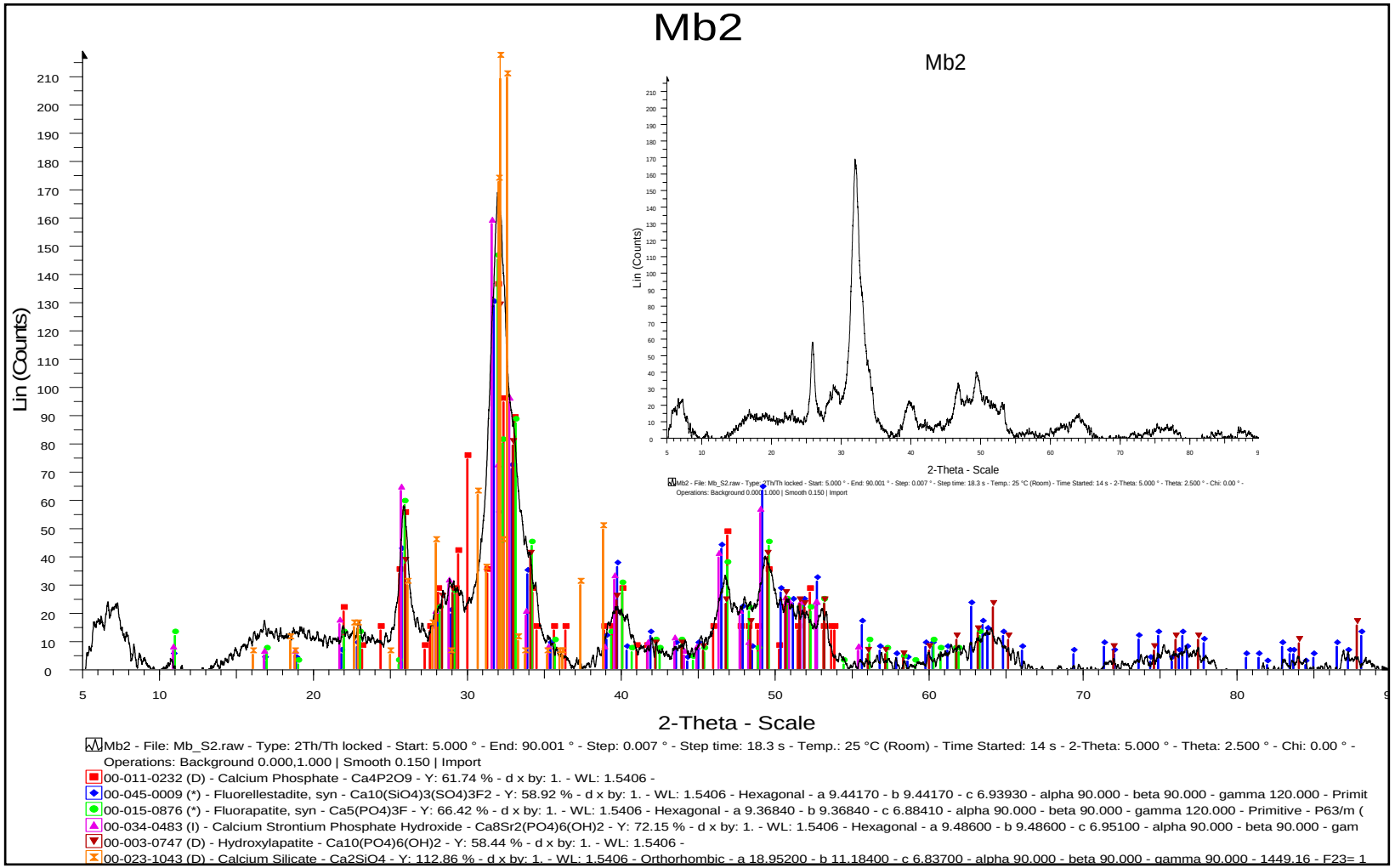

Figure 6.4. Sample (Mb2) modern bone diffractogram before and after mineral loading.

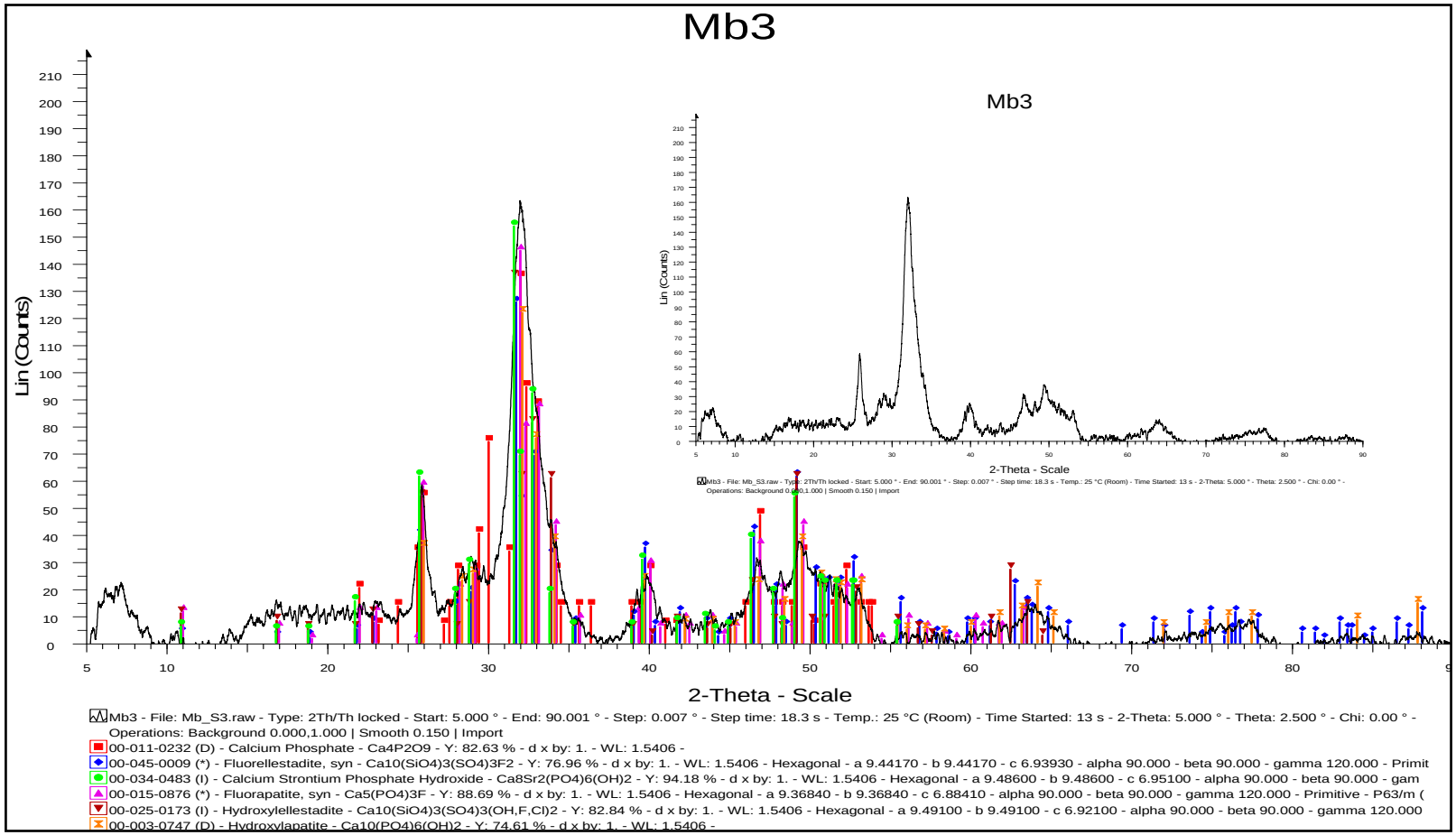

Figure 6.5. Sample (Mb3) modern bone diffractogram before and after mineral loading.

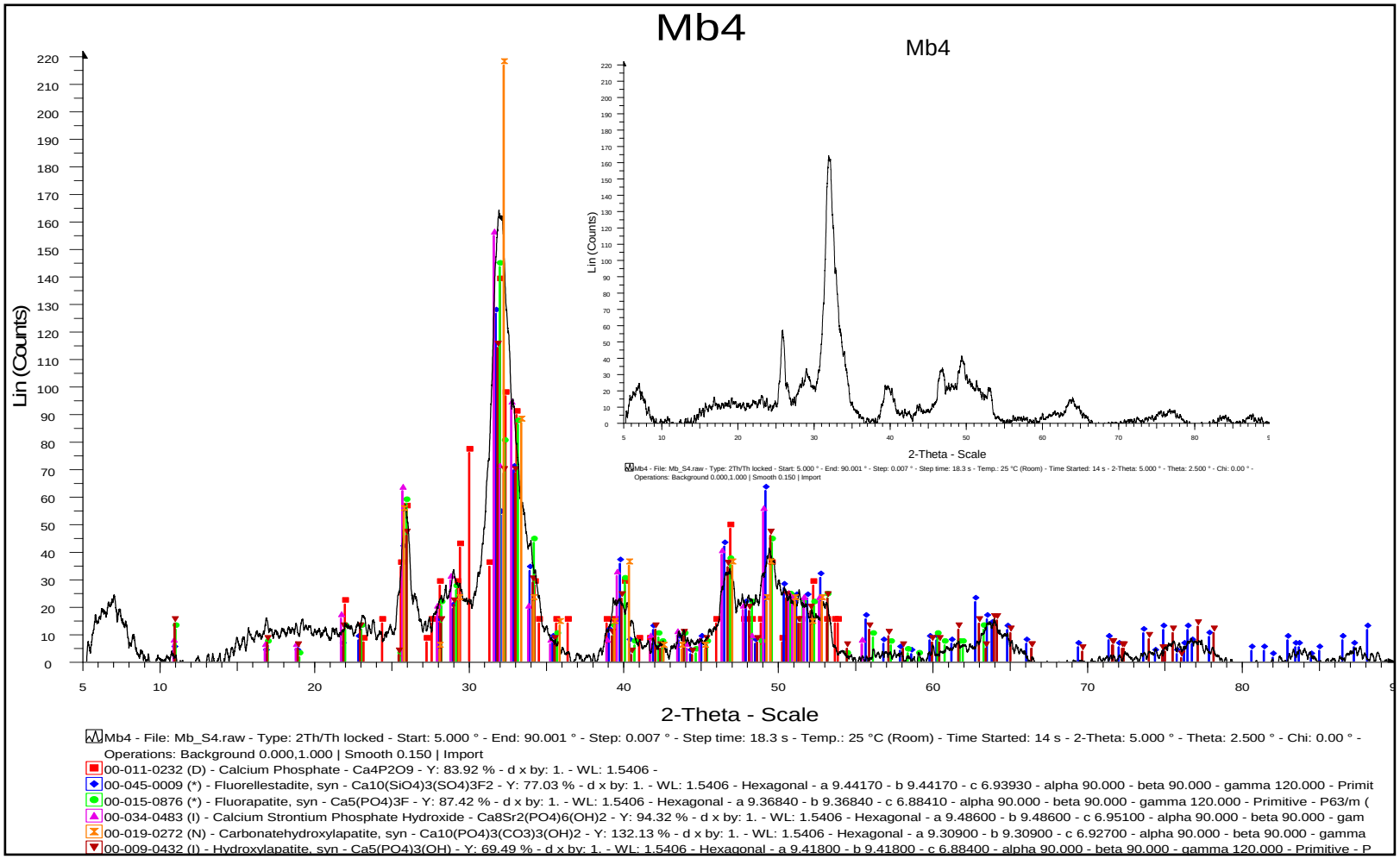

Figure 6.6. Sample (Mb4) modern bone diffractogram before and after mineral loading.

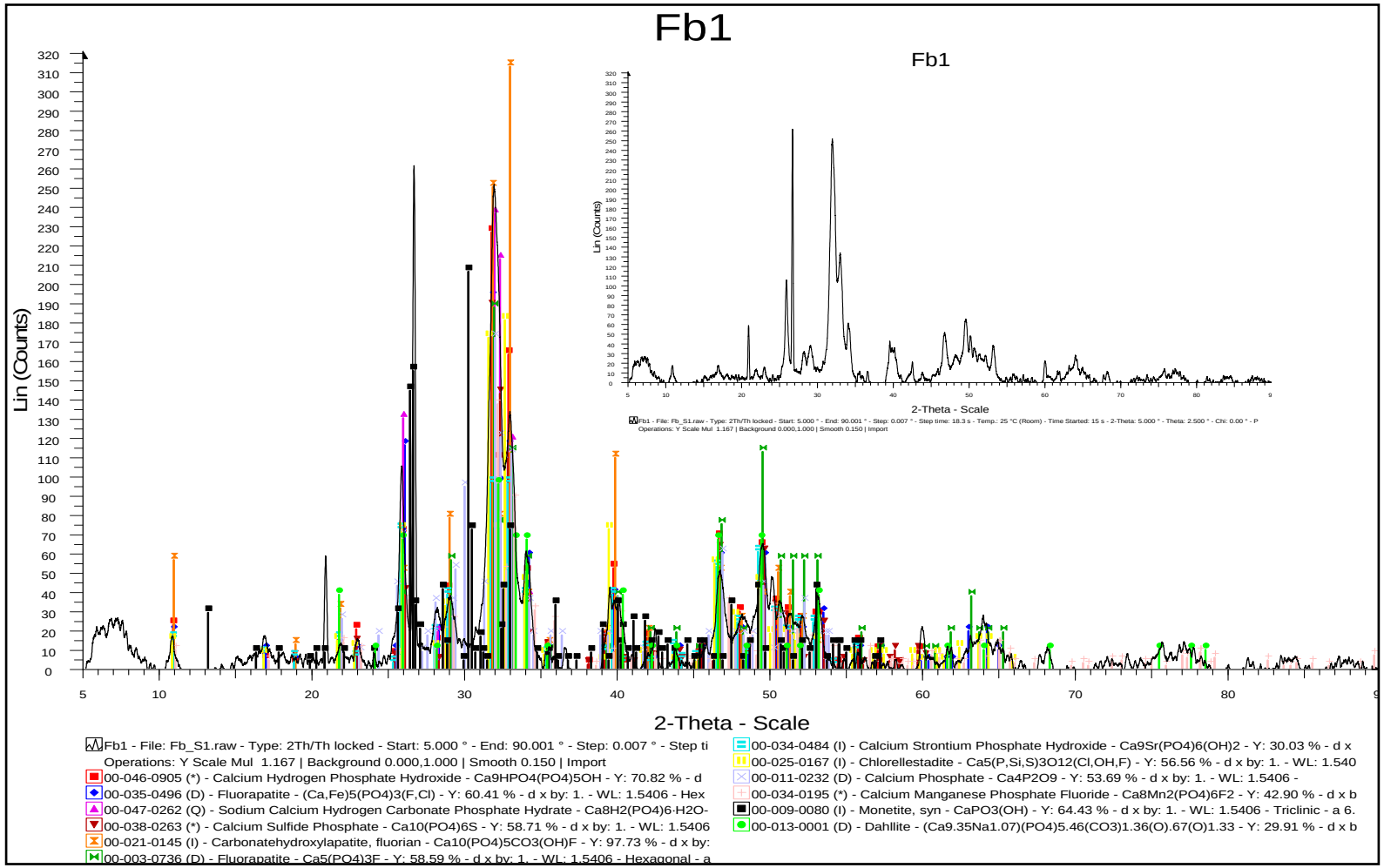

Figure 6.7. Powder X-ray diffraction patterns of fossil bone sample (Fb1) before and after mineral loading.

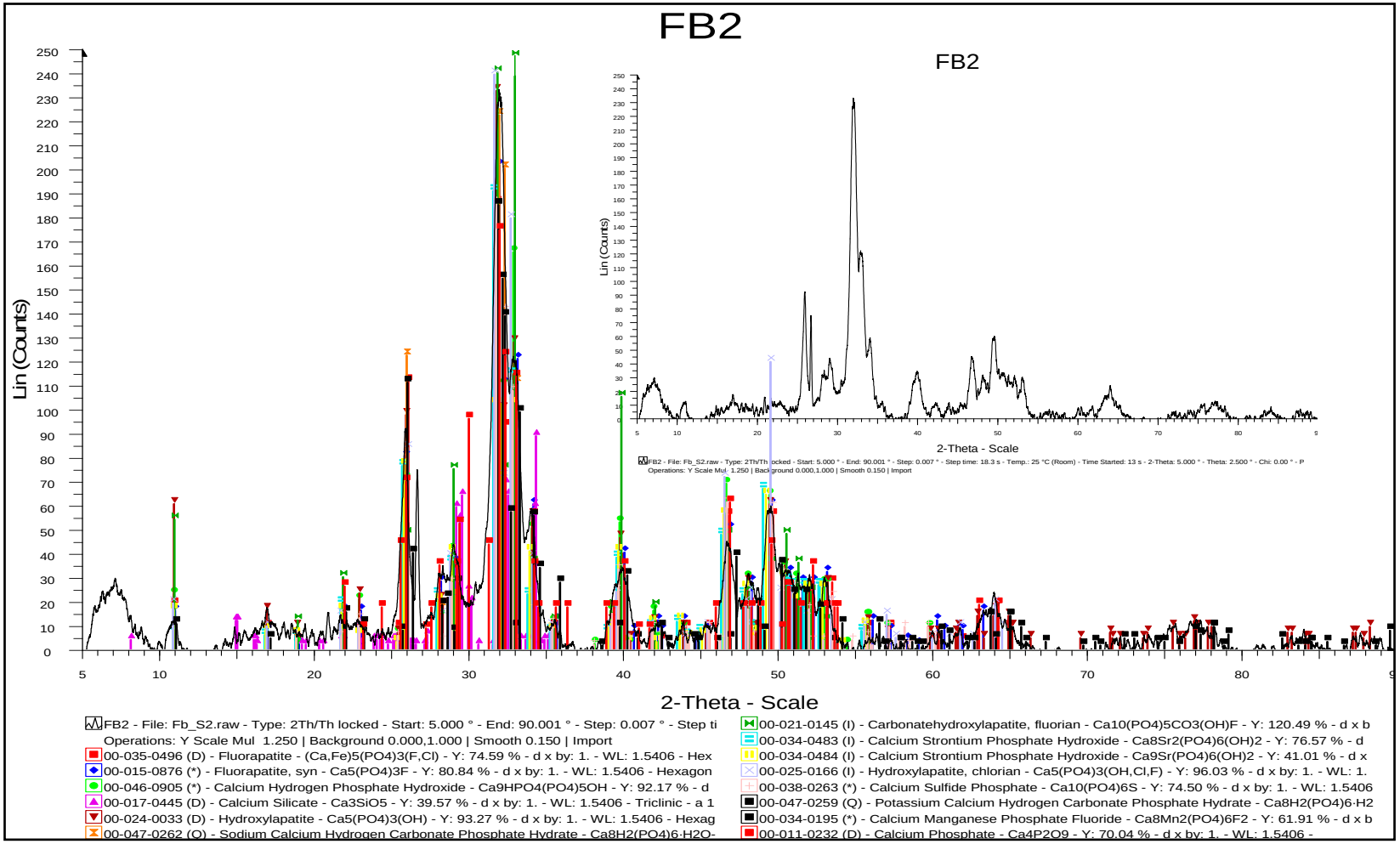

Figure 6.8. Powder X-ray diffraction pattern of fossil bone sample (Fb 2) before and after mineral loading.

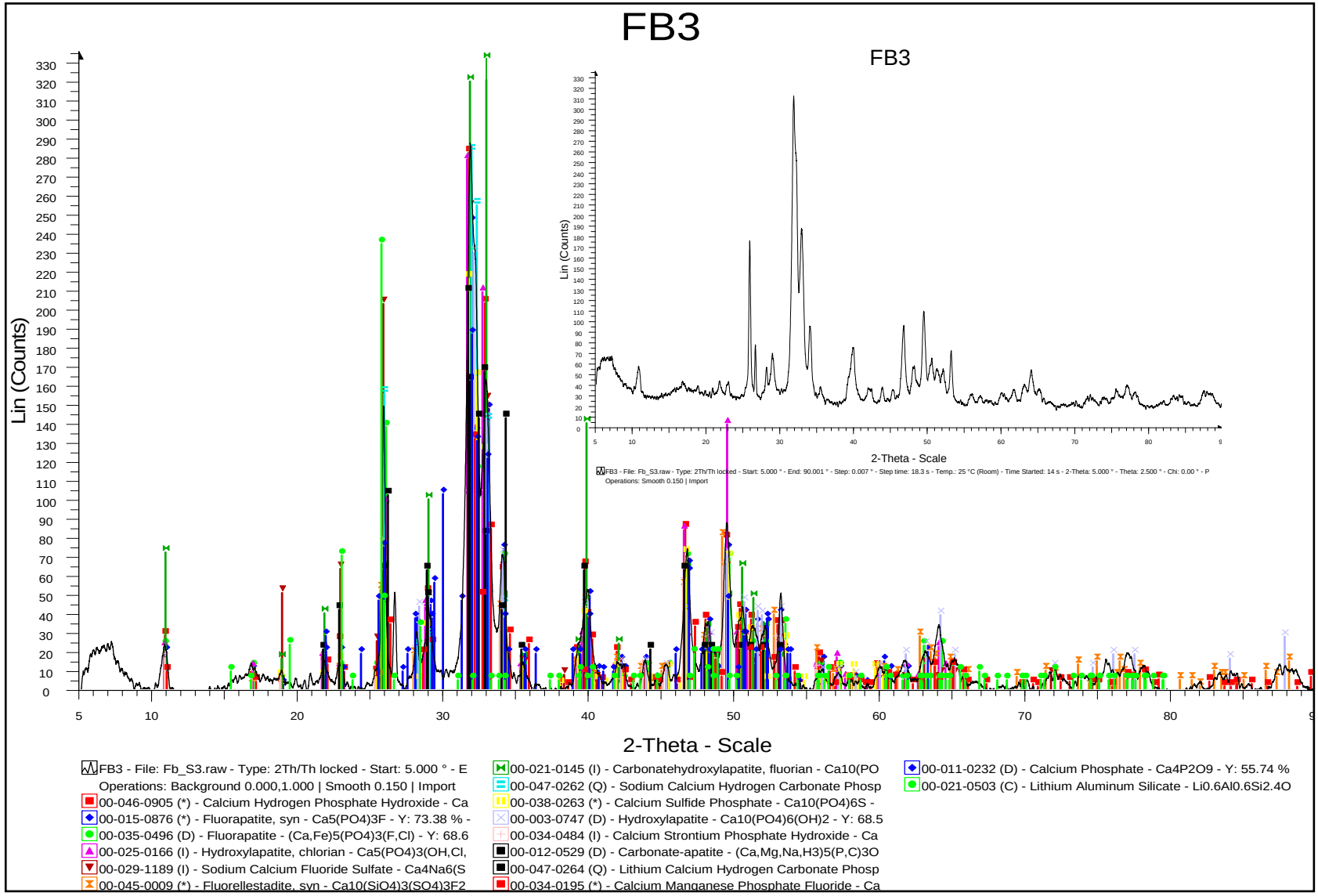

Figure 6.9. Powder X-ray diffraction patterns of fossil bone (FB 3) before and after mineral loading.

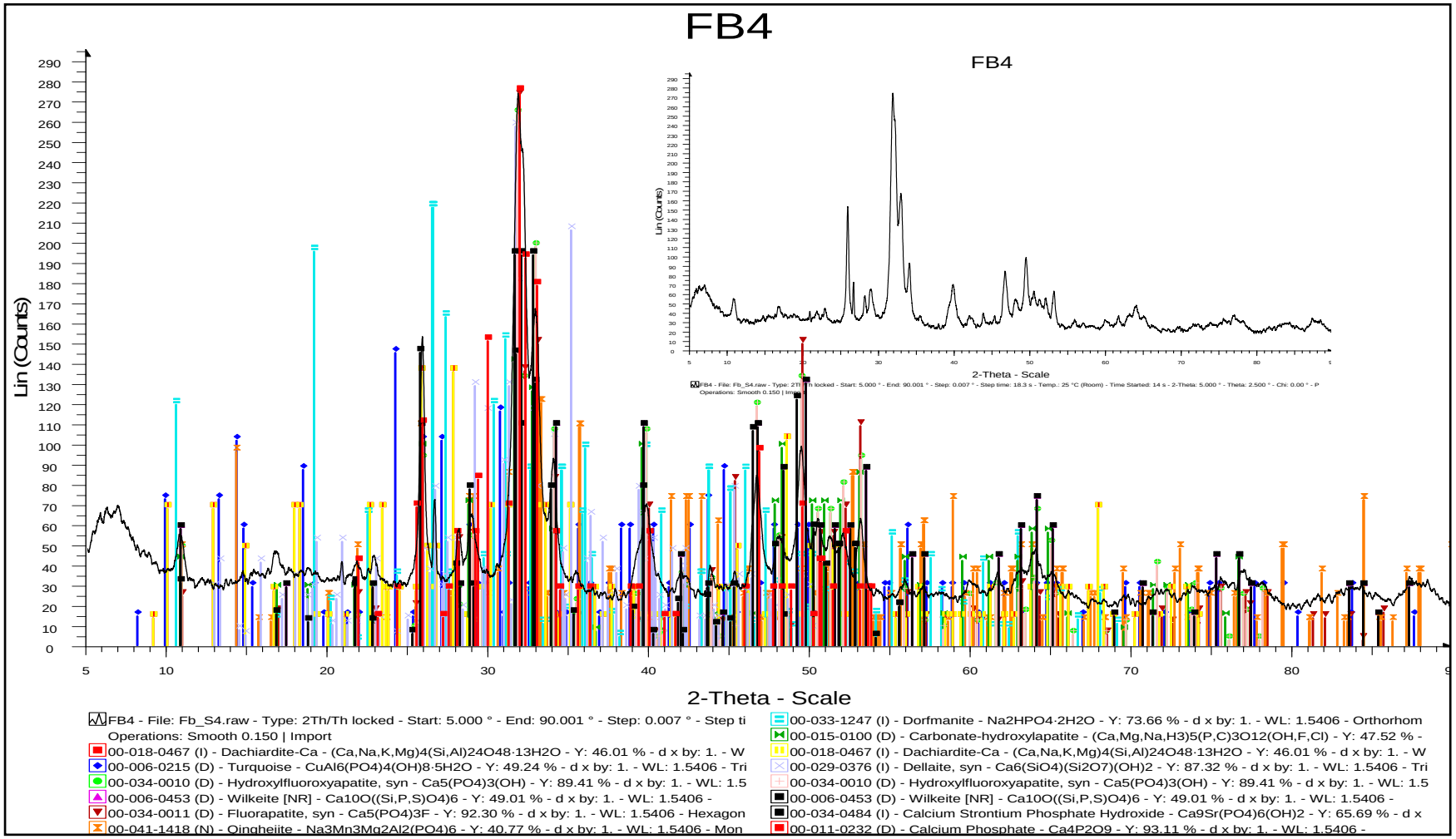

Figure 6.10. Powder X-ray diffraction patterns of fossil bone (FB 4) before and after mineral loading.

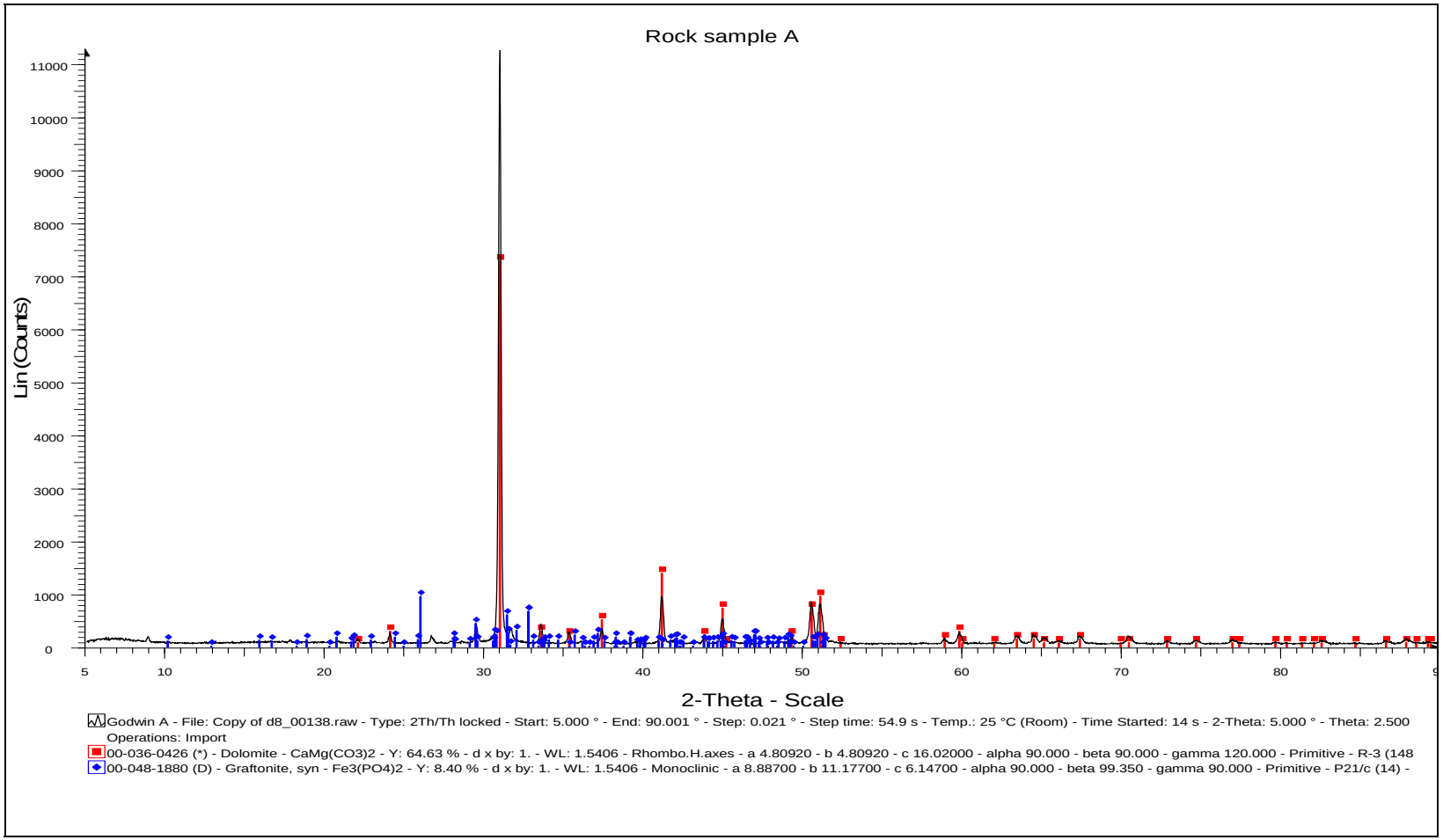

Figure 6.11. Powder X-ray diffraction patterns of rock (sample A) after mineral loading. The sample is mainly composed of dolomite.

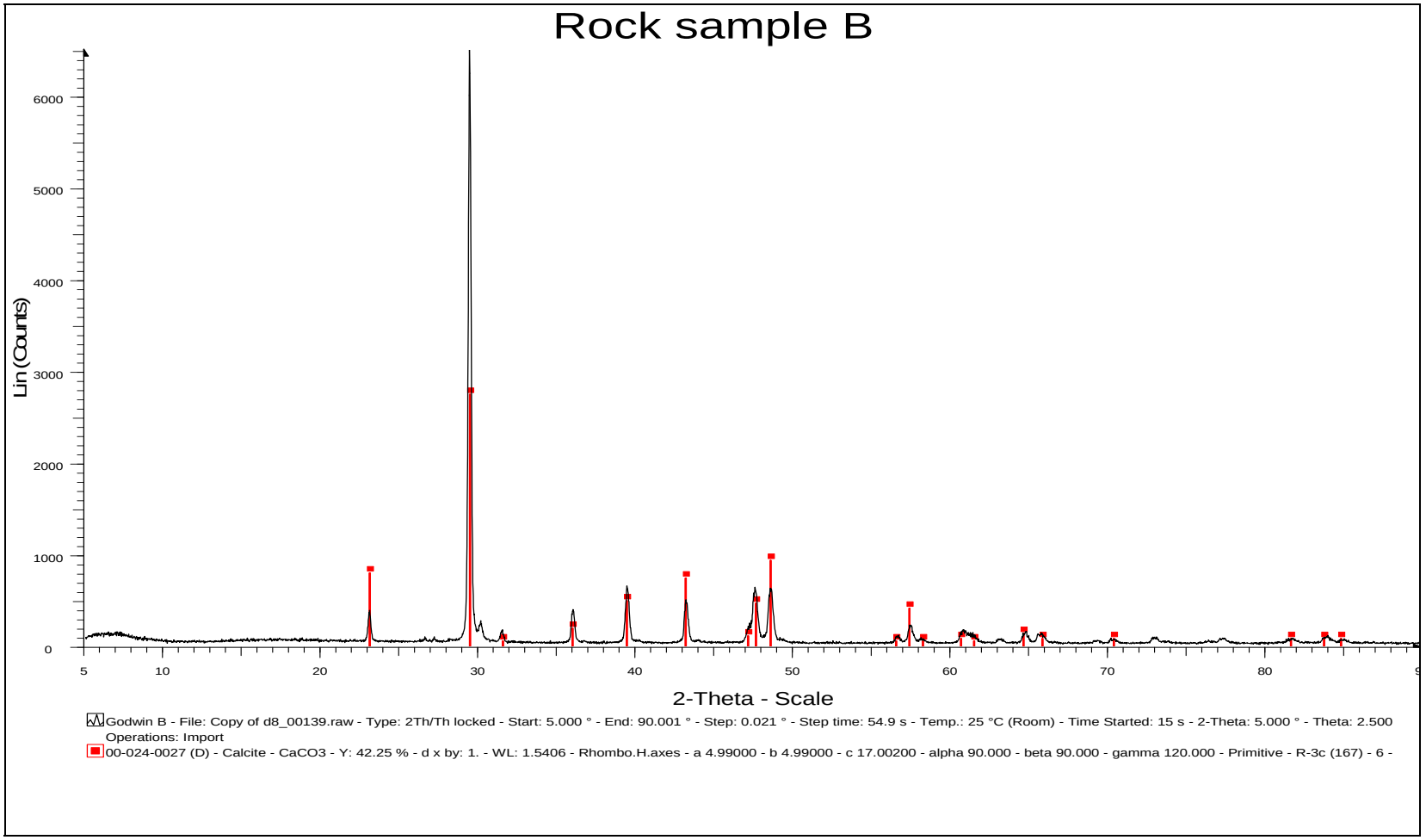

Figure 6.12. Powder X-ray diffraction patterns of rock (sample B) after mineral loading. The sample is exclusively composed of calcite.

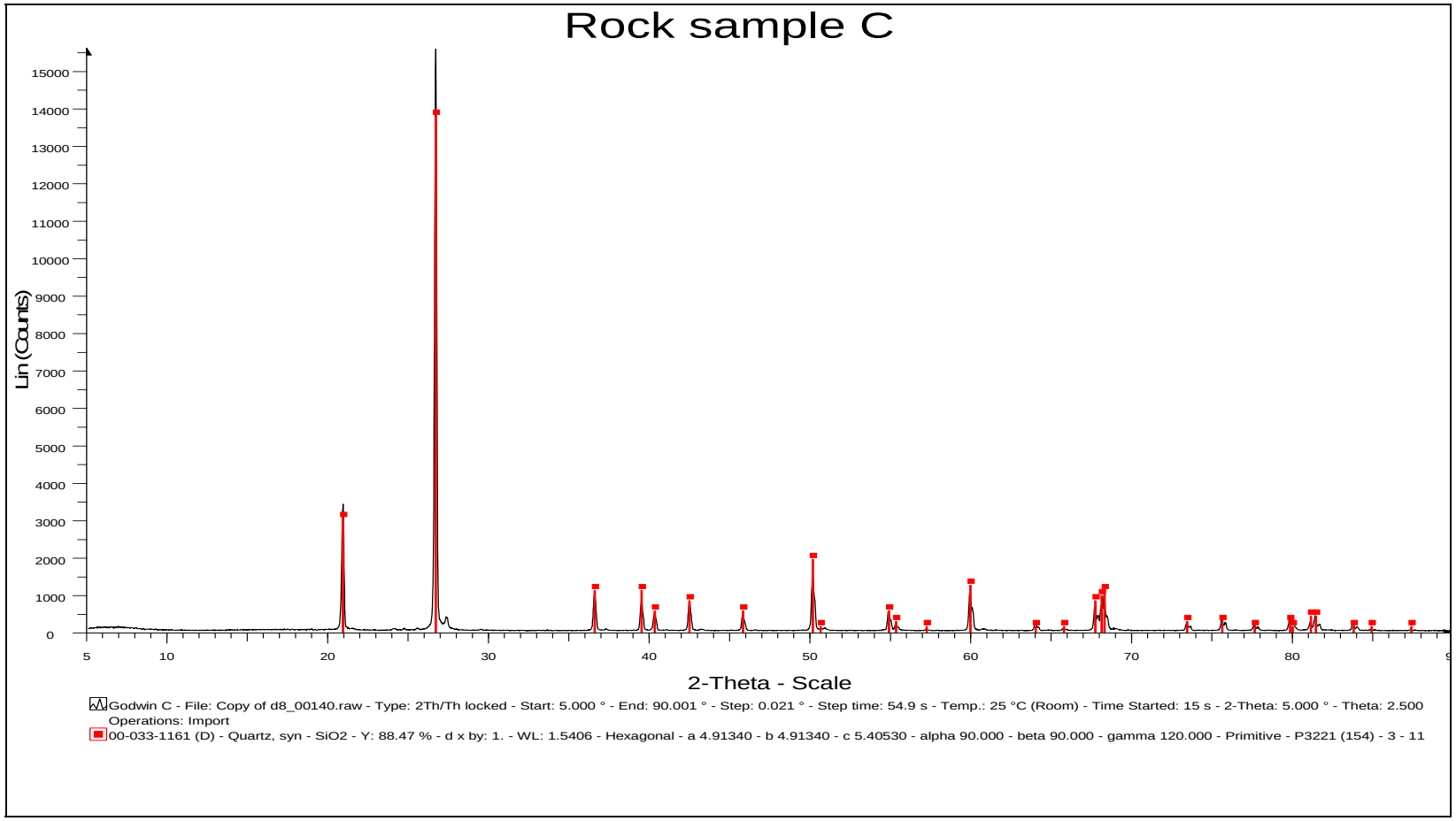

Figure 6.13. Powder X-ray diffraction patterns of rock (sample C) after mineral loading. The sample is exclusively composed of quartz.

The modern bone (Mb1) diffraction data (Figure 6.3) indicate that the sample is composed of the following minerals; hydroxyapatite ($Ca_{10}(PO_4)_6(OH)_2$), Calcium Strontium Phosphate Hydroxide ($Ca_8Sr_2(PO_4)_6(OH)_2$), Fluorellestadite, syn ($Ca_{10}(SiO_4)_3(SO_4)_3F_2$), Fluorapatite, syn ($Ca_5(PO_4)_3F$), Calcium Phosphate ($Ca_4P_2O_9$), with all the peaks of greatest intensity falling within the range of 25° to 35 ° 2θ. Outside this range it was difficult to measure the peaks due to the lack of definition of individual peaks.

The diffraction pattern (Figure 6.4) indicates the presence of: hydroxyapatite ($Ca_{10}(PO_4)_6(OH)_2$), Calcium Strontium Phosphate Hydroxide ($Ca_8Sr_2(PO_4)_6(OH)_2$), Fluorellestadite, syn ($Ca_{10}(SiO_4)_3(SO_4)_3F_2$), Fluorapatite, syn ($Ca_5(PO_4)_3F$), Calcium Phosphate ($Ca_4P_2O_9$) minerals with all the peaks of greatest intensity still falling within the range of 25° to 35 ° 2θ. The peaks become more diffuse as we move away from this range indicating that the sample was not quite crystalline but rather amorphous and therefore these peaks were not well defined.

Sample (Mb3) Figure (6.5) consisted of the following minerals; hydroxyapatite ($Ca_{10}(PO_4)_6(OH)_2$), Calcium Strontium Phosphate Hydroxide ($Ca_8Sr_2(PO_4)_6(OH)_2$), Fluorellestadite, syn ($Ca_{10}(SiO_4)_3(SO_4)_3F_2$), Fluorapatite, syn ($Ca_5(PO_4)_3F$), Calcium Phosphate ($Ca_4P_2O_9$), with the well defined peaks lying between 25° 2θ and 35 ° 2θ. The other part of the diffraction pattern shows very broad peaks demonstrating lack of crystallinity in modern bones.

The following minerals were identified in the modern bone sample (Mb4) Figure 6.6; hydroxyapatite ($Ca_{10}(PO_4)_6(OH)_2$), Calcium Strontium Phosphate Hydroxide ($Ca_8Sr_2(PO_4)_6(OH)_2$), Fluorellestadite, syn ($Ca_{10}(SiO_4)_3(SO_4)_3F_2$), Fluorapatite, syn ($Ca_5(PO_4)_3F$), Calcium Phosphate ($Ca_4P_2O_9$) as indicated by the diffraction pattern of the sample. These minerals were identified where the peaks were well defined and just like in the case of other modern bone samples outside the range of (25° to 35 ° 2θ), no minerals were identified due to the lack of definition of individual peaks.

The fossil bone (Fb1) diffraction data (Figure 6.7) indicate that the sample constitutes the following minerals; Calcium Sulfide Phosphate, ($Ca_{10}(PO_4)_6S$), Calcium Manganese Phosphate Fluoride, ($Ca_8Mn_2(PO_4)_6F_2$), Calcium Phosphate, ($Ca_4P_2O_9$), Chlorellestadite, $Ca_5(P,Si,S)_3O_{12}(Cl,OH,F)$, Fluorapatite, $(Ca,Fe)_5(PO_4)_3(F,Cl)$,

Monetite, syn, ($CaPO_3(OH)$), Dahllite, (Ca9.35Na1.07)(PO4)5.46(CO3)1.36(O).67(O)1.33, Calcium Strontium Phosphate Hydroxide ($Ca_8Sr_2(PO_4)_6(OH)_2$), Fluorapatite, ($Ca_5(PO_4)_3F$), Sodium Calcium Hydrogen Carbonate Phosphate Hydrate ($Ca_8H_2(PO_4)_6{\cdot}H_2O$-$NaHCO_3$-$H_2O$) and Carbonatehydroxylapatite, fluorian, ($Ca_{10}(PO_4)_5CO_3(OH)F$). The X-ray diffraction patterns indicate that the fossil samples are more crystalline and have larger crystals as compared to their modern sample counterparts.

Calcium Phosphate, ($Ca_4P_2O_9$), Calcium Manganese Phosphate Fluoride, ($Ca_8Mn_2(PO_4)_6F_2$), Fluorapatite, $(Ca,Fe)_5(PO_4)_3(F,Cl)$, Calcium Strontium Phosphate Hydroxide ($Ca_8Sr_2(PO_4)_6(OH)_2$), Fluorapatite, syn, ($Ca_5(PO_4)_3F$), Sodium Calcium Hydrogen Carbonate Phosphate Hydrate ($Ca_8H_2(PO_4)_6{\cdot}H_2O$-$NaHCO_3$-$H_2O$), Potassium Calcium Hydrogen Carbonate Phosphate Hydrate, ($Ca_8H_2(PO_4)_6{\cdot}H_2O$-$KHCO_3$-$H_2O$), Carbonatehydroxylapatite, fluorian, ($Ca_{10}(PO_4)_5CO_3(OH)F$), Hydroxylapatite, chlorian, ($Ca_5(PO_4)_3(OH,Cl,F)$), Hydroxylapatite ($Ca_5(PO_4)_3(OH)$), Calcium Silicate, (Ca_3SiO_5) minerals are contained in fossil bone (FB 2) sample Figure 6.8. Comparison of the fossil bone diffraction data with the standard modern bone sample (e.g Figure 6.3.1) indicate mineral contamination following bone burial. The diffraction peaks are well defined demonstrating better crystallinity relative to the modern bone sample.

The fossil bone sample (FB 3), Figure 6.9 is composed of Calcium Phosphate, ($Ca_4P_2O_9$), Calcium Manganese Phosphate Fluoride, ($Ca_8Mn_2(PO_4)_6F_2$), Fluorapatite, $(Ca,Fe)_5(PO_4)_3(F,Cl)$, Calcium Strontium Phosphate Hydroxide ($Ca_8Sr_2(PO_4)_6(OH)_2$), Fluorapatite, syn, ($Ca_5(PO_4)_3F$), Fluorellestadite, syn ($Ca_{10}(SiO_4)_3(SO_4)_3F_2$), Sodium Calcium Hydrogen Carbonate Phosphate Hydrate ($Ca_8H_2(PO_4)_6{\cdot}H_2O$-$NaHCO_3$-$H_2O$), Carbonatehydroxylapatite, fluorian, ($Ca_{10}(PO_4)_5CO_3(OH)F$), Hydroxylapatite, chlorian, ($Ca_5(PO_4)_3(OH,Cl,F)$), Hydroxylapatite ($Ca_5(PO_4)_3(OH)$), Carbonate-apatite, $(Ca,Mg,Na,H_3)_5(P,C)_3O_{12}(OH,Cl,F)$, Calcium Sulfide Phosphate, ($Ca_{10}(PO_4)_6S$), Sodium Calcium Fluoride Sulfate, ($Ca_4Na_6(SO_4)_6F_2$), Dellaite, syn, ($Ca_6(SiO_4)(Si_2O_7)(OH)_2$), Lithium Calcium Hydrogen Carbonate Phosphate Hydrate, ($Ca_8H_2(PO_4)_6{\cdot}H_2O$-$Li_2CO_3$-$H_2O$) and Lithium Aluminum Silicate, ($Li0.6Al0.6Si_2.4O_6$) minerals. The presence of exogenous minerals in this fossil bone

sample (Figure FB 3) shows mineral alteration from the original biological mineral phase(s) of the modern bone.

The fossil bone (FB 4) diffraction data Figure (6.10) indicate that the sample comprises the following minerals: Calcium Phosphate, ($Ca_4P_2O_9$), Fluorapatite, syn, ($Ca_5(PO_4)_3F$), Hydroxylapatite ($Ca_5(PO_4)_3(OH)$), Calcium Silicate, (Ca_3SiO_5), Dellaite, syn, ($Ca_6(SiO_4)(Si_2O_7)(OH)_2$), Dachiardite- Ca, $(Ca,Na,K,Mg)_4(Si,Al)_{24}O48{\cdot}13H_2O$, Carbonate-hydroxylapatite, $(Ca,Mg,Na,H_3)_5(P,C)_3O_{12}(OH,F,Cl)$, Calcium Strontium Phosphate Hydroxide ($Ca_8Sr_2(PO_4)_6(OH)_2$), Wilkeite [NR], ($Ca_{10}O((Si,P,S)O_4)_6$), Hydroxylfluoroxyapatite, syn, ($Ca_5(PO_4)_3(OH)$). Relative to the modern bone diffraction results like all other fossil bone samples analysed, this sample indicates mineral contamination following bone burial. These exogenous minerals represent both the mineral and elemental composition of the burial environment. These elements became incorporated into the bone matrix during bone diagenesis through one or a combination of the following mechanisms: exchange with natural bone constituents i.e. heteroionic exchange, deposition in unfilled voids or defects, and/or adsorption on the bone surface.

Discussion

The diffractograms show a clear distinction between the modern and archaeological samples. The modern samples produced profiles of diffuse blunted peaks with poor definition (see Figures 6.3-6.6) and therefore few minerals were identified as compared to fossil bones. Contrary to this, fossil bones yielded patterns with much sharper, more distinct peaks of greater intensity (Figures 6.7-6.10). Thus the least well-preserved bone (fossil) yielded the highest cumulative X-ray peak intensities and the lowest cumulative peak widths (i.e. well-defined peaks meaning the material is crystalline), while the best preserved material (modern bones) had the lowest cumulative peak intensity and the highest cumulative peak widths (i.e. diffuse meaning the material is amorphous). The unloaded diffraction patterns for both the fossil and modern bones clearly show this difference. This observation supports the fact that the fossil specimens have been exposed to diagenetic processes for much longer periods as compared to modern specimen, and thus are more mineralized (as

confirmed by well defined diffraction peaks) and diagenetically altered. The modern diffraction data indicate that all of the samples are composed more or less of the same minerals; hydroxyapatite ($Ca_{10}(PO_4)_6(OH)_2$), Calcium Strontium Phosphate Hydroxide ($Ca_8Sr_2(PO_4)_6(OH)_2$), Fluorellestadite, syn ($Ca_{10}(SiO_4)_3(SO_4)_3F_2$), Fluorapatite, syn ($Ca_5(PO_4)_3F$), Calcium Phosphate ($Ca_4P_2O_9$), with all the peaks falling within the range of 25° 2θ to 35 ° 2θ.

From the results obtained all fossil samples displayed unquestionable extensive alteration from the original mineral phase relative to their modern counterparts. However, the diffraction data obtained indicate that all modern bone samples are composed exclusively of the mineral hydroxylapatite.

Calcite, dolomite and quartz minerals are common in the Cradle of Humankind caves (e.g. Gladysvale cave) as indicated by rock PXRD results in Table 6.1 and Figures 6.11; 6.12 and 6.13. Decomposition/weathering products deriving from calcite, dolomite and quartz are dominant mineral phases in fossil bones (see Figure 6.7-10). Some of these minerals are found to be present in almost all fossil samples and these include; Calcium Manganese Phosphate Fluoride, ($Ca_8Mn_2(PO_4)_6F_2$), Calcium Strontium Phosphate Hydroxide ($Ca_8Sr_2(PO_4)_6(OH)_2$), Fluorapatite, syn ($Ca_5(PO_4)_3F$), Calcium Phosphate ($Ca_4P_2O_9$). The presence of Fluorapatite, Calcium Strontium Phosphate Hydroxide, Fluorapatite, Manganese Phosphate Fluoride and Calcium Silicate indicate diagenetic alteration from original, unaltered bone mineral hydroxylapatite ($Ca_{10}(PO_4)_6(OH)_2$). Fe, Mn, Sr, Si, Al, F and Cl were found to be present in the form of Calcium Silicate (Ca_3SiO_5) , Dachiardite- Ca $(Ca,Na,K,Mg)_4(Si,Al)_{24}O_{48}\cdot 13H_2O$), Fluorapatite $(Ca,Fe)_5(PO_4)_3(F,Cl)$, Calcium Manganese Phosphate Fluoride ($Ca_8Mn_2(PO_4)_6F_2$), Calcium Strontium Phosphate Hydroxide ($Ca_9Sr(PO_4)_6(OH)2$) minerals. The presence of these elements is also confirmed by ICP-AES results in which they were found to occur at higher levels in the fossil bones. Therefore there is evidence that diagenetic Sr, Si, Fe, Mn, Al, F and Cl have become structurally incorporated within the fossil bones analysed here. The presence of authigenic quartz-containing minerals such as Fluorellestadite, syn ($Ca_{10}(SiO_4)_3(SO_4)_3F_2$) and Calcium Silicate ($Ca_3SiO_5$) in the bones indicate that soluble silica was the major component in the groundwater. The sampling area contains a lot of silica as confirmed by ICP-AES (Figure 6.1) and XRD (Figure 6.13)

results and this is the most probable source of silica. This study revealed that minerals are responsible for the infill of bone voids during diagenesis. From the results the most common infill minerals are carbonates ($Ca_8H_2(PO_4)_6{\cdot}H_2O$-$NaHCO_3$-$H_2O$, $Ca_{10}(PO_4)_5CO_3(OH)F$), sulphides ($Ca_{10}(PO_4)_6S$) and phosphates ($Ca_9Sr(PO_4)_6(OH)_2$, $Ca_8Mn_2(PO_4)_6F_2$, $Ca_9HPO_4(PO_4)_5OH$). These findings are similar to some extent with the XRD results reported by Wings, (2004) in which the most common fossil bone infill minerals were carbonates ($CaCO_3$, $FeCO_3$, $BaCO_3$), sulphates ($BaSO_4$, $CaSO_4$), oxides (FeO, Fe_2O_3) and sulphides (FeS, ZnS). Therefore precipitation and mineral replacement are both complex diagenetic physicochemical processes which take place during infilling of the openings in the bone (Downing and Park, 1998). It has been documented that exogenous elements may become incorporated into the bone matrix by several different mechanisms, including exchange with natural bone constituents, i.e. heteroionic exchange, deposition in unfilled voids or defects, and adsorption on the bone surface (Neuman and Neuman, 1958). Thus in this case fluoride and chloride ions substituted hydroxide ion, carbonate ion (CO_3^{2-}) substitute phosphate ion (PO_4^{3-}) and strontium and aluminium substituted calcium in the hydroxylapatite matrix, whereas Mn, Fe, and Si normally fill voids and defects (Lambert *et al*., 1985) without necessarily undergoing heteroionic exchange with the bone mineral.

Secondary minerals and apatite alteration

The mineral replacement results observed in this study (Figure 6.7-6.10) are in total agreement with the findings of several previous similar studies and can be best attributed to pseudomorphic type of replacement reactions, having been more pronounced in fossil bones relative to modern bones. Pseudomorphic replacement reactions form the basis of the process of fossilisation, where the original biological remains are replaced by minerals such as calcite, quartz or opal (e.g., Groecke *et al*., 1999; Kizil'shtein, 2006; Pewkliang *et al*., 2008).

Several authors (e.g., Thornber, 1975a; Cole, 1983; Wilkin and Barnes, 1996; Cole and Chakraborty, 2001; Eda *et al*., 2006; Hunger and Benning, 2007) have greatly underestimated the role of fluids in such pseudomorphic reactions, and have limited replacement reactions chiefly as diffusion driven movement of cations within a solid.

Harland (1994) clearly explained this mechanism as involving the preservation of the anionic structural framework, whereas cations appear to freely interchange through larger atomic sites or interconnected channels within the structure. Contrary to this, detailed studies have proven that even simple ‘‘cation exchange” or ‘‘leaching” reactions may not proceed by simple cation diffusion, but rather may involve dissolution and reprecipitation processes in which the structure of the primary mineral is totally disrupted/broken down by dissolution prior to secondary mineral precipitation (Putnis and Putnis, 2007; Xia *et al*., 2009). Thus in this case the fossil bone mineral hydroxylapatite underwent dissolution and partial demineralisation reaction followed by the precipitation, re-mineralization and recrystallization of Calcium Strontium Phosphate Hydroxide ($Ca_8Sr_2(PO_4)_6(OH)_2$), Fluorellestadite, syn ($Ca_{10}(SiO_4)_3(SO_4)_3F_2$), Fluorapatite, syn ($Ca_5(PO_4)_3F$), Calcium Phosphate ($Ca_4P_2O_9$) as secondary minerals. Hence both leaching and incorporation of cations have resulted in a change in the stoichiometry of the parent hydroxylapatite crystal giving rise to these secondary minerals. The rate of these diagenetic variables; bone dissolution and demineralization followed by mineral precipitation, re-mineralization and recrystallization are site-specific and liable to depend on the hydrological, microbiological and chemical composition of soil water as this affects the solubility product of (these minerals) as well as determining some principal ionic concentrations. In this model/mechanism the rate of bone primary mineral (i.e. hydroxylapatite) dissolution was greatly increased by the nucleation and growth of secondary minerals on its surface through the process of re-mineralization. In this case the analyzed bone samples were buried in cave soil and not in water logged sediments, in this solution-transport limited environment, dissolution of the primary mineral hydroxylapatite, resulted in the formation of a locally enriched solution, which increased the super-saturation with respect to secondary minerals and that promoted the rate of their nucleation and growth. At some point and time, these reactions may reach a steady state in which the rate of growth of secondary minerals will be equal to the rate of dissolution of the hydroxylapatite bone mineral. At this state, the buried fossil bone can be chemically defined and quantified with certainty; though this can be complicated by the fact that most burial conditions are very dynamic and thus the steady state is rarely reached.

Table 6.1. Different minerals contained in different bone samples.

Mineral	Formula	FBS 1	FBS 2	FBS 3	FBS 4	MBS1	MBS2	MBS3	MBS4	RS A	RS B	RS C
Calcium Phosphate	$Ca_4P_2O_9$	+	+	+	+	+	+	+	+			
Fluorapatite	$Ca_5(PO_4)_3F$	+										
Fluorapatite, syn	$Ca_5(PO_4)_3F$		+	+	+	+	+	+	+			
Hydroxylapatite	$Ca_{10}(PO_4)_6(OH)_2$			+			+	+				
Fluorapatite	$(Ca,Fe)_5(PO_4)_3(F,Cl)$	+	+	+								
Hydroxylapatite	$Ca_5(PO_4)_3(OH)$		+									
Calcium Silicate	Ca_3SiO_5		+				+					
Fluorellestadite, syn	$Ca_{10}(SiO_4)_3(SO_4)_3F_2$			+		+	+	+	+			
Calcite	$CaCO_3$										+	
Quartz	SiO_2											+
Dolomite	$CaMg(CO_3)_2$									+		
Hydroxylapatite, chlorian	$Ca_5(PO_4)_3(OH,Cl,F)$		+	+								
Calcium Sulfide Phosphate	$Ca_{10}(PO_4)_6S$	+										
Dachiardite- Ca	(Ca,Na,K,Mg)4(Si,Al)24O4 8·13H2O				+							

Carbonatehydroxylapatite, syn	$Ca_{10}(PO_4)_3(CO_3)_3(OH)_2$								+	
Hydroxylellestadite	$Ca_{10}(SiO_4)_3(SO_4)_3(OH,F,Cl_2$							+		
Potassium Calcium Hydrogen Carbonate Phosphate Hydrate	$Ca_8H_2(PO_4)_6{\cdot}H_2O$-$KHCO_3$-$H_2O$		+							
Carbonate-hydroxylapatite	$(Ca,Mg,Na,H_3)_5(P,C)_3O_{12}(OH,F,Cl)$				+					
Calcium Hydrogen Phosphate Hydroxide	$Ca_9HPO_4(PO_4)_5OH$	+	+	+						
Calcium Manganese Phosphate Fluoride	$Ca_8Mn_2(PO_4)_6F_2$	+								
Sodium Calcium Hydrogen Carbonate Phosphate Hydrate	$Ca_8H_2(PO_4)_6{\cdot}H_2O$-$NaHCO_3$-$H_2O$	+	+	+		+				
Carbonate-apatite	$(Ca,Mg,Na,H_3)_5(P,C)_3O_{12}(OH,Cl,F)$			+						
Hydroxylapatite, syn	$Ca_5(PO_4)_3(OH)$								+	

Calcium Strontium Phosphate Hydroxide	$Ca_8Sr_2(PO_4)_6(OH)_2$		+			+	+	+	+		
Strontium Aluminum Oxide	$Sr_3Al_2O_6/3SrO{\cdot}Al_2O_3$										
Calcium Strontium Phosphate Hydroxide	$Ca_9Sr(PO_4)_6(OH)_2$	+	+	+	+						
Wilkeite [NR]	$Ca_{10}O((Si,P,S)O_4)_6$				+						
Monetite, syn	$CaPO_3(OH)$	+									
Hydroxylfluoroxyapatite, syn	$Ca_5(PO_4)_3(OH)$				+						
Chlorellestadite	$Ca_5(P,Si,S)_3O_{12}(Cl,OH,F)$	+									
Dahllite	(Ca9.35Na1.07)(PO4)5.46(CO3)1.36(O).67(O)1.33	+									
Dellaite, syn	$Ca_6(SiO_4)(Si_2O_7)(OH)_2$			+	+						
Calcium Sulfide Phosphate	$Ca_{10}(PO_4)_6S$	+		+							
Calcium Manganese Phosphate Fluoride	$Ca_8Mn_2(PO_4)_6F_2$	+	+	+							
Lithium Aluminum	Li0.6Al0.6Si2.4O6			+							

Silicate						
Carbonatehydroxylapatite, fluorian	$Ca_{10}(PO_4)_5CO_3(OH)F$	+	+	+		
Lithium Calcium Hydrogen Carbonate Phosphate Hydrate	$Ca_8H_2(PO_4)_6{\cdot}H_2O$-$Li_2CO_3$-$H_2O$			+		
Sodium Calcium Fluoride Sulfate	$Ca_4Na_6(SO_4)_6F_2$			+		

6. 4. Bone porosity, density and water absorption

6. 4.1 Bone porosity

Porosity measurement results are shown in Figure 6.14 with error bars included. The porosity results have shown that fossil bones are highly porous as compared to their modern counterparts. This is a direct result of the diagenesis process. The large increase in porosity observed in fossil specimens is mainly due to the microbial attack resulting in increased bone pore sizes which ultimately lead to rapid interaction of bone specimens with ground water and thus accelerates rate of dissolution. Hence the loss of micro-porosity with gain in macro-porosity increased interaction of ground water with the bone. Thus bone material, both the mineral and the organic fractions were lost due to microbial attack, the most common mechanism of bone deterioration, resulting in a bone becoming more susceptible to hydrolytic infiltration. Therefore this increased the rate of leaching of bone components, with the overall increase in bone porosity.

From the results obtained it can be postulated that fossil bones had undergone alteration during the early stages of diagenesis that resulted in significant changes in the bone mineral leading to disruption of the protein–mineral association of the bone resulting in collagen loss and further increases in porosity. Thus with the breaking down of mineral–protein bonds, both fractions (i.e. the mineral and the protein) were exposed to diagenetic agents, among others the soil water. The mineral-protein bond(s) dissociation substantially led to increased bone porosity, which in turn increased the rate of hydrolytic infiltration which further increased the rate of bone degradation and porosity, as illustrated also by scanning electron micrographs results in Figure 6.2. The following authors supported this mechanism as being responsible for increase in fossil bone porosity relative to their modern counterparts: Nielsen-Marsh *et al*. (2000); Pike *et al*. (2001); Collins *et al*. (2002).

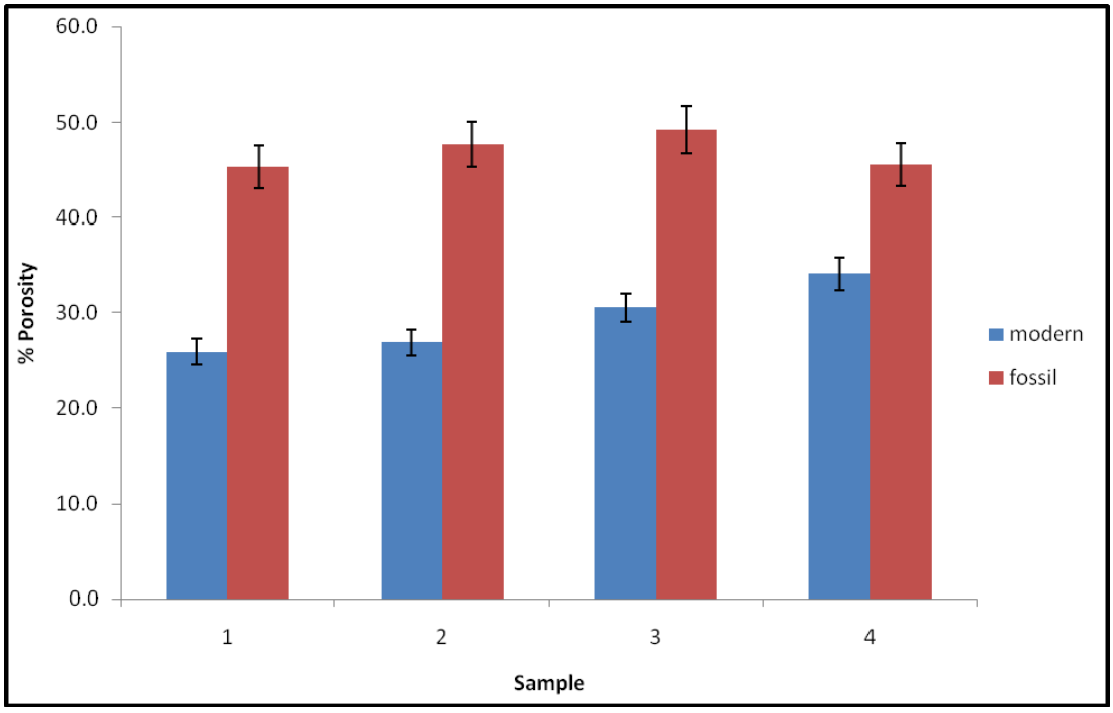

Figure 6.14. Variation in porosity measurements done on modern bone versus fossil bone samples.

Microbially attacked bone has a large increase in porosity which will allow increased interaction with soil water and thus potentially accelerate the bone mineral dissolution process (Smith *et al.,* 2007) leading to an increase in porosity. The bone porosity results are in strong agreement with the morphological examination results (Figure 6.2) done on the same samples in which the fossil bones display numerous deep pores and cracks relative to the modern bones, reflecting the extent of microbial post-mortem destruction. The scanning electron micrographs (Figure 6.2) show microbial post-mortem destruction of the fossil bone, a process which occurs in the initial phases of bone diagenesis and which has caused considerable alteration (i.e. increase) to the fossil bone pore structure. These initial degradation processes determine bone preservation in the environment and the kind of information available from the bone such as DNA or collagen, mineral isotope, and elemental uptake profiles. Hence from the results obtained, modern bones show less alteration at gross (Figure 6.14), microscopic (Figure 6.2) and elemental levels (Figure 6.1) from the living state and consequently have retained much of the original fragments of original bio-molecules

for example collagen (Figure 6.17) as compared to fossil bones, which are displaying totally opposite results from modern bones in all the measured parameters.

6.4.2. Bone density

Figure 6.15 shows the results of bone density. From these results, fossil bones have lower density as compared to modern bones. As a result of the increase in porosity of fossil bones, the specimens suffer severe leaching of both the mineral and organic fractions. This results in decrease in mass leading to lower density values (Figure 6.15) as compared to their modern bone counterparts which have not lost much of the bone matter. The high density measurements in modern bones demonstrated that little exogenous elements (also confirmed by ICP AES results Figure 6.1) and minerals (confirmed by PXRD results Figure 6.3-6.6) have been added in modern bones relative to fossil bones, thus decay and deterioration processes were more pronounced in fossil bones relative to the modern bones.

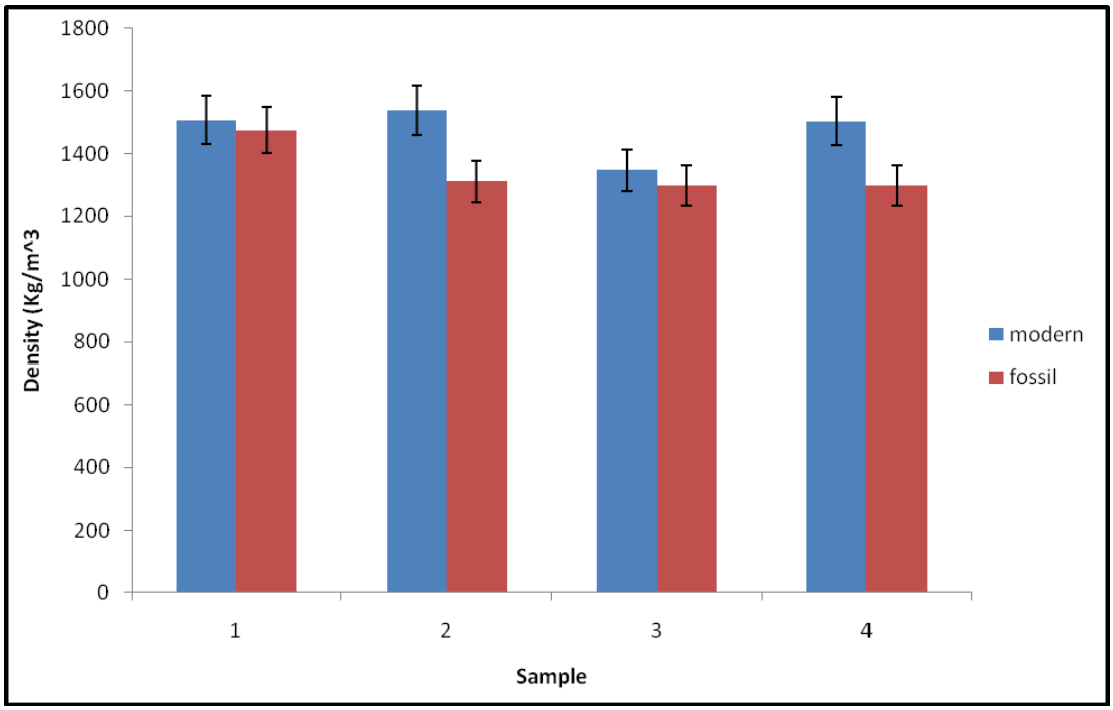

Figure 6.15. Bone density results of modern versus fossil bone samples.

6.4.3 Water absorption

Due to an increase in porosity and leaching, fossil bones possess numerous vacant pore spaces as compared to modern bones, hence the higher water absorption values (Figure 6.16) than the modern bones. Basing on the bone porosity, density and water absorption results obtained, it can be concluded that modern bones have higher bulky density compared to fossil bones, while fossil bone displayed higher porosity and water absorption values. Therefore bones with higher porosity (fossil) have low bulk density, where bulk density (or Volume density) is defined as a measure of the density of a bone including vacant pore spaces (Smith *et al.,* 2008).

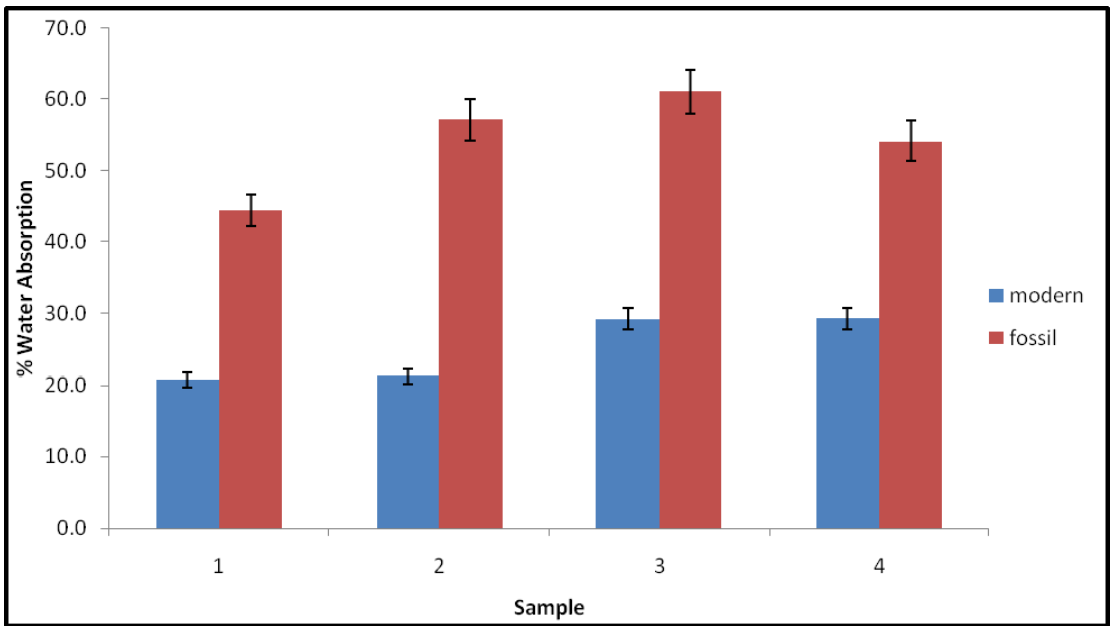

Figure 6.16. Bone water absorption results of modern versus fossil bone samples.

6.5 Carbon, Hydrogen, Nitrogen (CHN) elemental analysis in fossil and modern bones.

Figures 6.17, 6.18 and 6.19 show the variation in nitrogen, carbon, and hydrogen percentage composition in the measured bone samples respectively. Results are reported as the average of two measurements.

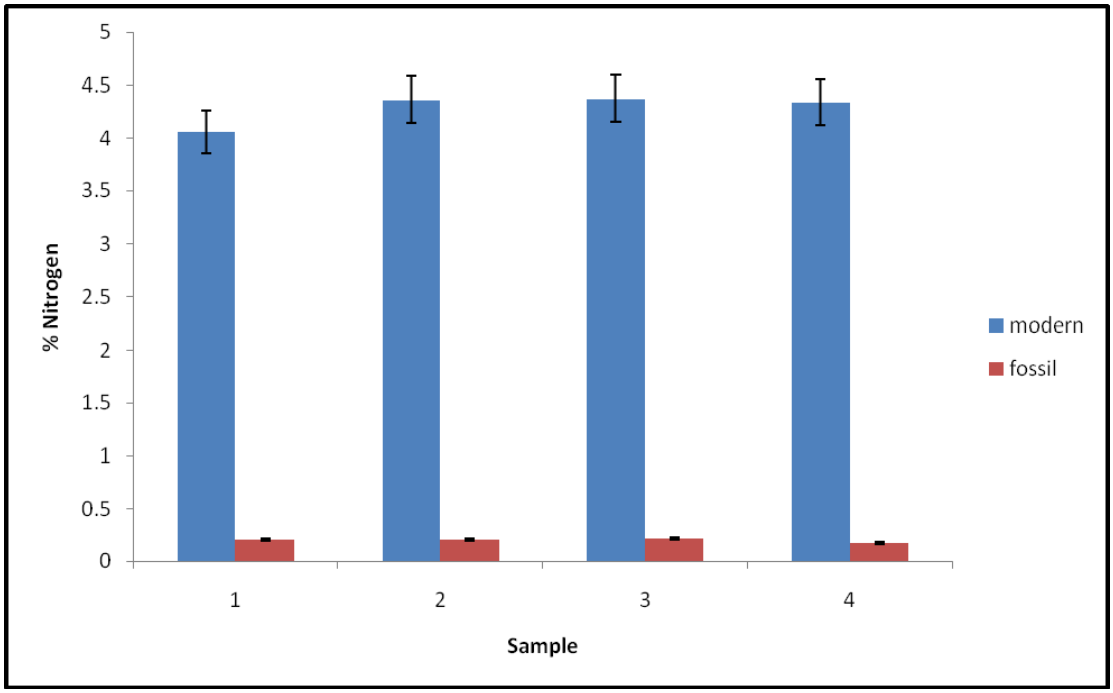

Figure 6.17. Variation in percentage nitrogen content measured in both the fossil and modern bones.

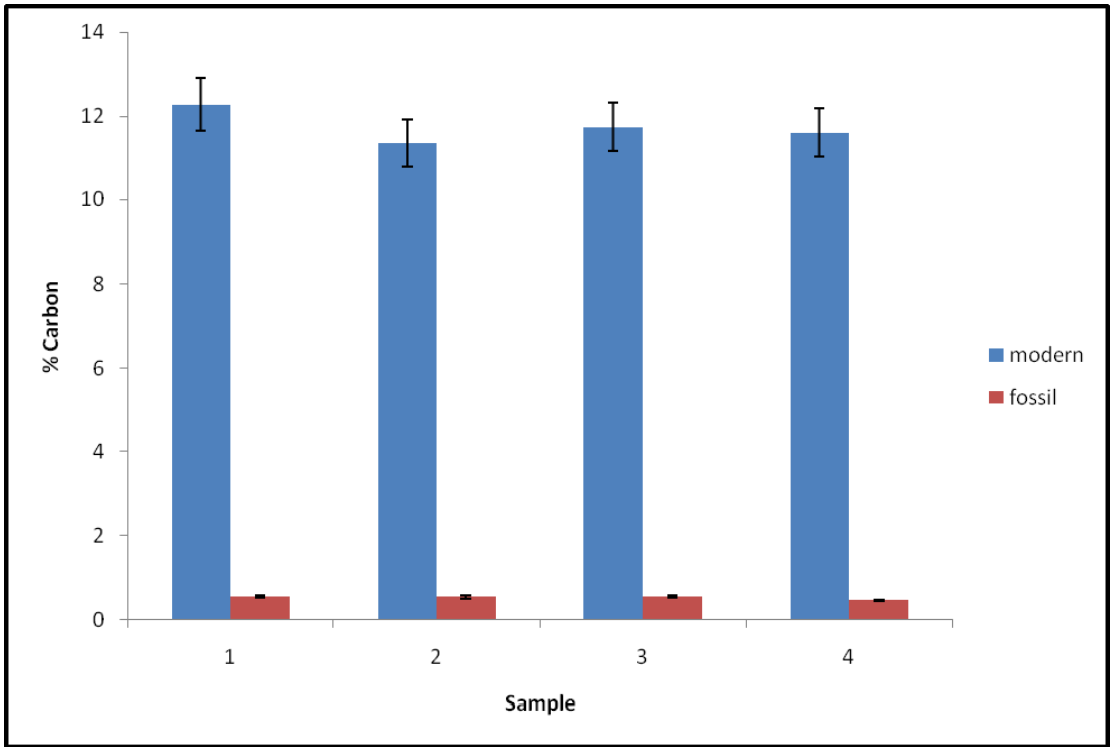

Figure 6.18. Variation in percentage collagenous carbon content measured in both the fossil and modern bones.

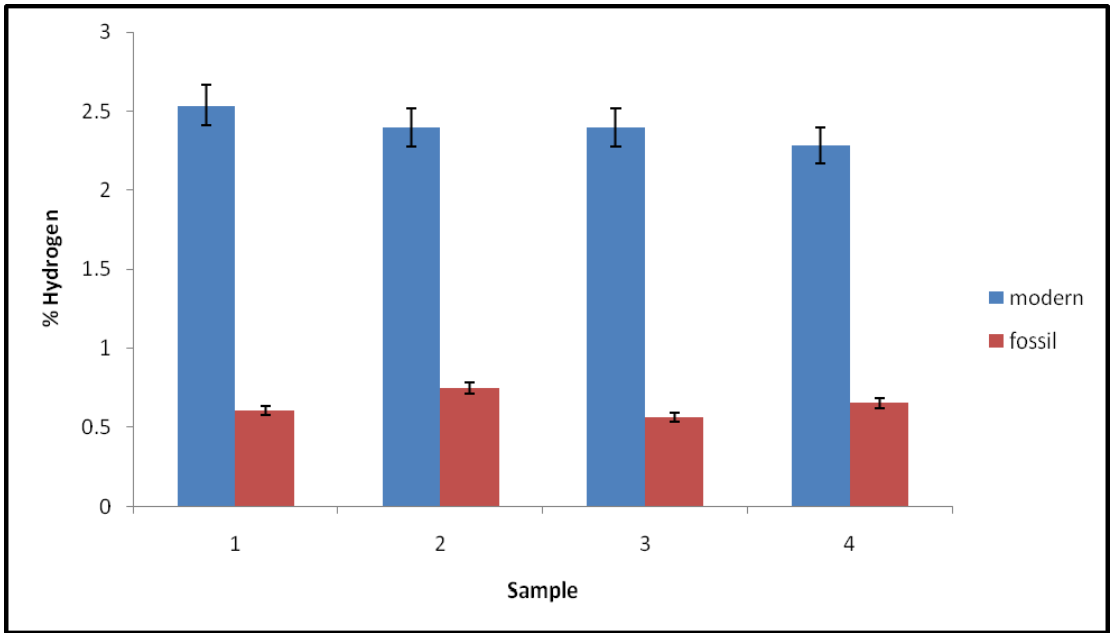

Figure 6.19. Variation in percentage hydrogen content measured in both the fossil and modern bones.

Discussion

The amount of nitrogen is low in fossil bones (Figure 6.17), i.e. only a little collagen is preserved. In modern bones the %N is high, indicating good preservation of collagen, and the histological structure is nearly intact as evidenced by the scanning electron micrographs (Figure 6.2). The same trend is observed in the percentage of collagenous carbon and hydrogen in Figures 6.18 and 6.19, respectively.

The results show that the nitrogen content of the fossil bones analyzed ranged from 0.175 to 0.213%. The nitrogen content of the modern bones analyzed ranged from 4.210% to 4.549%. The values found for %N for the modern bone are in agreement with the values found in previous similar studies. According to Bocherens *et al*. (2005) the nitrogen content values expected for modern bones are 4.3±0.6%, and according to a study by Tütken (2003), fresh bones contain approximately (4±0.5 wt.% N). Reiche *et al*. (2003) also reported that modern bones contain about 4 wt %N and 11 wt% C within the organic phase. For %N in bones, the key value is 0.4%, which corresponds to a collagen loss of around 90%, and which also corresponds to

the lower limit for bones that still yield collagen with well preserved stable isotopic signatures.

Fossil and modern bones were defined based on this value: (1) bones with less than 0.4% nitrogen, which have lost more than 90% of their original collagen, and (2) bones with more than 0.4% nitrogen, which have retained at least 10% of the original collagen (after Bocherens *et al*., 2005).

From the results, Figure 6.17 all the fossil bone samples have lost a larger proportion of residual nitrogen that correlates to the remaining organic phase fraction mainly collagen, though they have managed to retain 4.375% to 5.325% of the original collagen bone content. Thus these bones have lost more than 90% of their original collagen, whereas modern bone results statistically suggest that they have retained more than 90% of their original collagen. This characteristic reflects the subsequent infilling of the fossil bone structure with authigenic cave minerals. In this case the infilling occurred while some organic material i.e. collagen was still in the bone sample, thus the samples still contain substantial organic material, which was sheltered from further diagenetic loss. However, in the case where the infilling occurred after the all the organic material had been lost, then the samples will not reflect any trace of nitrogen.

Both collagenous (%Ccoll) and non-collagenous (%Cncoll) carbon percentages were calculated from the measured total carbon (%Cb) percentages in the bone using the following equation (Bocherens *et al*., 2005):

$$\%Cncoll=\%Cb-(2.7*\%Nb) \qquad (6.1)$$

where 2.7*%Nb stands for the percentage of carbon coming from the collagen still present in the bone, after the work by Bocherens *et al*. (2005). The results are shown in Table 6.2

The results obtained for the percentage of non-collagenous carbon content in modern bones are exceptionally comparable to those reported by Bocherens *et al*. (2005), in which the non-collagenous carbon content was around 1.4% for modern bones. None of the fossil bones contained more than 0.250% non-collagenous carbon; all the samples contained much less amounts, with values as low as 0.014%. Whilst modern bones recorded values not less than 1.470% non-collagenous carbon. This is an

indication that the fossil bones have already lost a significant amount of carbon from its mineral component as compared to their modern counterparts. On average, modern bones contained more collagenous carbon than fossil bones (11.75% versus 0.540%) and this category yielded the bones with the highest amounts of collagenous carbon, with %Ccoll as high as 12.28%. Among modern bones, almost no specimen contained less than 11.00% collagenous carbon, while no fossil bone specimen contained more than 0.6% collagenous carbon. Thus fossil bones have undergone significant alteration at both molecular and elemental levels due to the diagenesis process relative to modern bones. All bones with a depletion of non-collagen carbon exhibit a collagen loss higher than 90%.

Table 6.2. CHN modern and fossil bone elemental analysis results.

ELEMENT	**%H**	**%C**	**%N**	**%Ccoll**	**%Cncoll**
FBSI	0.606	0.808	0.208	0.562	0.246
FBS2	0.750	0.565	0.204	0.551	0.014
FBS3	0.564	0.774	0.213	0.575	0.199
FBS4	0.652	0.592	0.175	0.473	0.120
MBS1	2.536	14.48	4.549	12.28	2.198
MBS2	2.397	13.14	4.210	11.37	1.773
MBS3	2.398	13.36	4.353	11.75	1.607
MBS4	2.281	13.08	4.300	11.61	1.470

The covariation of nitrogen and non-collagenous carbon in both the fossil and the modern bones allows one to predict the most probable sequence of bone diagenesis in Gladysvale cave. From Table 6.2 the loss of non-collagenous carbon, which corresponds to carbon in the mineral fraction of bone (Bocherens *et al*., 2008), started only when at least nine tenths of the collagen had already been lost. The percentage carbon and nitrogen results for the fossil bone obtained (Figures 6.17 and 6.18)

together with the PXRD results (Figures 6.3-6.10) which displayed an increase in bone crystallinity in fossil bones, are in strong agreement with those from a similar study done by Bocherens *et al*. (2008), in which crystallinity index was observed to increase in bones which had lost most of their collagen. Therefore collagen tends to protect the bone mineral phase which is poorly crystalline (amorphous), a phenomenon described in detail in previous similar studies (e.g. Collins *et al*., 1995; Person *et al*., 1996; Wess *et al*., 2001) of experimentally and naturally altered bones. Nevertheless, mineral deposition in bone, for instance carbonate-containing minerals, in bone may occur even before the complete loss of collagen, since bones which still contain more than 95% (modern bones Table 6.2) original collagen exhibit significant increases in non-collagenous carbon (Table 6.2). This is further evidenced by the presence of exogenous elements e.g. Si and Sr found in Calcium Strontium Phosphate Hydroxide ($Ca_8Sr_2(PO_4)_6(OH)_2$) and Fluorellestadite, syn ($Ca_{10}(SiO_4)_3(SO_4)_3F_2$) minerals in modern bones (Figure 6.3-6). This is probably because such minerals including calcite were deposited in the natural cavities of bone tissue, such as Haversian canals and blood vessel cavities, even when collagen was still present (Bocherens *et al*., 2008), during the early stages of diagenesis. However, the amount of non-collagenous carbon that results from carbonate-containing mineral (e.g. calcite) uptake generally increases with collagen loss, as voids left behind by the collagen degradation process become filled by mineral-containing solutions. This mechanism is supported by the PXRD results (Table 6.5) in which the fossil bones contain many exogenous minerals incorporated through mineral infilling of bone voids, followed by precipitation and recrystallization processes.

Conclusion

Fossil bones from Gladysvale cave exhibit a very narrow range of preservation states. Using the nitrogen and carbon contents as proxies for bone preservation, the values are much lower in fossil bones relative to modern bones. The differences in preservation states of fossil and modern bones do not only have implications for the preservation of biogeochemical signals in bones, such as those recorded in the elemental signatures of collagen, but rather also for the survival of bones themselves

in the geochemical environment. From the results obtained (Figures 6.17; 6.18 and Table 6.2), bones that have lost much of their collagen and part of their mineral carbon are visibly putrid and deteriorating, as confirmed by the scanning electron micrographs (Figure 6.2) showing larger pore spaces and high porosity (Figure 6.14) in fossil bones relative to modern bones. Large pore spaces in bones point to microbial attack, therefore microbial attack affected these other diagenetic parameters as well. Hence increased microbial attack resulted in the decrease % 'collagen' remaining as shown by fossil bone %N results. Thus the well preserved specimens i.e. modern bones (Table 6.2, Figure 6.17) have high % collagen, high bulk density (Figure 6.15) and low porosity values (Figure 6.14). Contrary to this, degraded fossil bones display low % collagen, low bulk density, large increases in porosity with the largest pores and consequent loss of density, these bones are therefore considered to be poorly preserved.

6.6 Redox, pH, X-ray microprobe, and XRF mapping results

6.6.1 Eh-pH

Field measurements; pH, reduction potentials, temperature and conductivity were carried out on the soil surrounding the fossil to infer on the soil chemistry of the burial environment and the results are presented in Table 6.3.

Table 6.3. Eh-pH results obtained in soil samples where the fossil bones were buried.

Soil sample	Temp (^{0}C)	pH	ORP (SHE) mV	Conductivity (µS cm^{-1})
S1	16.6	8.22	547.4	210
S2	16.4	8.25	537.0	124
S3	16.3	8.11	575.3	157

From the results obtained Table 6.3, it shows that the bones were buried on the surface under highly oxidising conditions. Such oxygen-rich environment during dry periods has resulted in a rapid degradation of the bone's organic matter and also favoured the activity of micro-organisms, which is visible on scanning electron micrographs results obtained (Figure 6.2). The analysed fossil bone samples were obtained from cave experiencing fluctuating hydrological regime depending on seasons i.e. experience much water during the rain season relative to the winter season. These water table fluctuations lead to the transport of bone constituents and exogenous species into and out of the bones, as confirmed by the elemental results (Figure 6.1). The degraded collagen, i.e. short polymers of amino acids, has been leached out due to an increased solubility in water leading to a rapid decrease in the percentage collagen as indicated by the amount of % nitrogen obtained in the bone (Figure 6.17).

The process of organic matter degradation and its ultimate leaching induced an increase in bone porosity in the fossil bone (Figure 6.14), which permitted the exogenous pore water containing dissolved chemical species to penetrate more deeply into the bone structure and to be in contact with a larger available surface of apatite crystals, giving way for substitution reactions. Therefore loss of collagen, the increased porosity and the intense flux of water gave rise to important dissolution/recrystallization processes resulting in the formation of mineral apatite crystals of a larger size in fossil bone compared to modern bone as shown by well defined fossil diffractogram peaks. Exogenous chemical species available in groundwater were incorporated into the apatite crystals and precipitated as secondary minerals during dissolution/recrystallization processes (PXRD Table 6.1). In addition to these processes bone alteration also proceeded by solubility-controlled mechanisms, precipitation, diffusion-reaction mechanisms and bacteria-controlled processes.

Transport of materials in and out of the bone as a result of water fluctuation patterns caused by seasonal rainfall also lead to the trapping of sediment particles in bone pores like quartz, clays and hence the ultimate precipitation of several secondary minerals in fossil bones. Reiche *et al*. (2003) pointed out that if these particles remain at the surface of the bone pores can act as diffusion barriers, obstructing water penetration and therefore do limit bone elemental enrichment to a certain extent.

Redox and soil acidity/alkalinity play a vital role in the survival and/or destruction of the bone in the geochemical environment. Since the geochemical conditions varies from one burial site (e.g. caves) to the other, both the rate and intensity of bone decay also varies, for this reason some burial site may ultimately be devoid of fossil bones, while others will yield many fossil bones. Hence variations in geochemical conditions for instance pH and Eh in the environmental resulted in differential state of bone preservation leading to spatial variation in bone abundance in different burial sites. In some cases the absence of bone in some burial sites used by prehistoric populations is not necessarily proof of no deposition but rather may be the result of complete bone dissolution, a phenomenon which is directly dependent on pH.

Hedges and Millard (1995) pointed out that all bone will potentially be at risk of complete dissolution depending on the acidity and hydrological activity of the soil water at the burial site. Dissolution results in a rapid increases the porosity of the bone and the greater the porosity of the bone the greater the rate of dissolution. Pike *et al*. (2001) described this feedback mechanism as catastrophic dissolution. Therefore the fossil bone samples analysed here have managed to survive catastrophic dissolution though they have undergone a significant degree of dissolution as confirmed by both the porosity and scanning micrographs results.

In a similar study carried out by Reiche *et al*. (2003), in which the level of contamination of bones from the emerged and immersed areas were compared, both types of bones were found to be highly contaminated by exogenous chemical species. Under this study they concluded that “bone enrichment by exogenous species is not only controlled by differences in porosity, but also by the groundwater chemistry and the presence of secondary minerals that fills pores”. Therefore the state of bone preservation is directly dependent on the geochemistry of the environment during burial.

6.6.2 X-ray microprobe and synchrotron-based XRF mapping analysis - surface elemental mapping of a fossil bone.

The synchrotron-based XRF mapping (Figure 6.21) was used for the detection of heavier elements (Pb, As, Sr, Cu) while EPMA technique was employed for the detection of relatively lighter elements (Figure 6.20), (Kuczumow *et al*., 2010).

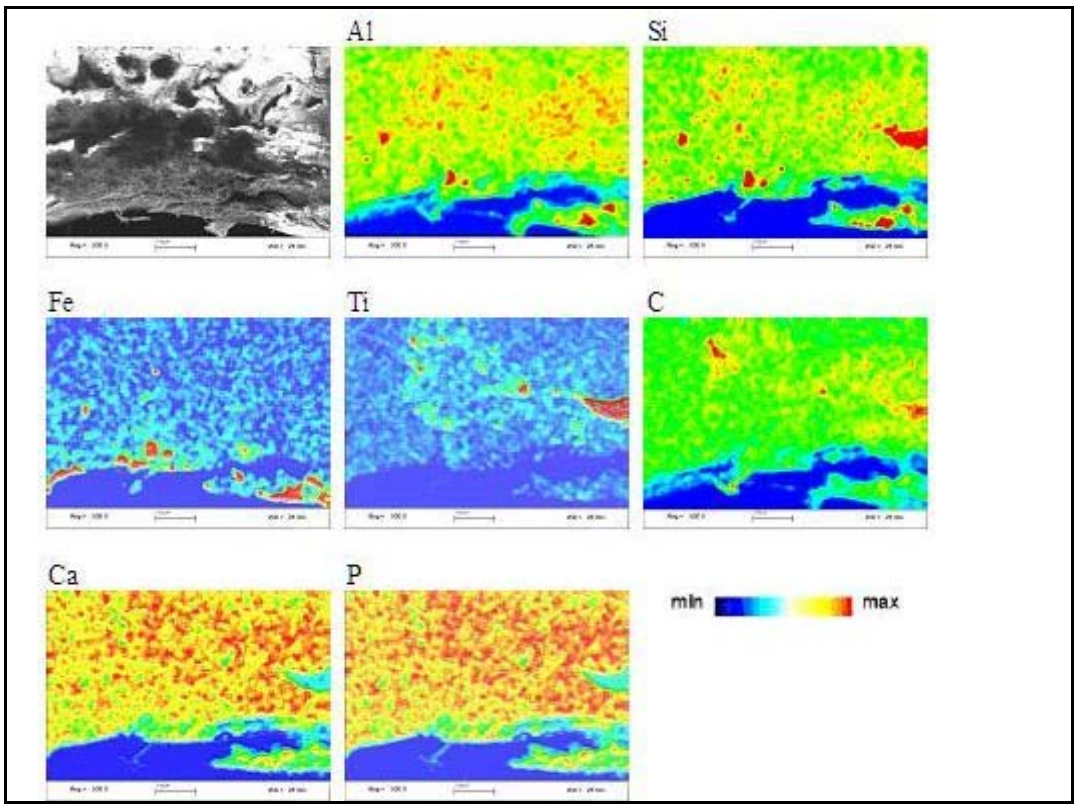

Figure 6.20. Maps of the elemental distribution in the fossil bone from EPMA: a) image from the QBSD detector; b) signal of AlKα_1; c) signal of SiKα_1; d) signal of FeKα_1; e) signal of TiKα_1; f) signal of CKα; g) signal of CaKα_1; h) signal of PKα_1, (Kuczumow *et al*., 2010).

Results from both the synchrotron-based XRF and EPMA techniques, have shown the presence of several exogenous elements. Calcium and phosphorous were detected in the entire bone area as a matrix elements. Strontium and Zinc were two elements

found to be scattered all over, with Zn presenting a stronger correlation with calcium (Figure 6.21). Iron was detected in areas where there are high strontium concentrations. Though, manganese and copper had the same distribution pattern as iron, they were associated with low intensities and were rather detected in the edge zone of the bone while iron penetrated deeper into the bone matrix. Silicon and aluminium share the similar distribution pattern. This is because the two elements occur naturally together as aluminosilicate in clays.

The inclusion of these exogenous elements is as a result of diagenetic alterations that have occurred to the bone morphology and porosity which includes among other physical changes: mechanical fracture seen on the edge zone of the bone sample (see Figure 6.21).

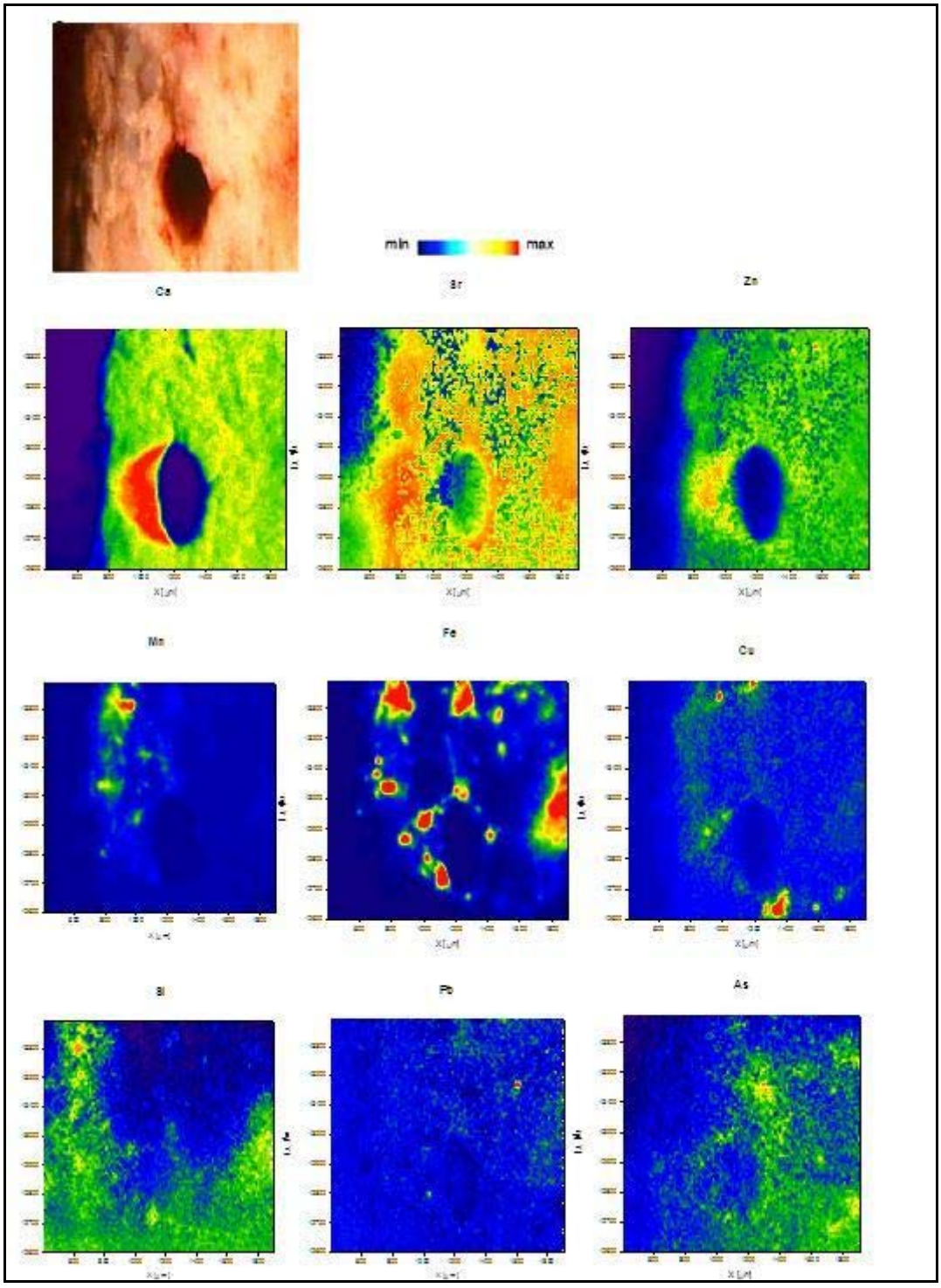

Figure 6.21. Elemental mappings of the fragment of fossil bone made with synchrotron-based XRF: A) optical image; B) Ca; C) Sr; D) Zn; E) Mn; F) Fe; G) Cu; H) Si; I) Pb; J) As mappings, (Kuczumow *et al*., 2010).

6.6.3 XRF mapping on fossil and modern bone specimen

6.6.3.1 XRF mapping modern bone specimen

Figure 6.22 is the optical image of the cross sectional area of a modern bone and Figure 6.23 illustrates its corresponding elemental distribution map.

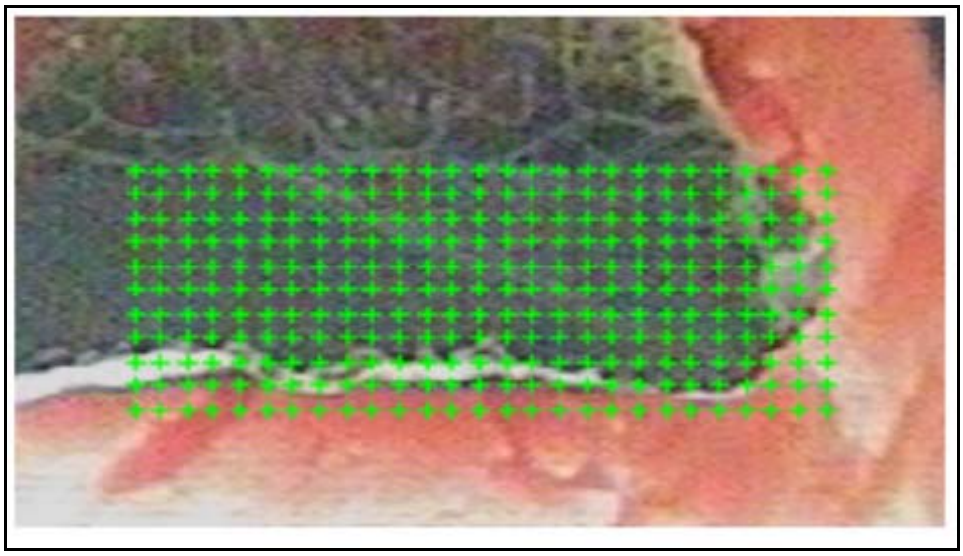

Figure 6.22. Optical image of the cross sectional area of a modern bone (MB3) with the green crosses marking measurement points.

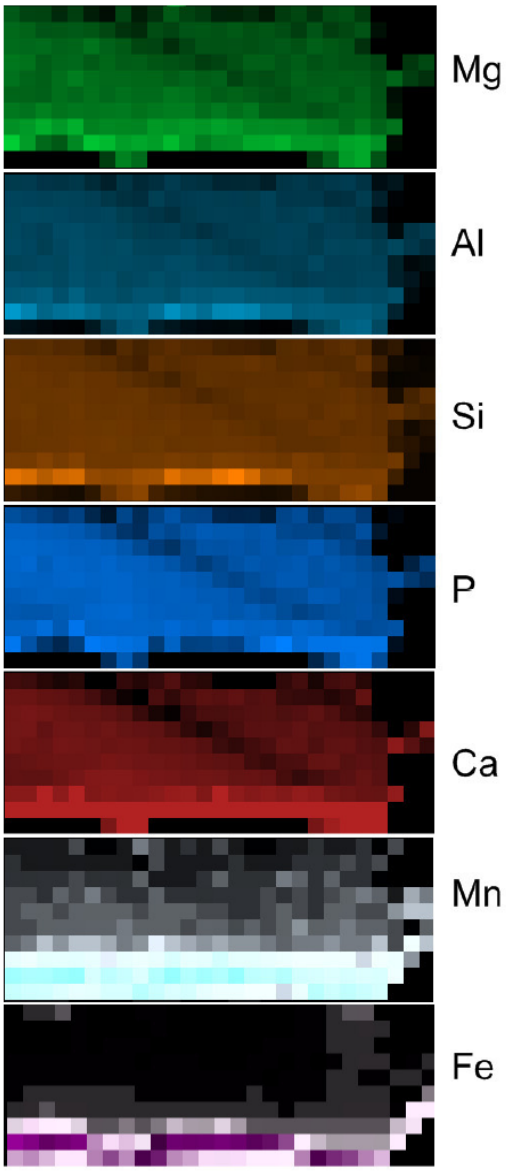

Figure 6.23. Elemental distribution XRF images for modern bone sample MB3. Where there is no strong intensity variation it means that no variation in element concentration within the bone could be found.

6.6.3.2 XRF mapping on fossil bone specimens

Figure 6.24 shows the optical image of the cross section of a fossil bone specimen and Figure 6.25 shows the XRF elemental map for the same sample. Figure 6.26 shows the optical image of the cross section of a fossil bone specimen (CD 21231) and Figure 6.27 is its X-ray fluorescence image.

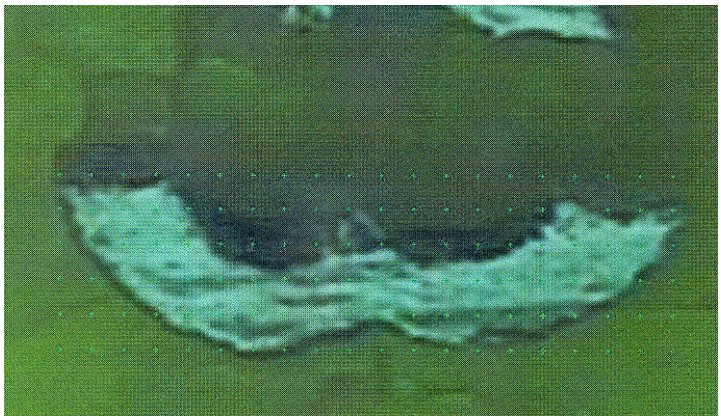

Figure 6.24. Optical image of the cross section of a fossil bone specimen. The green dots represent the target area of the analysis, (Kuczumow *et al*., 2010).

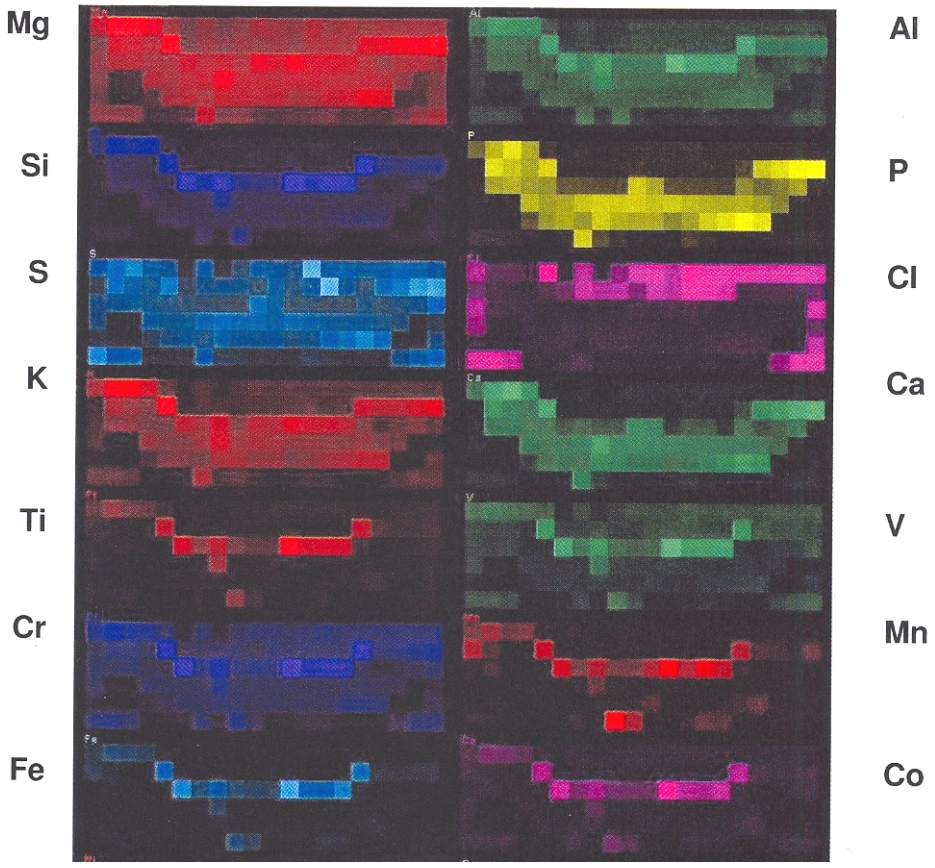

Figure 6.25. XRF image for sample CD 21245 at 1 mm resolution of a cross section of a fossil bone fragment, (Kuczumow *et al*., 2010).

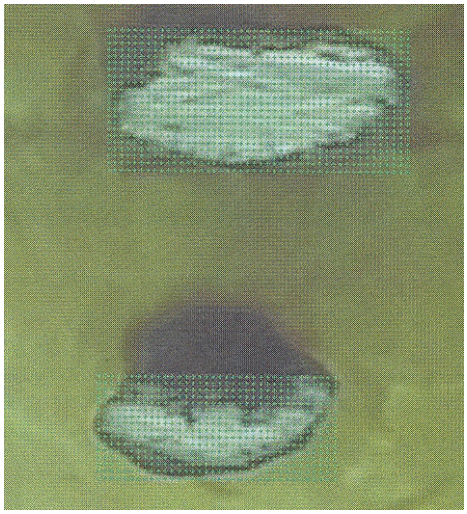

Figure 6.26. Optical image of the cross section of a manganese oxide coated fossil bone specimen. The green dots represent the target area of the analysis, (Kuczumow *et al*., 2010).

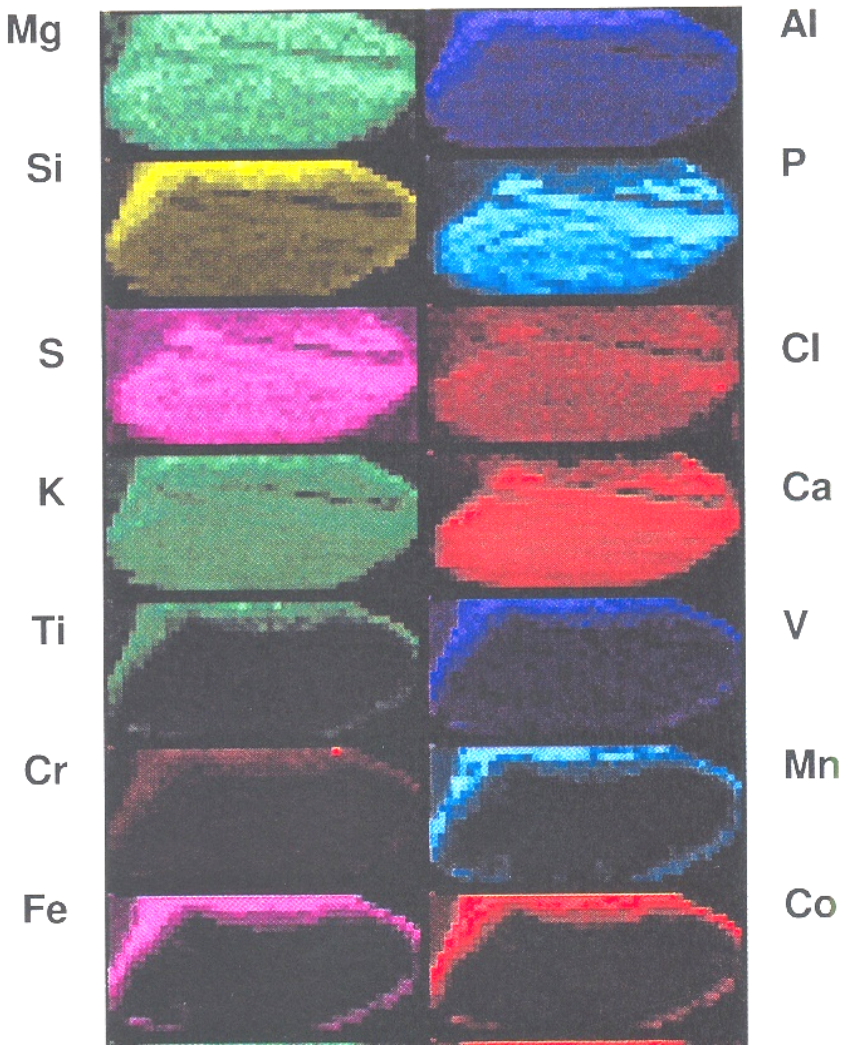

Figure 6.27. X-ray fluorescence image for the cross section of a fossil bone fragment sample CD 21231, (Kuczumow *et al*., 2010).

Discussion

For all the XRF-maps obtained, the brighter the colour the higher the X-ray intensity for that particular element. Different colours between elements are meaningless.

Figure 6.23 shows the distribution map from the modern bone sample for several elements. High intensities for Ca and P were found. Elements like Mg, Al and Si were found to be are equally distributed throughout the bone. There is a decrease in intensity of all displayed elements (except iron and manganese) at the transition from spongiform to solid bone.

Manganese and iron are associated with very low intensities and are only observed on the bones outer surface. On the other hand the fossil bone results (Figures 6.25 and 6.27) are showing lower calcium and phosphorous intensity on the regions on the cross sectional surface area where silicone and aluminium are high on the bone surface. Thus exogenous these elements (iron, manganese, silicone and aluminium) are occupying surface voids where phosphorous and calcium intensity is low in fossil bones (Figures 6.25 and 6.27). The replacement of calcium and phosphorous by these elements is a direct result of diagenetic elemental substitutions occurring within the bone matrix following dissolution, precipitation, recrystallization and mineral replacement (both leaching and enrichment) reactions taking place in and on the bone surface. Overall relative to fossil specimens, the modern bones are characterized by higher concentration of P and Ca and lower concentration of Fe and Mn. In general the results are indicating a higher intensity (i.e. concentration) of exogenous elements in the fossil bone relative to their modern counterpart. This is a result of alterations occurring during diagenesis.

Cave environment limits transport of solutions, hence dissolution of the primary mineral results in the formation of a locally enriched solution composed mainly of soluble mobile metal compounds, thereby facilitating uptake and diffusion of different elements into the buried bone. The fossil maps results suggested that the rate of element diffusion and ultimately the penetration depth into the bone varies from one element to another. Manganese is mainly located on the fossil bone surface and crack edges whereas iron is showing deeper penetration into the bone matrix. Lo´pez-Gonza´lez, *et al*. (2006) described the cave environment as being wet, mildly alkaline, and oxidizing, which is in agreement with the results obtained in this study (Table 6.3 and Figure 2.5 in Chapter Two). From the results obtained (Table 6.3) the soil pH values ranged from 8.00-8.25 and the redox potentials are in the range of well-oxidizing conditions. Under these soil conditions (relatively high pH and oxidizing redox) the alkali metals Na and K and the alkaline earth metals Ca and Mg are the most abundant soluble cations, while the transition metals Cu, Fe, and Mn are the least abundant, and the alkaline earth metals Sr and Ba and the transition metal Zn are of intermediate availability (Pate *et al*., 1989). Under these cave conditions, the stable forms of iron and of manganese are hydrates and manganese oxide compounds, respectively. Precipitation of these highly insoluble hydrates and oxides varies with

pH (Karkanas *et al*., 2000) and tend to form crusts and coatings in caves (White, 1976) and on surfaces of fossil bones.

The three oxidation states of Mn in the aqueous environment of soils are Mn^{2+}, Mn^{3+}, and Mn^{4+} (Figure 2.5 in Chapter Two). Of these three states, Mn^{2+} is soluble and hence the most dominant state of Mn in soil solution, while Mn^{3+} is insoluble and unstable in the soil solution and is often spontaneously transformed into Mn^{2+} or Mn^{4+}, depending on redox potential. Mn^{4+} is also insoluble and precipitates into various Mn oxides and hydroxides. Mn^{2+} is thermodynamically stable when under anoxic conditions and low pH, while the stability of Mn^{3+} and Mn^{4+} is highly favoured by oxic conditions and high pH, where they occur as insoluble Mn oxyhydrooxides and oxides (Kleiwicki and Morgan, 1998, 1999). Under oxic soil conditions and a pH range of 5-8, the insoluble Fe^{3+}-oxide phases are thermodynamically favoured while reduction of Fe to soluble Fe^{2+} requires suboxic or anoxic conditions. Contrary to this, insoluble Mn-oxide mineral species are stable only at the highest pE's and pH's and soluble Mn^{2+} is thermodynamically stable even under oxic conditions. In general the soluble Mn^{2+} is stable when pH is below 8, above this pH Mn^{2+} will precipitate as solid $MnCO_3$ under reducing conditions (McBride, 1994) and as insoluble Mn oxyhydrooxides and oxides under oxidizing conditions. Cornell and Schwertmann, (1996), "pointed out that Fe^{2+} spontaneous oxidizes to Fe^{3+} in the presence of O_2 at pH values below 3", whereas Mn in the same situation needs a pH around 8.5 - 9.0 to get a spontaneously oxidation. Figure 2.5 in Chapter Two is a stability diagram showing at which pH and pE different forms of Mn and Fe are stable. Since the redox plateau of MnO_2 is above that of Fe^{2+}, it means that MnO_2 has the potential to oxidize Fe^{2+} to Fe^{3+}, generating Mn^{2+} in the process according to the following reaction (Asghar and Kanehiron 1981):

$$MnO_2 + 4\ H^+ + 2\ Fe^{2+} \leftrightarrow Mn^{2+} + 2\ H_2O + 2\ Fe^{3+} \qquad (6.2)$$

Lo´pez-Gonza´lez *et al.*, (2006) proposed that the deposition is superficially produced on bone surfaces before penetration of the metallic deposits into the bone. From the XRF mapping results (Figures 4.9-4.12), iron, manganese, silicone and aluminium are occupying surface voids where phosphorous and calcium intensity is low. This is indicative of diagenetic alteration (i.e. elemental enrichment and/or leaching

following mineral dissolution/precipitation reactions) which has occurred within the bone matrix prior to the ionic substitution by these elements on the Ca positions in the hydroxylapatite lattice. The increase of these elements in the bone is directly proportional to loss of organic matter that is, as the organic collagen matter decays, the bone becomes more susceptible to diagenetic additions. This is also conformed by ICP-AES results (Figure 6.1) in which the concentration of these metals together with other exogenous elements were found to be higher in fossil specimen relative to their modern counterparts. Among other factors that can affect the extent of elemental penetration is the nature of the bone (i.e. factors such as are porosity, fractured and/or had developed cracks before or during the burial). Therefore the more porous the bone is, the deeper the penetration. Thus mineral oxides, hydrates and carbonates precipitates along these fractures and voids created by organic decay. Similarly, quartz (SiO_2,) is commonly contaminated by colloidal or clay-sized material containing aluminium, iron and manganese [Kyle, (1986), that is precipitation of quartz in these voids has lead to presents of Mn, Al and Fe in the fossil bone matrix (Figures 6.21; 6.25 and 6.27).

Conclusion

Elemental enrichment due to the uptake and diffusion of chemical elements in to the fossil bone, leaching of elements out of the bone and/or other alteration processes changes the chemical composition of bones relative to the original bone composition. However, detailed studies show that the alteration process proceeds via several mechanisms such as cation exchange, cation diffusion, dissolution and reprecipitation among others and is directly dependent on the local soil/sediment solution chemistry in which the bones were buried. As already been outlined by other authors (Downing and Park, 1998; Pate *et al*., 1989; Piepenbrink, 1989; Williams and Marlow, 1987), that "precipitation, recrystallization and mineral replacement are some of the dominant complex diagenetic physicochemical processes which take place during infilling of bone voids throughout the process of diagenesis", diffusion of exogenous elements into the bone results in supersaturation of the bone solution and the ultimate mineral precipitation, recrystallization and mineral replacement due to increased nucleation and crystal growth rate.

Therefore a combination of geochemical processes, including oxidation–reduction, adsorption, and precipitation, governs the subsurface transport and distribution of these elements.

6.7 Burnt bones: Differentiating between burning and oxide staining

Figure 6.28 shows the results of the bone cleaning operation.

Burnt bone before cleaning	After cleaning	Fe/Mn coated bone - before cleaning	After cleaning
 S1		 S4	
 S2		 S5	
 S3		 S6	

Figure 6.28. Bone cleaning results.

6.7.1 Elemental analysis of carbon, hydrogen, nitrogen and sulphur composition in burnt bones by CHNS

Table 6.4 shows the results of both burnt and coated bone elemental analyses done on three samples under each category. As illustrated in Chapter Five section 5.3 in Figure 5.3 (category 1), Figure 5.4 (category 2), Figure 5.5 (category 3) and Figure 5.6 (category 4), bone samples, were grouped into four categories according to their physical outward appearance: black, greyish-brown, Chalky-white and mineral coated unburned bones respectively.

Table 6.4. CHNS burnt and coated bone elemental analysis results.

Element	**%C**	**%H**	**%N**	**%S**
Category 1 (back)	32.93	3.150	8.038	0.483
	26.72	1.828	2.980	0.033
	26.48	2.250	nd	nd
Category 2 (greyish-brown)	15.22	1.411	3.325	nd
	14.32	1.462	2.732	0.144
	14.86	1.228	3.075	nd
Category 3 (chalky-white)	9.923	1.197	2.061	0.086
	9.394	1.127	2.167	nd
	8.820	1.048	2.192	nd
Category 4 (coated unburned bone)	0.666	0.398	0.170	nd
	0.523	0.521	0.344	nd
	0.481	0.597	nd	0.042

Results are reported as the average of two measurements.

6.7.2 ICP-AES bone surface elemental analysis

The concentrations were reported as average concentrations for three measurements in Tables 6.5 and 6.6. The elements of interest were Cr, Fe, Ca, Ba, Al, Zn, V, Co, Mn and Cu.

6.7.3 Determination of self ignition temperature of organic materials found together with the burnt bones

The organic materials (23.00 g except for leaves) found from the same site as the burnt bones were placed in a crucible and heated in an oxygen rich environment in a Gallenhamp muffle furnace to determine their self ignition temperature. The rate of heating was set at 20^{o}C/ min. the results are displayed in Figure 6.29.

Table 6.5. ICP AES burnt bones elemental analysis results.

Mass used = 0.1 g								**mg kg^{-1}**			
Sample	**Type**	**Al**	**Ca**	**Co**	**Cr**	**Ba**	**Cu**	**Fe**	**Mn**	**V**	**Zn**
S1	**<x>**	**3 448**	**42 364**	**6.4**	**37.44**	**3 054**	**2.463**	**535.5**	**93.1**	**56.65**	**2 709**
	Rsd	9.799	1.829	1.776	3.656	0.591	3.23	0.257	0.27	4.486	0.537
S2	**<x>**	**134.2**	**27 410**	**8.507**	**33.55**	**59.55**	**1.89**	**756.2**	**77.03**	**51.04**	**247.6**
	Rsd	1.466	4.016	9.656	3.892	1.366	2.835	6.102	1.961	5.657	1.485
S3	**<x>**	**455.3**	**19 069**	**9.767**	**28.37**	**31.16**	**nd**	**354.4**	**48.37**	**9.302**	**165.1**
	Rsd	1.023	2.133	0.858	3.884	0.602		0.306	2.292	6.197	0.51

Table 6.6. ICP-AES mineral coated bone elemental analysis results.

Mass=0.1 g								**mg kg^{-1}**			
Sample	Type	**Al**	**Ca**	**Co**	**Cr**	**Ba**	**Cu**	**Fe**	**Mn**	**V**	**Zn**
S4	**<x>**	**710.5**	**368 561**	**9.7691**	**113.8**	**71.94**	**16.87**	**799.3**	**1 065**	**nd**	**183.4**
	Rsd	2.570	1.322	5.559	0.674	0.357	2.763	5.329	1.32		0.294
S5	**<x>**	**2 343**	**291 361**	**11.49**	**150.7**	**163.1**	**15.63**	**1 884**	**2 022**	**22.98**	**242.6**
	Rsd	7.798	0.73	4.135	0.181	0.581	5.324	1.543	0.495	8.201	0.449
S6	**<x>**	**6 293**	**30 815**	**12.59**	**185.8**	**116.8**	**18.66**	**5 642**	**3 298**	**80.73**	**156.7**
	Rsd	0.554	1.069	2.855	0.778	0.935	2.36	0.794	0.292	3.259	0.995

Sample	Image	Average Ignition temp/^{o}C
Leaves		382
Twigs		423
Very fine free drooping		450
Fine drooping (in lump form)		462
Small nuts droopings		492
Small nuts plus fine drooping		495
Big marula		526

Figure 6.29. Determination of self ignition temperature of organic materials found in the vicinity of burnt bones.

Discussion

An insignificant amount of free carbon is found in mineral coated bone (category 4, Table 6.4). The quantity of char is directly related to the observed blackening. Blackened bones (those which were burnt between 300^{o}C and 400^{o}C) contain most char i.e. free carbon-reaching 32.93%. Relatively low percentage of free carbon was found in greyish-brown (bones heated at 500^{o}C to 600^{o}C) due to oxidation of the carbon in the organic molecule to carbon dioxide. Generally there is a continuous decrease in carbon, nitrogen and sulphur with the rise in temperature due to the extent of oxidation and this is always accompanied by loss of weight of the bone specimen. The presents of small amounts of nitrogen indicates that some proteins were still present in these bones. For fossil samples, the nitrogen amount is a good approximation of the remaining protein content. Very little char was observed in light-coloured specimens (those heated at 700-800^{o}C, the bone is chalky white and extremely light and brittle- i.e. almost complete combustion had occurred). At such elevated temperatures the bone matrix has lost much of its structure, (morphology) resulting in development of wide and deep cracks, often infiltrated by iron, manganese dioxide, and many other metal oxides. Thus the disappearance of the original microstructure of the bone is largely due to precipitation of secondary mineral, dissolution/recrystallization of the hydroxylapatite mineral (Brain, 1993) and ionic substitution within the hydroxylapatite crystal lattice.

It has also been observed that burned bones are more fragile or brittle compared to the unburned bones (the mineral coated bones) in an experimental context, and that their mechanical strength varies as a function of the extent to which the bones were burned (Stiner *et al*., 1995). Generally gross microscopic surface characteristics such as colour, cracking and warping, and degree of calcination, are typical specimen properties that are normally manipulated to characterize the degree of exposure to a heat source or lack thereof.

From the ICP AES results (Table 6.1) coated bones contained a higher concentration of selected analysed elements as compared to burnt bones. Thus loss of organic compounds during burning results in a bone becoming more susceptible to hydrolytic infiltration hence increases the rate of leaching of elements. It can be therefore assumed that the bone organic matter do protect or bind the elements (i.e. mineral

phases) from alteration. When these elements become organic free, the above experimental data suggest loss of structure of the bone apatite resulting in subsequent loss of bone elements in burnt bones. From the ignition temperatures obtained (Figure 6.29) it can be concluded that self ignition could have happened considering low ignition temperature of the organic material found together with the burnt bones.

CHAPTER SEVEN

CONCLUSION

Fossil and modern bone characterization was successfully achieved through the study of the geochemical aspects of bone diagenesis using a variety of physicochemical techniques including; scanning electron microscopy (SEM), porosity and density measurements, powder X-ray diffraction (PXRD), X-ray fluorescence-mapping (XRF-mapping), carbon, hydrogen, nitrogen, sulphur analyzer (CHNS) and inductively coupled plasma atomic emission spectroscopy (ICP AES).

These analytical techniques were employed to qualitatively and quantitatively determine the sample's post-mortem; mineral occurrence, loss and/or gain, elemental loss and/or gain, even at trace level, and examine the elemental distribution patterns across bone transverse sections; hence providing information on the local and global crystallinity of bone apatite, the precipitation of foreign minerals in the bone matrix and the presence of preserved collagen. This was achieved by comparison of the elemental amounts in fossil bones with those in modern, as well as soil in which the fossil bones were buried.

All fossil bones were found to contain calcium phosphate mineral; this is because phosphates released during crystal dissolution were involved in the recrystallisation of any remaining bone dahllite crystals. Elemental enrichment has been found to be more prevalent in fossil bones due to the incorporation of authigenic minerals from the burial environment during the fossilisation process of the bone. The post-mortem elemental enrichment and/or loss are directly linked to the relative density and porosity of the specimen. Despite the fact that the amounts of most elements are variable, some exceptional markers, such as Fe and Mn, are elevated in nearly all fossil bones and reflect a diagenetic signal from the burial environment. This trend has been observed in several studies (Parker and Toots, 1970; Lambert *et al*., 1982, 1985; Schoeninger *et al*., 1989; Bocherens *et al*., 1994; Denys *et al*., 1996; Greenlee, 1996; Kohn *et al*., 1999; Reiche *et al*., 1999; Goodwin *et al*., 2007). Thus biological apatite had incorporated Mn and Fe as well as other cations as substitute ions at all the

Ca (i.e. cation) positions in its crystal structure. Fossil specimens were also found to contain slightly higher levels of Ca and P relative to modern bones signifying the infiltration of these elements from the surrounding environment into the bone. The higher levels of Ca in fossil bones can also be attributed to the fact that Gladysvale cave is formed from dolomite ($CaMg(CO_3)_2$), and calcite ($CaCO_3$) minerals. Both minerals contain a lot of Ca, thus Ca entered the fossil bone through a simple diffusion process following their dissolution along the groundwater flow-path. ICP AES results also show a pattern of Al, Ti, Mn, Fe, Cr, Zn, Cu, and V enrichment in fossil bones relative to modern bones.

As already established, bone diagenesis leading to the preservation of skeletal tissue over geological time is a highly complex phenomenon involving the physical, chemical, histological and mechanical alterations that occur at different time scales from the time of death and depend on the prevailing local geochemical conditions (Clarke and Barker, 1993; Hedges and Millard, 1995; Hedges, 2002; Reiche *et al*., 2003; Trueman *et al*., 2004). Hence in this study preservation covered molecular/elemental/mineral preservation and retention of biogenic geochemical signals of which both depend directly on a restricted degree of bone–soil water interaction during the process of diagenesis.

The microscopic nature/condition of fossil bones show poor preservation relative to modern bones, with mineral recrystallisation and remineralization processes being some of the dominant diagenetic parameters/activities as indicated by the PXRD results. The fossil specimens have been exposed to diagenetic processes for a longer period and thus are more mineralized (as confirmed by well defined diffraction peaks) and diagenetically altered relative to modern bones. All the investigated modern specimens are microscopically well-preserved, not intensely mineralized (as indicated by diffuse PXRD peaks). From the results obtained from the PXRD, modern bones are poorly crystalline (i.e. are amorphous to a certain extent). The amorphous nature of these modern bones is correlated to a high amount of organic matter. In contrast to this, fossil bones are crystalline and this increase in crystallinity is correlated or attributed to loss of organic matter, especially carborn in the carbonate hydroxylapatite mineral. Therefore the bone organic matter protects or binds the mineral phase from alteration in modern bones. However, when the bone minerals are

organic matter-free, as in most fossil samples, then loss of the structural bone apatite is the main factor that results in the increase of crystallinity. The nature of these results is in agreement with the work done by Pfretzschner (2000) and Tütken (2003).

The results from the porosity studies indicated that the fossil specimens are highly porous as compared to their modern counterparts. One of the major factors contributing to this observation is the interaction of the bone with the ground water i.e. the bone's pore structure. Hedges and Millard (1995) pointed out that the entire bone will potentially be under threat of dissolution depending on the acidity and hydrological activity of the soil water at a given site. The increase in bone porosity of fossil bone relative to their modern counterparts can be attributed to the fact that microbially attacked bone (fossil specimens) has a large increase in porosity, which allowed increased interaction with soil water and thus potentially accelerated the bone mineral dissolution process (Smith *et al.,* 2007) leading to an increase in porosity.

The self ignition temperature of organic matter found in the vicinity of burnt bones was relatively low, which was assumed to have caused a spontaneous ignition of this organic matter (bat guano), resulting in burning of the bones. CHNS was employed for free carbon which occurs in large amounts in char. Results of the CHNS have shown insignificant amounts of free carbon is found in mineral coated bone. The quantity of char is directly linked to the observed blackening. Blackened bones (those which were burnt between 300^{o}C and 400^{o}C) contain most char since they had the highest amount of carbon. Relatively low percentages of free carbon were found in greyish-brown (bones heated at 500^{o}C to 600^{o}C) as compared to blackened bones due to oxidation of the carbon in the organic molecule to carbon dioxide. No char was anticipated in light-coloured specimens (those heated at 700^{o}C-800^{o}C, the bone is chalky-white and extremely light and brittle i.e. complete combustion could have occurred).

From the obtained ICP-AES results coated bones contained a higher concentration of selected analyzed elements as compared to burnt bones. Thus from both CHNS and ICP-AES analysis done, the burnt fossil bones contained less amounts of elements compared to their coated counterparts simply due to major alterations in bone mineralogy that occurs when bones are heated. This is simply because burned bones

lost their mechanical coherence, thereby increasing their susceptibility to hydrolytic infiltration leading to increased leaching of the bone mineral components.

Finally, the results following the cleaning process has shown that the majority of the bones were indeed burned, of which a few were burned and stained. These observations were based on comparison of the cleaning results of burnt bones against unburned (mineral coated bones).

Though several studies have been done on bone characterization, little effort if any has been made to combine and compare morphological, mineralogical, and chemical information for both modern and fossil bone from the same geological area (in South Africa). The other major drawback of previous studies is that they concentrated mainly on chemical trends of bulk materials and seldom investigated the mechanisms by which chemical compositions and mineralogy alterations occur during the bone burial period.

I therefore consider this study (in our knowledge), to be the first to characterize the morphological, mineralogical, and chemical features of fossils and compare them with those of the modern bone specimens from the same geological area, and also to investigate the possible mechanisms by which bone chemical compositions, morphological and mineralogical alterations occur during bone diagenesis in varying geochemical environments.

Such information (i.e. the characterization data) can be used in future work, to come up with a diagenesis model that can predict dominant diagenetic processes prevailing in different geochemical environments. Hence predicting the extent of bone preservation in varying environmental conditions i.e. whether fossils are likely to survive or not, thereby answering the most critical question: why do fossils occur in one site and not another? Furthermore the data can also be used for fingerprinting the origin of fossils that are out of context, study of the original mineral composition of an individual (fossil) and for direct dating of radioactive material in fossils.

PUBLICATIONS

E. Cukrowska, **Nhauro, G**., Menter, C. Burned bones: Differentiating between burning and mineral coating and investigation of the possible cause of the fire, (Article in preparation).

CONFERENCE

The South African Chemical Institute (SACI). 2009. University of Witwatersrand, Johannesburgy, South Africa.

REFERENCES

Acocks, J. P. H. 1953. Veld types of South Africa. *Mem. Bot. Surv. S. Afr.* **28:** 1-192.

Ali, M. Y. 1995. Carbonate cement stratigraphy and timing of diagenesis in a Miocene mixed carbonate-clastic sequence, off shore Sabah, Malaysia: constraints from cathodoluminescence, geochemistry, and isotopic studies. Sediment. *Geology*. **99:** 191–214.

Andrews, P., Cook, J. 1985. Natural modifications to bones in a temperate setting. *Man*. **20:** 675-691.

Antolak, A. J., Bench, G. S. 1994. PIXEF: the Livermore PIXE spectrum analysis package. Nuclear Instruments & Methods in Physics Research. Section B, Beam Interactions with Materials and Atoms. **90:** 596–601.

Antolak, A. J., Bench, G. S., Morse, D. H., 1994. IMAP: a complete Ion Micro-Analysis Package for the nuclear microprobe. Nuclear Instruments & Methods in Physics Research. Section B, Beam Interactions with Materials and Atoms. **85:** 597–601.

Asara, J. M., Garavelli, J. S., Slatter, D. A., Schweitzer, M. J., Freimark, L. M., Phillips, M., Cantley, L. C. 2007. Interpreting sequences from mastodon and *Tyrannosaurus rex*, *Science*. **317:** 1324–1325.

Asara, J. M., Schweitzer, M. H., Freimark, L. M., Philllips, M., Cantley, L. C. 2007. Protein Sequences from Mastodon and *Tyrannosaurus rex* revealed by Mass Spectrometry, *Science*. **316:** 280–285.

Avery, D. M., 1995. A preliminary assessment of the micro-mammalian remains from Gladysvale Cave, South Africa. *Palaeont. Afr*. **32:** 1-10.

Bacquet, G., Truong, V. Q., Vignoles, M., Trombe, J. C., Bonel, G. 1981. ESR of CO_2 in x-irradiated tooth enamel and A-type carbonated aoatite. *Calcified Tissue International*. **33:** 105–199.

Bada, J. L., Miller, S. L. 1970. The kinetics and mechanism of the reversible non-enzymatic deamination of aspartic acid. *Journal of the American Chemical Society*. **92 (9):** 2774–2782.

Ballomo, R. V. 1993. A Methodological Approach for Identifying Archaeological Evidence of fire Resulting from Human Activities. *Journal of Archaeological Science*. **20:** 525-553.

Barber, B. H., Berger, L. R. 2002. Field Guide to the Cradle of Humankind: Sterkfontein, Swartkrans, Kromdraai & Environs World Heritage Site. Abbot, P. & Villiers, H. Eds, pp. 11. Struik Publishers, South Africa.

Barbetti, M. 1986. Traces of Fire in the Archaeological Record, Before One Million Years Ago? *Journal of Human Evolution.* **15:** 771-781.

Behrensmeyer, A. K., Gordon, K. D., Yanagi, G.T. 1989. Nonhuman bone modification in Miocene fossils from Pakistan. In R. Bonnichsen and M. H. Sorg, Eds. *Bone Modification*. Centre for the Study of the First Americans, pp. 99-120. Orono: University of Maine Centre for the Study of the First Americans. Thompson-Shore Inc. United States of America.

Bell, L. S. 1990. Paleopathology and Diagenesis: An SEM evaluation of structural changes using backscattered electron imaging. *Journal of Archaeological Science*. **17:** 85–102.

Berger, L. R., 1992. Early hominin fossils discovered at Gladysvale Cave, South Africa. *South Africa Journal of Science.* **88:** 362.

Berger, L. R., Keyser, A. W., Tobias, P. V., 1993. Brief Communication: Gladysvale: first early hominin site discovered in South Africa since 1948. *American Journal of Physical Anthropology.* **92:** 107-111.

Berger, L. R., Tobias, P. V., 1994. New discoveries at the early hominin site of Gladysvale, South Africa. *South Africa Journal of Science*. **90:** 223-226.

Berna, F., Matthews, A., Weiner, S. 2004. Solubilities of bone mineral from archaeological sites: the recrystallization window. *Journal of Archaeological Science.* **31:** 867–882.

Birks, L. S., Hergoltz, H. K. 1978 . *X-Ray Spectrometry*, vol. 2.

Blumberg, W. E. 1981. The study of hemoglobin by electron paramagnetic spectroscopy, Methods Enzymol. **76:** 312–329.

Bocherens, H., Brinkman, D. B., Dauphin, Y. O., Mariotti, A. 1994. Microstructural and geochemical investigations on Late Cretaceous archosaur teeth from Alberta, Canada. *Canadian Journal of Earth Sciences.* **31:** 783–792.

Bocherens, H., Drucker, D., Billiou, D., Geneste, J. M., Kervazo, B. 2008. Grotte Chauvet (Ardèche, France): A "natural experiment" for bone diagenesis in karstic context. *Palaeogeography*, *Palaeoclimatology, Palaeoecology.* **266:** 220–226.

Bocherens, H., Drucker, D., Billiou, D., Moussa, I. 2005. Une nouvelle approche pour évaluer l'état de conservation de l'os et du collagène pour les mesures isotopiques (datation au radiocarbone, isotopes stables du carbone et de l'azote). *L'Anthropologie.* **109:** 557–567.

Bocherens, H., Tresset, A., Wiedemann, F., Giligny, F., Lafage, F., Lanchon, Y., Mariotti, A. 1997. Bone diagenetic evolution in two French Neolithic sites. *Bulletin de la Société Géologique de France*. **168:** 555–564.

Borgese, L., Zacco, A., Bontempi, E., Clombi, P., Bertuzzi, R., Ferretti, E., Tenini, S., Depero, L. E. 2009. Total reflection of X-ray fluorescence (TXRF): A mature technique for environmental chemical nanoscale metrology. *Measurement Science and Technology.* **20 (8):** 084027

Boscher-Barre, N., Trocellier, P. 1993. Nuclear Instruments and Methods in Physics Research. Section B, Beam Interactions with Materials and Atoms. **73:** 413– 416.

Bowel, R. 2007. Multi-Elemental Determination of Geological Samples using ICP-OES and ICP-MS –which technique and when? *Newsletter for the Association of Applied Geochemists. Explore.* **136:** 2-7.

Brain, C. K. 1993. The Occurrence of burnt Bones at Swartkrans and Their Implications for the Control of Fire by Early Hominids, pp. 230-233.

Brenn, R., Ch Haug, Klar, U., Zander, S., Alt, K. W., Jamieson, D. N., Lee, K. K., Schutkowski, H. 1999. Nuclear Instruments & Methods in Physics Research. Section B, Beam Interactions with Materials and Atoms. **158:** 270– 274.

Briggs, D., Seah, M. P. 1990. Practical Surface Analysis, Auger and X-ray Photoelectron Spectroscopy, 2nd Edition, Wiley, Chichester, UK, **1:** 473.

Broadhurst, J. L, Hansen, Y and Petrie, J. G. 2007. Waste characterisation and water-related impact predictions for solid mineral wastes: a new approach, Report to the Water Research Commission, by ISBN 978-1-77005-576-6, Report No 1550/1/07

Brown, P. L., Ritchie, I. M., Bennett, J. W., Comarmond, M. J., Timms, G. P. 2000. Geochemical kinetic modelling of acid rock drainage. In *ICARD 2000 - International Conference on Acid Rock Drainage.* Denver, USA.

Bruckschen, P., Bruhn, F., Meijer, J., Stephan, A., Veizer, J. 1995. Diagenetic alteration of calcitic fossil shells: proton microprobe (PIXE) as a trace element tool. Nuclear Instruments & Methods in Physics Research. Section B, Beam Interactions with Materials and Atoms. **104:** 427–431.

Butler, R. F. 1992. *Paleomagnetism: Magnetic Domains to Geologic Terrains.*

Callens, F. J., Verbeck, R. M. H., Matthys, P. F. A., Martens, L. C., Boesman, E. R. 1987. The contribution of CO_3^{3-} and CO_2^- to the ESR spectrum near g=2 of powdered human tooth enamel. *Calcified Tissue International.* **41:** 124–129.

Canfield, D. E., Raiswell, R., Bottrell, S. 1992. The reactivity of sedimentary iron minerals toward sulfide. *American Journal of Science*. **292:** 659-683.

Carvalho, M. L., Brito, J., Barreiros, M. A. 1998. *X-ray Spectrometry*. **27:** 198–204.

Carvalho, M. L., Casaca, C., Pinheiro, T., Marques, J. P., Chevallier, P., Cunha, A. S. 2000. Nuclear Instruments and Methods in Physics Research. Section B, Beam Interactions with Materials and Atoms. **168:** 559– 565.

Carvalho, M. L., Marques, A. F., Brito, J. 2003. American Institute of Physics, X-ray and Inner-Shell Processes, in: A. Bianconi, A. Marcelli, N.L. Saini (Eds.), 19th International Conference on X-ray and Inner-Shell Processes, 24 January 2004. Universidade de Lisboa, Lisboa**,** Portugal. AIP Conference Proceeding 652, pp. 522–528.

Carvalho, M. L., Marques, J. P., Marques, A. F., Casaca, C. 2004. *X-ray Spectrometry*. **33:** 55–60.

Carvalho, M. L., Marquesa, A. F., Lima, M. T., Reus, U. 2004. Trace elements distribution and post-mortem intake in human bones from Middle Age by total reflection X-ray fluorescence *Spectrochimica Acta* Part B **59:** 1251– 1257

Cevc, P., Schara, M. 1972. Electron paramagnetic resonance study of irradiated tooth enamel. *Radiation Research.* **51:** 581–589.

Child, A. M. 1995. Microbial taphonomy of archaeological bone. *Studies in Conservation*. **40:** 19–30.

Child, A. M. 1995. Towards an understanding of the microbial decomposition of archaeological bone in the burial environment. *Journal of Archaeological Science*. **22:** 165–174.

Chillón, B. S., Alberdi, M. T., Leone, G., Bonadonna, F. P., Stenni, B., Longinelli, A. 1994. Oxygen isotope composition of fossil equid tooth and bone phosphate: An archive of difficult interpretation, *Palaeogeography, Palaeoclimatology, Palaeoecology*. **107:** 317–328.

Clarke, J. B., Barker, M. J. 1993. Diagenesis in Iguanodon bones from the Wealden Group, Isle of Wight, southern England, Kaupia-Darmst. *Beitrage zur Naturgeschichte.* **2:** 57–65.

CoBabe, E., Pratt, L. M. 1995. Molecular and isotopic compositions of lipids in bivalve shells: a new prospect for molecular paleontology, *Geochimica et Cosmochimica Acta*. **59 (1):** 87–95.

Cole, D. R. 1983. Theory and application of adsorption and ion exchange reaction kinetics to in situ leaching of ores. In Leaching and Diffusion in Rocks and their Weathering Products (ed. S. S. Augustithis). Theophrastus Publications S.A., Athens.

Cole, D. R., Chakraborty, S. 2001. Rates and mechanisms of isotopic exchange. In Stable Isotope Geochemistry. Reviews in Mineralogy and Geochemistry (eds. J. W. Valley and D. R. Cole). Mineralogical Society of America.

Collins, M. J., Nielsen-Marsh, C. M., Hiller, J., Smith, C. I., Roberts, J. P., Prigodich, R. V.,Wess, T. J., Csapo, J., Millard, A., Turner-Walker, G., 2002. The survival of organic matter in bone: a review. *Archaeometry.* **44:** 383–394.

Collins, M. J., Riley, M. S., Child, A. M., Turner-Walker, G. 1995. A basic mathematical simulation of the chemical degradation of ancient collagen, *Journal of Archaeological Science.* **22:** 175–183.

Connolly, J. R. 2007. Introduction to X-Ray Powder Diffraction, pp. 1-9.

Cukrowska, E. M., Pole, S., McCarthy, T. S., Backwell, L. and Steininger, C. 2005. The chemical removal of manganese dioxide coatings from fossil bone. Fifth International Bone Diagenesis Meeting. University of Cape town, South Africa, pp 36.

DeNiro, M. J., Weiner, S. 1988. Organic matter within crystalline aggregates of hydroxyapatite: a new substrate for stable isotopic and possibly other biogeochemical analyses of bone. *Geochimica et Cosmochimica Acta*. **52:** 2415–2423.

Denys, C., William, C. T., Dauphin, Y., Andrews, P., Fernández-Jalvo, Y. 1996. Diagenetical changes in Plesitocene small mammal bones from Olduvai Bed-1. *Palaeogeography, Palaeoclimatology, Palaeoecology.* **126:** 121–134.

Doi, Y., Aoba, T., Okazaki, M., Takahashi, J. 1980. Orientation of carbonate ions in human tooth enamel studied with the use of the carbonate radical ion. *Journal of Dental Research.* **59:** 1473–1477.

Doi, Y., Aoba, T., Okazaki, M., Takahashi, J., Moriwaki, Y. 1981. Enriched carbonate apatites studied by ESR: comparison with human tooth apatites. *Calcified Tissue International*. **33:** 81–82.

Doi, Y., Aoba, T., Takahashi, J., Moriwaki 1979. Analysis of paramagnetic centers in X-ray-irradiated enamel, bone, and carbonate-containing hydroxyapatite by electron spin resonance spectroscopy. *Calcified Tissue International*. **28:** 107–112.

Dongarrà G., Manno, E., Sabatino, G., Varrica, D. 2009. Geochemical characteristics of waters in mineralised area of Peloritani Mountains (Sicily, Italy). *Applied Geochemistry*. **24:** 900–914

Downing, K. F., Park, L. E., 1998. Geochemistry and early diagenesis of mammal-bearing concretions from the Sucker Creek Formation (Miocene) of southeastern Oregon. Palaios. **13:** 14-27.

Drucker, D., Bocherens, H., Mariotti, A., Lévêque, F., Vandermeersch, B., Guadelli, J.L., 1999. Conservation des signatures isotopiques du collagène d'os et de dents du Pléistocène Supérieur (Saint-Césaire, France): implications pour les reconstitutions des régimes alimentaires des Néandertaliens. Bull. Mém. Soc. Anthropol. Paris **11:** 289–305.

Eda, K., Uno, Y., Nagai, N., Sotani, N., Chen, C., Whittingham, M. S., 2006. Structure-inheriting solid-state reactions under hydrothermal conditions. *Journal of Solid State Chemistry*. **179:** 1453–1458.

Efremov, J. A. 1940. Taphonomy: a new branch of palaeontology. *Pan America Geologist*. **74(2):** 81-93.

Eighmy, J. L. 1980. Archaeomagnetic Dating: A Handbook for Archaeologists.

Eighmy, J. L., Sternberg, R. S., eds. 1990. Archaeomagnetic Dating.

El-Korashy, S. A. 2003. Studies on divalent ion uptake of transition metal cations by calcite through crystallization and cation exchange process. *Journal of Materials Science*. **38:** 1709–1719.

Elliott, T. A., Grime, G. W., 1993. Examining the diagenetic alteration of human bone material from a range of archaeological burial sites using nuclear microscopy. Nuclear Instruments and Methods in Physics Research. Section B, Beam Interactions with Materials and Atoms. **77:** 537–547.

Elorza, J., Asitbia, H., Murelaga, Z., Suberbiola, X. P. 1999. Francolite as a diagenetic mineral in dinosaur and other Upper Cretaceous reptile bones (Lano, Iberian Peninsula) microstructural, petrological and geochemical features, *Cretaceous Research*. **20:** 169–187.

Engström, A., Björnerstedt, R., Clemedson, C. J. 1957. *Bone and Radiostrontium.* Stockholm: Almqvist and Wiksell.

Esaka, F., Watanabe, K., Onodera, T., Taguchi, T., Magara, M., Usuda, S. (2003). The use of Si carriers for aerosol particle collection and subsequent elemental analysis by total-reflection X-ray fluorescence spectrometry. *Spectrochimica Acta* Part B. **58:** 2145–2155.

Evangelou, V. P. 1998. Environmental Soil and Water Chemistry: Principles and Applications. A Wiley-Interscience Publication. John Wiley and Sons, Inc.pp. 131-141, 243-258.

Farquharson, M. J., Speller, R. D., Brickley, M. 1997. Measuring bone mineral density in archaeological bone using energy-dispersive low angle X-ray scattering techniques. *Journal of Archaeological Science.* **24:** 765–772.

Faure, G. 1992. Principles and Applications of Inorganic Geochemistry: A Comprehensive Textbook for Geology Students. Macmillan Publishing Company, New York.

Flohr, M. J. K. 1997. X-Ray Powder Diffraction. U.S. Department of the Interior U.S. Geological Survey, pp. 1-2.

Forbes, E. A., Posner A. M., Quirk, J. P. 1976. The specific adsorption of divalent Cd, Co, Cu, Pb and Zn on goethite. *Journal of Soil Science*. **27:** 154-166.

Frank J. M., Wensheng Y., Jennifer A. 1995. The speciation of Fe(OH) and Fe(III) in natural waters. *Marine Chemistry.* **50:** 21-39

Gaines, R. V., Skinner, H. C. W., Foord, E. E., Mason, B., Rosensweig, A. 1997. *Dana's New Mineralogy*, John Wiley & Sons, New York.

Garcı´a-Sa´nchez A. and A ´ lvarez-Ayuso E. 2002. Sorption of Zn, Cd and C on calcite. Application to purification of industrial wastewaters. *Minerals Engineering*. **15:** 539–547.

Geoffrey, M., Tochon-Danguy, H. J. 1985. Long lived radicals in irradiated apatites of biological interest: an e.s.r. study of apatite samples treated with $^{13}CO_2$. *International Journal of Radiation Biology.* **48:** 621–633.

Goldstein, J., Newbury, D. E., Joy, D.C., Lyman, C. E., Echlin, P., Lifshin, E., Sawyer, L. C., Michael, J. R., 2003. Scanning Electron Microscopy and X-ray Microanalysis, Third Edition. Springer Science + Business Media, Inc., New York. i–xix+1–689.

Gomez, S., Preoteasa, E. A., Harangus, L., Iordan, A., Grambole, D., Hermann, F. 2006. Micro-PIXE and histochemical studies of Zn and Ca distribution in normal bone. Nuclear Instruments & Methods in Physics Research. Section B, Beam Interactions with Materials and Atoms. **249:** 673–676.

Gonzalez-Reimers, E., Arnay-de-la- Rosa., M., Velasco-Vasquez, J., Galindo-Martin, L., E., Delgado-Ureta, Santolaria-Fernandez, F. 1999. *American Journal of Human Biology*. **11:** 405– 410.

Goodwin, M. B., Grant, P. G., Bench, G., Holroyd, P. A. 2007. Elemental composition and diagenetic alteration of dinosaur bone: Distinguishing micron-scale spatial and compositional heterogeneity using PIXE. *Palaeogeography, Palaeoclimatology, Palaeoecology.* **253:** 458–476.

Goren-Inbar, N., Melamed, Y., Alperson, N., Kislev, E. M., Simchoni, O., Ben-Nun, A., Werker, E. 2004. Evidence of Hominin Control of Fire at Gesher Benot Ya`aqov, Israel. *Science.* **304:** 725-727.

Grant, W. D., Long P. E. 1985. Environmental microbiology. In *Handbook of Environmental Chemistry* (ed. O. Hutzinger). The Natural Environment and the Biogeochemical Cycles. Springer. **1**, Part D, pp. 125-237.

Greenlee, D. M. 1996. An electron microprobe evaluation of diagenetic alteration in archaeological bone. In: Orna, M.V. Ed., Archaeological Chemistry: Organic, Inorganic, and Biochemical Analysis. Reviews in Mineralogy and Geochemistry. Mineralogical Society of America, Washington, D.C., pp. 455–488.

Grimme, H. 1968. Die Adsorption von Mn, Co, Cu, and Zn durch Goethit aus verduennten Löesungen. *Z. Pflanzenernaehr. Dueng. Bodenkd*. **121,** 55-65

Groecke, D. R., Hesselbo, S. P. and Jenkyns H. C. 1999. Carbon isotope composition of Lower Cretaceous fossil wood: Ocean– atmosphere chemistry and relation to sea-level change. *Geology.* **27:** 155–158.

Gross, S. R., Weiner, S. and Bar-Yosef, O. 1997. Black –Coloured bones in Hayonim Cave, Israel: Differential between burning and oxide staining. *Journal of Archaeological Science.* **24:** 439-446.

Grün, R., Schwarcz, H. P., Zymela, S. 1987. Electron spin resonance dating of tooth enamel. *Canadian Journal of Earth Sciences.* **24:** 1022–1037.

Grupe, G. and Piepenbrink, H. 1989. Impact of microbial activity on trace element concentrations in excavated bones. *Applied Geochemistry.* **4:** 293-298.

Guarino, F. M., Angelini, F., Vollono, C., Orefice, C. 2006. Bone preservation in human remains from the Terme del Sarno at Pompeii using light microscopy and scanning electron microscopy. *Journal of Archaeological Science.* **33.** 513-520.

Gutierrez, M. A. 2001. Bone Diagenesis and Taphonomic History of the Paso Otero 1 Bone Bed, Pampas of Argentina. *Journal of Archaeological Science.* **28:** 1277–1290.

Gutierrez, M. A. 2001. Bone Diagenesis and Taphonomic History of the Paso Otero 1 Bone Bed, Pampas of Argentina. *Journal of Archaeological Science.* **28:** 1277–1290.

Hagelberg, E. E., Bell, L. S., Aleen, T., Boyde, A., Jones, S. J., Clegg, J. B. 1991. Analysis of ancient bone DNA: techniques and applications, *Philosophical Transactions of the Royal Society of London.* B. **333:** 399–407.

Hare, P. E. 1980. Organic Geochemistry of Bone and its Relation to the Survival of Bone in the Natural environment.In: A. K. Behrensmeyer and A. P. Hill, Editors, Fossil in the making, University of Chicago Press, Chicago, IL.

Harland, C. E. 1994. Ion Exchange: Theory and Practice. Royal Society Chemistry, Cambridge.

Hedges, R. E. M. and Law, I. A. 1989. Radiocarbon dating of bone. *Applied Geochemistry.* **4:** 249–253

Hedges, R. E. M. and Millard, A. R., Pike, A. W. G. 1995. Measurements and Relationships of Diagenetic Alteration of Bone from Three Archaeological Sites. *Journal of Archaeological Science.* **22:** 201–209.

Hedges, R. E. M., 2002. Bone diagenesis: An overview of processes. *Archaeometry*. **44:** 319–328.

Hedges, R. E. M., Millard A. R., Pike, A. W. G. 1995. Measurements and relationships of diagenetic alteration of bone from three archaeological sites, *Journal of Archaeological Science*. **22:** 201–209.

Hedges, R. E. M., Millard, A. R., 1995. Bones and groundwater towards the modelling of diagenetic processes. *Journal of Archaeological Science.* **22:** 155-165.

Hedges, R. E. M., Millard, A. R., Pike, A. W. G., 1995. Measurements and relationships of diagenetic alteration of bone from three archaeological sites. *Journal of Archaeological Science.* **22:** 201–209.

Hem J. D., Lind C. J. 1983. Non equilibrium models for predicting forms of precipitated manganese oxides. *Geochimica et Cosmochimica Acta.* **47:** 2037-2046.

Henderson, P., Marlow, C. A., Molleson, T. I., Williams, C. T. 1983. Patterns of chemical change during bone fossilization. *Nature.* **306:** 358–360.

Hubert, J. F., Panish, P. T., Chure, D. J., Prostak, K. S. 1996. Chemistry, microstructure, petrology and diagenetic model of Jurassic dinosaur bones, Dinosaur National Monument, Utah. *Journal of Sedimentary Research*. **66:** 531–547.

Hueda-Tanabe, Y., Soler-Arechalde, A. M., Urrutia-Fucugauchi, J., Barba, L.,Manzanilla, L., Rebolledo-Vieyra, M., Goguitchaichvili, A. 2004. Archaeomagnetic studies in central Mexico-dating of Mesamerican lime-pasters. *Physics of the Earth and Planetary Interiors*. **147:** 269-283.

Hunger, S., Benning, L. G. 2007. Greigite: a true intermediate on the polysulfide pathway to pyrite. *Geochemical Transactions*. **8:** 1.

Jack, R. W., Schwarcz, H. P. 1995. Tests for Diagenesis in Tooth Enamel: ESR Dating Signals and Carbonate Contents. *Journal of Archaeological Science.* **22:** 251–255

Jackes, M., Sherburne, R., Lubell, D., Barker, C., Wayman, M. 2001. Destruction of microstructure in archaeological bone: a case study from Portugal. *International Journal of Osteoarchaeology.* **11 (6):** 415–432.

Jacques, L., Ogle, N., Moussa, I., Kalin, R., Vignaud, P., Brunet, M., Bocherens, H. 2008. Implications of diagenesis for the isotopic analysis of Upper Miocene large mammalian herbivore tooth enamel from Chad. *Palaeogeography, Palaeoclimatology, Palaeoecology*, **266:** 200–210

Jenne, E. A. 1968. Controls on Mn, Fe, Co, Ni, Cu and Zn concentrations in soils and water: the significant role of hydrous Mn and Fe oxides. In R.F. Gould, Eds. Trace Inorganics in Water. *Advances in Chemistry Series.* pp.73

Karasek, F. W., Clement, R. E. 1988. Basic Gas Chromatography – Mass Spectrometry, Elsevier Science Publishers, New York.

Kizil'shtein, L. 2006. Pyritization of fossil mollusk shells and some problems of supergene sulfide formation. *Lithology and Mineral Resources.* **41:** 570–575.

Kniewald, G., Kozar, S., Brajkovic, D., Bagi, C., Branica, M. 1994. Trace metal levels in fossil human bone from the Bezdanjaca necropolis in Croatia. *The Science of the Total Environment*. **151:** 71-76.

Kobayashi, E., Suzuki, K. T. 1990. Biological discrimination between calcium and strontium in the kidney and bone of calcium deficient growing rats. *Journal of Trace Elements in Experimental Medicine*. **3:** 327–336.

Kohn, M. J. 1999. You are what you eat, *Science.* **283:** 335–336.

Kohn, M. J., Cerling, T. E. 2002. Stable isotope compositions of biological apatite, in: M.J. Kohn, J. Rakovan, J.M. Hughes (Eds.), Phosphates: Geochemical, geobiological, and materials importance, *Reviews in Mineralogy and Geochemistry*. **48:** 455–488.

Kohn, M. J., Law, J. M. 2006. Stable isotope chemistry of fossil bone as a new paleoclimate indicator. *Geochimica et Cosmochimica Acta.* **70:** 931–946.

Kohn, M. J., Schoeninger, M. J., Barker, W. W. 1999. Altered states: effects of diagenesis on fossil tooth chemistry. *Geochimica et Cosmochimica Acta.* **63 (18):** 2737–2747.

Kostial, K., Gruden, N., Durakovic, A. 1969. Intestinal absorption of calcium-47 and strontium-85 in lactating rats. *Calcium Tissue Res*. **4:** 13–19.

Kowalewska, M., Szwedo, J. 2009. Examination of the Baltic amber inclusion surface using SEM techniques and X-ray microanalysis. *Palaeogeography, Palaeoclimatology, Palaeoecology.* **271:** 287–291.

Krumbein, W. C., Garrels, R.M., 1952. Origin and classification of chemical sediments in terms of pH and oxidation-reduction potentials. *Journal of Geology*. **60:** 1-33.

Kuczumow, A., Cukrowska, E., Stachniuk, A., Gaweda, R., Mroczka, R., Paszkowicz, W., Skrzyiec, k., Falkenberg, R., Backwell, L. 2010. Investigation of chemical change in bone material from South Africa fossil hominid deposits. *Journal of Archaeological Science.* **37:** 107-115.

Kyle, J. H. 1986. Effect of post-burial contamination on the concentrations of major and minor elements in human bones and teeth-the implications for palaeodietary research. *Journal of Archaeological Science*. **13:** 403-416.

Lacruz, R. S., Brink, J. S., Hancox, P. J., Skinner, A. R., Herries, A., Schmid, P., Berger, L. R., 2002. Palaeontology and geological context of a middle Pleistocene faunal assemblage from the Gladysvale Cave, South Africa. *Palaeontol. Afr*. **38:** 99-114.

Lacruz, R., Ungar, P, Hancox, P. J., Brink J. S., Berger, L. R. 2003. Gladysvale : fossils, strata and GIS analysis. *South African Journal of Science*. **99:** 283-284.

Lambert, J. B., Simpson, S. V., Szpunar, C. B., Buikstra, J. E. 1985. Bone diagenesis and dietary analysis. *Journal of Human Evolution*. **14:** 477–482.

Lambert, J. B., Vlasak, S. M., Thometz, A. C. 1982. A comparative study of the chemical analysis of ribs and femurs in woodland populations. *American Journal of Physical Anthropology*. **59:** 289–294.

Landmesser, M. 1994. Zur Entstehung von Kieselhölzern, extraLapis. **7:** 49–80.

Lawrence, D. R. 1979. Diagenesis of fossils – fossil diagenese. In (R. W. Fairbridge and D. Jablonski, Eds.) *Encyclopedia of Paleontology*, pp. 245-247.

Lee-Thorp, J. A., Van der Merwe, N. J. 1991. Aspects of the chemistry of modern and fossil biological apatites, *Journal of Archaeological Science*. **18:** 343–351.

Leggett, R. W., 1992. Fractional absorption of ingested barium in adult humans. *Health Physics*. **62:** 556–561.

Linford, P., 2004. Archaeomagnetic dating. *Physics Education*. **39:** 145-154.

Louër, D., Mittemeijer, J. E. 2000. Powder Diffraction in Materials Science, pp. 1-6 (editer Rennes, Stuttgart).

Lowenstam, H. A., Weiner, S. 1989. *On Biomineralization*. New York: Oxford University Press.

Lyman, L. R. 1994. Vertebrate Taphonomy. Cambridge manuals in Archaeology, Cambridge University Press.

Marion G. M., Crowley, J. K., Thomson, B. J., Kargel, J. S., Bridges, N. T., Hook, S. J., Baldridge A., Brown , A. J. , Ribeiro da Luz, B., de Souza Filho C. R. 2009. Modeling aluminum–silicon chemistries and application to Australian acidic playa lakes as analogues for Mars, *Geochimica et Cosmochimica Acta.* **73:** 3493–3511.

Martin, R. B., Burr, D. B., Sharkey, N.A., 1998. Skeletal Tissue Mechanics. Springer-Verlag, New York, NY.

McCarthy, T., Rubidge, B. 2005. The Story of Earth & Life: A Southern African Perspective on a 4.6-Billion-Year Journey. Harvey, L. & Reid, R. Eds, pp. 284-285. Struik Publishers, South Africa.

McKinley, J. P., Zachara, J. M. Smith, S. C., Liu, C. 2007. Cation exchange reactions controlling desorption of $^{90}Sr^{2+}$ from coarse-grained contaminated sediments at the Hanford site, Washington. *Geochimica et Cosmochimica Acta.* **71:** 305–325.

McLean, F. C., Urist, M. R., 1968. Bone: An Introduction to the Physiology of Skeletal Tissue, Third edition. Chicago: University of Chicago Press, pp24.

Millard, A. R., Hedges, R. E. M. 1999. A diffusion-adsorption model of uranium uptake by archaeological bone. *Geochimica et Cosmochimica Acta.* **60:** 2139–2152.

Nelson, D. A., Sauer. N. J. 1984. An evaluation of post depositional changes in the trace element content of human bone. *American Antiquity*. **49:** 14l-l47.

Neuman, W. F., Neuman, M. W. 1958. *The Chemical Dynamics of Bone Material*, pp. 705-712. Chicago, IL. University of Chicago Press.

Newesely, H. 1980. Berliner Beitrage zur Archaometrie. **5:** 175.

Nicu, M., Ionascu, l., Dragolici F., Turcanu, C., Rotarescu, G. H. 2007. XRF application for diffusion studies in radioactive waste cemented matrix. *Romanian Journal of Physics*. **52:** 287–294.

Nielsen-Marsh, C. M., Gernaey, A., Turner-Walker, G., Hedges, R., Pike, A., Collins, M., 2000. The chemical degradation of bone. In: Cox, M., Mays, S. (Eds.), Human Osteology In Archaeology and Forensic Science. Greenwich Medical Media, London, pp. 439–454.

Nielsen-Marsh, C. M., Hedges, R.E.M., 2000. Patterns of diagenesis in bone I: The effects of site environments. *Journal of Archaeological Science.* **27:** 1139–1150.

Olson, B. H. 1983. Microbial mediation of biogeochemical cycling of metals. In *Applied Environmental Geochemistry* (ed. I. Thornton), pp. 201-229. Academic Press.

Orr, P. J., Kearns, S. L., Briggs, D. E. G. 2002. Backscattered electron imaging of fossils exceptionally-preserved as organic compressions. Palaios, *Research Letter Society for Sedimentary Geology*. **517:** 110–117.

Pålsgård, E., Johansson, C., Li, G., Grime, G. W., Triffitt, J. T. 1997. Bone growth and bone development in the presence of implants or after induced leg-lengthening studied using the Oxford scanning proton microprobe. Nuclear Instruments & Methods in Physics Research. Section B, Beam Interactions with Materials and Atoms. **130:** 431–438.

Pan, Y., Fleet, M., 2002. Compositions of the apatite-group minerals: substitution mechanisms and controlling factors. In: Kohn, M.J., Rakovan, J., Hughes, J.M. (Eds.), Phosphates: Geochemical, Geobiological, and Materials Importance. Reviews in Mineralogy & Geochemistry. Mineralogical Society of America, Washington, D.C., pp. 13–50.

Parker, R. B., Toots, H. 1970. Minor elements in fossil bone. *Geological Society of America Bulletin.* **81:** 925–932.

Parkman, R. H., Charnock, J. M., Livens, F. R., Vaughan, D. J. 1998. A study of the interaction of strontium ions in aqueous solution with surfaces of calcite and kaolinite. *Geochimica et Cosmochimica Acta.* **62:** 1481–1492.

Pate, F. D, Hutton, J. T., Norrish, K. 1989. Ionic exchange between soil solution and bone: toward a predictive model. *Applied Geochemistry.* **4:** 303-316.

Pate, F. D. and Hutton, J. T. 1988. The use of soil chemistry data to address post-mortem diagenesis in bone mineral. *Journal of Archaeological Science.* **15:** 729 -739.

Penel, G. L., Rey, G., Bres, C. E. 1998. *Calcified Tissue International*. **63:** 475.

Person, A., Bocherens, H., Mariotti, A., Renard, M. 1996. Diagenetic evoluation and experimental heating of bone phosphosphate. *Palaeogeagraphy, Palaeoclimatology, Palaeoecology*. **126:** 135-149.

Person, A., Bocherens, H., Saliège, J. F., Paris, F., Zeitoun, V., Gérard, G. 1995. Early diagenetic evolution of bone phosphate: An X-ray diffractometry analysis, *Journal of Archaeological Science*. **22:** 211–221.

Pewkliang, B., Pring, A., Brugger, J. 2008. The formation of precious opal: Clues from the opalization of bone. *The Canadian Mineralogist.* **46:** 139–149.

Pfretzschner, H. U. 1998. Frühdiagenetische Prozesse bei der Fossilisation von Knochen, *Neues Jahrbuch fur Geologie und Palaontologie Abhandlungen*. **210 (3):** 369–397.

Pfretzschner, H. U. 2000. Microcracks and fossilization of Haversian bone, *Neues Jahrbuch fur Geologie und Palaontologie Abhandlungen.* **216 (3):** 413–432.

Pfretzschner, H. U. 2000. Pyrite formation in Pleistocene long bones — a case of very early mineral formation during diagenesis. *Neues Jahrbuch für Geologie und Paläontologie Abhandlungen.* **217:** 143–160.

Pfretzschner, H. U. 2001. Iron oxides in fossil bone, *Neues Jahrbuch fur Geologie und Palaontologie. Abhandlungen*. **220 (3):** 417–429.

Pfretzschner, H. U. 2004. Fossilization of Haversian bone in aquatic environments, *Comptes. Rendus. Palevol*. **3:** 605–616.

Pfretzschner, H. U. 2004. Fossilization of Haversian bone in aquatic environments. *Comptes. Rendus. Palevol.* **3:** 605–616.

Pickering, R., Hancox, P. J., Lee-Thorp, J. A., Gru¨n, R., Mortimer, G. E., Malcolm, M., Berger, L. R. 2007. Stratigraphy, U-Th chronology, and paleoenvironments at Gladysvale Cave: Insights into the climatic control of South African hominin-bearing cave deposits, *Journal of Human Evolution*. doi:10.1016/j.jhevol.2007.02.005.

Pike, A. W. G., Nielsen-Marsh, C. M., Hedges, R. E. M., 2001. Modelling bone dissolution under different hydrological regimes. Archaeological Sciences '97. Proceedings of the Conference Held at Durham. BAR International series, Oxford. **939:** 127–132.

Pike, A. W. G., Richards, M. P. 2002. Diagenetic Arsenic Uptake in Archaeological Bone. Can we Really Identify Copper Smelters? *Journal of Archaeological Science.* **29:** 607–611.

Poole, I., Lloyd, G. E. 2000. Alternative SEM techniques for observing pyritised fossil material. *Review of Palaeobotany and Palynology.* **112:** 287–295.

Posner, A. S. 1969. Crystal chemistry of bone mineral. *Physiological Reviews.* **49:** 760-792.

Preoteasa, E. A., Georgescu, R., Ciortea, C., Fluerasu, D., Harangus, L., Iordan, A., Severcan, F., Boyar, H., Preoteasa, E., Piticu, I., Pantelica, D., Gherodunescu, V. 2004. Standardless PIXE analysis of thick biomineral structures. *Analytical and Bioanalytical Chemistry*. **379:** 825–841.

Price, D. T., Schoeninger, M. J. and Armelagos, G. J. 1985. Bone Chemistry and Past Behaviour: an Overview. *Journal of Human Evolution*. **14:** 419-447.

Price, T. D, Blitz, J., Burton, J. and Ezzo, A. J., 1992. Diagenesis in prehistoric bone: problems and solutions. *Journal of Archaeological Science*. **19:** 513-529.

Putnis, A., Putnis, C. V. 2007. The mechanism of re-equilibration of solids in the presence of a fluid phase. *Journal of Solid State Chemistry*. **180:** 1783–1786.

Radosevich, S. C. 1993. The six deadly sins of trace element analysis: a case of wishful thinking in science. In: Sandford MK, editor. Investigations of ancient human

tissue. Chemical analyses in anthropology. Gordon and Breach Science Publishers, pp. 269–332.

Rafalska, J. K., Engel, M. H. and Lanier, W. P. 1991. Retardation of amino acids incorporated into melanoidins, *Geochimica et Cosmochimica Acta.* **55:** 3669–3675.

Raiswell, R., Berner, R. A., 1985. Pyrite formation in euxinic and semi-euxinic sediments. *American Journal of Science*. **285:** 710-724

Reiche, I., Quattropani, L. F., Calligaro, C., Salomon, J., Bocherens, H., Charlet, L., Menu, M. 1999. Trace element composition of archaeological bones and postmortem alteration in the burial environment. Nuclear Instruments & Methods in Physics Research. Section B, Beam Interactions with Materials and Atoms. **150:** 656–662.

Reiche, I., Quattrropani, F. L., Vignaud, C., Bocherens, H., Charlet, L., Menu, M. 2003. A multi-analytical study of bone diagenesis: the Neolithic site of Bercy (Paris, France). *Measurement Science and Technology*. **14:** 1608-1619.

Roberts, M. L., Grant, P. G., Bench, G. S., Brown, T. A., Frantz, B. R., Morse, D. H., Antolak, A. J. 1999. The stand-alone microprobe at Livermore. Nuclear Instruments & Methods in Physics Research. Section B, Beam Interactions with Materials and Atoms. **158:** 24–30.

Ruiz-Agudo, E., Putnis, C.V., Jime´nez-Lo´pez, C., Rodriguez-Navarro, C. 2009. An atomic force microscopy study of calcite dissolution in saline solutions: The role of magnesium ions *Geochimica et Cosmochimica Acta.* **73:** 3201–3217.

Schiegl, S., Goldberg, P., Bar-Yosef, O., Weiner, S. 1996. Ash deposits in Hayonim and Kebara Caves, Israel: macroscopic, microscopic and mineralogical observations, and their archaeological implications. *Journal of Archaeological Science.* **23:** 763–781.

Schmidt, A. 2007. Archaeology, Magnetic Methods. Encyclopedia of Geomagnetism and Paleomagnetism. David Gubbins and Emilio Herrero-Bervera (eds) Springer, New York, pp. 23-31.

Schoeninger, M. J. 1979. Diet and status at Chalcatzingo: some empirical and technical aspects of strontium analysis. *American Journal Physical Anthropology.* **51:** 295-310.

Schoeninger, M. J., Moore, K. M., Murray, M. L., Kingston, D. J. 1989. Detection of bone preservation in archaeological and fossil samples. *Applied Geochemstry.* **4:** 281-292.

Schweitzer, H. M., Avci, R., Collier ,T. and Goodwin , M. B. 2008. Microscopic, Chemical and molecular methods for examining fossil preservation. *Comptes Rendus palevol*. **7:** 159-184.

Schweitzer, M. H., Marshall, M., Carron, K., Bohle, D. S., Busse, S. C., Arnold, E. V., Barnard, D., Horner, J. R., Starkey, J. R. 1997. Heme compounds in dinosaur trabecular bone, *Proceedings of the National Academy of Sciences.* USA, **94:** 6291–6296.

Schweitzer, M. H., Suo, Z., Avci, R., Asara, J. M., Allen, M. A., Teran, A. F., Horner, J. R. 2007. Analyses of soft tissue from *Tyrannosaurs rex* suggest the presence of protein, *Science* **316:** 277–280.

Schweitzer, M. H., Watt, J. A., Avci, R., Forster, C. A., Krause, D. W., Knapp, L., Rogers, R. R., Beech, I., Marshall, M. 1999. Keratin immuno-reactivity in the Late Cretaceous bird, *Rahonavis ostromi*, *Journal of Vertebrate Paleontology*. **10 (4):** 712–722.

Shinomiya, T., Shinomiya, K., Orimoto, C., Minami, T., Tohno, Y., Yamada, M., 1998. In- and out-glows of elements in bones embedded in reference soils. *Forensic Science International.* **98:** 109–118.

Shipman, P., Foster, G., Schoeninger, M. J. 1984. Burnt Bones and Teeth: An Experimental Study of Colour, Morphology, Crystal Structure and shrinkage. *Journal of Archaeological Science*. **11:** 307-325.

Sillen, A. 1989. Diagenesis of the inorganic phase of cortical bone. In: Price, T. D. (Ed.), Bone Chemistry and Past Behaviour. Cambridge University Press, Cambridge, pp. 211–229.

Sillen, A., Hoering, T. 1993. Chemical characterization of burnt bones from Swartkrans. In (C. K. Brain, Ed.) *Swartkrans. A Cave's Chronicle of Early Man*. Transvaal: Transvaal Museum Monograph No. **8:** 242–249.

Sillen, A., Parkington, J.,1996. Diagenesis of bones from Eland's Bay Cave. *Journal of Archaeological Science*. **23:** 535–542.

Sips, A. J. A. M., Barto, R., Netelenbos, J.C., Van der Vijgh, W. J. F., 1997. Preclinical screening of the applicability of strontium as a marker for intestinal calcium absorption. *American Journal of Physiology Endocrinology Metabolism*. **272:** E422–E428.

Skinner, W. C. H. 2004. Mineralogy of Bone. In: O. Selinus, Ed. Essentials of Medical Geology impacts of the Natural Environment on Public Health. pp 667-693.

Smith, C. I., Craig, O. E., Prigodich, R. V., Nielsen-Marsh, C. M., Jans, M. M. E., Vermeer, C., Collinse, M. J. 2005. Diagenesis and survival of osteocalcin in archaeological bone. *Journal of Archaeological Science*. **32:** 105–113.

Smith, C. I., Faraldo, M. and Fernandez-Jalvo. Y. 2008. The precision of porosity measurements: effects of sample pre-treatment on porosity measurements of modern and archaeological bone. *Palaeogeography, Palaeoclimatology, Palaeoecology*. doi:10.10.1016/j.palaeo.2008.03.028, pp. 1-8.

Smith, C. I., Faraldos, M., Fernández-Jalvo, Y. 2008. The precision of porosity measurements: Effects of sample pre-treatment on porosity measurements of modern and archaeological bone. *Palaeogeography, Palaeoclimatology, Palaeoecology*. **266:** 175–182

Smith, C. I., Nielsen-Marsh, C. M., Jans, M. M. E. Collins, M. J. 2007. Bone diagenesis in the European Holocene I: patterns and mechanisms. *Journal of Archaeological Science*. **34:** 1485-1493.

Spencer, H., Warren, J. M., Kramer, L., Samachson, J., 1973. Passage of calcium and strontium across the intestine in man. *Clinical Orthopaedics and Related Research*. **91:** 225–234.

Sposito, G. 1989. *The chemistry of Soils.* Oxford University Press. USA.

Stankiewicz, B. A., Briggs, D. E. G., Evershed, R. P. 1997. Chemical composition of Paleozoic and Mesozoic fossil invertebrate cuticles as revealed by pyrolysis–gas chromatography/mass spectrometry, *Energy and Fuels.* **11 (3):** 515–521.

Stankiewicz, B. A., Briggs, D. E. G., Evershed, R. P., Flannery, M. B., Wuttke, M. 1997. Preservation of chitin in 25-million-year-old fossils. *Science*. **276:** 1541–1543.

Stankiewicz, B. A., Mastalerz, M., Kruge, M. A., Van Bergen, P. F., Sadowska, A. 1997. A comparative study of modern and fossil cone scales and seeds of conifers: A geochemical approach, *New Phytologist*. **135:** 375–393.

Stankiewicz, B. A., Poinar, H. N., Briggs, D. E. G., Evershed, R. P., Poinar Jr, G. O. 1998. Chemical preservation of plants and insects in natural resins, *Proceedings of the Royal Society of London*. B **265:** 641–647.

Stathopoulou, E., Theodorou, G., Panayides, L. 2005. Black bones from Aghia Napa, Cyprus: oxide staining vs. burning. Fifth International Bone Diagenesis Meeting: University of Cape Town, South Africa, pp. 44.

Stidham, T. A., 2004. Plio-Pleistocene Birds from the Hominin-Bearing Cave Deposits of Gauteng Province, South Africa. In: Proceedings Geoscience Africa 2004. University of the Witwatersrand, Johannesburg, South Africa, pp. 622. Abstract Volume.

Stiner, M. C., Kuhn, S. L., Surovell, T. A., Goldberg, P., Meignen, L., Weiner, S., Bar-Yosef, O. 2001. Bone preservation in Hayonim Cave (Israel): A Macroscopic and Mineralogical study. *Journal of Archaeological Science*. **28:** 643–659.

Stiner, M. C., Kuhn, S. L., Weiner, S. and Bar-Yosef, O. 1995. Differential burning, recrystallization, and fragmentation of archaeological bone. *Journal of Archaeological Science.* **22:** 223–237.

Suetsugu, Y., Takahashi, Y., Okamura, F. P. and Tanaka, J. 2000. *Journal of Solid State Chemistry*. **155:** 292.

Sung, W., Morgan, J. J. 1981. Oxidative removal of Mn(I1) from solution catalysed by the y-FeOOH (Iepidocrocite) surface. *Geochimica et Cosmochimica Acta*. **45:** 2377–2383

Tang, S. M., Orlic, I., Yu, K. N., Sanchez, J. L., Thong, P. S. P., Watt, F., Khoo, H. W., 1997. Nuclear microscopy study of fish scales. Nuclear Instruments and Methods in Physics Research. Section B, Beam Interactions with Materials and Atoms. **130:** 396–401.

Tapper, U., Vuorinen, H., Mussalo-Rauhama, H. 1990. Nuclear Instruments & Methods in Physics Research. Section B, Beam Interactions with Materials and Atoms. **49:** 245–249.

Taylor, R. E., Hare, P. E., White, T. D. 1995. Geochemical Criteria for Thermal Alteration of Bone. *Journal of Archaeological Science*. **22:** 115-119.

Thomas, K. J. S., Carlson, S. J., 2004. Microscale ^{18}O and ^{13}C isotope analysis of an ontogenetic series of the hadrosaurid dinosaur Edmontosaurus: implications for physiology and ecology. *Palaeogeography, Palaeoclimatology, Palaeoecology*. **206:** 257–287.

Thornber, M. R. 1975. Supergene alteration of sulphides. I: A chemical model based on massive nickel sulphide deposits at Kambalda, Western Australia. *Chemical Geology*. **15:** 1–14.

Toots, H. 1963. The chemistry of fossil bones from Wyoming and adjacent states. *Contribution in Geology*. 2 69–80.

Trueman, C. N. 1999. Rare earth element geochemistry and taphonomy of terrestrial vertebrate assemblages. *Palaios*. **14:** 555–568.

Trueman, C. N. G., Behrensmeyer, A. K., Tuross, N., Weiner, S. 2004. Mineralogical and compositional changes in bones exposed on soil surfaces in

Amboseli National Park, Kenya: diagenetic mechanisms and the role of sediment pore fluids. *Journal of Archaeological Science.* **31:** 721–739.

Trueman, C. N., Behrendsmeyer, A. K., Potts, R., Tuross, N. 2006. High-resolution records of location and stratigraphic provenance from the rare earth element composition of fossil bones. *Geochimica et Cosmochimica Acta*. **70:** 4343–4355.

Trueman. C. N., Palmer, M. R., Field, J., Privat, K., Ludgate, N., Chavagnac, V., Eberth, D. A., Cifelli, R., Rogers, R. R. 2008. Comparing rates of recrystallisation and the potential for preservation of biomolecules from the distribution of trace elements in fossil bones. *Comptes Rendus Palevol.* **7:** 145–158.

Tütken, T. 2003. Die Bedeutung der Knochenfrühdiagenese für die Erhaltungsfähigkeit in vivo erworbener Element— und Isotopenzusammensetzungen in fossilen Knochen. On-line Dissertation, Universität Tübingen. http://w210.ub.uni-tuebingen. de/dbt/volltexte/2003/962/.

Tütken, T., Vennemann, T. W., Pfretzschner H.-U. 2008. Early diagenesis of bone and tooth apatite in fluvial and marine settings: Constraints from combined oxygen isotope, nitrogen and REE analysis. *Palaeogeography, Palaeoclimatology, Palaeoecology.* **266:** 254–268.

Tuross, N., Behrensmeyer, A. K., Eanes, E. D., Fisher, L. W., Hare, P. E. 1989. Molecular preservation and crystallographic alterations in a weathering sequence of wildebeest bones. *Applied Geochemistry*. **4:** 261–270.

Van Bergen, P. F., Collinson, M. E., Briggs, D. E. G., de Leeuw, J. W., Scott, A. C., Evershed, R. P., Finch, P. 1995. Resistant biomacromolecules in the fossil record, *Acta Botanica Neerl*. **44 (4):** 319–342.

Vaniman, D. T., Chipera, S. J. 1996. Paleotransport of lanthanides and strontium recorded in calcite compositions from tuffs at Yucca Mountain, Nevada, USA. *Geochimica et Cosmochimica Acta.* **60:** 4417–4433.

Vickerman, J. C., Brown, A., Reed, N. M. 1989. Secondary Ion Mass Spectrometry: Principles and Applications, Oxford University. Press, New York.

Waldron. H. A. 1983. On the post-mortem accumulation of lead by skeletal tissues. *Journal of Archaeological Science.* **10:** 35-40.

Walker, A., Zimmerman, M. R., Leakey, R. E. F. 1982. A possible case of hypervitaminosis A in *Homo erectus. Nature.* **296:** 248-250.

Walrafen, G. E., Chu, Y.C. 2000. Nature of collagen-water hydration forces: a problem in water structure. *Chemical Physics*. **258:** 427–446.

Walser, M., Robinson, B. H. B. 1963. Renal excretion and tubular reabsorption of calcium and strontium. In: Wasserman, R. H. (Ed.), Transfer of Calcium and Strontium across Biological Membranes. Academic Press, New York, pp. 305–326.

Weiner, S., Bar-Yosef, O. 1990. States of preservation of bones from prehistoric sites in the Near East: a survey. *Journal of Archaeological Science*. **17 (2):** 187–196.

Weiner, S., Price, P. 1986. Disaggregation of bone into crystals. *Calcified Tissue International.* **39:** 365–375.

Weiner, S., Traub, W., 1992. Bone structure: from ångstroms to microns. *FASEB Journal*. **6:** 879–885.

Wess, T., Alberts, I., Hiller, J., Drakopoulos, M., Chamberlain, A. T., Collins, M., 2001. Microfocus small angle X-ray scattering reveals structural features in archaeological bone samples: detection of changes in bone mineral habit and size. *Calcified Tissue International*. **70:** 103–110.

Wilkin, R. T., Barnes, H. L. 1996. Pyrite formation by reaction of iron monosulfides with dissolved inorganic and organic sulfur species. *Geochimica et Cosmochimica Acta*. **60:** 4167–4179.

Williams, C. T. 1989. Trace elements in fossil bone. *Applied Geochemistry.* **4:** 247-248.

Wilson, L., Pollard, M. 2002. Here today, gone tomorrow? Integrated experimentation and geochemical modeling in studies of archaeological diagenetic change. *Accounts of Chemical Research.* **35:** 644–51.

Wings, O. 2004. Authigenic minerals in fossil bones from the Mesozoic of England: poor correlation with depositional environments. *Palaeogeography, Palaeoclimatology, Palaeoecology.* **204:** 15-32.

Wogelius, R. A., Fraser, D. G., Wall, G. R., Grime, G. W. 1997. Trace element and isotopic zonation in vein calcite from the Mendip Hills, UK, with spatial-process correlation analysis. *Geochimica et Cosmochimica Acta.* **61:** 2037–2051.

Wright, L. E., Schwarcz, H. P. 1996. Infrared and isotopic evidence for diagenesis of bone apatite at Dos Pilas, Guatemala: palaeodietary implications. *Journal of Archaeological Science*. **23 (6):** 933–944.

Wu, X., Orlic, I., Tang, S. M., Wang, Y., Wang, X., Zhu, J. 1997. Analysis of dinosaur samples by nuclear microscopy. Nuclear Instruments & Methods in Physics Research. Section B, Beam Interactions with Materials and Atoms. **130:** 308–314.

Wycoff, R. W. G. 1972. The Biochemistry of Animal Fossils, Scientechnica Blake, R. E., O'Neil, J. R., Garcia, G. A. 1997. Oxygen isotope systematics of biologically mediated reactions of phosphate: I. Microbial degradation of organophosphorous compounds, *Geochimica et Cosmochimica Acta*. **20:** 4411–4422.

Xia, F., Brugger, J., Chen, G., Ngothai, Y., O'Neill, B., Putnis, A., Pring, A. 2009. Mechanism and kinetics of pseudomorphic mineral replacement reactions: A case study of the replacement of pentlandite by violarite. *Geochimica et Cosmochimica Acta.* **73:** 1945–1969.

Yellepeddi, R., Bapst, A., Bonvin, D. 1996. Application of an Intergrated XRF-XRD spectrometer. Colloque C4, *supplkment au Journal de Physique III*. **6:** 781-788.

Zazzo, A., Lécuyer, C., Mariotti, A. 2004. Experimentally-controlled carbon and oxygen isotope exchange between bioapatites and water under inorganic and microbially mediated conditions. *Geochimica et Cosmochimica Acta.* **68:** 1–12.

Zipkin, I. 1970. Inorganic Composition of bone. In *Biological Calcification: Cellular and Molecular Aspects* (H. Schraer, Ed.), Appleton-Century-Crofts, New York, pp. 69–104.

APPENDIX 1. ICP AES and XRF results for rock elemental analysis

Table 1A.1. ICP-AES rock elemental analysis results (mg kg^{-1})

Sample	Type	Al	Ba	Ca	Cr	Cs	Fe	K	Li	Mg	Mn	P	Sb	Si	Sn	Sr	Ti	Zn
RS.A	**<x>**	**nd**	**1607**	**230565**	**nd**	**1507**	**316.5**	**5495**	**5.871**	**23448**	**5354**	**407.1**	**314.3**	**33690**	**6.706**	**58.72**	**38.45**	**63.59**
	rsd		0.676	2.940		0.809	5.294	6.381	2.566	2.423	1.208	1.134	1.794	0.4825	5.642	0.7	2.104	6.095
RS.B	**<x>**	**191.2**	**43.80**	**345262**	**43.13**	**41.31**	**270.1**	**158.1**	**3.772**	**5736**	**177.0**	**5177**	**373.3**	**5252**	**37.97**	**147.9**	**19.39**	**55.46**
	rsd	3.278	3.976	2.604	4.012	2.516	0.662	2.141	3.488	3.925	2.951	2.026	2.905	3.998	7.500	0.707	4.321	6.009
RS.C	**<x>**	**517.1**	**8.602**	**2071**	**26.61**	**8.279**	**2622**	**181.2**	**2.917**	**385.9**	**72.04**	**435.0**	**282.4**	**244461**	**97.80**	**19.48**	**32.90**	**11.032**
	rsd	0.571	3.379	2.468	5.130	3.307	4.132	3.876	5.086	0.388	0.566	1.084	1.637	0.571	4.109	0.353	2.517	2.022

Table 1A.2. XRF results for rock analysis

mineral	%SiO_2	%Al_2O_3	%Fe_2O_3	%FeO	%MnO	%MgO	%CaO	%K_2O	%TiO_2	%P_2O_5	LOI	T. mass
S.A	2.556	0.621	0.128	1.004	0.986	36.58	57.68	0.091	0.365	0.183	45.65	100.43
S.B	nd	0.136	0.017	0.085	0	1.409	98.42	0.017	0.034	0.068	42.04	100.95
S.C	99.35	0.169	0.03	0.279	0.01	0.05	0.139	0	0.01	0.02	0.18	100.66

APPENDIX 2. ICP AES results for modern bones, fossil bones and soil elemental analysis

Table 2A.1. ICP-AES modern bones elemental analysis results (mg kg^{-1})

Sample	Type	Ca	Cr	Na	Cu	Fe	K	Li	Mg	Mn	Ba	Al	Pb	P	S	Sn	Si	Sr	Zn
MBS1	**<x>**	**345 628**	**77.02**	**9 007**	**17.34**	**282.6**	**141.7**	**3.047**	**8 179**	**160.0**	**92.80**	**91.40**	**44.68**	**157 240**	**6 076**	**47.18**	**23388**	**361.0**	**188.4**
	rsd	0.415	1.827	2.773	5.412	6.385	2.714	3.862	0.701	2.022	0.902	4.751	6.219	1.751	5.528	5.291	2.937	0.700	1.068
MBS2	**<x>**	**385 358**	**110.1**	**9 384**	**16.92**	**276.0**	**160.6**	**3.093**	**7 831**	**174.9**	**103.6**	**63.96**	**55.65**	**174 559**	**5 880**	**48.33**	**4763**	**431.2**	**304.9**
	rsd	0.414	0.934	1.626	7.014	0.654	2.088	3.964	0.390	0.868	0.849	4.055	8.071	1.504	5.621	5.326	4.868	0.691	0.932
MBS3	**<x>**	**414 189**	**81.54**	**7 537**	**16.06**	**487.5**	**122.7**	**2.934**	**7 969**	**396.2**	**106.3**	**164.9**	**49.37**	**182 186**	**4 620**	**44.51**	**14264**	**397.1**	**207.9**
	rsd	0.416	1.787	2.202	6.431	0.421	3.923	1.976	0.347	3.652	0.801	3.310	7.673	1.094	6.161	3.552	6.452	0.778	0.809
MBS4	**<x>**	**315 553**	**81.19**	**6 211**	**20.65**	**346.8**	**117.9**	**3.041**	**7 508**	**415.9**	**92.53**	**157.8**	**52.27**	**148 159**	**2 145**	**49.97**	**13509**	**379.9**	**158.5**
	rsd	0.279	1.086	1.000	5.806	3.402	2.948	3.583	0.443	0.748	0.546	3.727	7.105	1.728	7.468	3.480	4.199	0.3803	0.892

Table 2A.2. ICP-AES fossil bones and soil elemental analysis results (mg kg^{-1})

Sample	Type	Ca	Cr	Cu	Fe	K	Li	Mg	Mn	Zn	Na	Al
FBS1	**<x>**	**436 392**	**143.3**	**39.33**	**10 650**	**115.2**	**9.659**	**2 576**	**8 258**	**285.0**	**498.8**	**8 074**
	rsd	0.606	1.498	4.005	1.711	0.998	2.333	0.965	0.599	1.383	0.555	3.994
FBS2	**<x>**	**427 165**	**134.2**	**86.85**	**9 608**	**136.7**	**8.515**	**3 164**	**4 354**	**681.1**	**389.0**	**9 511**
	rsd	0.575	1.279	3.605	1.504	0.369	2.353	1.333	0.655	4.286	0.335	7.767
FBS3	**<x>**	**369 416**	**238.2**	**126.9**	**3 393**	**72.46**	**9.579**	**3 801**	**6 988**	**1 379**	**536.7**	**4 679**
	rsd	0.333	1.2095	1.801	1.619	1.239	1.683	1.927	0.885	2.794	1.017	1.021
FBS4	**<x>**	**348 133**	**92.21**	**98.04**	**3 958**	**77.37**	**6.817**	**3 863**	**8 231**	**1 292**	**435.7**	**4 208**
	rsd	0.645	0.342	1.361	2.212	0.861	1.7935	0.554	0.980	2.794	0.404	9.777
SOIL S1	**<x>**	**100 351**	**124.1**	**99.63**	**36 982**	**434.5**	**26.08**	**2 783**	**15 679**	**421.7**	**251.9**	**20 832**
	rsd	5.197	2.057	3.489	0.733	1.925	1.559	0.658	0.868	1.071	1.325	2.367
SOIL S2	**<x>**	**62 970**	**193.8**	**104.8**	**38 963**	**441.4**	**28.74**	**3 221**	**14 770**	**380.3**	**261.3**	**22 528**
	rsd	0.695	1.206	1.068	1.084	0.904	1.076	0.389	0.548	0.484	0.870	2.675
SOIL S3	**<x>**	**60 915**	**131.1**	**104.2**	**35 898**	**522.7**	**27.90**	**3 999**	**13 950**	**395.7**	**200.4**	**19 995**
	rsd	0.094	2.06	2.735	0.872	0.123	2.415	3.092	0.669	1.767	2.03	2.838

Table 2A.2. ICP-AES fossil bones and soil elemental analysis results (mg kg^{-1})

Sample	Type	Ba	Ti	Sr	P	Pb	S	Si	Sn	V
FBS1	**<x>**	**167.9**	**312.3**	**123.7**	**185 891**	**127.4**	**4 645**	**1 705**	**82.57**	**24.6**
	rsd	0.841	3.422	0.762	1.340	8.113	5.613	1.111	4.895	6.227
FBS2	**<x>**	**194.4**	**297.3**	**343.7**	**178 057**	**157.7**	**3 796**	**908.7**	**86.15**	**23.11**
	rsd	1.269	1.955	1.108	4.953	4.94	5.127	4.523	2.928	4.402
FBS3	**<x>**	**433.7**	**317.4**	**226.0**	**165 235**	**144.2**	**4 859**	**335.0**	**76.21**	**15.91**
	rsd	0.79	0.799	0.7955	1.515	6.7795	3.695	3.467	5.8615	7.262
FBS4	**<x>**	**405.5**	**122.2**	**205.5**	**190 811**	**148.0**	**5 021**	**1 192**	**81.53**	**12.45**
	rsd	0.906	1.388	0.925	2.145	3.4645	7.3815	1.256	5.918	4.713
SOIL S1	**<x>**	**295.8**	**1 416**	**62.37**	**28 699**	**116.3**	**2 247**	**26 279**	**68.72**	**51.17**
	rsd	1.014	9.543	1.072	1.565	8.5755	14.34	0.606	7.289	1.975
SOIL S2	**<x>**	**308.3**	**1 829**	**64.83**	**23 810**	**101.3**	**2 341**	**11 351**	**69.42**	**66.16**
	rsd	0.769	8.471	0.85	2.539	4.23	9.93	5.477	4.402	2.240
SOIL S3	**<x>**	**301.8**	**2 093**	**51.62**	**21 623**	**129.3**	**2 790**	**4 343**	**104.2**	**56.26**
	rsd	0.757	2.862	1.035	4.242	6.943	9.296	0.264	8.885	4.468

APPENDIX 3. Photographs of features in the study area (Cradle of Humankind, Gauteng, S.A)

(a) (b)

Figure 3A.1. A view of the sampling site (a) outside the cave (b) 45 metres below the ground level, where modern bone samples were obtained

(a) (b)

Figure 3A.2. A view of the sampling site (a) outside the cave (b) inside the cave, where fossil bone and soil samples were obtained

APPENDIX 4. Properties of individual acid (in an acid mixture) employed during sample digestion

Nitric acid

Nitric acid is a strong oxidising agent and hence it was employed for its oxidising and as its acidic properties as well as for the destruction of organic matter. The other advantage being that nitric acid forms invariably soluble salts.

Hydrochloric acid

Hydrochloric acid is non-oxidizing agent; in fact it is reducing towards some higher oxidation states of metals, for example Ce(IV), Te(VI), Mn(IV), Mn(VII). It was used for the attack of inorganic matrices yielding/giving metal chlorides which are known to be soluble except or few elements like Ag, TI and Pb. Thus HCl was employed for its powerful complexing properties, thereby aiding sample dissolution. The main challenge with hydrochloric acid is that it forms volatile chlorides such as those of Hg, Ge, As, Sb, and Se.

Hydrofluoric Acid

This is a weak, non-oxidising acid and was basically used to destroy difficult silicate matrices. After using HF boric acid was added to combine with any residual traces of fluoride prior to analysis using ICP to avoid damage of the quartz component(s) on the instrument. Exceptional great care was taken when handling HF. Gloves entirely freee from any pinholes, were always used, since HF causes painful bums that are slow to heal and it can pass through the skin to attack the bone.

Hydrogen Peroxide acid

It is one of the most powerful laboratory oxidants. H_2O_2 was used to aid in dissolving the resistant bone matrix.